

February
1105.5
Northrop B-35/4



UNCLASSIFIED

GRANDMUM REPORT

Redacted

~~CONFIDENTIAL~~ MR No. L5L27
~~UNCLASSIFIED~~ ~~Inactive~~
 TESTS OF A 1/7-SCALE SEMISPAN MODEL OF
 THE XB-35 AIRPLANE IN THE
 LANGLEY 19-FOOT PRESSURE TUNNEL
 By Jerome Teplitz, Gerald G. Kayten
 and Patrick A. Cancro

JAN 16 1946

*Suitable for
indexing (Revised
2-7-46)*

CLASSIFICATION CANCELLED

Authority RF 2284 Date 12/4/53
EO 128108
By J.H. 2/19/54 See



FOR REFERENCE

NOT TO BE TAKEN FROM FILE

NATIONAL ADVISORY COMMITTEE FOR AERONAUTICS

UNCLASSIFIED

UNCLASSIFIED

NACA LANGLEY MEMORIAL AERONAUTICAL LABORATORY

MEMORANDUM REPORT

for the

Air Technical Service Command, Army Air Forces

~~CONFIDENTIAL~~

MR No. L5L27

UNCLASSIFIED
TESTS OF A 1/7-SCALE SEMISPAN MODEL OF

THE XB-35 AIRPLANE IN THE

LANGLEY 19-FOOT PRESSURE TUNNEL

By Jerome Teplitz, Gerald G. Kayten
and Patrick A. Cancro

SUMMARY

A 1/7-scale semispan model of the XB-35 airplane was tested in the Langley 19-foot pressure tunnel, primarily for the purpose of investigating the effectiveness of a leading-edge slot for alleviation of stick-fixed longitudinal instability at high angles of attack caused by early tip stalling, and a device for relief of stick-free instability caused by elevon up-floating tendencies at high angles of attack. The device consisted of an elevon tab linked to a free-floating "flipper" located at the outboard end of the elevon so that the up-floating tendency would be transmitted to the elevon tab by means of the flipper, thus introducing an elevon down-floating tendency.

The results indicated that the slot was not adequate to provide the desired improvement in stick-fixed stability. The tab-flipper device provided appreciable improvement in stick-free stability and two of the linkage combinations tested (with full-span elevon tab) gave satisfactory variations of control force with airspeed for all conditions except that in which the wing-tip "pitch-control" flap was fully deflected. The improvement in control-force characteristics, however, was accompanied by a detrimental effect on stick-fixed stability because of the pitching moments produced by the elevon tab deflection.

~~CONFIDENTIAL~~

UNCLASSIFIED

At a constant angle of attack, moreover, the flipper-linked tab acted in the manner of a balancing tab, causing a reduction in elevon rolling effectiveness and indicating possible overbalance of lateral control forces in certain conditions.

INTRODUCTION

The Northrop XB-35 airplane is a proposed bomber of the flying wing type powered by four submerged engines driving pusher propellers. The trailing edge consists almost entirely of control surfaces and flaps. Both longitudinal and lateral control are provided by a pair of trailing-edge control surfaces ("elevons") linked for simultaneous deflection as elevators as well as differential deflection as ailerons.

The investigation of reference 1 and data obtained by Northrop Aircraft, Inc. in flight tests of a flying model of the XB-35 have indicated poor stick-fixed and stick-free static longitudinal stability at low speeds, attributed largely to early stalling at the tips and along the trailing edge of the highly swept-back and tapered wing. The primary purpose of the present investigation was to determine the effects of a leading-edge tip slot installed for improvement of the stick-fixed longitudinal stability and to determine in three-dimensional flow the feasibility of an arrangement designed to eliminate the severe elevon up-floating tendencies (and the resulting stick-free instability) at high angles of attack. This arrangement consisted of a free-floating "flipper" linked to an elevon tab. The flipper, detached from the outboard end of the elevon, was intended to respond readily to the forces causing the elevon up-floating tendency. Upward deflection of the flipper would cause upward deflection of the elevon tab, thus reducing the up-floating tendency of the elevon itself. The arrangement was investigated to some extent in two-dimensional flow in the Langley stability tunnel, and the results were presented in reference 2. On the basis of these results, an elevon incorporating the flipper device was installed on a 1/7-scale semispan model to be tested with a reflection plane in the 19-foot pressure tunnel. The semispan model was selected in order to obtain the information at a relatively high Reynolds number and a low Mach number.

~~CONFIDENTIAL~~

UNCLASSIFIED

SYMBOLS AND COEFFICIENTS

The symbols and coefficients used herein are defined as follows:

C_L	lift coefficient	$(L/q_0 S)$
C_D	drag coefficient	$(D/q_0 S)$
C_m	pitching-moment coefficient	$(M/q_0 S c)$
C_l	rolling-moment coefficient	$(L'/4q_0 S b)$
C_n	yawing-moment coefficient	$(N/4q_0 S b)$
C_{h_e}	elevon hinge-moment coefficient	$(H/q_0 b_e \bar{c}_e^2)$
Δh	loss in total pressure from free stream	
q_0	free-stream dynamic pressure	$(\frac{1}{2} \rho_0 V_0^2)$
R	Reynolds number	$(\rho_0 V_0 c / \mu_0)$
M	Mach number	(V_0 / a_0)
ρ	mass density of air	
μ	coefficient of viscosity of air	
a	velocity of sound in air	
δ	control deflection, positive when trailing edge is down	
α	angle of attack, measured with respect to root chord line	
V_i	indicated airspeed, miles per hour	

where

L	lift
D	drag
M	pitching moment about center of gravity, positive when tending to depress tail

~~CONFIDENTIAL~~
UNCLASSIFIED

- L' rolling moment about center of gravity, positive when tending to depress right wing
- N yawing moment about center of gravity, positive when tending to retard right wing
- H elevon hinge moment, positive when tending to deflect elevon down
- h total pressure
- S semispan wing area (40.82 sq ft on model) $\left[4000.36 \text{ ft}^2 \text{ FULL SCALE} \right]$
- b semispan of wing (12.29 ft on model); in $pb/2V$, b refers to complete span
- c mean aerodynamic chord of wing (3.75 ft on model)
- V airspeed
- b_e elevon span (4.53 ft on model)
- \bar{c}_e elevon root-mean-square chord (0.552 ft on model)
- p rolling velocity

Subscripts:

- o free stream
- l duct entrance
- i slot inboard station
- h slot outboard station
- e elevon
- t tab
- F flipper
- p pitch control
- f flap
- l landing

MODEL AND TESTS

Tunnel Installation

The 1/7-scale semispan model of the XB-35 airplane was mounted in the Langley 19-foot pressure tunnel in conjunction with a true reflection plane. A gap of approximately 3/32 inch between the root section of the model and the reflection plane was maintained for the tests by means of an automatic telescoping mechanism within the model. The model was mounted on a two-support system with one strut exposed to the air stream and the other strut within the structure comprising the reflection plane. The general arrangement of the model installation is shown in figures 1 and 2.

Model

The subject model incorporated some of the latest design features of the XB-35 airplane. The aspect ratio was 7.36 and the taper ratio 4:1. NACA symmetrical sections were used: 65(318)-019 section at the root, and 65,3-018 at the construction tip. The wing was twisted about the 25-percent-chord line to give 4° geometric washout. The dihedral and sweepback of the 25-percent-chord line were 1° and 23°7', respectively, instead of 2° and 21°56' as in reference 1. Plan and elevation views of the model are given in figure 3.

The entire trailing edge of the wing was made up of control surfaces: a lift flap at the root, an elevon intermediate, a small flipper immediately outboard of the elevon, and a pitch-control flap at the tip.

The lift, or landing, flap (fig. 4) was of the split type modified to carry a portion of the trailing edge of the wing with it when deflected. It was approximately 22 percent of the chord and extended from 3.60 to 38.59 percent of the semispan. For the present tests, the flap was either deflected 43.3° or retracted.

The pitch-control flap, located at the wing tip in order to realize the maximum moment arm due to sweepback, extended inboard to 78.64 percent of the semispan. It was of the plain, sealed type, with approximately constant

~~CONFIDENTIAL~~

UNCLASSIFIED

chord. Designed for upward deflection to 35° to provide trim in pitch, the pitch-control flap was deflected during the tests only when the landing flap was deflected. The settings were 0° , -14.1° , and -34.1° . Details are given in figure 5.

The elevon installation consisted of an 18-percent (approximate) chord sealed internally balanced elevon with an overhang 40.6 percent of the elevon chord. The elevon extended from 38.23 percent to 75.89 percent along the semispan. It was equipped with a 25-percent-elevon-chord full-span tab divided equally in two spanwise sections.

Just outboard of the elevon and having a span approximately $1/16$ of that of the elevon was the so-called flipper. It consisted of a straight-sided unbalanced and unsealed surface with a 25-percent-chord full-span tab. The flipper was connected to the elevon tab through a linkage extending along the elevon hinge line so that the flipper and elevon tab deflected as a unit independent of elevon deflection. The unit was statically balanced and arranged so that the flipper could be connected to either half-span or full-span elevon tab or disconnected to float by itself. The linkage was such that the elevon tab deflected upward as the flipper floated up. It was possible to obtain only two linkage ratios of flipper to elevon tab, namely 2:1 and 1:1. The flipper tab was linked so as to deflect oppositely to the flipper with a linkage ratio of either 1:1 or 1:2. The flipper tab could also be locked at a given setting. Elevon and flipper details are given in figures 6 and 7. For these tests, the elevon had a deflection range of $\pm 20^\circ$ and the flipper had a deflection range of $\pm 18^\circ$.

The seal across the balance was koroseal-impregnated voile of sufficient length to avoid tautness at the extreme elevon deflections. The elevon balance chamber was divided into four spanwise units by three elevon-support brackets containing bearings, to help reduce friction caused by lack of rigidity. Copper tubes were located within the balance chambers to record the pressures across the seal of the balance.

Elevon hinge moments were measured by a resistance-type wire strain gage located approximately midway along

the elevon span. Hinge-moment measurements are believed accurate to within approximately $\Delta C_h = \pm 0.004$. The elevon deflection was adjusted by remote control. The positions of the elevon and of the inboard half-span elevon tab were indicated by NACA control-position indicators. It was possible to determine the position of the outboard semispan elevon tab only when the inboard and outboard tab sections were operated as a unit.

The leading-edge slot extended from 74 to 94 percent of the semispan. For most of the tests the slot was opened only when the landing flap was deflected. Slot details are given in figure 8 and the installation is shown in figure 3.

For some of the tests a split rudder was installed on the model. The rudder was composed of metal plates extending practically the full length of the pitch-control flap on both the upper and lower surfaces and held in place by wedge blocks to a total included angle of 120° . Split rudder details are shown in figure 5.

The duct entrance at the leading edge of the wing and the duct exits immediately forward of the landing flap were simulated on the model. Provision was made for measuring the quantity of air through the duct by the use of static and shielded total-head tubes at a station in the duct entrance.

Tests

The subject tests of the 1/7-scale semispan model of the XB-35 airplane were made in the Langley 19-foot pressure tunnel with the air in the tunnel compressed to a density of approximately 0.0055 slug per cubic foot. The Reynolds and Mach numbers at which the tests were made were approximately 7,500,000 and 0.12, respectively.

Preliminary tests.— Because of the possible effect of air flow through the induction system on elevon hinge moments, preliminary tests were made with the duct exit doors both deflected and neutral. Through the limited range available for control of internal air flow, the effects of the difference were negligible, and the actual tests were made with the duct exit doors set at neutral.

Figure 9 presents the resulting variation with angle of attack of the ratio of duct entrance velocity to free-stream velocity, V_1/V_0 .

In order to determine the effects of leakage between the wing-root section and the reflection plane, several tests were made with the end gap sealed by flexible sheet material. On the basis of these check tests, it was determined that end leakage had negligible effect on the lift and stalling characteristics of the model. The tests discussed in the remainder of the report are those made with the gap unsealed.

To determine the effectiveness of the elevon balance seal, the region immediately above the upper-surface vent was subjected to a pressure greater than atmospheric. The effectiveness of the seal is expressed in terms of the "leakage factor," which may be defined as the ratio $\frac{p_1 - p_2}{p_3 - p_4}$, where p_1 is the pressure in the balance chamber above the seal, p_2 is the pressure in the chamber below the seal, p_3 is the pressure above the upper-surface vent, and p_4 is the (atmospheric) pressure below the lower-surface vent. For the model seal arrangement used in the tests, the leakage factor was approximately 0.96.

Lift and stalling characteristics.- Model stalling characteristics were determined from observations of tufts of wool yarn attached to the upper surface of the wing at 20, 30, 40, 50, 60, 70, 80, 90, and 95 percent of the wing chord and spaced approximately 7 inches spanwise. Tuft surveys were made with the landing flap and pitch-control flap neutral, leading-edge slot open and closed, and with the landing flap deflected 43.3° for several pitch-control flap deflections, slot open and closed.

The effects of the leading-edge slot on the aerodynamic characteristics were investigated. Except for these tests made specifically to determine the effects of the slot, the slot was generally closed throughout the tests with landing flap retracted, and open during the tests with landing flap deflected. Some tests were made to determine the effect of pitch-control flap deflection on the air flow through the slot. Racks of one static-and three total-head tubes were placed in each

of two sections in the slot exit to measure the air-flow velocity and pressure recovery at the exit of the slot.

The effects of fixed transition were noted for a few tests by affixing a 0.032-inch diameter wire on the upper surface of the wing at each of two positions, 15 and 3 percent of the chord along the complete semispan.

Longitudinal stability and control.- In order to obtain general elevon- and tab-effectiveness data, a series of tests was made in which the half-span and the full-span elevon tabs were set at different angles for various elevon deflections through the angle-of-attack range. During these tests the elevon tab and the flipper were not linked together.

With the elevon tab linked to the flipper and the combination allowed to float freely, tests were made at various elevon deflections through the speed range, using different linkage ratios between the flipper and the elevon tab and between the flipper and the flipper tab. Both the half-span and the full-span elevon tabs were used in these tests. The tests were planned to determine a combination of variables that would give the best improvement in control-force characteristics. The combinations tested are listed in the following table:

δ_{f_1} (deg)	Elevon tab span	Elevon tab linkage	Flipper tab linkage	Limit to flipper up deflection	Figure no.
0	Half (outboard)	$\delta_{t_{e_o}} = \delta_F$	$\delta_{t_F} = -\delta_F$	-----	31
43.3	-----do-----	$\delta_{t_{e_o}} = \delta_F$	$\delta_{t_F} = -\delta_F$	-----	32
0	Half (inboard)	$\delta_{t_{e_i}} = \delta_F$	$\delta_{t_F} = -\delta_F$	-----	33
43.3	-----do-----	$\delta_{t_{e_i}} = \delta_F$	$\delta_{t_F} = -\delta_F$	-----	34
0	Full	$\delta_{t_e} = \delta_F$	$\delta_{t_F} = 0$	-----	35
43.3	-----do-----	$\delta_{t_e} = \delta_F$	$\delta_{t_F} = 0$	-----	36
0	-----do-----	$\delta_{t_e} = \frac{1}{2}\delta_F$	$\delta_{t_F} = 0$	-----	37
43.3	-----do-----	$\delta_{t_e} = \frac{1}{2}\delta_F$	$\delta_{t_F} = 0$	-----	38
0	-----do-----	$\delta_{t_e} = \delta_F$	$\delta_{t_F} = -\frac{1}{2}\delta_F$	-----	39
43.3	-----do-----	$\delta_{t_e} = \delta_F$	$\delta_{t_F} = -\frac{1}{2}\delta_F$	-----	40
0	-----do-----	$\delta_{t_e} = \delta_F$	$\delta_{t_F} = -\delta_F$	-7.5°	41
43.3	-----do-----	$\delta_{t_e} = \delta_F$	$\delta_{t_F} = -\delta_F$	-7.5°	42
0	-----do-----	$\delta_{t_e} = \delta_F$	$\delta_{t_F} = -\delta_F$	-----	43
43.3	-----do-----	$\delta_{t_e} = \delta_F$	$\delta_{t_F} = -\delta_F$	-----	44

For some of the tests the elevon tab was disconnected from the flipper and allowed to float freely with and without "cords" at its trailing edge. The cords were actually splines consisting of balsa strips 1/16 inch high and 1/8 inch wide extending along the complete span of the elevon tab.

RESULTS AND DISCUSSION

Data and Corrections

All results were reduced to standard nondimensional coefficients so that the results apply to a complete-span wing. Moments were computed about a center-of-gravity location at 21.74 percent of the mean aerodynamic chord and 4.58 percent mean aerodynamic chord above the root chord line on the basis of the latest design information received from the contractor. (The horizontal location corresponds to 25 percent mean aerodynamic chord based on the specifications of reference 1.) The corrected results are presented in graphical form. The corrections applied to the data are described as follows:

A stream angle correction determined from surveys made with the reflection plane and strut fairing in place was applied to the angle of attack and the drag coefficient. In addition, an empirical blocking correction (reference 3) was applied to the dynamic pressure. No tare corrections were applied to the lift, drag, or pitching moments for the effects of the drag and interference of the model support system. Increments in coefficients due to control deflections may be considered correct, neglecting small changes in tare values due to their deflection.

Jet-boundary interference corrections were applied to the angle of attack, drag coefficient, and rolling- and yawing-moment coefficients. These corrections were calculated by methods similar to those outlined in reference 4. No jet-boundary corrections were applied to the lift, pitching-moment, and elevon-hinge-moment coefficients. Rolling- and yawing-moment coefficients measured with the elevon neutral were used as tares in order to make the net rolling- and yawing-moment coefficients equal to zero when the elevon deflection was zero. The complete corrections to the gross data are as follows:

$$C_D = C_{D_{\text{gross}}} + 0.0188C_L^2$$

$$\alpha = \alpha_{\text{tunnel}} + 1.27C_L$$

~~CONFIDENTIAL~~

UNCLASSIFIED

$$C_L = 0.881(C_{L_{\text{gross}}} - C_{L_{\text{tare}}})$$

$$C_n = C_{n_{\text{gross}}} - C_{n_{\text{tare}}} + (-0.0453)C_L C_L$$

Effects of Fixed Transition

The results of tests made with transition fixed on the upper surface of the wing are presented in figures 10 through 14. Although the characteristics of the wing with transition fixed at 15 percent of the chord differed only slightly from those of the wing with natural transition, the differences in the case of the wing with transition fixed at 3 percent of the chord were appreciable. The differences included increased drag coefficients, decreased maximum lift coefficients and lift-curve slopes, reduced pitching-moment-curve slopes, and increased elevon up-floating tendencies. Although the 3-percent transition represented an extreme roughness condition, it appears that results of the present tests, the majority of which were made with natural transition, may be somewhat optimistic.

Effects of Leading-Edge Slot

The results of force tests with the slot open and closed are presented in figures 15, 16, 17, and 18. In general, the effects of the slot on the aerodynamic characteristics were very small. With landing and pitch flaps retracted, an increase of only 0.02 in the maximum lift coefficient was obtained by opening the slot, and longitudinal stability near maximum lift was increased slightly. The small increase in drag coefficient at low values of lift coefficient is a minor consideration inasmuch as the slot on the airplane will probably remain closed at high speeds. For the landing-flap deflected conditions, similarly slight beneficial effects of the slot were shown with the pitch flap neutral but were not apparent with the pitch flap deflected -14.1° and -34.1° .

The results of the stall studies are presented in figures 19, 20, and 21. With the landing and pitch flaps retracted, the stall with slot closed began at the outboard

end of the elevon and progressed inboard and outboard until at maximum lift the outer 75 percent of the wing was stalled. The stall pattern with slot open was practically no different, except that a small stalled region was noted behind the outboard end of the slot at low lift coefficients. Except for stalling on the deflected flap itself, the stall pattern with flaps deflected was quite similar to that with flaps retracted and did not vary appreciably with pitch-flap deflection. As in the case of the retracted flaps, the stalling characteristics with landing flap deflected 43.3° and pitch flap deflected -34.1° were essentially unchanged by the leading-edge slot.

It has been shown in reference 5 that a slot span of approximately 30 to 50 percent of the wing span is needed in order to afford appreciable relief from tip-stalling difficulties on this type of swept-back tailless airplane. The present slot is considerably smaller (about 20 percent) and would therefore not be expected to yield much improvement, although its effectiveness might possibly be increased somewhat by a change in spanwise location. Moreover, the absence of any noticeable flow improvement over the region behind the slot as indicated by the tuft studies suggests the possibility of imperfect aerodynamic design of the slot entry. As shown in reference 6, difficulties of this nature obtained with similar installations have been relieved by modification of the slot entry. In its present configuration, the slot has little effect on elevon hinge moments (figs. 17 and 18).

The effect of pitch-flap deflection on air flow through the leading-edge slot is shown in figures 22 and 23. The air-flow velocity at both the inboard and outboard survey stations decreased with upward pitch-flap deflection, although the variation was greater at the outboard station. The variation in slot exit pressure-recovery coefficient with pitch-flap deflection was small and did not indicate any distinct trend.

Longitudinal Stability and Control

Elevon tab characteristics. - Basic characteristics of the outboard half-span and the full-span elevon tab are presented in figures 24, 25, 26, and 27. As shown

~~CONFIDENTIAL~~

UNCLASSIFIED

by the figures, tab effectiveness is markedly decreased at the higher lift coefficients, particularly in the case of the half-span tab, which is on the outboard portion of the elevon. This would indicate that if a half-span tab were to be used, the inboard tab would be more desirable. It is seen also that tab deflection causes considerable change in pitching moment, especially at high or moderate negative elevon deflections. At $\delta_e = -10^\circ$ with landing and pitch flaps fully deflected, for example, a change of full-span tab setting from 0° to -10° at $C_L = 0.6$ causes as much change in pitching-moment coefficient as approximately -6° or -7° of elevon deflection. The effect of tab deflection on pitching moment is less pronounced, but still appreciable, at higher lift coefficients.

Longitudinal characteristics with elevon tab neutral.— Curves of α , C_m , and C_{h_e} against C_L are shown in figures 28 and 29 for the model with elevon tabs neutral. The pitching-moment curves, plotted for a rather extreme forward center-of-gravity position, do not exhibit the pronounced unstable slopes at high lift coefficients shown in most of the previous test results for this design computed for more rearward center-of-gravity positions.

The results show that with landing flap both retracted and deflected, the hinge-moment coefficients at constant δ_e increase rapidly in a negative direction at angles of attack approaching maximum lift, demonstrating in effect pronounced negative values of the hinge-moment parameter $\partial C_{h_e} / \partial \alpha$ at high lift coefficients. It is shown in reference 2 that this value must be either zero or positive for all angles of attack in the flight range in order to eliminate the control-force reversal encountered in the flight tests of a flying model of the XB-55 airplane made by Northrop Aircraft, Inc.

Inasmuch as a zero or positive value of $\partial C_{h_e} / \partial \alpha$ betokens a stable control-force variation only for a stable variation of elevator angle with airspeed, inspection of these hinge-moment curves alone does not suffice for the determination of an arrangement providing satisfactory control-force characteristics. Curves of elevon deflection and elevon hinge moment for trim through

the speed range are shown in figure 30 for several center-of-gravity locations covering the probable operating range for the airplane.

In the determination of the curves of elevon-deflection and hinge-moment variations with indicated airspeed, the airplane weight was assumed to be 160,000 pounds. Hinge-moment coefficients for trim (zero pitching moment) were shown in preference to control forces because results independent of both mechanical boost and trim-tab adjustment are thereby made possible. For practical purposes, a positive slope of the curve of hinge-moment coefficient against airspeed over any portion of the curve may be considered as indicating an unsatisfactory control-force variation (from trim) at the airspeeds in question. As indicated in figure 30, the variation of control force with airspeed for the airplane with zero elevon-tab deflection is unstable at low speeds.

Longitudinal characteristics with tab-flipper arrangement. Pitching-moment and hinge-moment data are shown in figures 31 through 46 for the tab-flipper arrangements by means of which improvement of the control-force characteristics was attempted. Curves of elevon deflection and elevon hinge moment for trim through the speed range are shown in figures 47 through 53 for several conditions of interest. Although none of the combinations tested showed completely satisfactory characteristics, it may be seen by comparison of figure 30 with figures 47 to 53 that some arrangements of the tab-flipper combination afforded noticeable improvement in the control-force characteristics. A direct linkage between the elevon tab and the flipper ($\delta t_e = \delta_F$) appeared best in this respect, provided the flipper received some boost in the form of flipper tab action. The greatest improvement with this direct linkage was obtained with maximum upward flipper deflection limited to -7.5° and a 1:1 ratio between the flipper and flipper-tab deflections ($\delta t_F = -\delta_F$) as shown in figure 47, or a 2:1 ratio of flipper to flipper-tab deflection ($\delta t_F = -\frac{1}{2}\delta_F$) with no -7.5° limitation to upward flipper deflection, as shown in figure 48. For these two combinations, satisfactory control-force variations are indicated throughout the speed range investigated, except for the -34.1° pitch-flap setting. As shown in figures 39 and 41,

the motion of the flipper-actuated elevon tab in the direction required for improvement of the control force characteristics is considerably reduced when the pitch flap is deflected -34.1° . It is believed that interference between the pitch flap and the flipper causes a change in flipper floating characteristics, but the test data did not permit further analysis of this effect. With the flipper tab held neutral (fig. 49) or with a 1:1 ratio of flipper to flipper tab and no -7.5° upward flipper deflection limitation (fig. 50) the improvement was less noticeable than that shown in figures 47 and 48.

As shown in figure 51, the elevon tab did not provide adequate improvement when linked so as to deflect 1° per 2° flipper movement ($\delta_{te} = \frac{1}{2}\delta_F$) with no flipper tab action. A tab extending over only half of the elevon span was found inadequate with even the direct linkage (figs. 52 and 53). In this respect, the inboard half-span tab appeared slightly more effective than the outboard tab.

Wherever the tab-flipper action caused an improvement in hinge-moment characteristics it also caused a reduction in stick-fixed stability as indicated by the variation of elevon deflection with airspeed. This effect is a result of the large pitching moments introduced by tab deflection and is inherent in the nature of the arrangement. Although an unstable elevon-deflection variation accompanied by a stable control-force variation might not be dangerous (the range of elevon movement involved, assuming a mechanical advantage $d\delta_e/d\delta_s = 0.729$ and a control-column length of 22 inches, corresponds to slightly more than a 5-inch travel at the top of control column), it would nevertheless be undesirable and might constitute a significant objection to the use of the tab-flipper device for improvement of the control force characteristics.

Data are presented in figures 54 to 59 for tests in which the tab was allowed to float freely with no flipper connection. Elevon-deflection and hinge-moment variations with airspeed for these conditions are shown in figures 60 and 61 and indicate that the plain tab did not have sufficiently high up-floating tendencies to cause the desired change in hinge-moment characteristics.

With splines at the trailing edge (to increase the up-floating tendency of the tab) the improvement was marked but not as great as that obtained with the best tab-flipper combinations.

Lateral Control

In order to indicate the possible influence of the free-floating tab-flipper combination on lateral control characteristics, curves of rolling-moment, yawing-moment, and elevon-hinge-moment coefficients against angle of attack are shown for a range of elevon settings in figures 62 through 67. These curves are presented only for the locked elevon tab ($\delta_{t_e} = 0$) and for the direct linkage of elevon tab and flipper tab to flipper ($\delta_{t_e} = \delta_F = -\delta_{t_F}$). The results are therefore not directly applicable to the best tab-flipper combinations.

Although some of the hinge-moment data in these curves are rather erratic, making analysis difficult, some comparison is possible between lateral control characteristics with tab fixed at $\delta_{t_e} = 0$ and with the tab-flipper combination floating freely. Estimated helix angles and control forces are shown in figures 68 and 69. In obtaining these curves, $\delta_e = 0$ was taken as the neutral setting. The actual neutral setting in flight would be that required for longitudinal trim and would vary with center-of-gravity position, power effects, etc. The helix angle was computed as
$$\frac{pb}{2V} = \frac{0.8C_l}{C_{l_p}}$$
 where a value of 0.467 was used for the damping coefficient C_{l_p} . The airplane weight was again considered to be 160,000 pounds and no mechanical boost was assumed. Hinge-moment coefficients were corrected for the effective change in angle of attack over the elevon due to rolling, but the influence of the small additional change in effective angle of attack at the flipper (because of the more outboard location of the flipper relative to the elevon) was neglected. Although it would not be possible to determine the effect of this factor without flipper and tab hinge-moment data, it was assumed that the effect would not be very great, inasmuch as the maximum difference in effective angles of attack for the cases presented in figures 68 and 69 would be approximately 0.4° .

Comparison of figure 68(a) with 69(a) and figure 68(b) with 69(b) shows that this tab-flipper arrangement caused overbalance at small deflections, and a reduction in rolling effectiveness. An explanation for these effects may be seen in the nature of the elevon tab behavior at constant angle of attack. Inasmuch as the elevon tab and the flipper are designed to operate as a unit independent of elevon deflection, the elevon tab tends to trail as the elevon is deflected, thereby acting as a balancing tab. This tab action is shown in figure 43(a) where for the same arrangement and configuration as that of figure 69(b) it may be seen that at $\alpha = 12^\circ$, elevon-tab deflection changes from 0° to 2.3° when the elevon is deflected upward from 0° to -5° .

The effects of this balancing-tab action, which apparently caused the reduction in $pb/2V$ as well as the overbalance, are illustrated more directly by the curves of hinge-moment and rolling-moment coefficients plotted against elevon deflection in figure 70. As shown in this figure, the slope $\partial C_{h_e} / \partial \delta_e$ is positive at small elevon angles with the tab-flipper combination floating freely. Although tendencies toward overbalance would be present with other tab-flipper combinations, actual overbalance might not exist, particularly if the neutral elevon settings were not in the vicinity of $\delta_e = 0^\circ$. The irregularities introduced in the variation of lateral-control force with control-wheel deflection, however, might nevertheless be undesirable.

SUMMARY OF RESULTS

The significant results of the 19-foot pressure-tunnel tests of a 1/7-scale semispan model of the XB-35 airplane may be summarized as follows:

1. The present leading-edge slot did not appear to be adequate to provide substantial relief of stick-fixed instability introduced by early tip stalling on the tapered, swept-back wing. Modification of the slot entry and an increase in slot span appeared desirable.

2. The elevon tab-flipper arrangement used in the model tests appeared capable of providing appreciable

~~CONFIDENTIAL~~

UNCLASSIFIED

improvement in static longitudinal control force characteristics over those with no tab-flipper device. Two of the combinations tested resulted in stable variations of elevon force with airspeed for all conditions except that in which the pitch flap was deflected -34.1° . These combinations were: (a) direct tab-flipper linkage ($\delta_{t_e} = \delta_F$), 1:1 ratio of flipper to flipper tab ($\delta_{t_F} = -\delta_F$) with a -7.5° limit to maximum upward flipper deflection; and (b) direct tab-flipper linkage ($\delta_{t_e} = \delta_F$), 2:1 ratio of flipper to flipper tab ($\delta_{t_F} = -\frac{1}{2}\delta_F$) without the -7.5° upper limit to flipper deflection.

3. When the flipper device was used with a half-span tab, the inboard half-span tab was found to be slightly more effective than the outboard half. Neither, however, produced adequate control-force improvement.

4. The beneficial effects of the tab-flipper device on control force characteristics were accompanied by an undesirable decrease in stick-fixed stability, because of the pitching moments produced by the tab.

5. The use of a plain elevon tab free-floating independently of the flipper did not result in the desired improvement of control force characteristics. Improvement was noted when the tab floating tendency was increased by the installation of trailing-edge "cords," but the device was not as effective as the better tab-flipper combinations.

6. At a given angle of attack, the action of the elevon tab in floating (with the flipper) independently of elevon deflection is similar to that of a balancing tab. This tab action causes a decrease in rolling effectiveness and may also lead to undesirable lateral

~~CONFIDENTIAL~~

UNCLASSIFIED

control force characteristics, possibly causing overbalance in certain conditions.

Langley Memorial Aeronautical Laboratory
National Advisory Committee for Aeronautics
Langley Field, Va.

Jerome Teplitz
Aeronautical Engineer

Gerald G. Kayten
Gerald G. Kayten
Aeronautical Engineer

Patrick A. Cancro
Electrical Engineer

Approved:

Clinton H. Dearborn
Clinton H. Dearborn
Chief of Full-Scale Research Division

ES

~~CONFIDENTIAL~~

REFERENCES

1. Sivells, James C., and Burgess, Jack: Tests in the NACA 19-Foot Pressure Tunnel of a 1/10.75-Scale Model of the Northrop XB-35 Tailless Airplane. NACA MR, Army Air Forces, Feb. 3, 1943.
2. Denaci, H. G., and Anderson, R. A.: Elevon Development for the XB-35 Airplane from Two-Dimensional-Flow Tests. NACA MR, Army Air Forces, Sept. 26, 1944.
3. Swanson, Robert S., and Gillis, Clarence L.: Wind-Tunnel Calibration and Correction Procedures for Three-Dimensional Models. NACA ARR No. L4E31, 1944.
4. Sivells, James C., Deters, Owen J., and Russell, Robert T.: Tests in the NACA 19-Foot Pressure Tunnel of a 4/29-Scale Semispan Model of the Consolidated XB-36 Airplane Wing. NACA MR, Army Air Forces, Oct. 5, 1943.
5. Stability Research Division: An Interim Report on the Stability and Control of Tailless Airplanes. NACA ACR No. L4H19, 1944.
6. Sweberg, Harold H., and Dingeldein, Richard C.: Summary of Measurements in Langley Full-Scale Tunnel of Maximum Lift Coefficients and Stalling Characteristics of Airplanes. NACA ACR No. L5C24, 1945.

~~CONFIDENTIAL~~

UNCLASSIFIED

FIGURE LEGENDS

Figure 1.- $\frac{1}{7}$ -scale semispan model of the XB-35 airplane mounted with a reflection plane in the NACA-Langley 19-foot pressure tunnel.

(a) Front view.

Figure 1.- Concluded.

(b) Rear view.

Figure 2.- Arrangement of the $\frac{1}{7}$ -scale XB-35 semispan model and reflection plane in the 19-foot pressure tunnel.

Figure 3.- Plan and elevation view of $\frac{1}{7}$ -scale XB-35 semispan model.

Figure 4.- Details of landing flap; $\frac{1}{7}$ -scale XB-35 semispan model.

Figure 5.- Details of pitch-control flap and rudder; $\frac{1}{7}$ -scale XB-35 semispan model.

Figure 6.- Details of elevon; $\frac{1}{7}$ -scale XB-35 semispan model.

Figure 7.- Details of flipper; $\frac{1}{7}$ -scale XB-35 semispan model.

Figure 8.- Typical section of leading edge slot. $\frac{1}{7}$ -scale XB-35 semispan model.

Figure 9.- Variation of duct entrance velocity ratio with angle of attack. $\frac{1}{7}$ -scale XB-35 semispan model.

Figure 10.- Effect of transition on aerodynamic characteristics. $\frac{1}{7}$ -scale XB-35 semispan model; $\delta_{f_l} = 0^\circ$; $\delta_{f_p} = 0^\circ$; slot closed; $\delta_e = 0^\circ$; $\delta_{t_e} = 0^\circ$; flipper locked; $R \approx 7,500,000$; $M \approx 0.12$.

FIGURE LEGENDS - Continued

Figure 11.- Effect of transition on aerodynamic characteristics. 1/7-scale XB-35 semispan model; $\delta_{f_l} = 0^\circ$; $\delta_{f_p} = 0^\circ$; slot open; $\delta_{t_e} = 0^\circ$; flipper locked; $R \approx 7,500,000$; $M \approx 0.12$.

(a) $\delta_e = 0^\circ$.

Figure 11.- Concluded.

(b) $\delta_e = -10^\circ$.

Figure 12.- Effect of transition on aerodynamic characteristics. 1/7-scale XB-35 semispan model; $\delta_{f_l} = 43.3^\circ$; $\delta_{f_p} = -34.1^\circ$; $\delta_{t_e} = 0^\circ$; flipper locked; slot closed; $R \approx 7,500,000$; $M \approx 0.12$.

(a) $\delta_e = 0^\circ$.

Figure 12.- Concluded.

(b) $\delta_e = -10^\circ$.

Figure 13.- Effect of transition on aerodynamic characteristics. 1/7-scale XB-35 semispan model; $\delta_{f_l} = 43.3^\circ$; $\delta_{f_p} = -34.1^\circ$; slot open; $\delta_{t_e} = 0^\circ$; flipper locked; $R \approx 7,500,000$; $M \approx 0.12$.

(a) $\delta_e = 0^\circ$.

Figure 13.- Concluded.

(b) $\delta_e = -10^\circ$.

Figure 14.- Effect of transition on aerodynamic characteristics. 1/7-scale XB-35 semispan model; $\delta_{f_l} = 43.3^\circ$; slot open; $\delta_e = 0^\circ$; $\delta_{t_e} = 0^\circ$; flipper locked; $R \approx 7,500,000$; $M \approx 0.12$.

(a) $\delta_{f_p} = 0^\circ$.

FIGURE LEGENDS - Continued

Figure 14.- Concluded.

$$(b) \delta_{fp} = -14.1^\circ.$$

Figure 15.- Effect of slot on aerodynamic characteristics; 1/7-scale XB-35 semispan model. $\delta_{f_l} = 0^\circ$; $\delta_{fp} = 0^\circ$; $\delta_e = 0^\circ$; $\delta_{t_{ei}} = 0^\circ$; $\delta_{t_{eo}} = 0^\circ$; flipper locked; $R \approx 7,500,000$; $M \approx 0.12$.

Figure 16.- Effect of slot on aerodynamic characteristics; 1/7-scale XB-35 semispan model. $\delta_{f_l} = 43.3^\circ$; $\delta_e = 0^\circ$; $\delta_{t_{ei}} = 0^\circ$; $\delta_{t_{eo}} = 0^\circ$; flipper locked; $R \approx 7,500,000$; $M \approx 0.12$.

Figure 17.- Effect of slot on aerodynamic characteristics; 1/7-scale XB-35 semispan model. $\delta_{f_l} = 0^\circ$; $\delta_{fp} = 0^\circ$; $\delta_e = 0^\circ$; $\delta_{t_{ei}} = 0^\circ$; $\delta_{t_{eo}} = 0^\circ$; flipper free-floating; $R \approx 7,500,000$; $M \approx 0.12$.

Figure 18.- Effect of slot on aerodynamic characteristics; 1/7-scale XB-35 semispan model. $\delta_{f_l} = 43.3^\circ$; $\delta_{fp} = -34.1^\circ$; $\delta_{t_{ei}} = 0^\circ$; $\delta_{t_{eo}} = -15^\circ$; flipper free-floating; $R \approx 7,500,000$; $M \approx 0.12$.

Figure 19.- Stall diagrams of the 1/7-scale semispan model of the XB-35 airplane. $\delta_{f_l} = 0^\circ$; $\delta_e = \delta_F = \delta_{t_e} = 0^\circ$, $\delta_{fp} = 0^\circ$, $R \approx 7,500,000$, $M \approx 0.12$.

Figure 20.- Stall diagrams of the 1/7-scale semispan model of the XB-35 airplane. $\delta_{f_l} = 43.3^\circ$, $\delta_{fp} = -34.1^\circ$, $\delta_e = \delta_F = \delta_{t_e} = 0^\circ$, $R \approx 7,500,000$, $M \approx 0.12$.

Figure 21.- Stall diagrams of the 1/7-scale semispan model of the XB-35 airplane. $\delta_{f_l} = 43.3^\circ$, $\delta_e = \delta_F = \delta_{t_e} = 0^\circ$, slot closed. $R \approx 7,500,000$, $M \approx 0.12$.

Figure 22.- Leading-edge slot exit-velocity ratios. 1/7-scale XB-35 semispan model; $\delta_e = \delta_{t_{ei}} = \delta_{t_{eo}} = 0^\circ$; flipper locked; $R \approx 7,500,000$; $M \approx 0.12$.

~~CONFIDENTIAL~~

UNCLASSIFIED

FIGURE LEGENDS - Continued

Figure 23.- Leading-edge slot exit pressure-recovery coefficients. 1/7-scale XB-35 semispan model; $\delta_e = \delta_{t_{ei}} = \delta_{t_{eo}} = 0^\circ$; flipper locked; $R \approx 7,500,000$; $M \approx 0.12$.

Figure 24.- Full-span elevon-tab effectiveness. 1/7-scale XB-35 semispan model; $\delta_{f_l} = 0^\circ$; $\delta_{f_p} = 0^\circ$; slot closed; flipper free-floating; $R \approx 7,500,000$; $M \approx 0.12$.

$$(a) \delta_e = 0^\circ.$$

Figure 24.- Continued.

$$(b) \delta_e = -5^\circ.$$

Figure 24.- Continued.

$$(c) \delta_e = -10^\circ.$$

Figure 24.- Concluded.

$$(d) \delta_e = -15^\circ.$$

Figure 25.- Full-span elevon-tab effectiveness. 1/7-scale XB-35 semispan model; $\delta_{f_l} = 43.3^\circ$; $\delta_{f_p} = -34.1^\circ$; slot closed; flipper free-floating; $R \approx 7,500,000$; $M \approx 0.12$.

$$(a) \delta_e = 0^\circ.$$

Figure 25.- Continued.

$$(b) \delta_e = -5^\circ.$$

Figure 25.- Continued.

$$(c) \delta_e = -10^\circ.$$

Figure 25.- Concluded.

$$(d) \delta_e = -15^\circ.$$

FIGURE LEGENDS - Continued

Figure 26.- Half-span elevon-tab effectiveness. 1/7-scale XB-35 semispan model; $\delta_{f_l} = 0^\circ$; $\delta_{f_p} = 0^\circ$; slot closed; $\delta_{t_{ei}} = 0^\circ$; flipper free-floating; $R \approx 7,500,000$; $M \approx 0.12$.

(a) $\delta_e = 0^\circ$.

Figure 26.- Continued.

(b) $\delta_e = -5^\circ$.

Figure 26.- Continued.

(c) $\delta_e = -10^\circ$.

Figure 26.- Concluded.

(d) $\delta_e = -15^\circ$.

Figure 27.- Half-span elevon-tab effectiveness. 1/7-scale XB-35 semispan model; $\delta_{f_l} = 43.3^\circ$; $\delta_{f_p} = -34.1^\circ$; slot open; $\delta_{t_{ei}} = 0^\circ$; flipper free floating; $R \approx 7,500,000$; $M \approx 0.12$.

(a) $\delta_e = 0^\circ$.

Figure 27.- Continued.

(b) $\delta_e = -5^\circ$.

Figure 27.- Continued.

(c) $\delta_e = -10^\circ$.

Figure 27.- Concluded.

(d) $\delta_e = -15^\circ$.

Figure 28.- Effect of elevon deflection on aerodynamic characteristics. 1/7-scale XB-35 semispan model; $\delta_{f_l} = 0^\circ$; $\delta_{f_p} = 0^\circ$; slot closed; $\delta_{t_e} = 0^\circ$; flipper free-floating; $\delta_{t_F} = -\delta_F$; $R \approx 7,500,000$; $M \approx 0.12$.

FIGURE LEGENDS - Continued

Figure 29.- Effect of elevon deflection on aerodynamic characteristics. 1/7-scale XB-35 semispan model; $\delta_{f_l} = 43.3^\circ$; $\delta_{f_p} = -34.1^\circ$; slot open; $\delta_{t_e} = 0^\circ$; flipper free-floating; $\delta_{t_F} = -\delta_F$; $R \approx 7,500,000$; $M \approx 0.12$.

Figure 30.- Variation of elevon deflection and hinge-moment with speed. XB-35 airplane, $\delta_{t_e} = 0^\circ$; $\delta_{t_F} = -\delta_F$; flipper free floating.

Figure 31.- Effects of free-floating outboard half-span elevon tab and flipper combination. 1/7-scale XB-35 semispan model; $\delta_{f_l} = 0^\circ$; $\delta_{f_p} = 0^\circ$; slot closed; $\delta_{t_{e0}} = \delta_F$; $\delta_{t_F} = -\delta_F$; $\delta_{t_{ei}} = 0^\circ$; $R \approx 7,500,000$; $M \approx 0.12$.

Figure 32.- Effects of free-floating outboard half-span elevon tab and flipper combination. 1/7-scale XB-35 semispan model; $\delta_{f_l} = 43.3^\circ$; $\delta_{f_p} = -34.1^\circ$; slot closed; $\delta_{t_{ei}} = 0^\circ$; $\delta_{t_{e0}} = \delta_F$; $\delta_{t_F} = -\delta_F$; $R \approx 7,500,000$; $M \approx 0.12$.

Figure 33.- Effects of free-floating inboard half-span elevon tab and flipper combination. 1/7-scale XB-35 semispan model; $\delta_{f_l} = 0^\circ$; $\delta_{f_p} = 0^\circ$; slot closed; $\delta_{t_{e0}} = 0^\circ$; $\delta_{t_{ei}} = \delta_F$; $\delta_{t_F} = -\delta_F$; $R \approx 7,500,000$; $M \approx 0.12$.

Figure 34.- Effects of free-floating inboard half-span elevon tab and flipper combination. 1/7-scale XB-35 semispan model; $\delta_{f_l} = 43.3^\circ$; slot open; $\delta_{t_{e0}} = 0^\circ$; $\delta_{t_{ei}} = \delta_F$; $\delta_{t_F} = -\delta_F$; $R \approx 7,500,000$; $M \approx 0.12$.

$$(a) \delta_{f_p} = -34.1^\circ.$$

Figure 34.- Continued.

$$(b) \delta_{f_p} = -14.1^\circ.$$

Figure 34.- Concluded.

$$(c) \delta_{f_p} = 0^\circ.$$

FIGURE LEGENDS - Continued

Figure 35.- Effects of free-floating full-span elevon tab and flipper combination. 1/7-scale XB-35 semispan model; $\delta_{f_l} = 0^\circ$; $\delta_{f_p} = 0^\circ$; slot closed; $\delta_{t_e} = \delta_F$; $\delta_{t_F} = 0^\circ$; $R \approx 7,500,000$; $M \approx 0.12$.

Figure 36.- Effects of free-floating full-span elevon tab and flipper combination. 1/7-scale XB-35 semispan model; $\delta_{f_l} = 43.3^\circ$; slot open; $\delta_{t_e} = \delta_F$; $\delta_{t_F} = 0^\circ$; $R \approx 7,500,000$; $M \approx 0.12$.

$$(a) \delta_{f_p} = -34.1^\circ.$$

Figure 36.- Continued.

$$(b) \delta_{f_p} = -14.1^\circ.$$

Figure 36.- Concluded.

$$(c) \delta_{f_p} = 0^\circ.$$

Figure 37.- Effects of free-floating full-span elevon tab and flipper combination. 1/7-scale XB-35 semispan model; $\delta_{f_l} = 0^\circ$; $\delta_{f_p} = 0^\circ$; slot closed; $\delta_{t_e} = 1/2\delta_F$; $\delta_{t_F} = 0^\circ$; $R \approx 7,500,000$; $M \approx 0.12$.

Figure 38.- Effects of free-floating full-span elevon tab and flipper combination. 1/7-scale XB-35 semispan model; $\delta_{f_l} = 43.3^\circ$; slot open; $\delta_{t_e} = 1/2\delta_F$; $\delta_{t_F} = 0^\circ$; $R \approx 7,500,000$; $M \approx 0.12$.

$$(a) \delta_{f_p} = -34.1^\circ.$$

Figure 38.- Continued.

$$(b) \delta_{f_p} = -14.1^\circ.$$

Figure 38.- Concluded.

$$(c) \delta_{f_p} = 0^\circ.$$

FIGURE LEGENDS - Continued

Figure 39.- Effects of free-floating full-span elevon tab and flipper combination. 1/7-scale XB-35 semispan model; $\delta_{f_l} = 0^\circ$; $\delta_{f_p} = 0^\circ$; slot closed; $\delta_{t_e} = \delta_F$; $\delta_{t_F} = -1/2\delta_F$; $R \approx 7,500,000$; $M \approx 0.12$.

Figure 40.- Effects of free-floating full-span elevon tab and flipper combination. 1/7-scale XB-35 semispan model. $\delta_{f_l} = 43.3^\circ$; slot open; $\delta_{t_e} = \delta_F$; $\delta_{t_F} = -1/2\delta_F$; $R \approx 7,500,000$; $M \approx 0.12$.

$$(a) \delta_{f_p} = -34.1^\circ.$$

Figure 40.- Continued.

$$(b) \delta_{f_p} = -14.1^\circ.$$

Figure 40.- Concluded.

$$(c) \delta_{f_p} = 0^\circ.$$

Figure 41.- Effect of free-floating elevon tab and flipper combination with flipper up deflection limited to -7.5° . 1/7-scale XB-35 semispan model; $\delta_{f_l} = 0^\circ$; $\delta_{f_p} = 0^\circ$; slot closed; $\delta_{t_e} = \delta_F$; $\delta_{t_F} = -\delta_F$; $R \approx 7,500,000$; $M \approx 0.12$.

Figure 42.- Effect of free-floating elevon tab and flipper combination with flipper up deflection limited to -7.5° . 1/7-scale XB-35 semispan model; $\delta_{f_l} = 43.3^\circ$; slot open; $\delta_{t_e} = \delta_F$; $\delta_{t_F} = -\delta_F$; $R \approx 7,500,000$; $M \approx 0.12$.

$$(a) \delta_{f_p} = -34.1^\circ.$$

Figure 42.- Continued.

$$(b) \delta_{f_p} = -14.1^\circ.$$

Figure 42.- Concluded.

$$(c) \delta_{f_p} = 0^\circ.$$

FIGURE LEGENDS - Continued

Figure 43.- Effect of elevon deflection on aerodynamic characteristics. 1/7-scale XB-35 semispan model; $\delta_{f_l} = 0^\circ$; $\delta_{f_p} = 0^\circ$; slot closed; $\delta_{t_e} = \delta_F$; $\delta_{t_F} = -\delta_F$; $R \approx 7,500,000$; $M \approx 0.12$.

Figure 44.- Effects of free-floating full span elevon tab and flipper combination. 1/7-scale XB-35 semispan model; $\delta_{f_l} = 43.3^\circ$; slot open; $\delta_{t_e} = \delta_F$; $\delta_{t_F} = -\delta_F$; $R \approx 7,500,000$; $M \approx 0.12$.

$$(a) \delta_{f_p} = -34.1^\circ.$$

Figure 44.- Continued.

$$(b) \delta_{f_p} = -14.1^\circ.$$

Figure 44.- Concluded.

$$(c) \delta_{f_p} = 0^\circ.$$

Figure 45.- Effects of split rudder on floating characteristics of free-floating elevon tab and flipper combination. 1/7-scale XB-35 semispan model; $\delta_{f_l} = 0^\circ$; $\delta_{f_p} = 0^\circ$; slot closed; $\delta_{t_e} = \delta_F$; $\delta_{t_F} = -\delta_F$; $R \approx 7,500,000$; $M \approx 0.12$.

Figure 46.- Effects of split rudder on floating characteristics of free-floating elevon tab and flipper combination. 1/7-scale XB-35 semispan model; $\delta_{f_l} = 43.3^\circ$; slot open; $\delta_{t_e} = \delta_F$; $\delta_{t_F} = -\delta_F$; $R \approx 7,500,000$; $M \approx 0.12$.

$$(a) \delta_{f_p} = -34.1^\circ.$$

Figure 46.- Continued.

$$(b) \delta_{f_p} = -14.1^\circ.$$

Figure 46.- Concluded.

$$(c) \delta_{f_p} = 0^\circ.$$

~~CONFIDENTIAL~~

UNCLASSIFIED

FIGURE LEGENDS - Continued

Figure 47.- Variation of elevon deflection and hinge-moment with speed. XB-35 airplane, $\delta_{t_e} = \delta_F$; $\delta_{t_F} = -\delta_F$; Flipper and elevon tab combination free floating; Maximum negative $\delta_F = -7.5^\circ$.

Figure 48.- Variation of elevon deflection and hinge-moment with speed. XB-35 airplane, $\delta_{t_e} = \delta_F$; $\delta_{t_F} = -1/2\delta_F$; flipper and elevon tab combination free floating.

Figure 49.- Variation of elevon deflection and hinge-moment with speed. XB-35 airplane, $\delta_{t_e} = \delta_F$; $\delta_{t_F} = 0^\circ$; flipper and elevon tab combination free floating.

Figure 50.- Variation of elevon deflection and hinge-moment with speed. XB-35 airplane, $\delta_{t_e} = \delta_F$; $\delta_{t_F} = -\delta_F$; flipper and elevon tab combination free floating.

Figure 51.- Variation of elevon deflection and hinge-moment with speed. XB-35 airplane, $\delta_{t_e} = 1/2\delta_F$; $\delta_{t_F} = 0^\circ$; flipper and elevon tab combination free floating.

Figure 52.- Variation of elevon deflection and hinge-moment with speed. XB-35 airplane, $\delta_{t_{e0}} = \delta_F$; $\delta_{t_{e1}} = 0^\circ$; $\delta_{t_F} = -\delta_F$; flipper and outboard elevon tab combination free floating.

Figure 53.- Variation of elevon deflection and hinge-moment with speed. XB-35 airplane, $\delta_{t_{e0}} = 0^\circ$; $\delta_{t_{e1}} = \delta_F$; $\delta_{t_F} = -\delta_F$; flipper and inboard elevon tab combination free floating.

Figure 54.- Effects of free-floating inboard half-span elevon tab. 1/7-scale XB-35 semispan model; $\delta_{f_l} = 0^\circ$; $\delta_{f_p} = 0^\circ$; slot closed; $\delta_{t_{e0}} = 0^\circ$; flipper free floating; $\delta_{t_F} = -\delta_F$; $R \approx 7,500,000$; $M \approx 0.12$.

FIGURE LEGENDS - Continued

Figure 55.- Effects of free-floating inboard half-span elevon tab. 1/7-scale XB-35 semispan model; $\delta_{f_l} = 43.3^\circ$; slot open; $\delta_{t_{e_0}} = 0^\circ$; flipper free floating; $\delta_{t_F} = -\delta_F$; $R \approx 7,500,000$; $M \approx 0.12$.

$$(a) \delta_{f_p} = -34.1^\circ.$$

Figure 55.- Continued.

$$(b) \delta_{f_p} = -14.1^\circ.$$

Figure 55.- Concluded.

$$(c) \delta_{f_p} = 0^\circ.$$

Figure 56.- Effects of free-floating full-span elevon tab. 1/7-scale XB-35 semispan model; $\delta_{f_l} = 0^\circ$; $\delta_{f_p} = 0^\circ$; slot closed; flipper free floating; $\delta_{t_F} = -\delta_F$; $R \approx 7,500,000$; $M \approx 0.12$.

Figure 57.- Effects of free-floating full-span elevon tab. 1/7-scale XB-35 semispan model; $\delta_{f_l} = 43.3^\circ$; slot open; flipper free floating; $\delta_{t_F} = -\delta_F$; $R \approx 7,500,000$; $M \approx 0.12$.

$$(a) \delta_{f_p} = -34.1^\circ.$$

Figure 57.- Continued.

$$(b) \delta_{f_p} = -14.1^\circ.$$

Figure 57.- Concluded.

$$(c) \delta_{f_p} = 0^\circ.$$

Figure 58.- Effects of free-floating full-span elevon tab with splines. 1/7-scale XB-35 semispan model; $\delta_{f_l} = 0^\circ$; $\delta_{f_p} = 0^\circ$; slot closed; flipper free floating; $\delta_{t_F} = -\delta_F$; $R \approx 7,500,000$; $M \approx 0.12$.

FIGURE LEGENDS - Continued

Figure 59.- Effects of free-floating full-span elevon tab with splines. 1/7-scale XB-35 semispan model; $\delta_{f_l} = 43.3^\circ$; slot open; flipper free floating; $\delta_{t_F} = -\delta_F$; $R \approx 7,500,000$; $M \approx 0.12$.

$$(a) \delta_{f_p} = -34.1^\circ.$$

Figure 59.- Continued.

$$(b) \delta_{f_p} = -14.1^\circ.$$

Figure 59.- Concluded.

$$(c) \delta_{f_p} = 0^\circ.$$

Figure 60.- Variation of elevon deflection and hinge-moment with speed. XB-35 airplane, $\delta_{t_F} = -\delta_F$; flipper and elevon tab (without splines) free floating separately.

Figure 61.- Variation of elevon deflection and hinge-moment with speed. XB-35 airplane, $\delta_{t_F} = -\delta_F$; flipper and elevon tab (with splines) free floating separately.

Figure 62.- Aileron characteristics with elevon tabs locked. 1/7-scale XB-35 semispan model; $\delta_{f_l} = 0^\circ$; $\delta_{f_p} = 0^\circ$; slot closed; flipper free floating; $\delta_{t_F} = -\delta_F$; $R \approx 7,500,000$; $M \approx 0.12$.

Figure 63.- Aileron characteristics with elevon tabs locked. 1/7-scale XB-35 semispan model; $\delta_{f_l} = 43.3^\circ$; $\delta_{f_p} = -34.1^\circ$; slot open; flipper free floating; $\delta_{t_F} = -\delta_F$; $R \approx 7,500,000$; $M \approx 0.12$.

Figure 64.- Aileron characteristics with a free-floating elevon tab and flipper combination. 1/7-scale XB-35 semispan model; $\delta_{f_l} = 0^\circ$; $\delta_{f_p} = 0^\circ$; slot closed; $\delta_{t_e} = \delta_F$; $\delta_{t_F} = -\delta_F$; $R \approx 7,500,000$; $M \approx 0.12$.

FIGURE LEGENDS - Concluded

Figure 65.- Aileron characteristics with a free-floating elevon tab and flipper combination. 1/7-scale XB-35 semispan model; $\delta_{f_l} = 43.3^\circ$; $\delta_{f_p} = -34.1^\circ$; slot open; $\delta_{t_e} = \delta_F$; $\delta_{t_F} = -\delta_F$; $R \approx 7,500,000$; $M \approx 0.12$.

Figure 66.- Aileron characteristics with a free-floating elevon tab and flipper combination. 1/7-scale XB-35 semispan model; $\delta_{f_l} = 43.3^\circ$; $\delta_{f_p} = -14.1^\circ$; slot open; $\delta_{t_e} = \delta_F$; $\delta_{t_F} = -\delta_F$; $R \approx 7,500,000$; $M \approx 0.12$.

Figure 67.- Aileron characteristics with a free-floating elevon tab and flipper combination. 1/7-scale XB-35 semispan model; $\delta_{f_l} = 43.3^\circ$; $\delta_{f_p} = 0^\circ$; slot open; $\delta_{t_e} = \delta_F$; $\delta_{t_F} = -\delta_F$; $R \approx 7,500,000$; $M \approx 0.12$.

Figure 68.- Variation of estimated helix angle and lateral control force with control-wheel deflection. XB-35 airplane with free-floating flipper. $\delta_{t_e} = 0^\circ$; $\delta_{t_F} = -\delta_F$.

(a) $\delta_{f_l} = 0^\circ$; $\delta_{f_p} = 0^\circ$; slot closed.

Figure 68.- Concluded.

(b) $\delta_{f_l} = 43.3^\circ$; $\delta_{f_p} = -34.1^\circ$; slot open.

Figure 69.- Variation of estimated helix angle and lateral control force with control-wheel deflection XB-35 airplane with free-floating elevon tab and flipper combination. $\delta_{t_e} = \delta_F$; $\delta_{t_F} = -\delta_F$.

(a) $\delta_{f_l} = 0^\circ$; $\delta_{f_p} = 0^\circ$; slot closed.

Figure 69.- Concluded.

(b) $\delta_{f_l} = 43.3^\circ$; $\delta_{f_p} = -34.1^\circ$; slot open.

Figure 70.- Effects of free floating elevon tab and flipper combination on lateral control characteristics. 1/7-scale XB-35 semispan model. $\delta_{f_l} = 43.3^\circ$; $\delta_{f_p} = -34.1^\circ$; $\alpha = 12^\circ$; flipper free floating; $\delta_{t_F} = -\delta_F$.

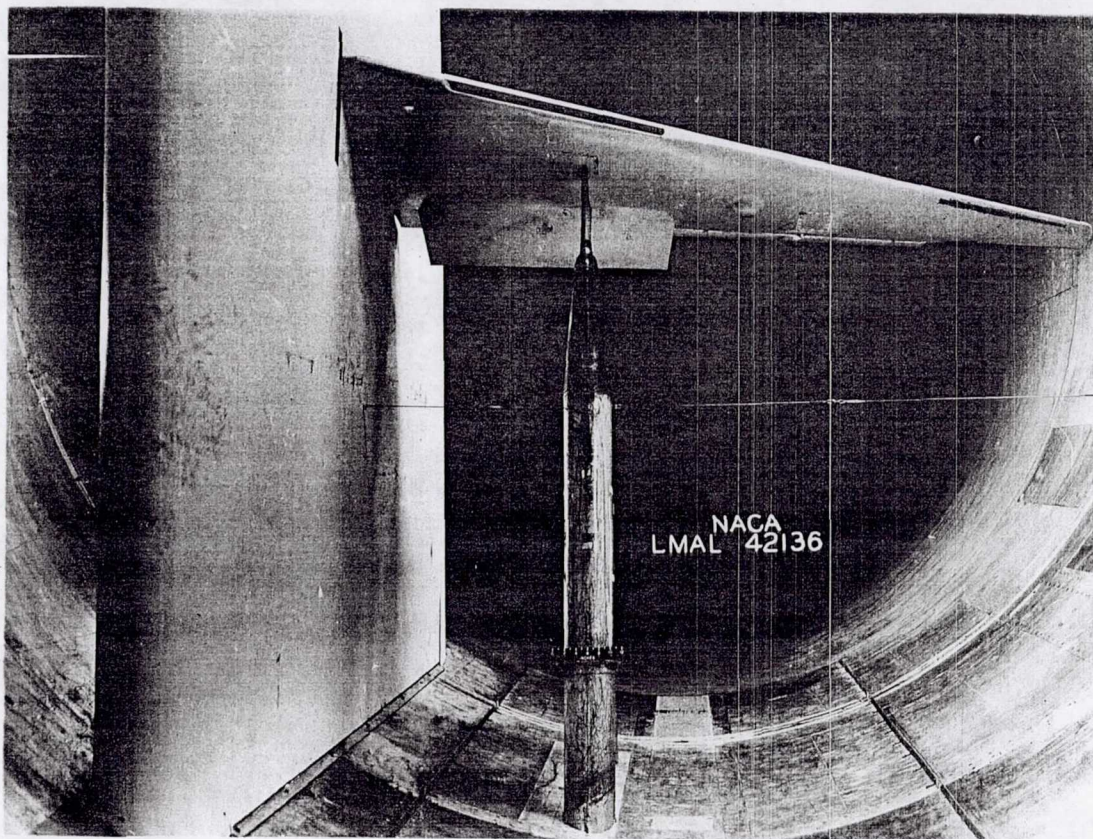
~~CONFIDENTIAL~~

UNCLASSIFIED

1845

UNCLASSIFIED

~~CONFIDENTIAL~~



(a) Front view.

Figure 1.- $\frac{1}{7}$ -scale semispan model of the XB-35 airplane mounted with a reflection plane in the NACA-Langley 19-foot pressure tunnel.

MR No. L5L27

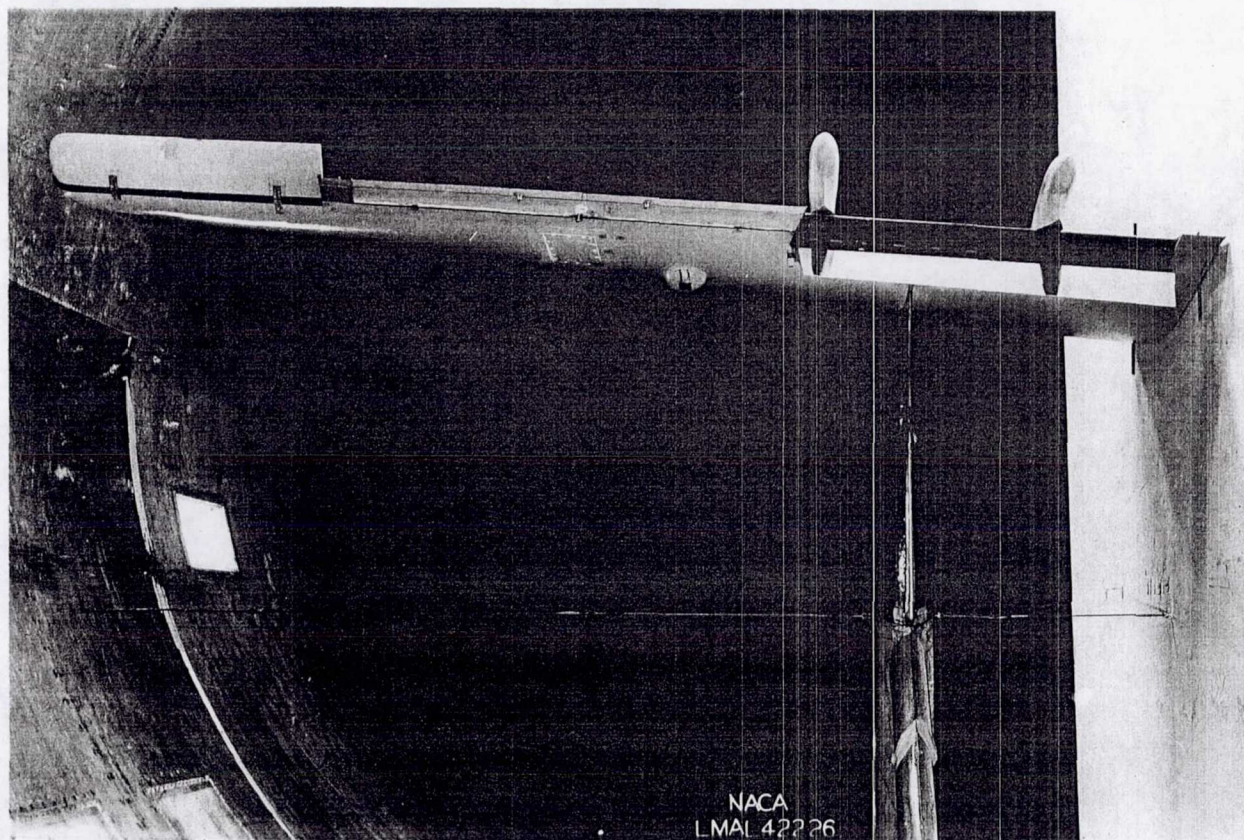
~~CONFIDENTIAL~~

UNCLASSIFIED

NATIONAL ADVISORY COMMITTEE FOR AERONAUTICS
LANGLEY MEMORIAL AERONAUTICAL LABORATORY - LANGLEY FIELD, VA.

1945

UNCLASSIFIED
~~CONFIDENTIAL~~



~~CONFIDENTIAL~~
UNCLASSIFIED

(b) Rear view.

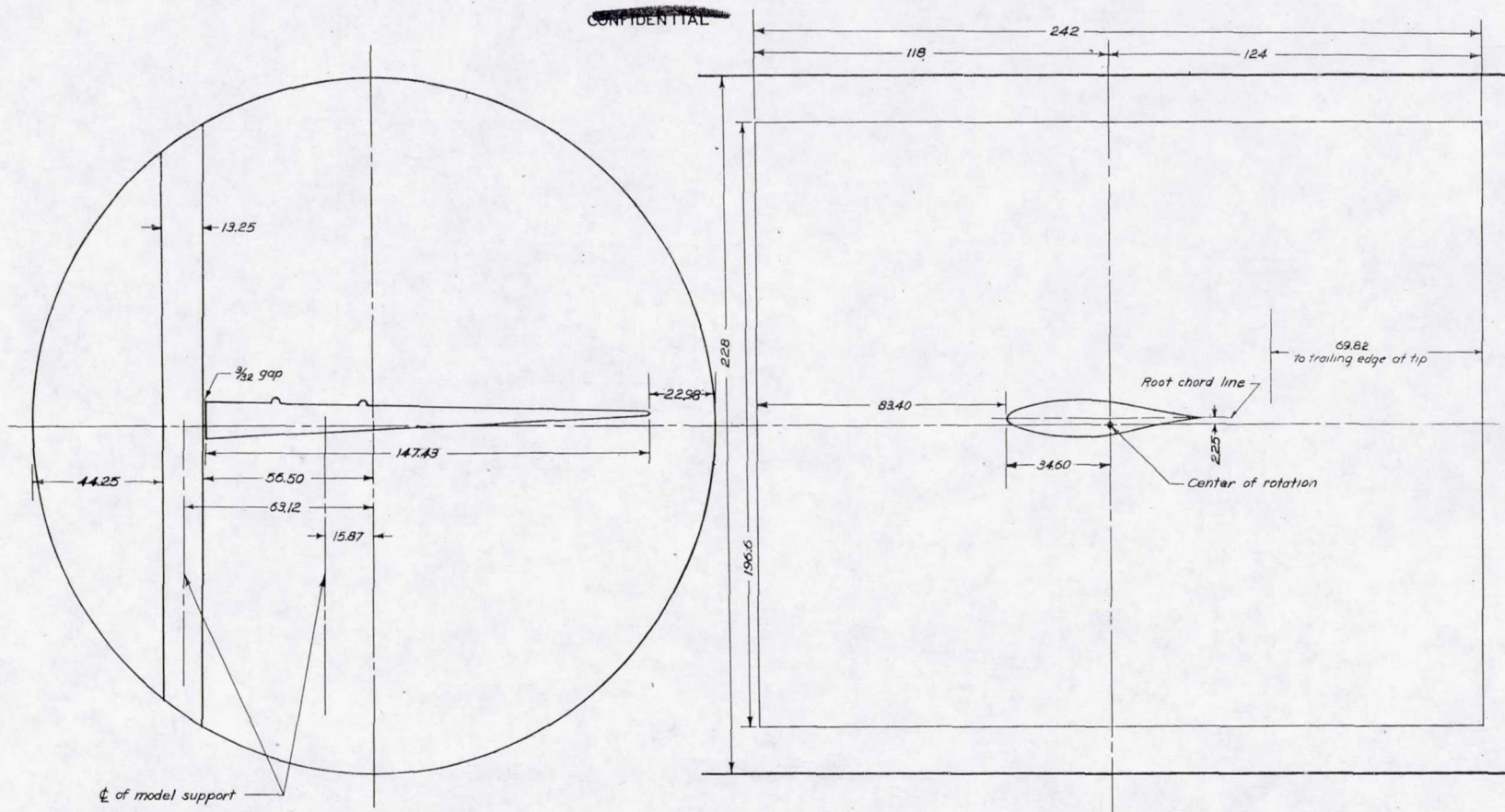
Figure 1.- Concluded.

NATIONAL ADVISORY COMMITTEE FOR AERONAUTICS
LANGLEY MEMORIAL AERONAUTICAL LABORATORY - LANGLEY FIELD, VA.

MR No. L5L27

UNCLASSIFIED

~~CONFIDENTIAL~~



All dimensions in inches

NATIONAL ADVISORY
COMMITTEE FOR AERONAUTICS

~~CONFIDENTIAL~~

Figure 2.- Arrangement of the 1/7-scale XB-35 semispan model and reflection plane in the 19-foot pressure tunnel.

UNCLASSIFIED

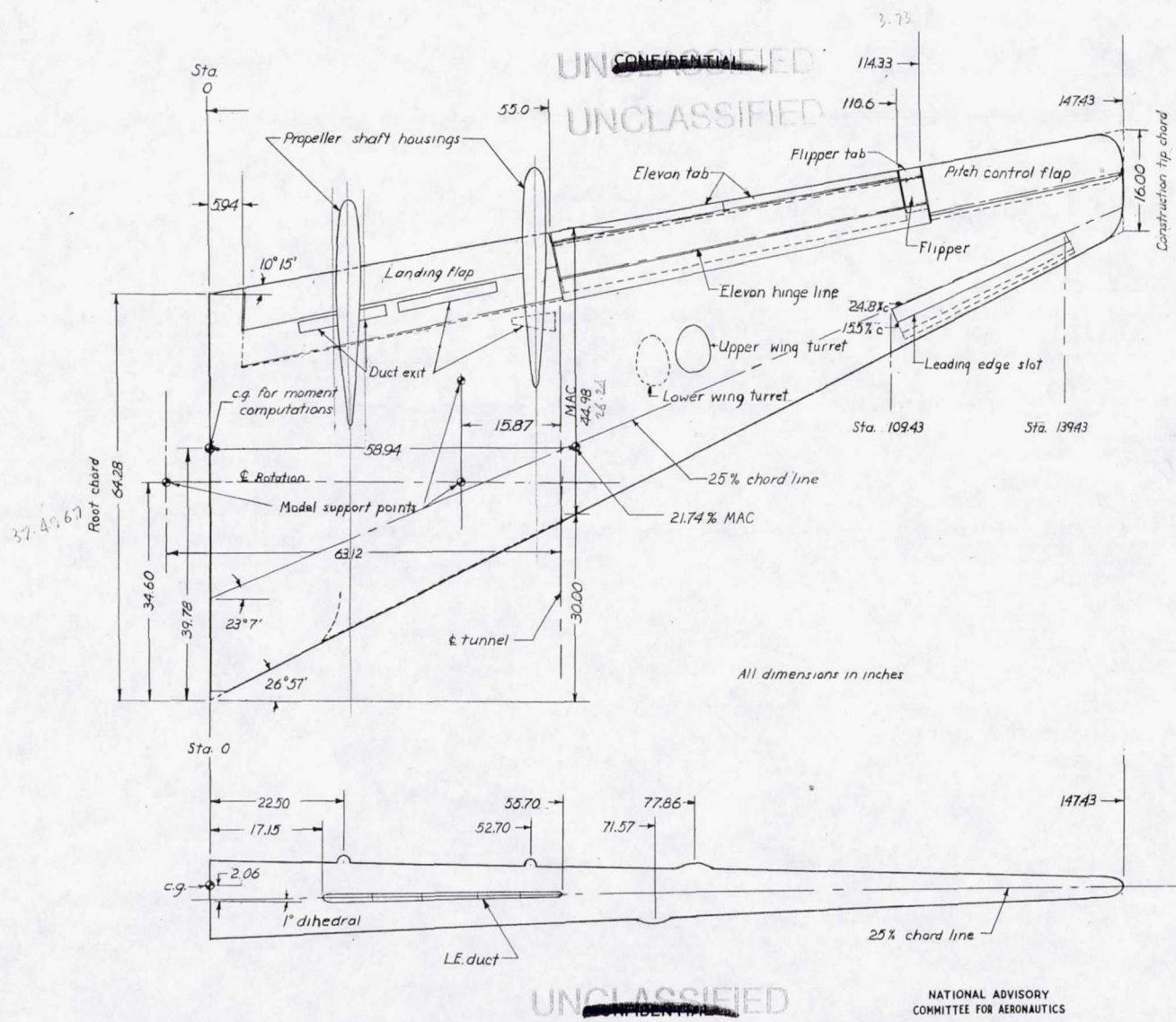
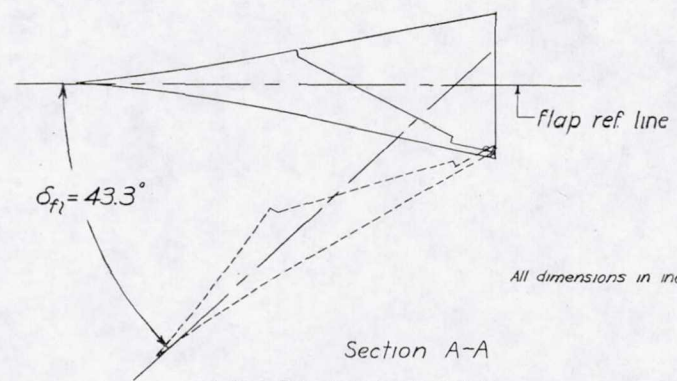
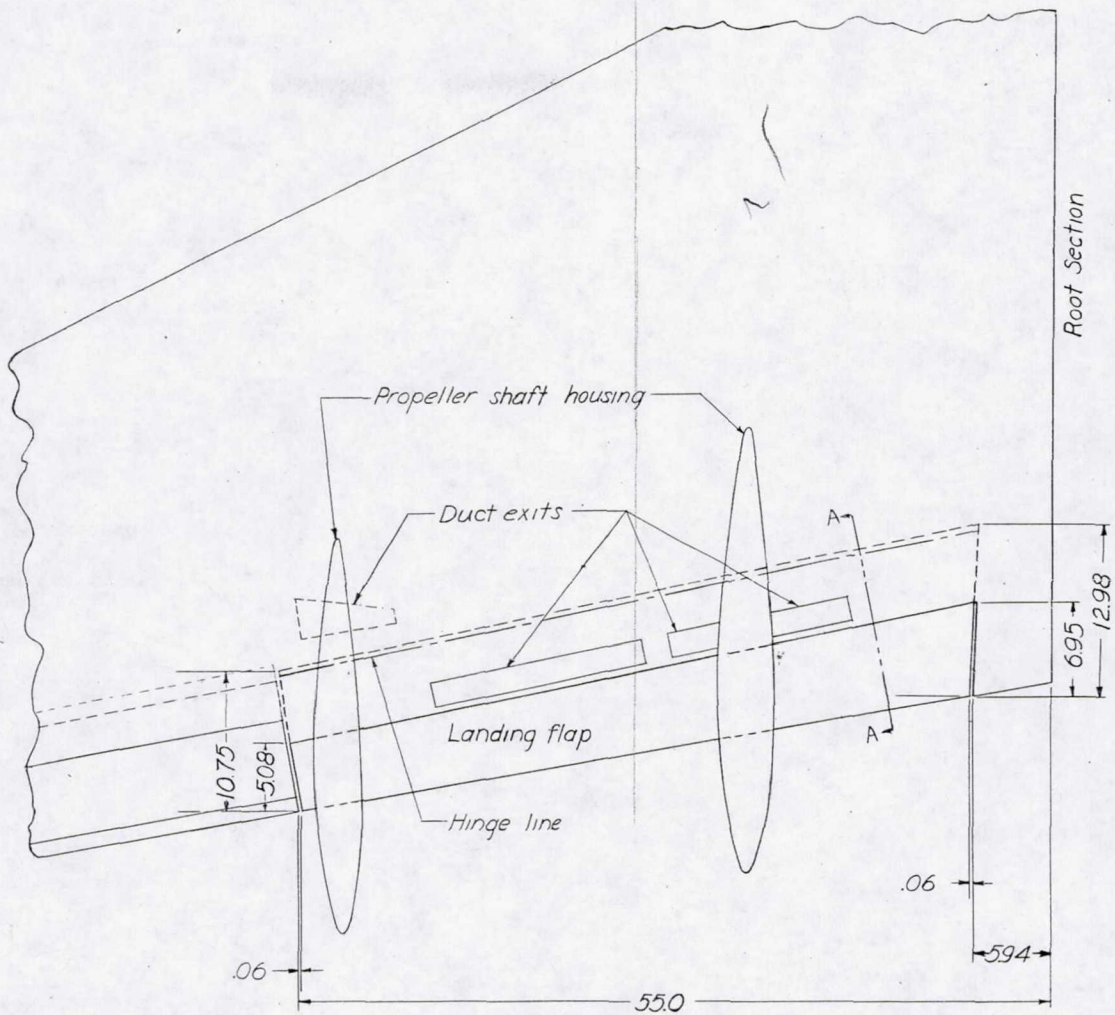


Figure 3.- Plan and elevation view of 1/4-scale XB-35 semispan model.

MR No. 15127

UNCLASSIFIED

~~CONFIDENTIAL~~



All dimensions in inches

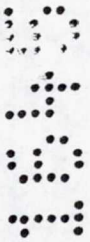
Section A-A

UNCLASSIFIED

NATIONAL ADVISORY COMMITTEE FOR AERONAUTICS

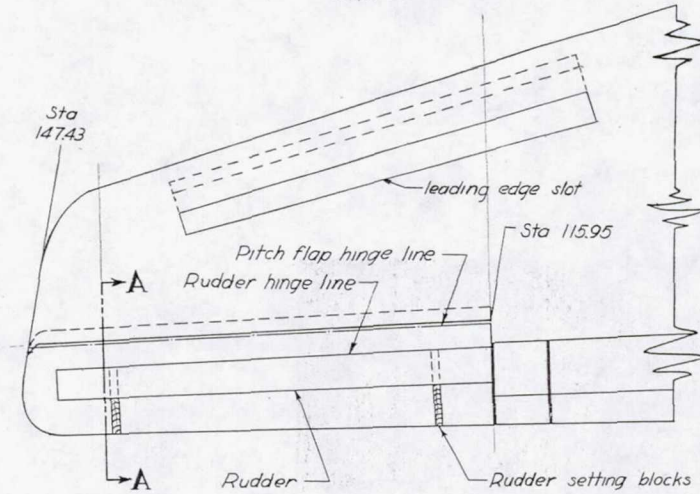
~~CONFIDENTIAL~~

Figure 4.-Details of landing flap. 1/2-scale XB-35 semispan model.



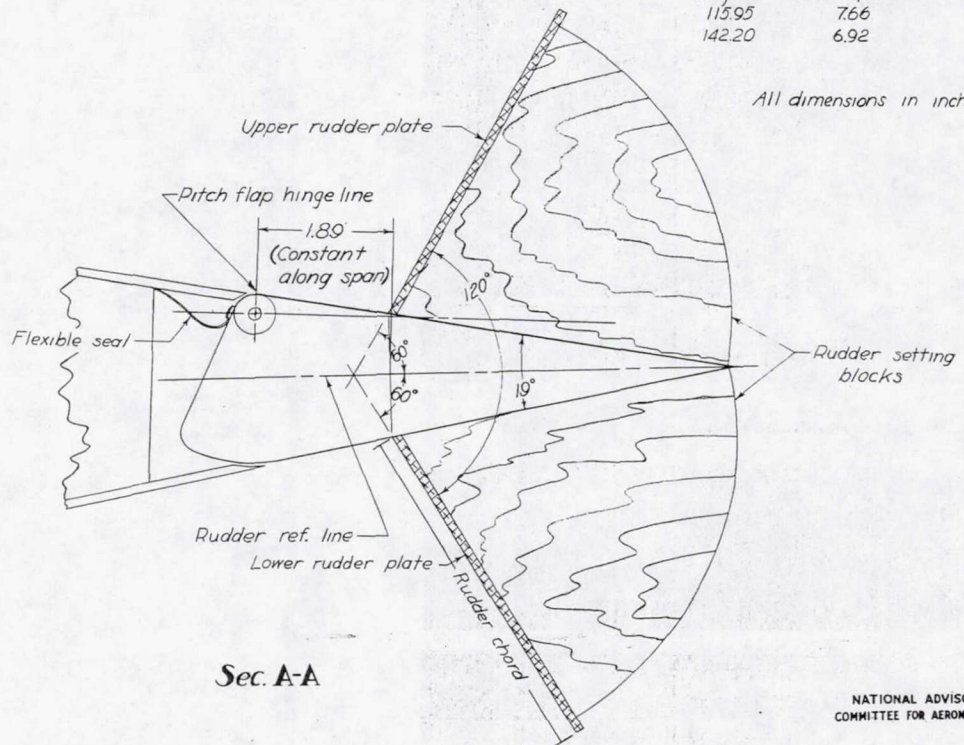
UNCLASSIFIED

~~CONFIDENTIAL~~



Wing Sta	Pitch flap chord	Rudder chord
115.95	7.66	5.71
142.20	6.92	5.00

All dimensions in inches



Sec. A-A

NATIONAL ADVISORY
COMMITTEE FOR AERONAUTICS

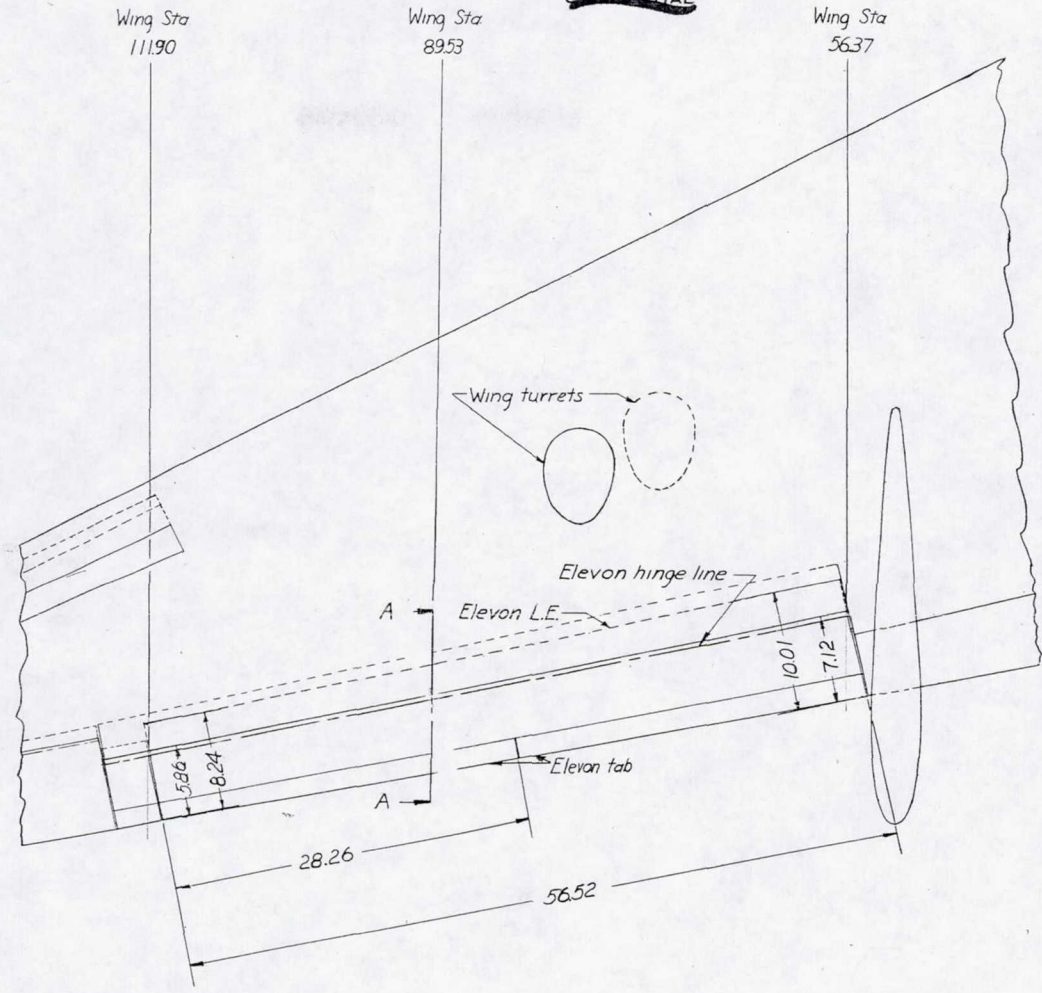
~~CONFIDENTIAL~~

Figure 5.-Details of pitch-control flap and rudder; 1/7-scale XB-35 semispan model.

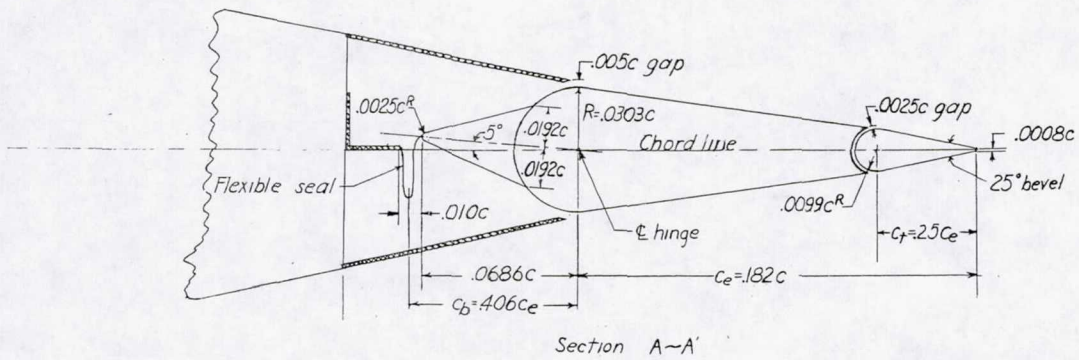
UNCLASSIFIED

UNCLASSIFIED

~~CONFIDENTIAL~~



All dimensions in inches



NATIONAL ADVISORY COMMITTEE FOR AERONAUTICS

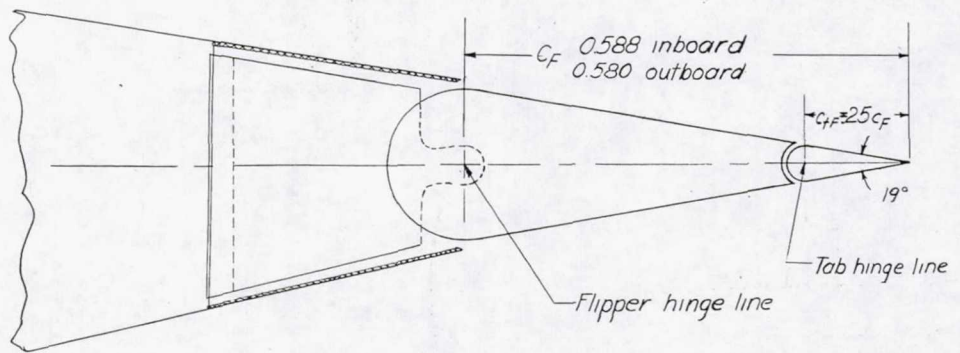
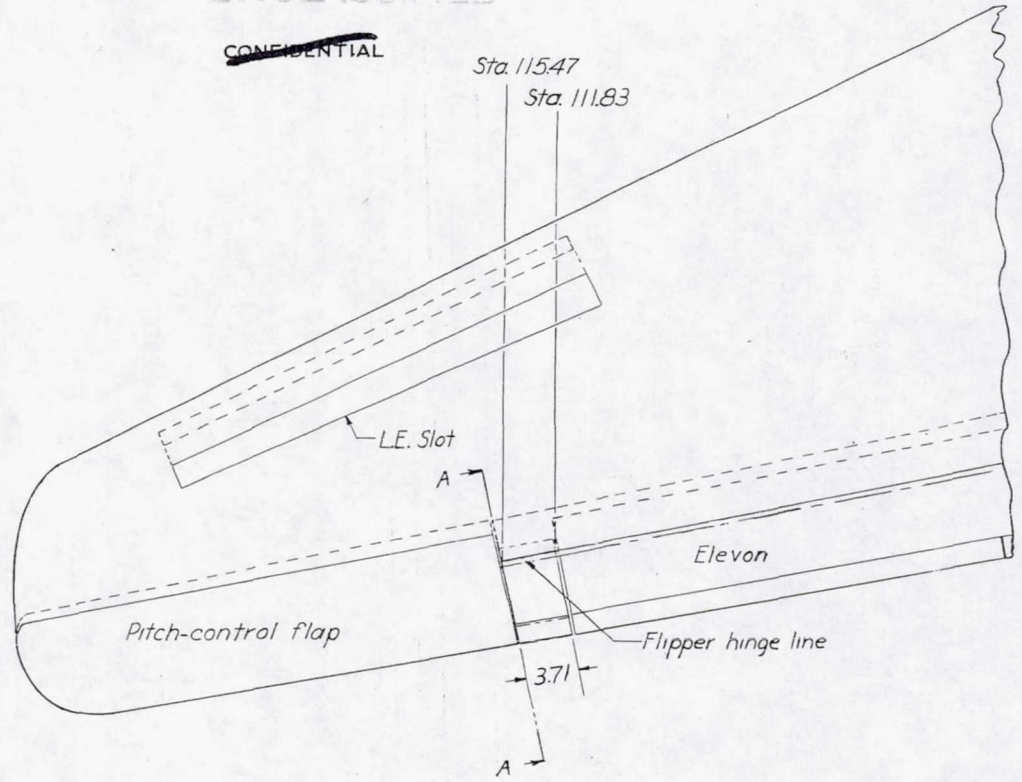
~~CONFIDENTIAL~~

Figure 6 - Details of elevon. 1/7-scale XB-35 semispan model.

UNCLASSIFIED

UNCLASSIFIED

~~CONFIDENTIAL~~



Section A-A

All dimensions in inches

UNCLASSIFIED

~~CONFIDENTIAL~~

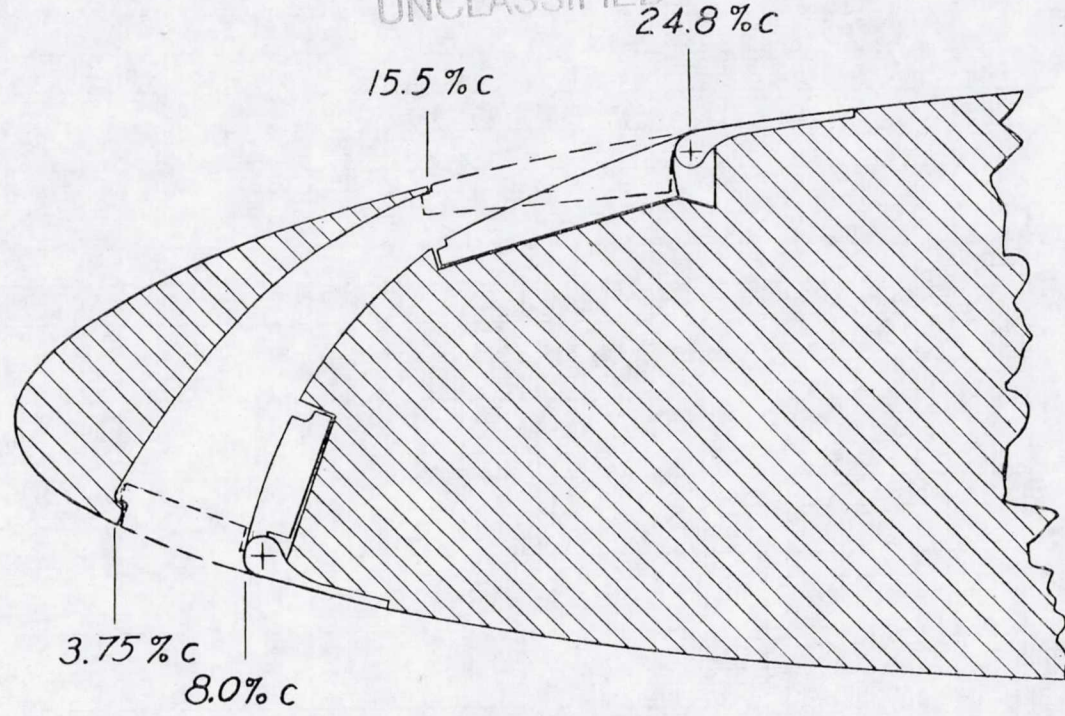
NATIONAL ADVISORY COMMITTEE FOR AERONAUTICS

Figure 7.-Details of flipper. 1/7-scale XB-35 semispan model.

1045

~~CONFIDENTIAL~~

UNCLASSIFIED



~~CONFIDENTIAL~~

NATIONAL ADVISORY
COMMITTEE FOR AERONAUTICS

UNCLASSIFIED

Figure 8. - Typical section of leading edge slot.
1/7-scale XB-35 semispan model.

MR No. L5L27

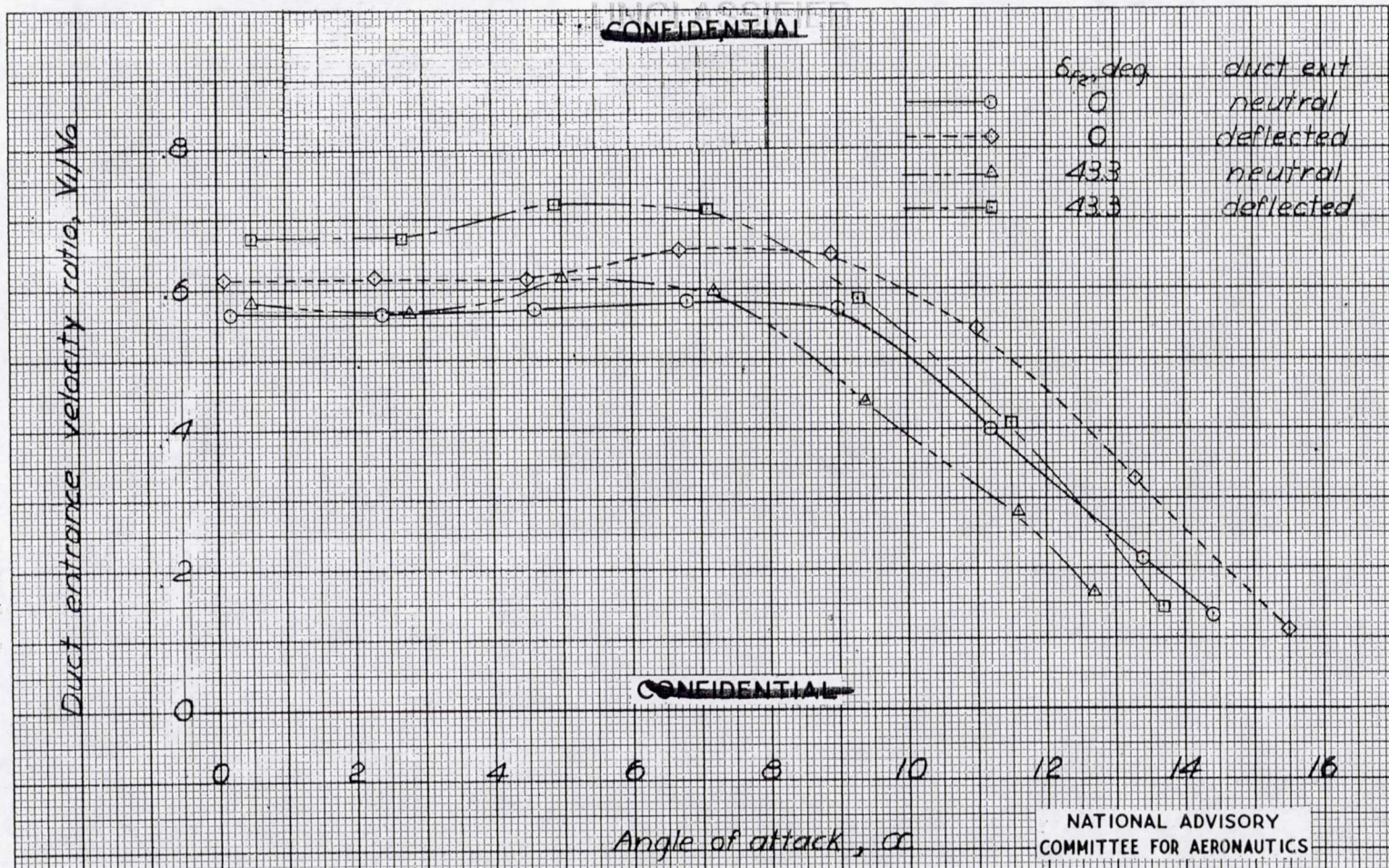
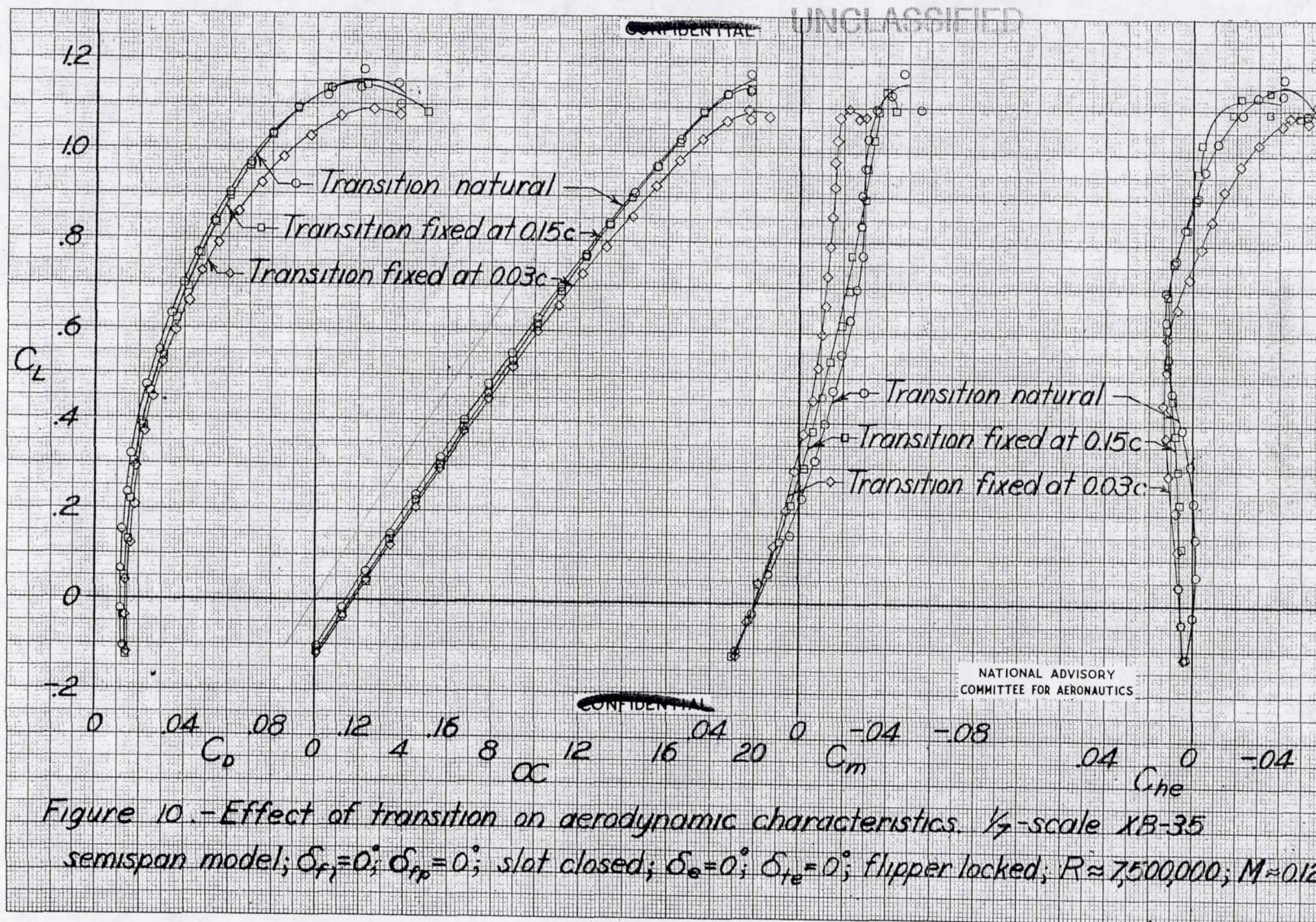
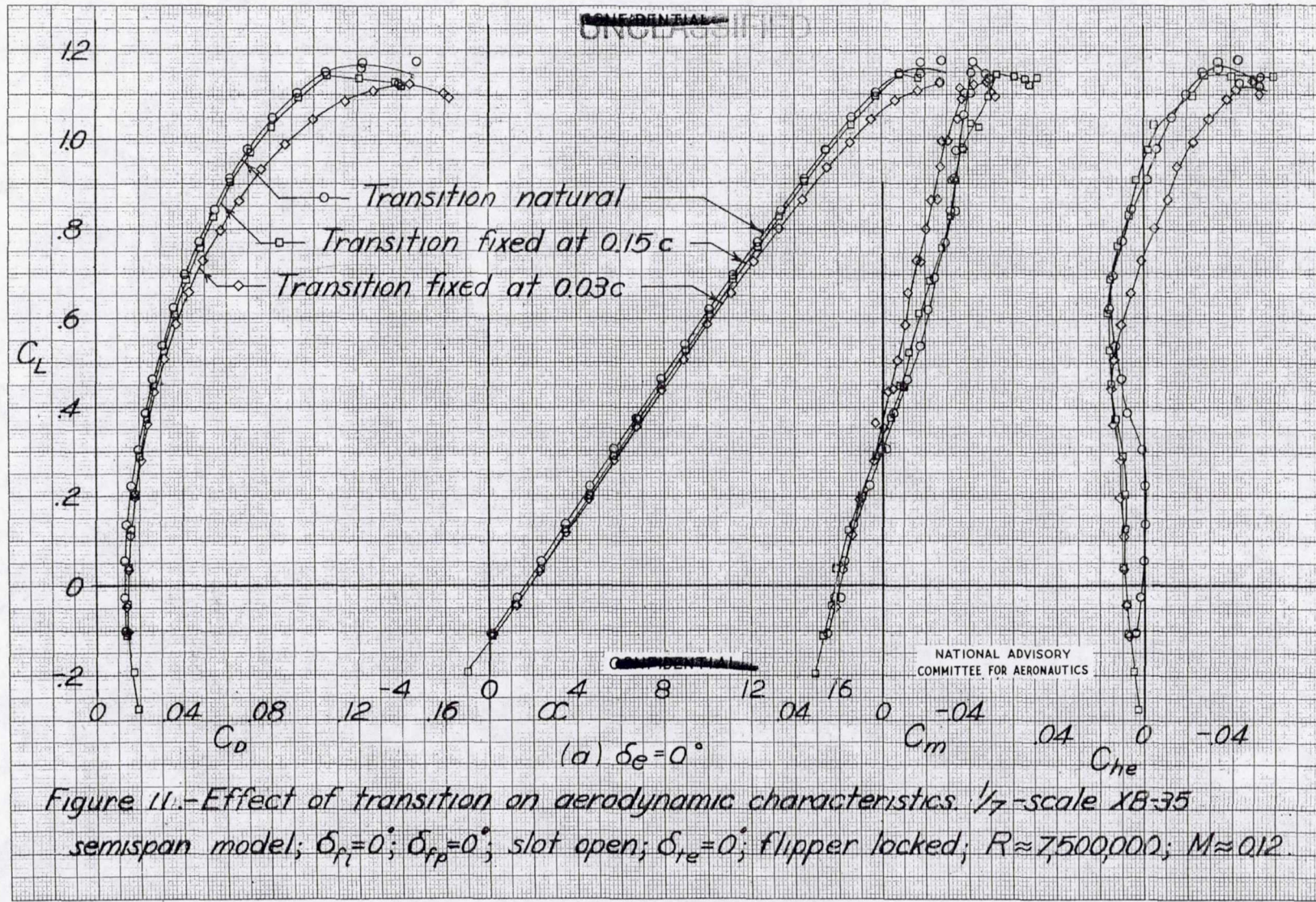


Figure 9 - Variation of duct entrance velocity ratio with angle of attack.

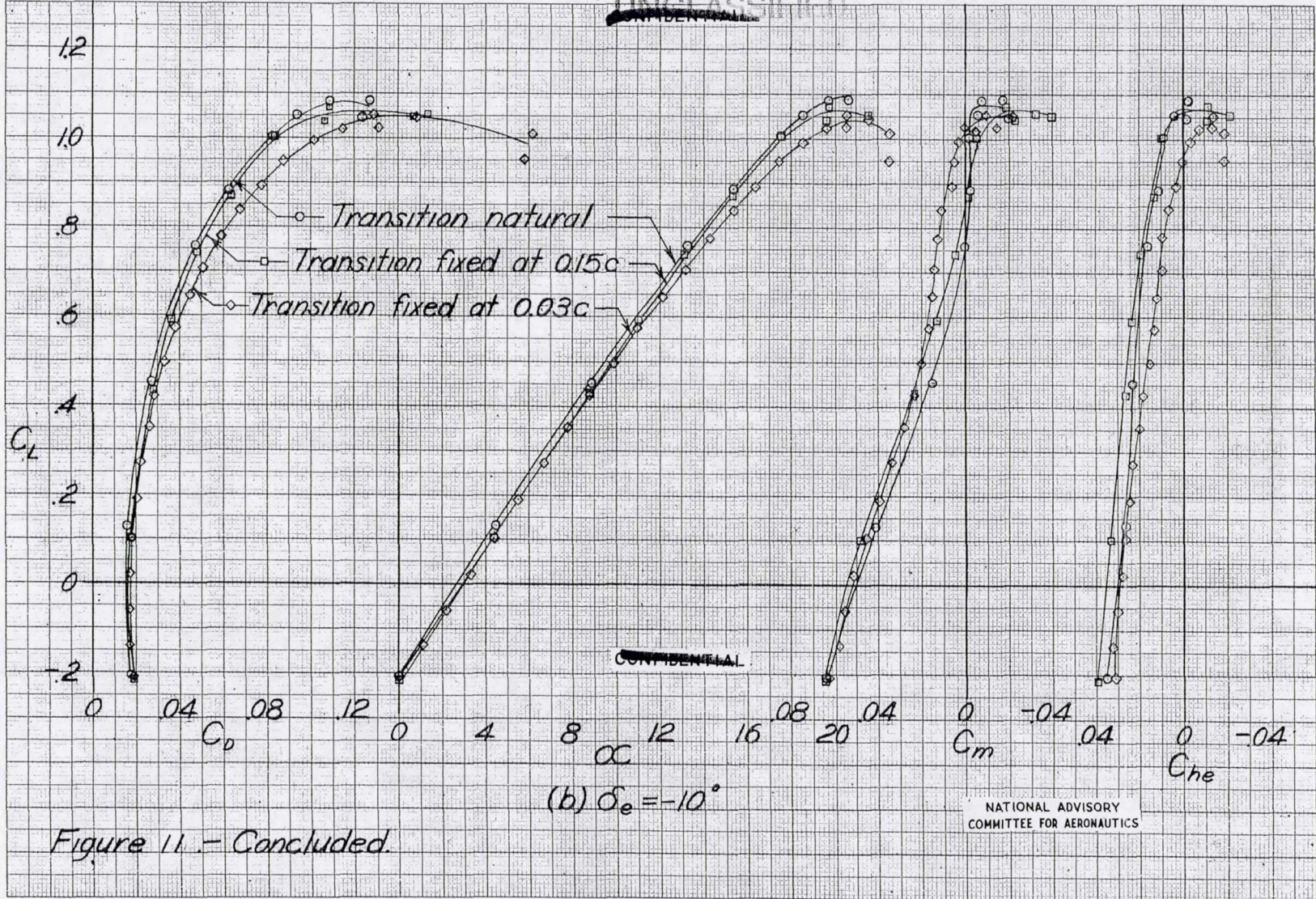
1/7-scale XB-35 semispan model.



UNCLASSIFIED



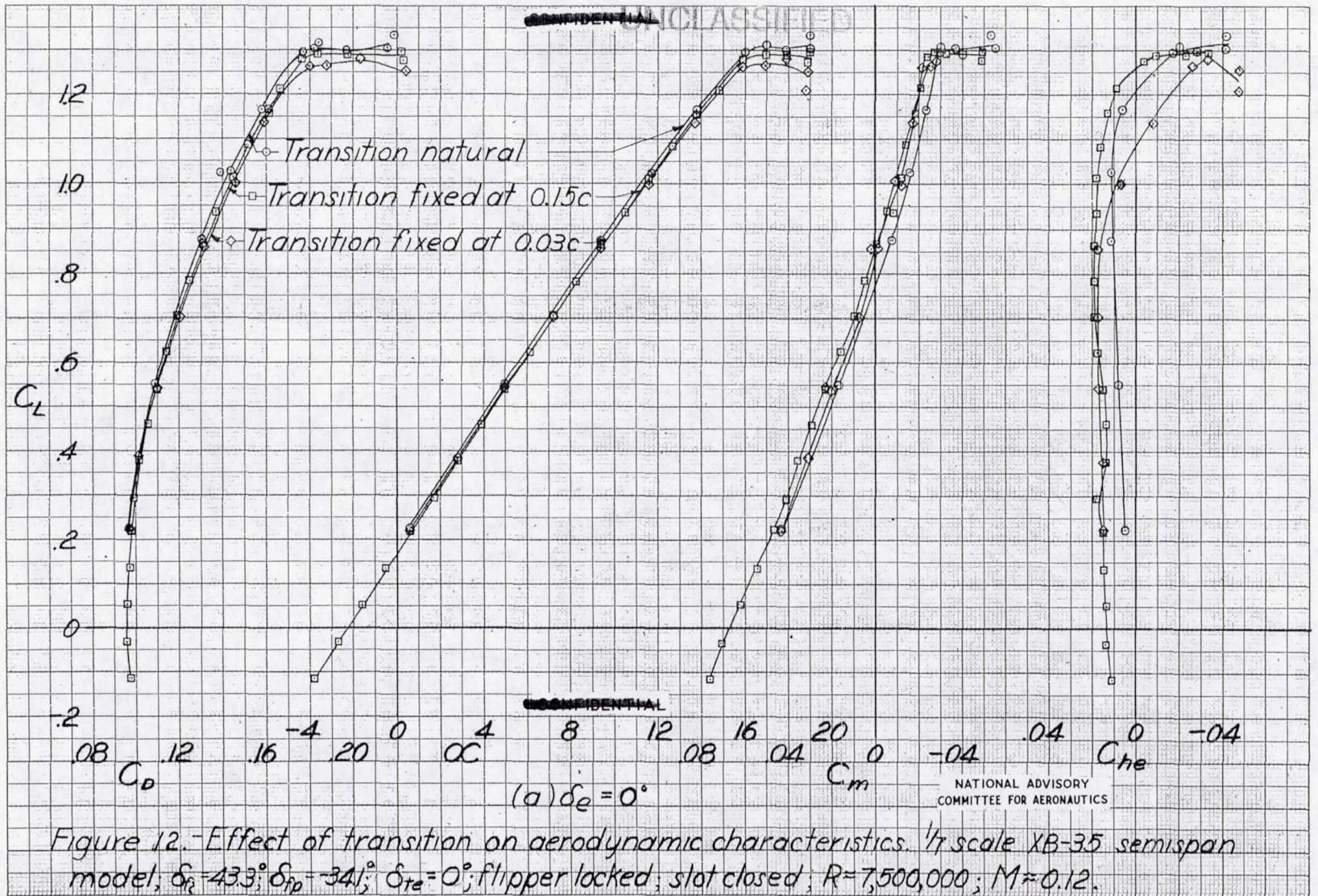
UNCLASSIFIED



UNCLASSIFIED

MR. NO. 1545

1941



MR No. L5L27

UNCLASSIFIED

UNCLASSIFIED

~~CONFIDENTIAL~~

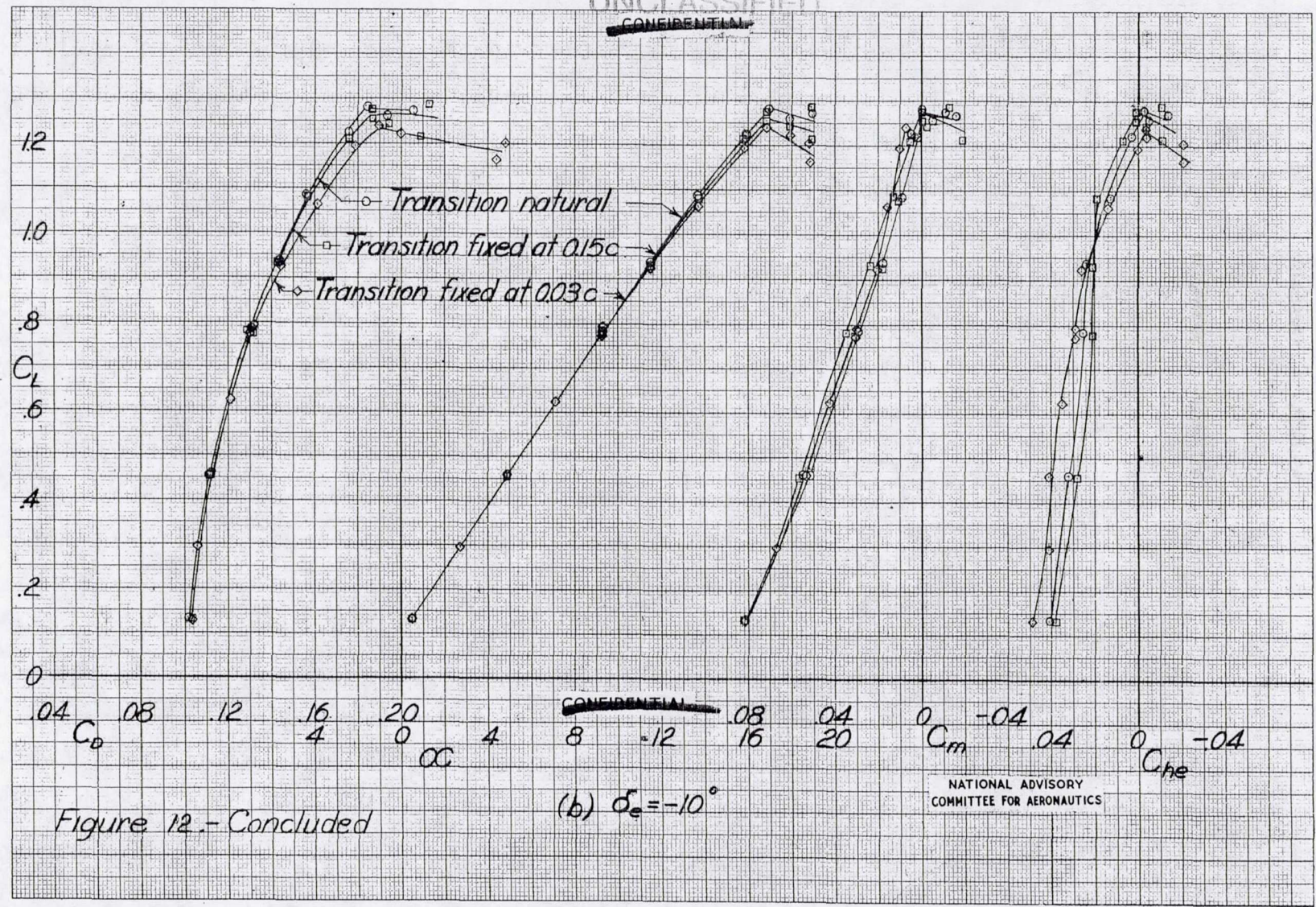


Figure 12.- Concluded

(b) $\alpha_e = -10^\circ$

UNCLASSIFIED

REF ID: A60571

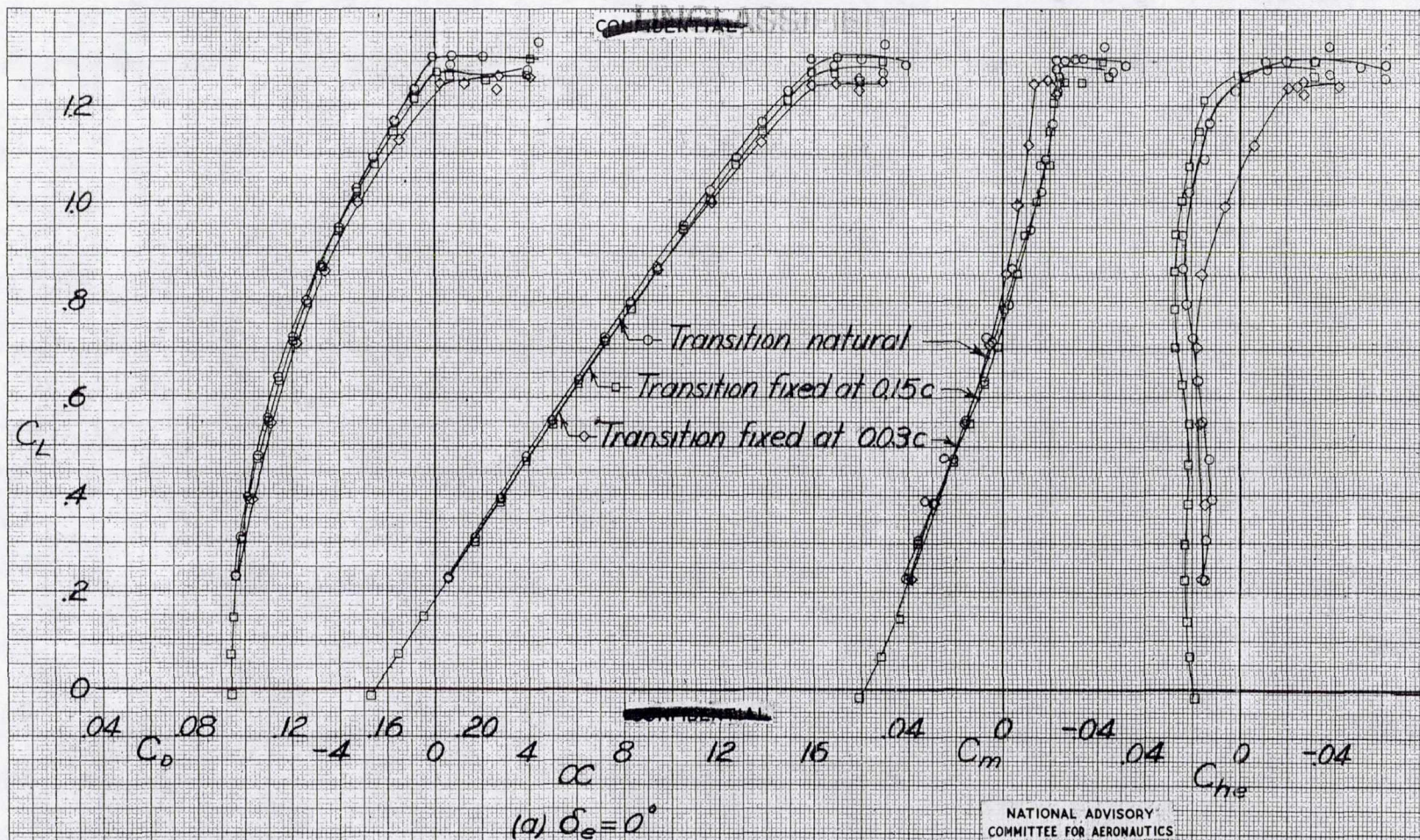
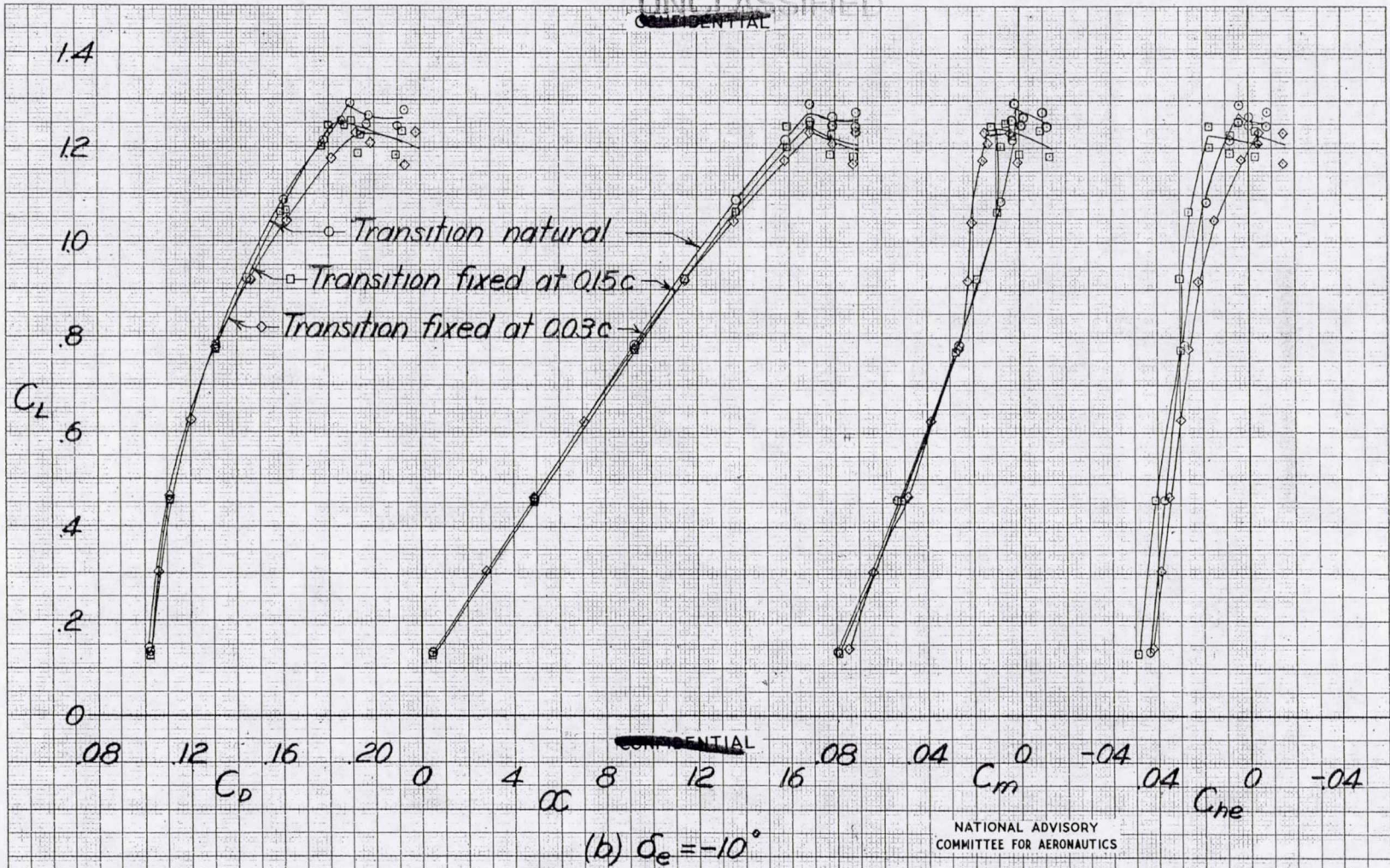


Figure 13.-Effect of transition on aerodynamic characteristics. $1/7$ -scale XB-35 semispan model; $\delta_{f1} = 43.3^\circ$; $\delta_{fp} = -34.1^\circ$; slot open; $\delta_{te} = 0^\circ$; flipper locked; $R \approx 7,500,000$; $M \approx 0.12$

UNCLASSIFIED
~~CONFIDENTIAL~~



NATIONAL ADVISORY
COMMITTEE FOR AERONAUTICS

Figure 13 - Concluded

UNCLASSIFIED

MR. NO. 13121

10451

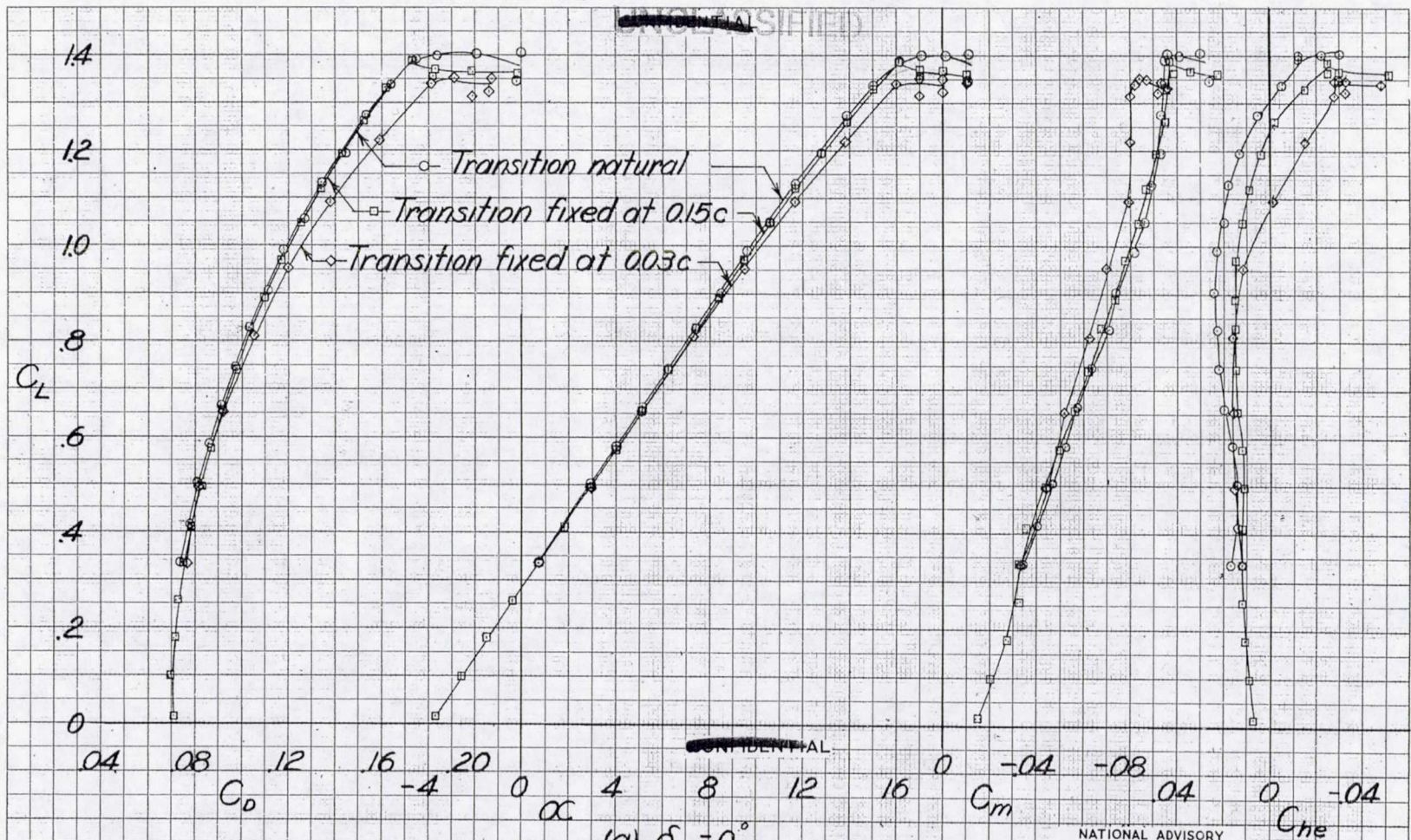


Figure 14.-Effect of transition on aerodynamic characteristics. $1/7$ -scale XB-35 semispan model; $\delta_{f1} = 43.3^\circ$; slot open; $\delta_e = 0^\circ$; $\delta_{te} = 0^\circ$; flipper locked; $R \approx 7,500,000$; $M \approx 0.12$.

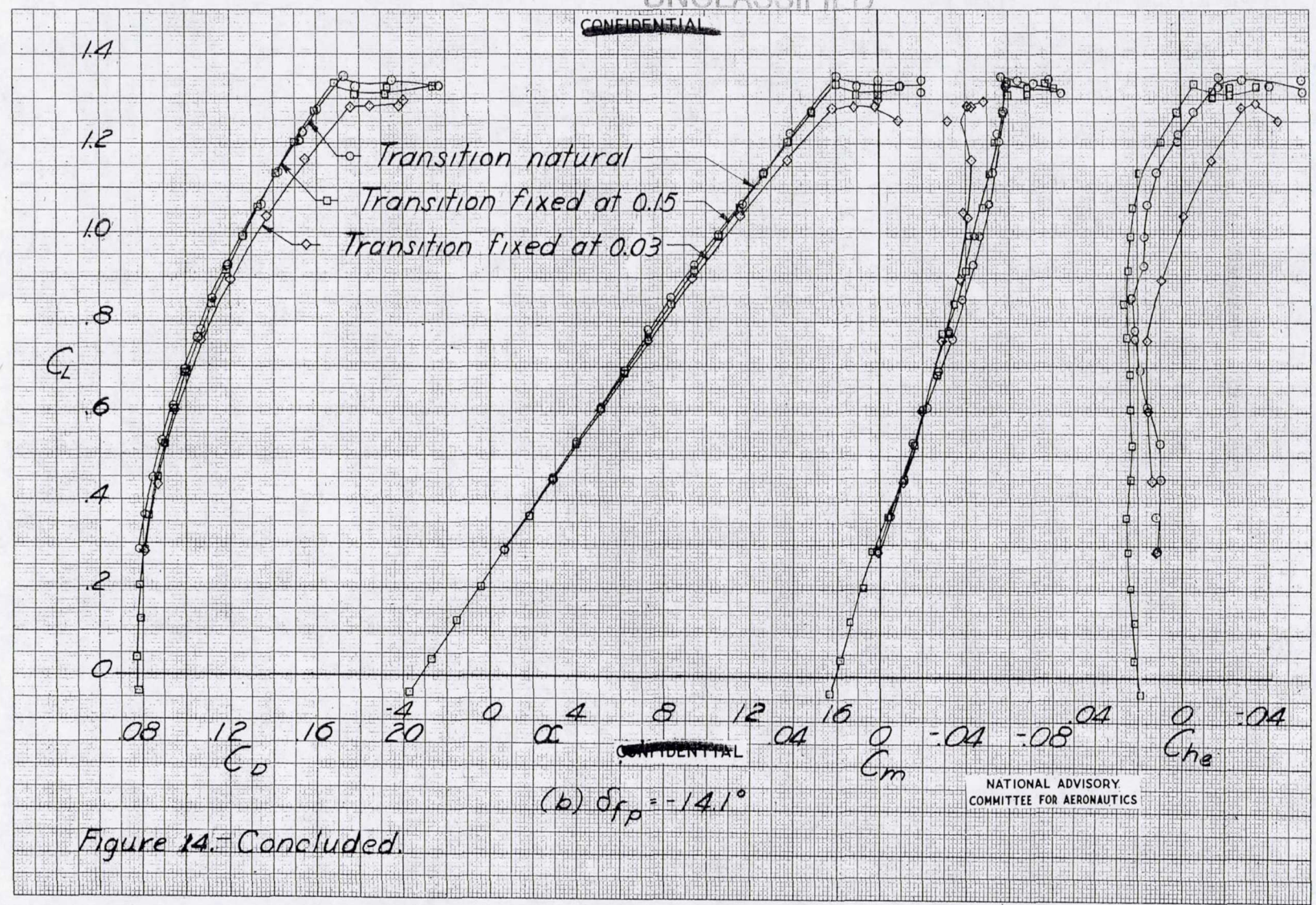
UNCLASSIFIED

MR No. L5L27

104511

UNCLASSIFIED

~~CONFIDENTIAL~~



~~CONFIDENTIAL~~

(b) $\delta_{fp} = -14.1^\circ$

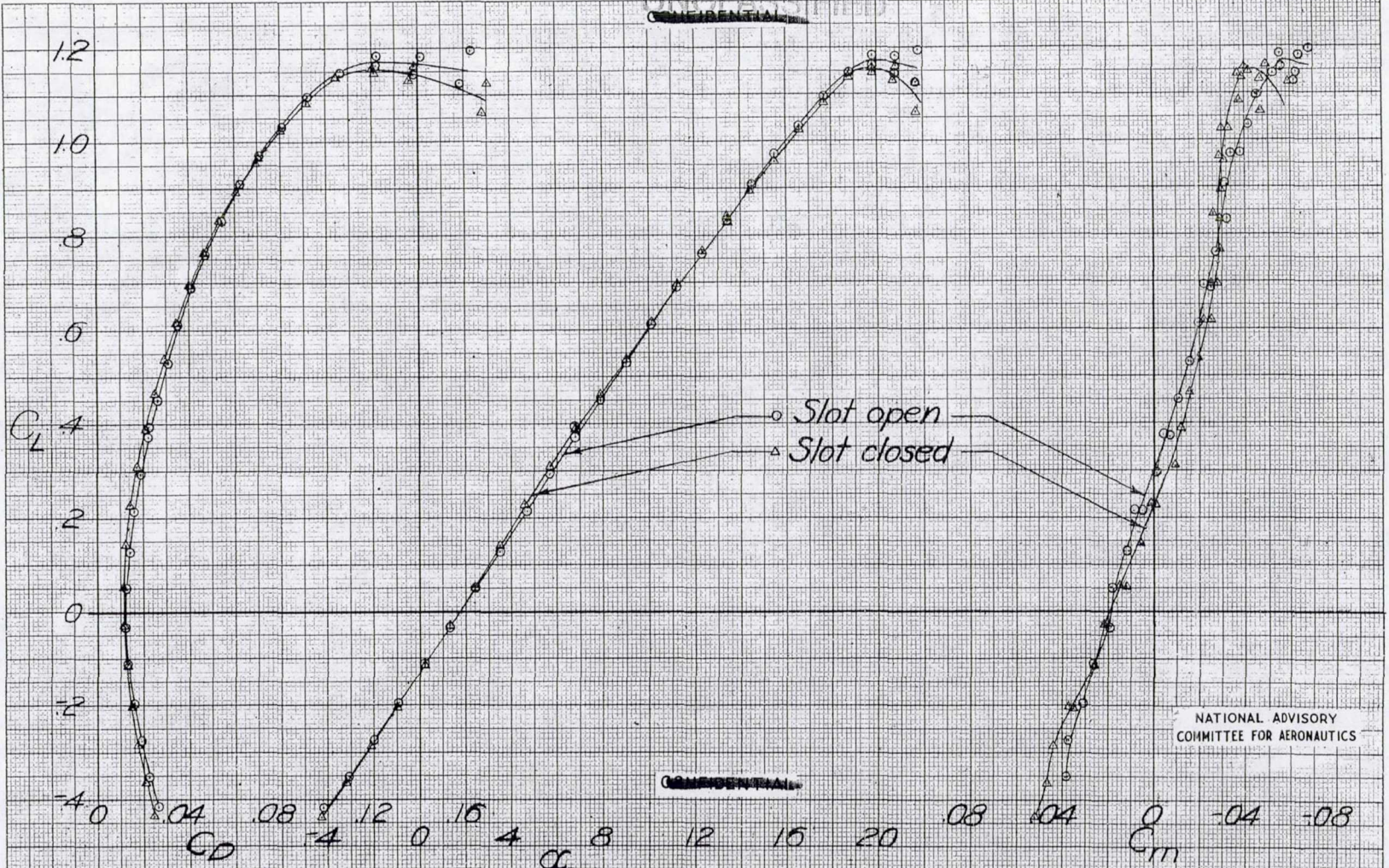
NATIONAL ADVISORY
COMMITTEE FOR AERONAUTICS

Figure 14.- Concluded.

UNCLASSIFIED

MR No. L5127

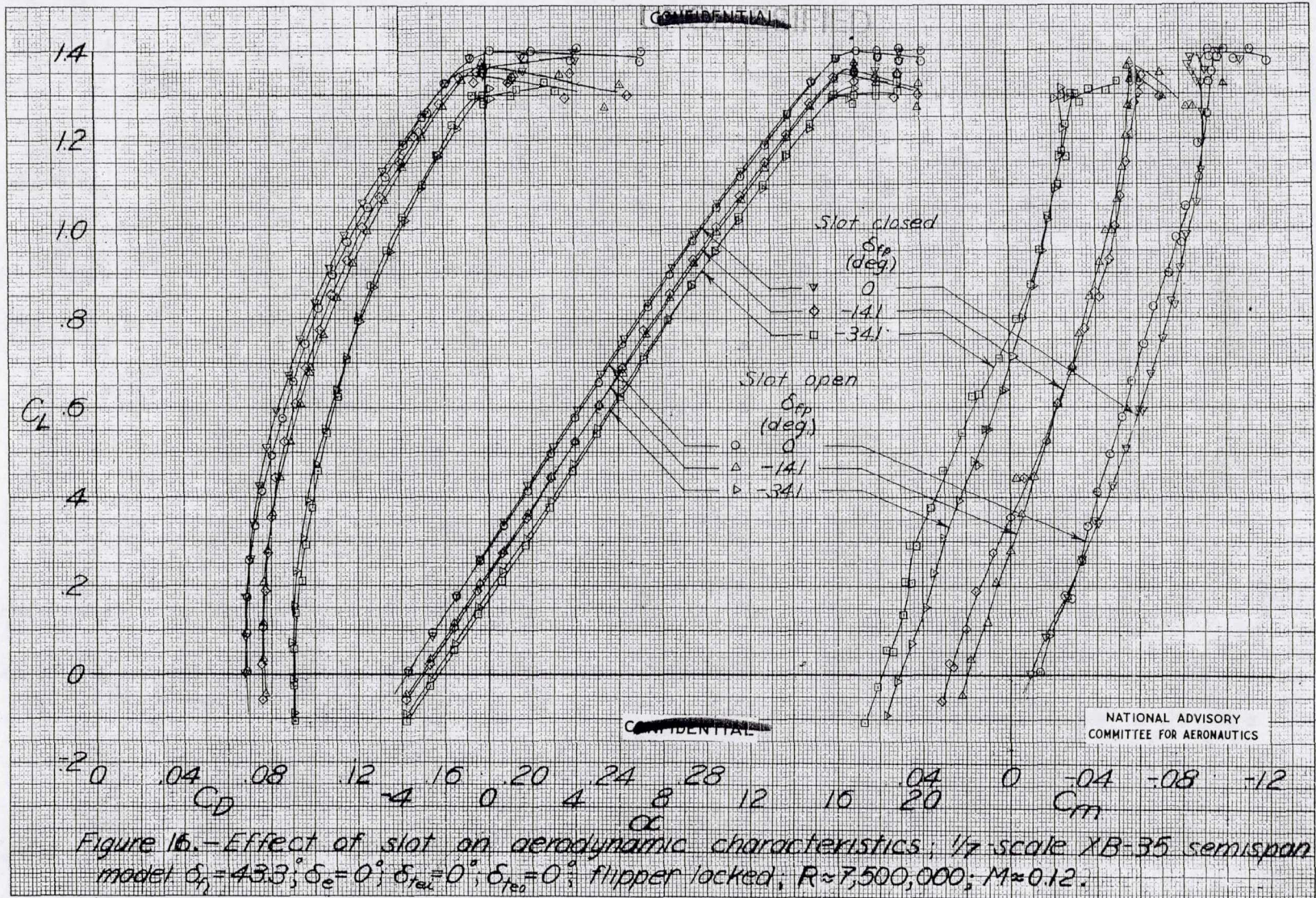
UNCLASSIFIED



CONFIDENTIAL

Figure 15.- Effect of slot on aerodynamic characteristics; 1/7-scale XB-35 semispan model. $\delta_{fp} = 0^\circ$; $\delta_e = 0^\circ$; $\delta_{rez} = 0^\circ$; $\delta_{reo} = 0^\circ$; flipper locked; $R \approx 7,500,000$; $M \approx 0.12$.

UNCLASSIFIED



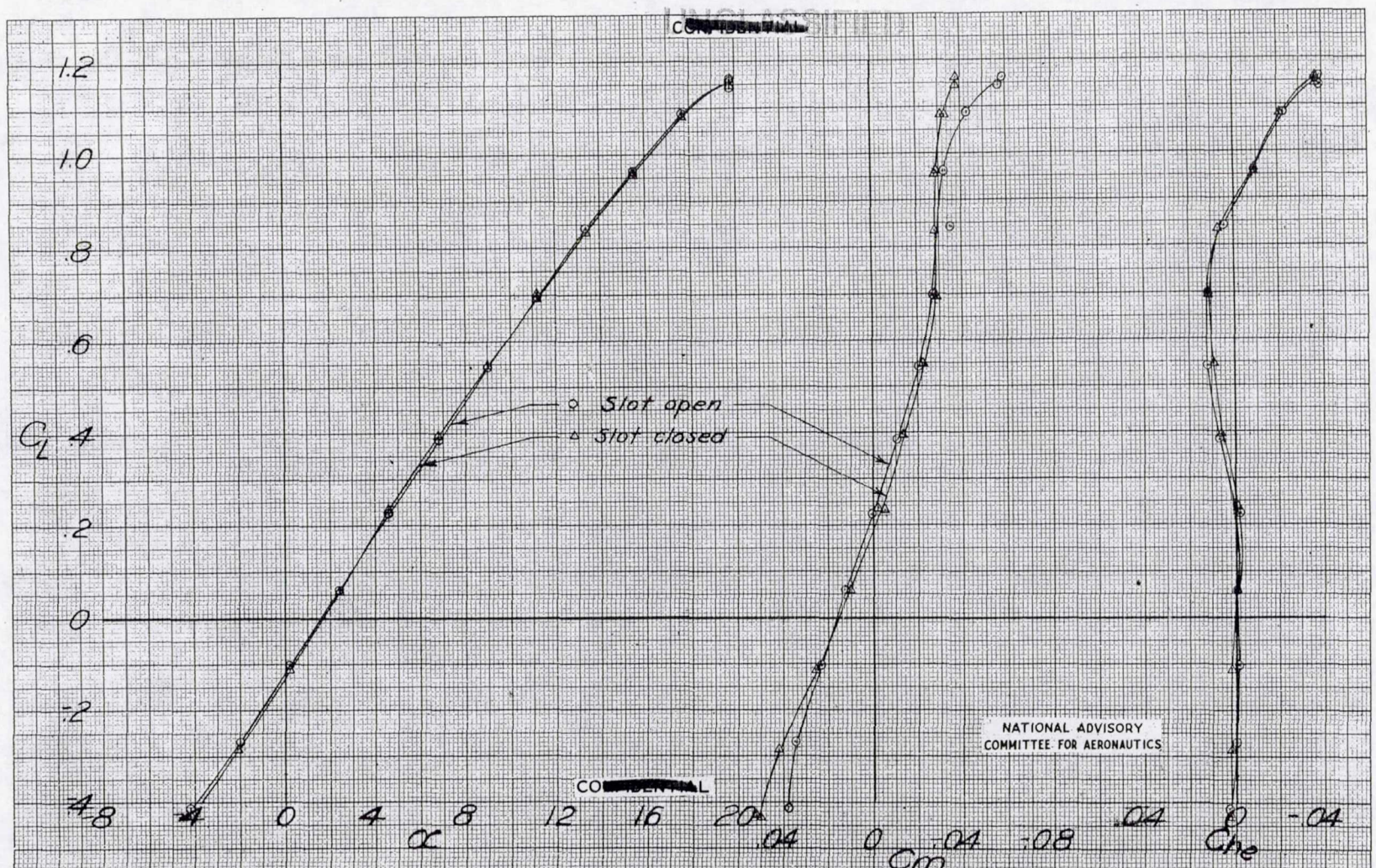
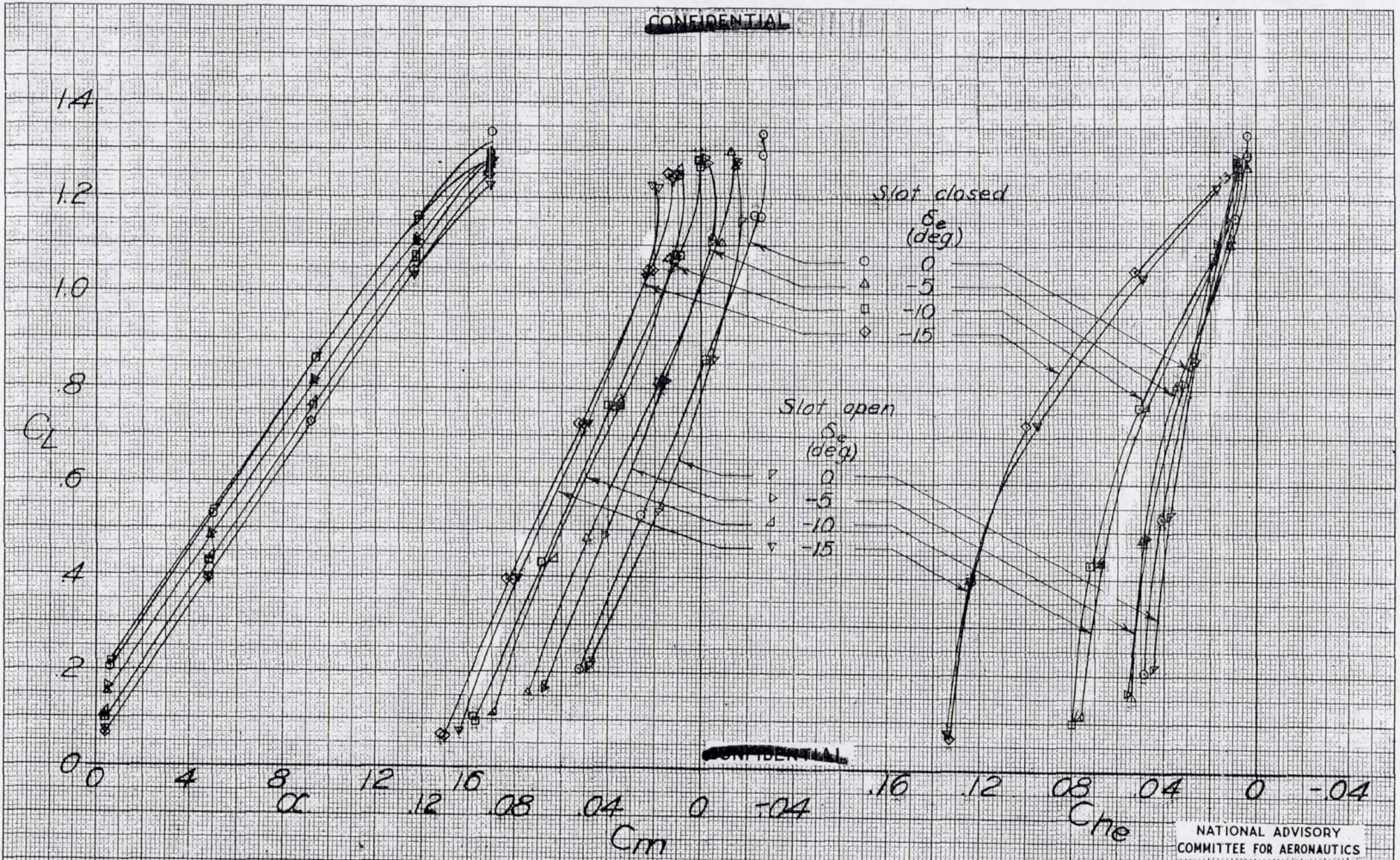


Figure 17. - Effect of slot on aerodynamic characteristics, 1/7-scale XB-35 semispan model. $\delta_{fi}=0^\circ$; $\delta_{fp}=0^\circ$; $\delta_a=0^\circ$; $\delta_{tal}=0^\circ$; $\delta_{leo}=0^\circ$; flipper free-floating; $R=7,500,000$; $M=0.12$.

NATIONAL ADVISORY COMMITTEE FOR AERONAUTICS

CONFIDENTIAL

CONFIDENTIAL



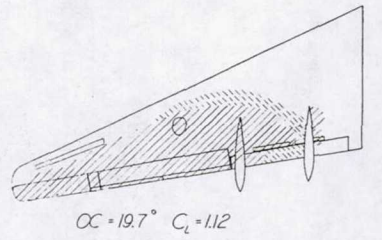
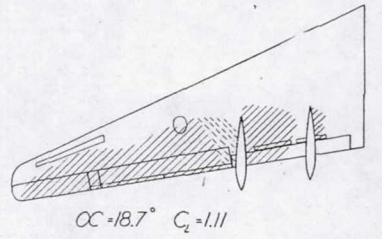
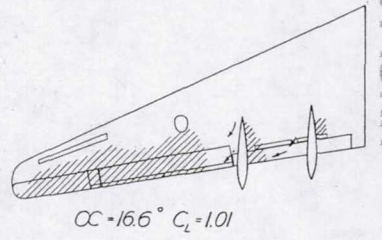
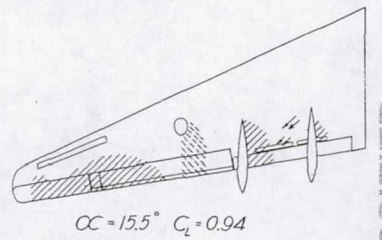
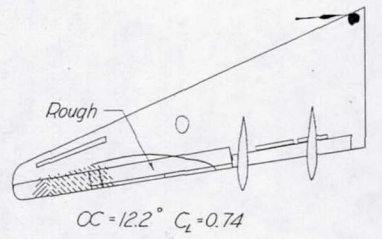
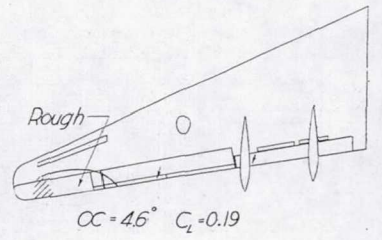
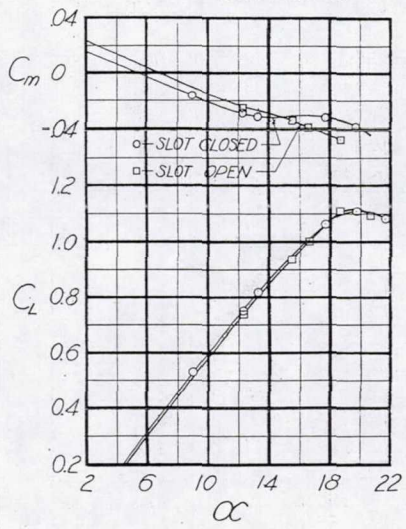
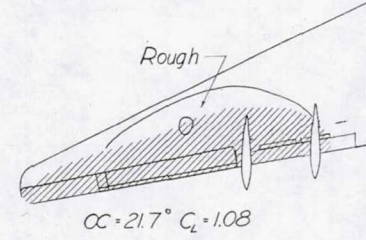
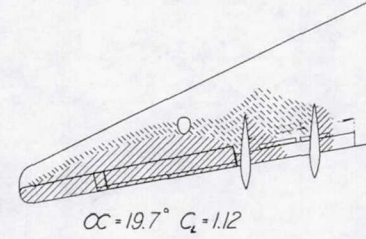
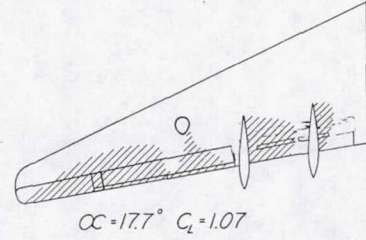
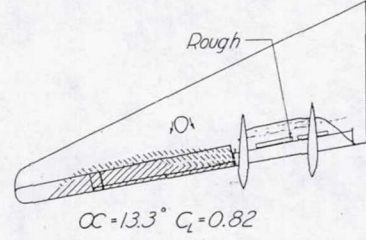
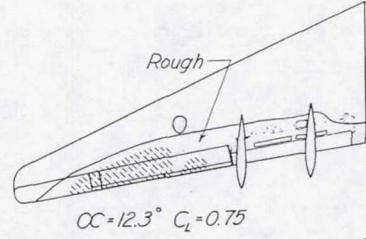
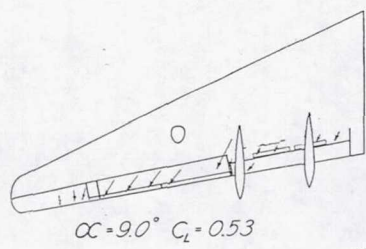
CONFIDENTIAL

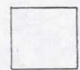



NATIONAL ADVISORY COMMITTEE FOR AERONAUTICS

Figure 18.- Effect of slot on aerodynamic characteristics; 1/4 scale XB-35 semispan model. $\delta_{fp} = 43.3^\circ$; $\delta_{fp} = -34.1^\circ$; $\delta_{red} = 0^\circ$; $\delta_{red} = -15^\circ$; flipper free-floating; $R = 7,500,000$; $M = 0.12$.

UNCLASSIFIED

~~CONFIDENTIAL~~



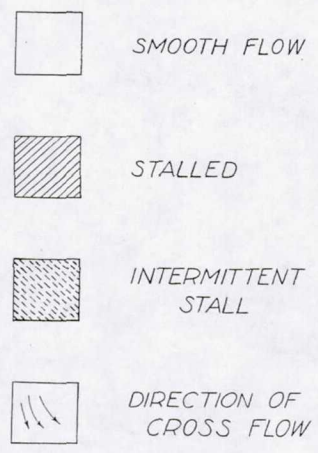
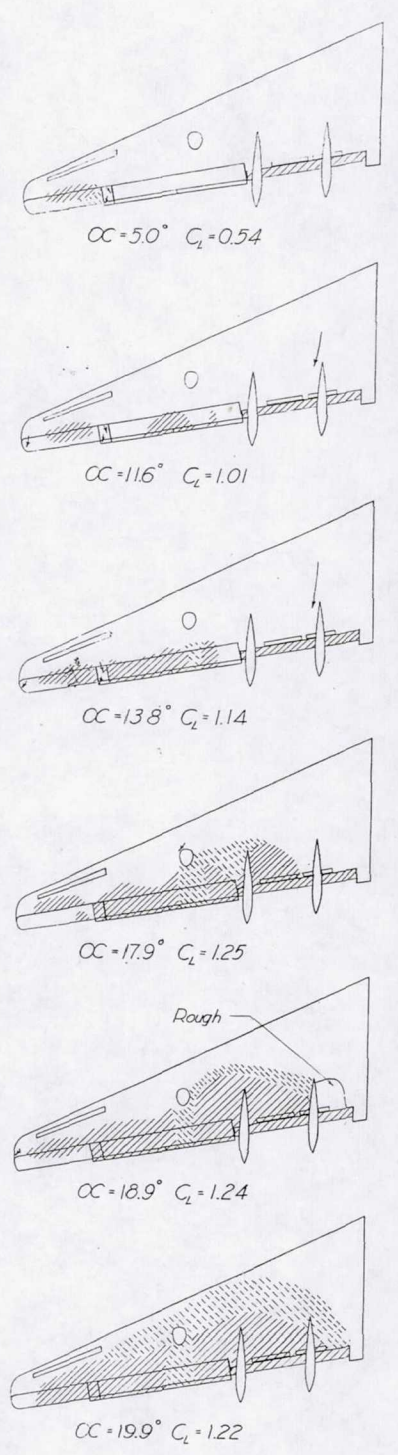
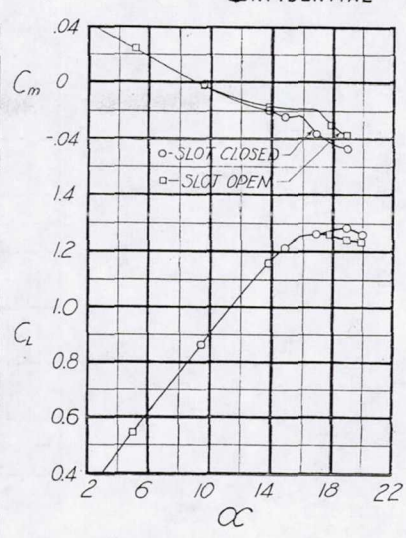
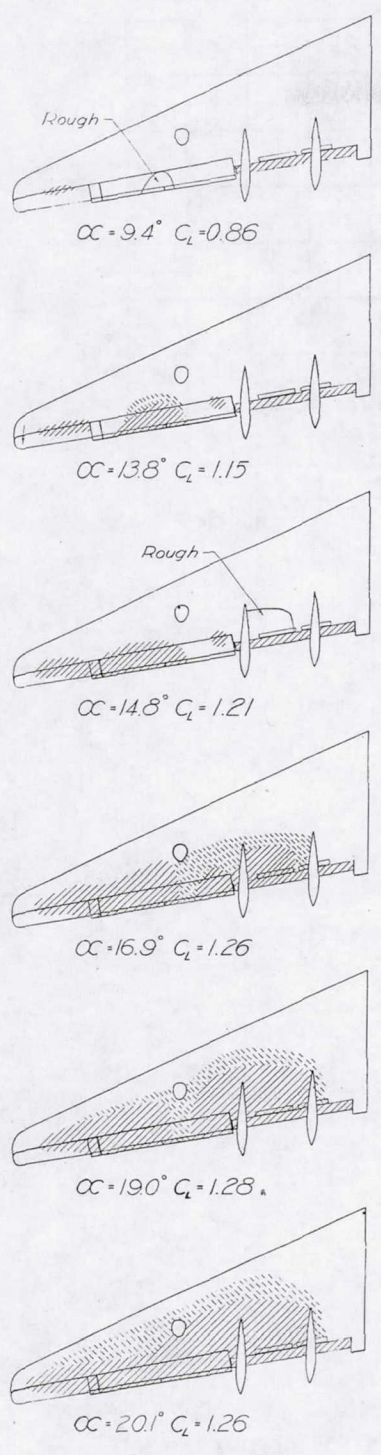
-  SMOOTH FLOW
-  STALLED
-  INTERMITTENT STALL
-  DIRECTION OF CROSS FLOW

NATIONAL ADVISORY COMMITTEE FOR AERONAUTICS.

~~CONFIDENTIAL~~

(a) Slot closed (b) Slot open
 Figure 19.- Stall diagrams of the 1/7-scale semispan model of the XB-35 airplane. $\delta_i = 0^\circ$, $\delta_e = \delta_F = \delta_{te} = 0^\circ$, $\delta_n = 0^\circ$, $R \approx 7,500,000$, $M \approx 0.12$.

~~CONFIDENTIAL~~



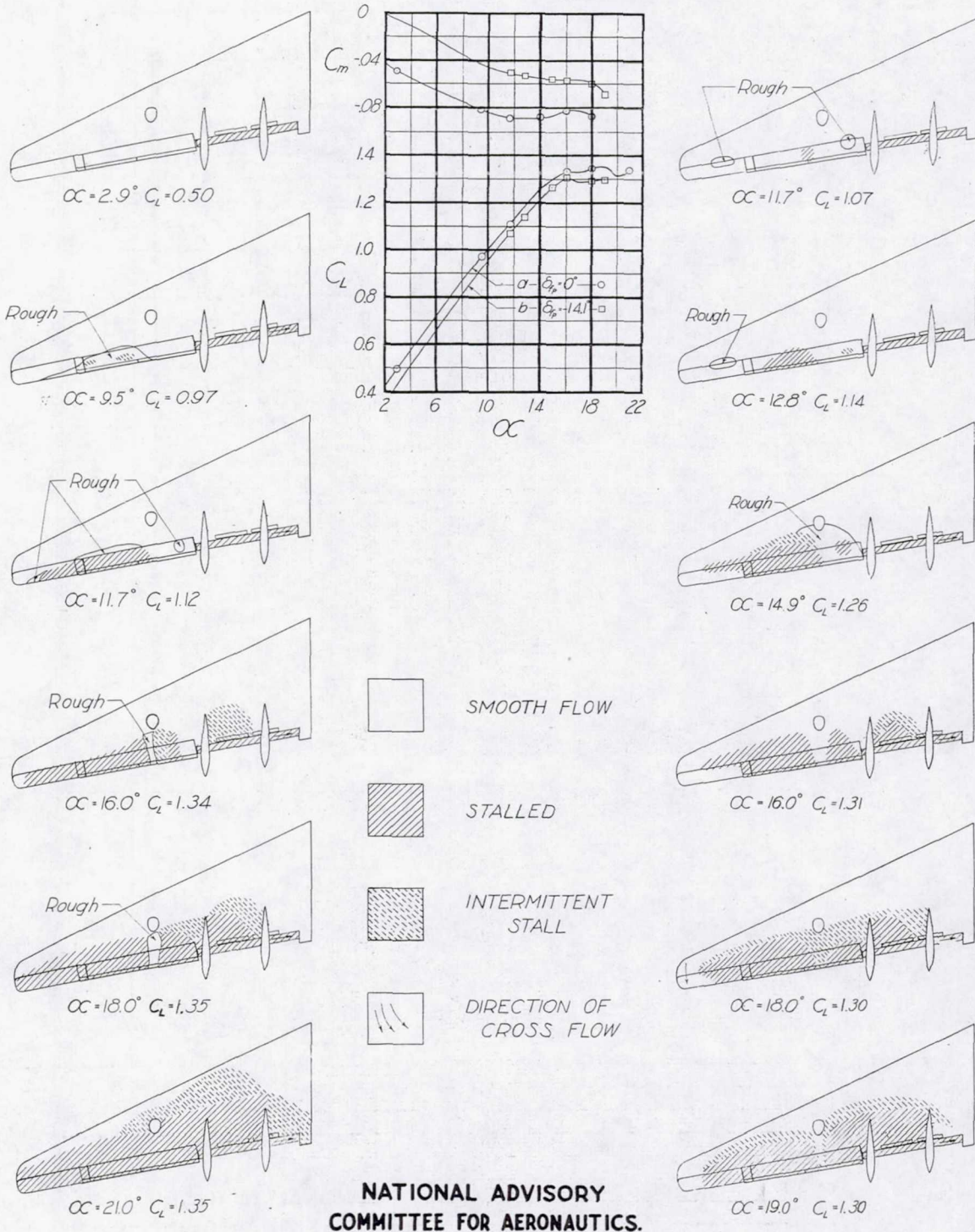
NATIONAL ADVISORY COMMITTEE FOR AERONAUTICS.

~~CONFIDENTIAL~~

(a) Slot closed (b) Slot open
 Figure 20.- Stall diagrams of the 1/7-scale semispan model of the XB-35 airplane. $\delta_t = 43.3^\circ$, $\delta_p = -34.1^\circ$, $\delta_e = \delta_r = \delta_c = 0^\circ$, $R = 7,500,000$, $M \approx 0.12$.

UNCLASSIFIED

~~CONFIDENTIAL~~



(a) $\delta_p = 0^\circ$ (b) $\delta_p = -14.1^\circ$
 Figure 21.- Stall diagrams of the 1/7-scale semi-span model of the XB-35 airplane. $\delta_f = 43.3^\circ$, $\delta_e = \delta_f - \delta_e = 0^\circ$, slot closed. $R \approx 7,500,000$, $M \approx 0.12$.

UNCLASSIFIED

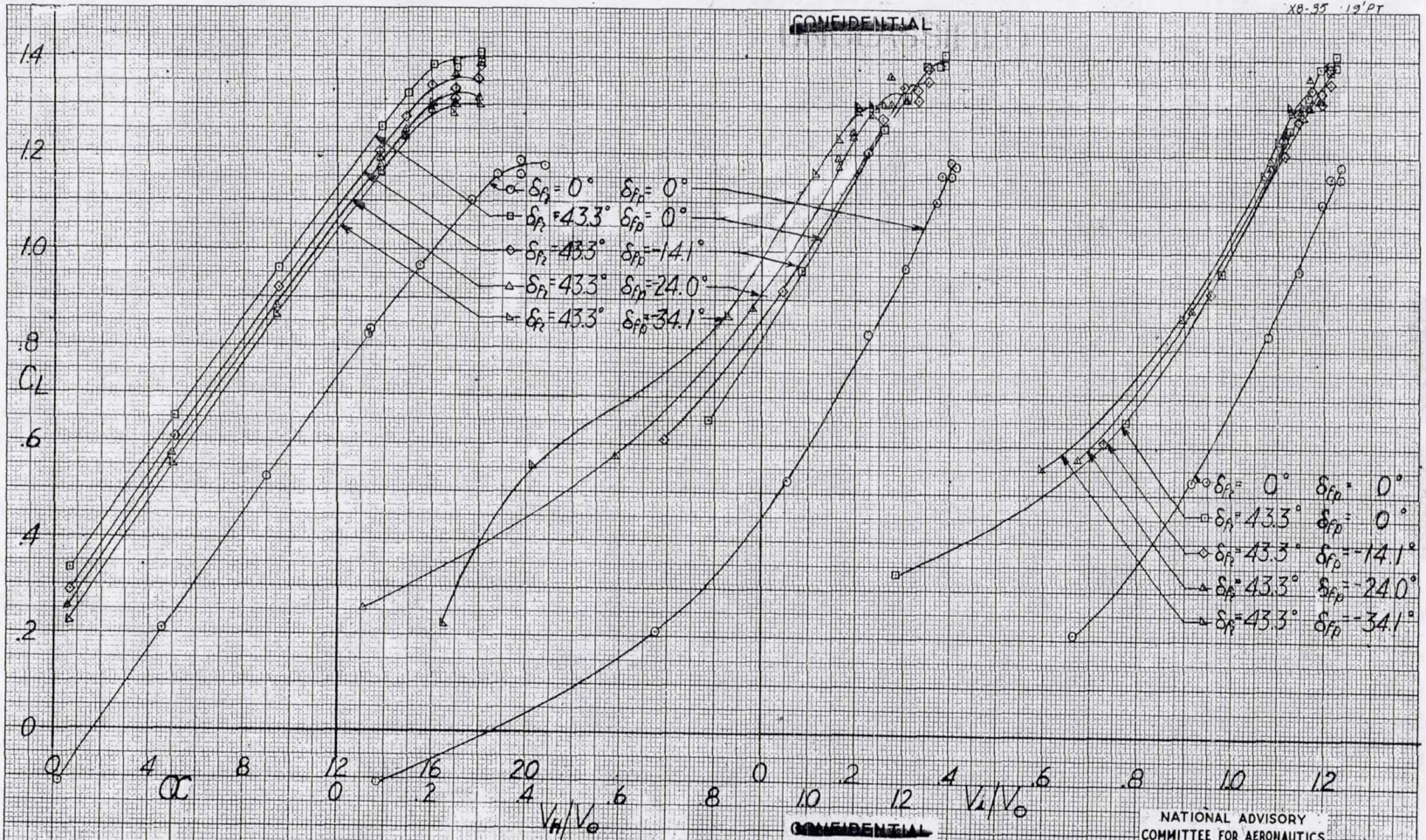
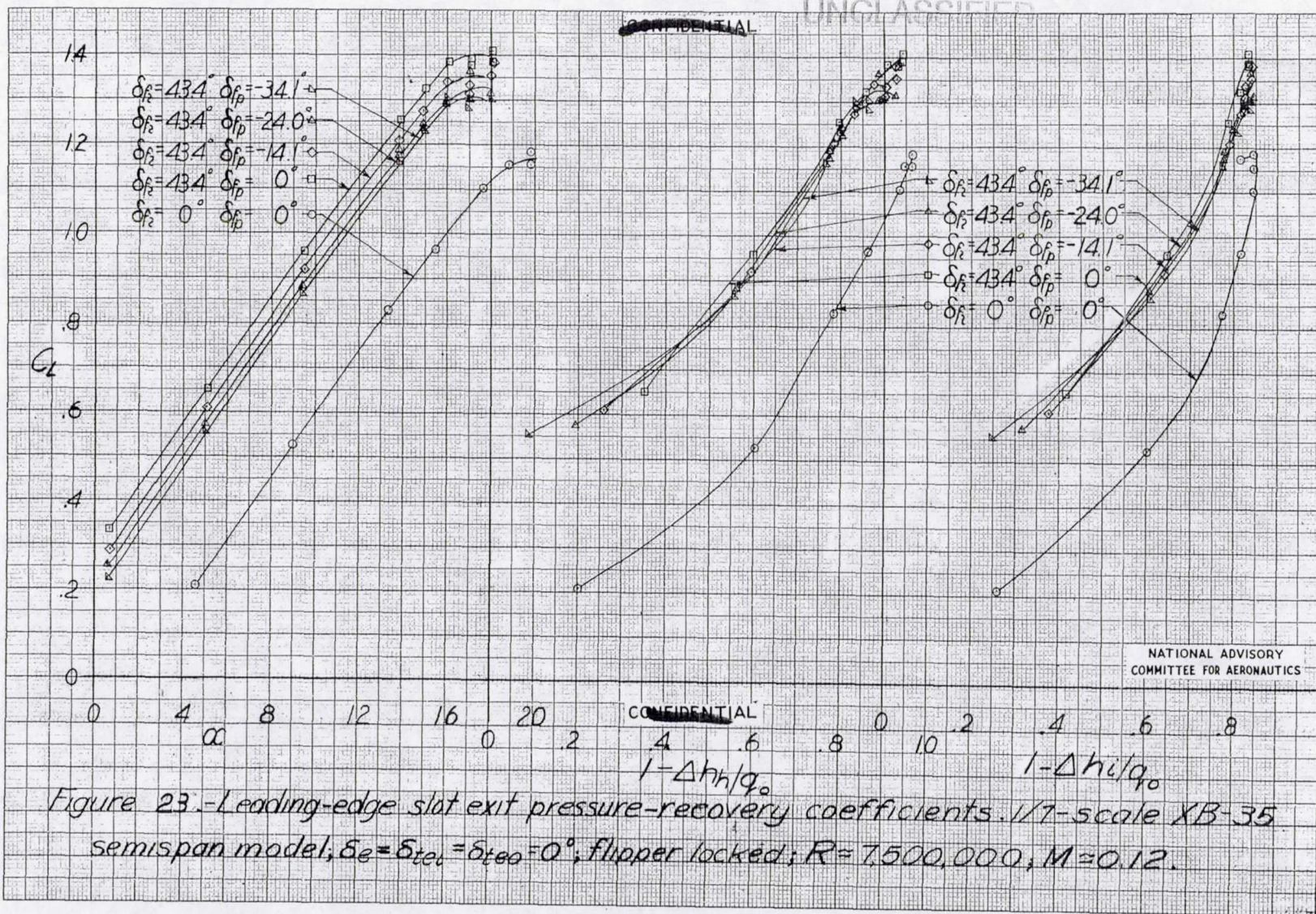
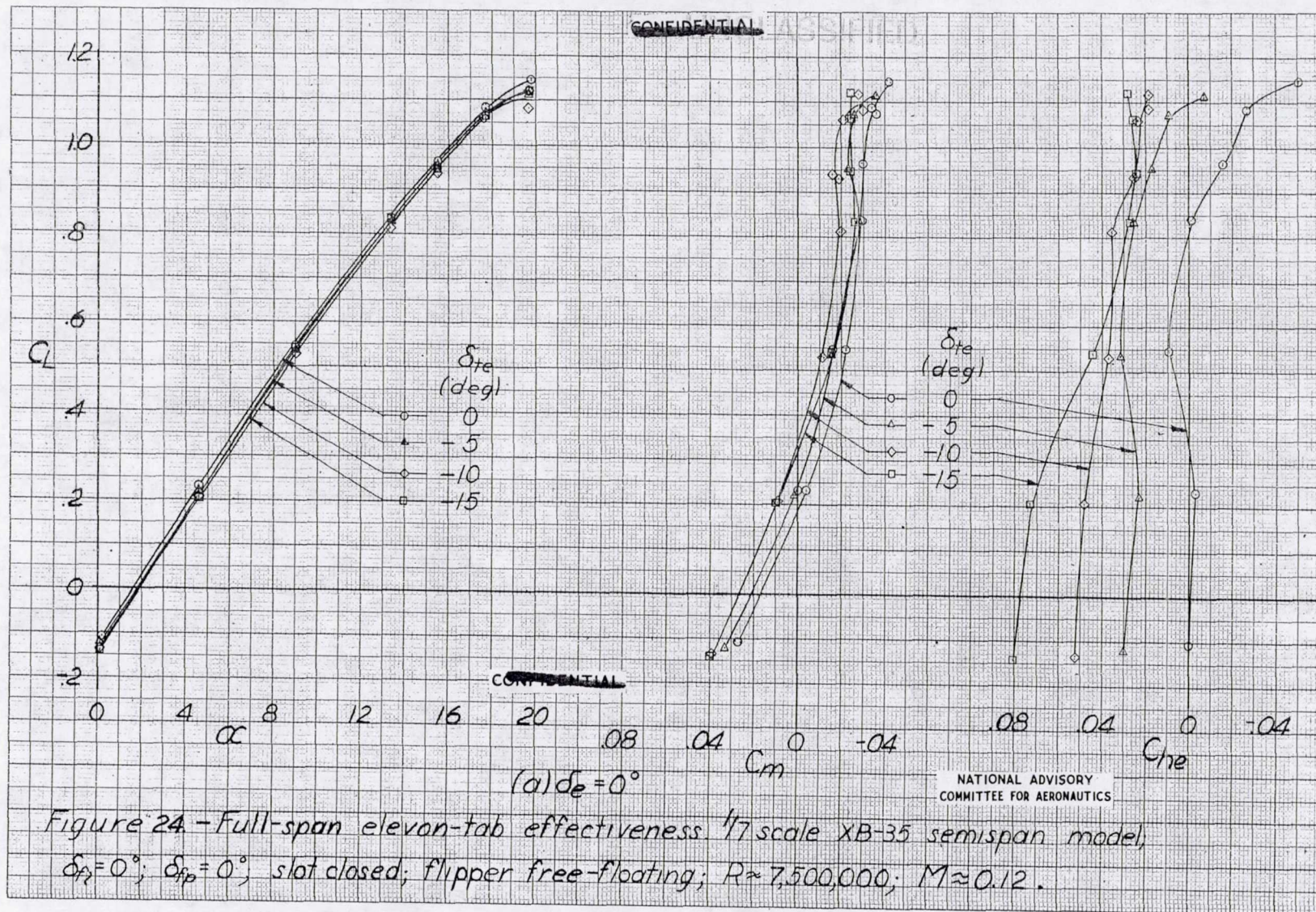


Figure 22₁ - Leading-edge slot exit-velocity ratios. 1/7-scale XB-35 semispan model; $\delta_e = \delta_{te1} = \delta_{te0} = 0^\circ$; flipper locked; $R=7,500,000$, $M=0.12$.

UNCLASSIFIED



16452



MR No. L5L27

UNCLASSIFIED

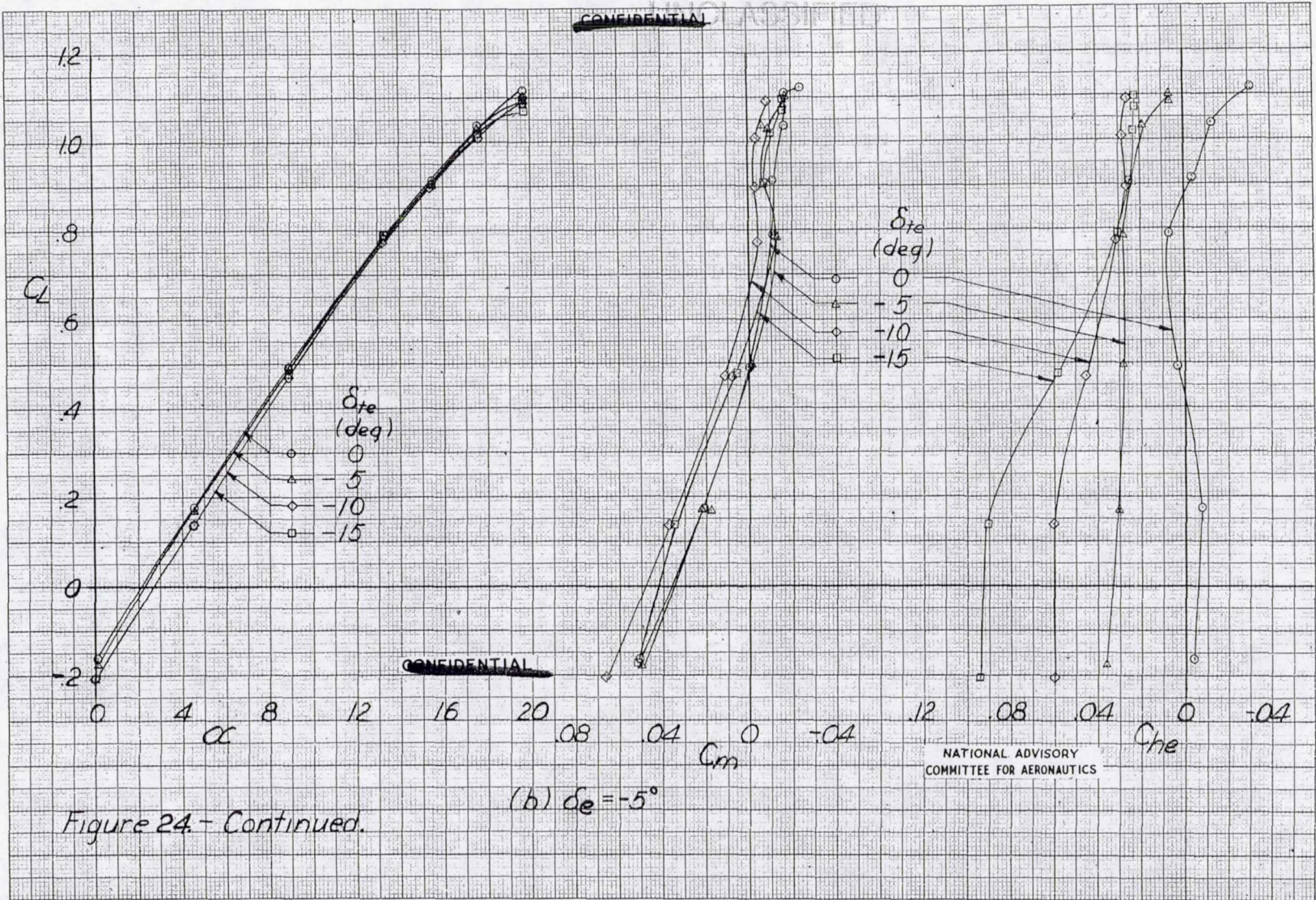


Figure 24 - Continued.

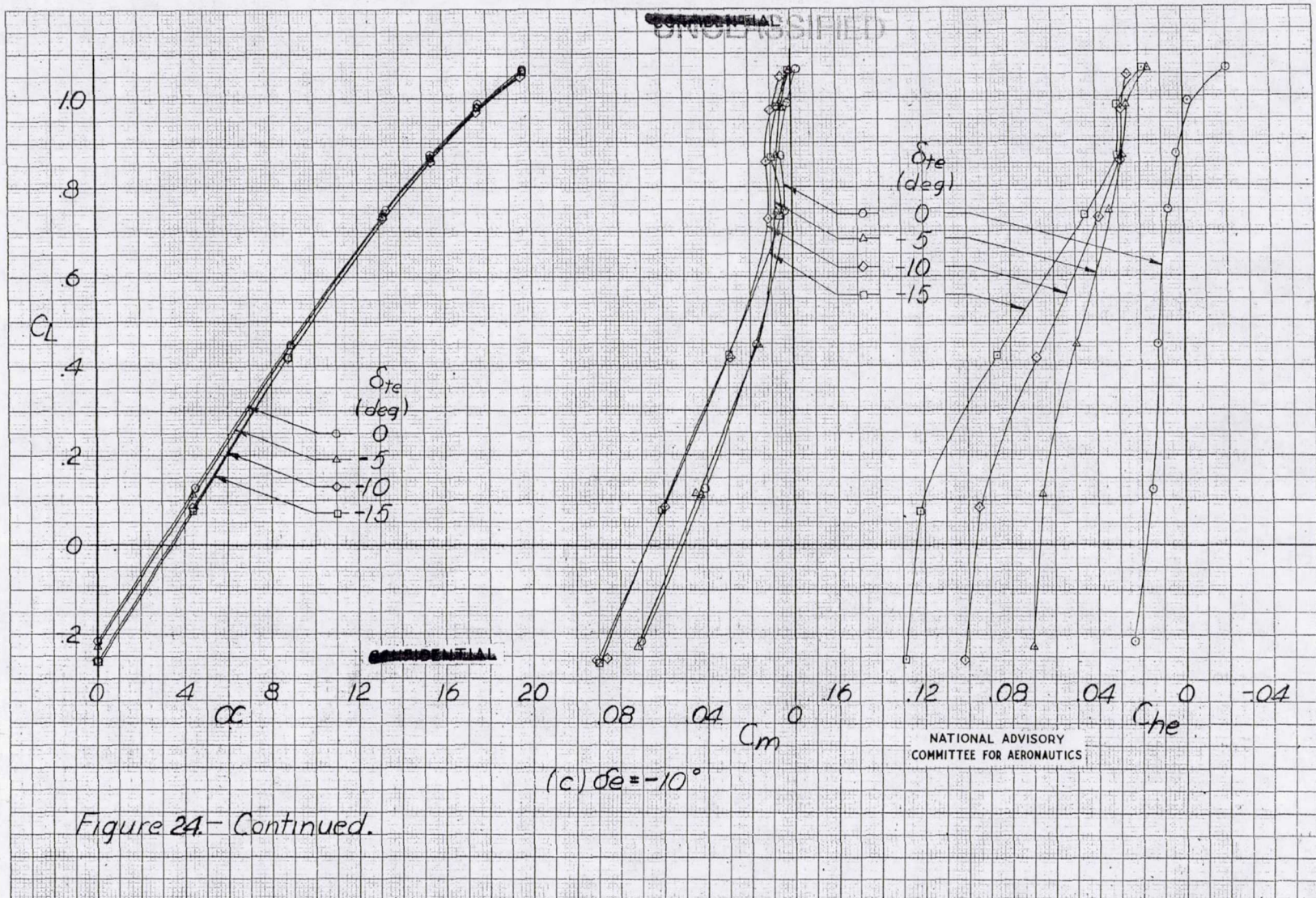
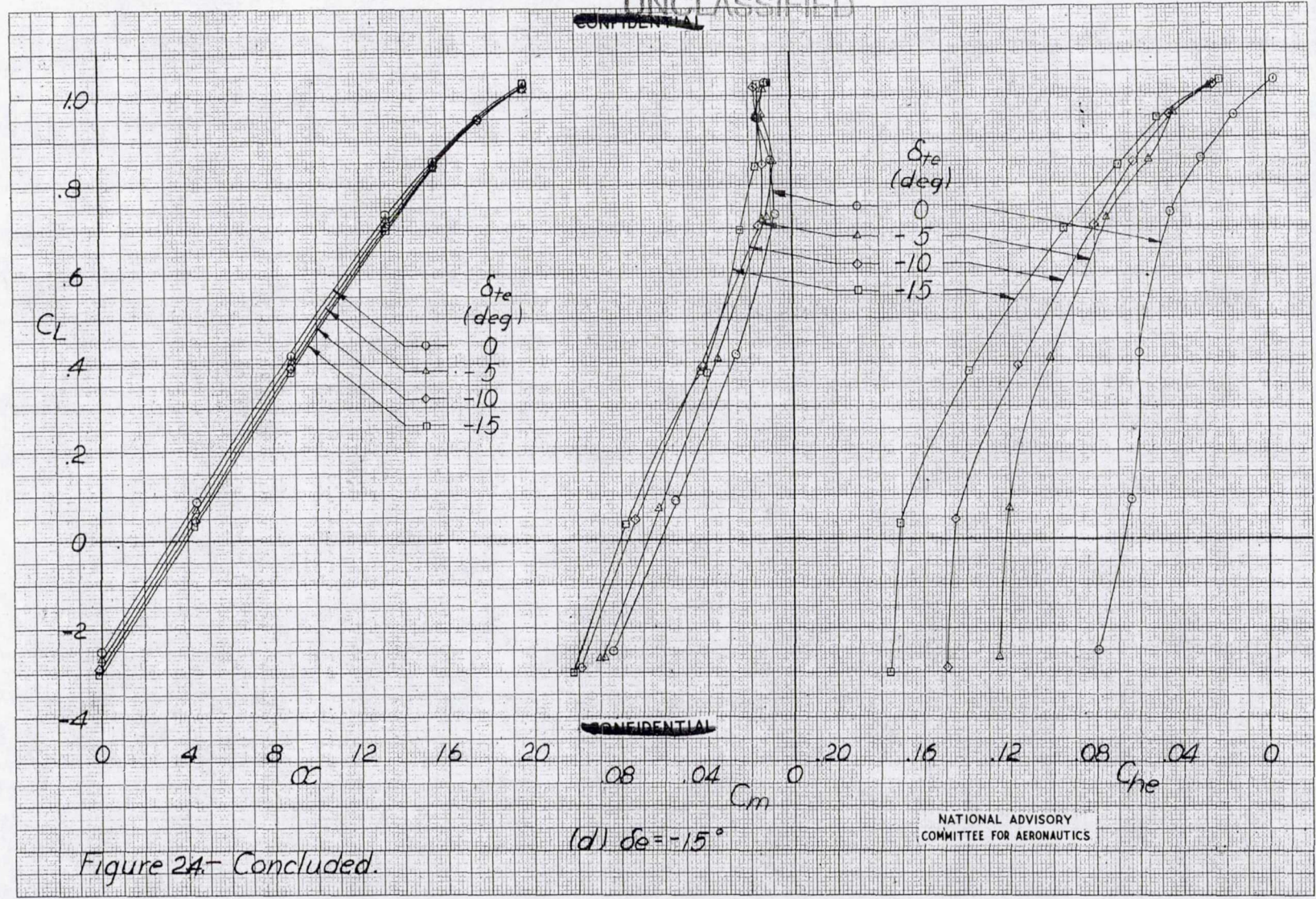


Figure 24- Continued.

UNCLASSIFIED
CONFIDENTIAL



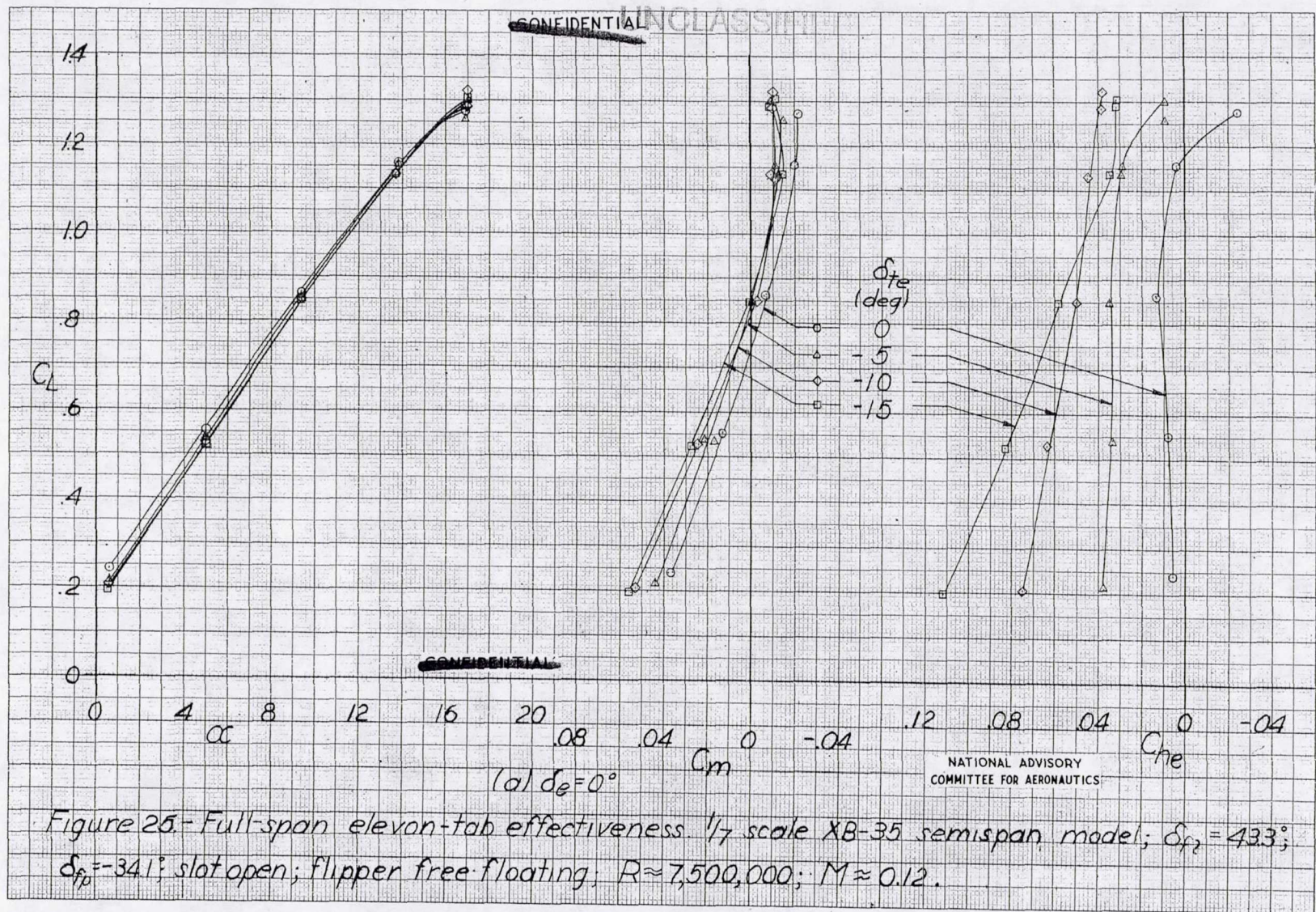
CONFIDENTIAL

(d) $\delta e = -15^\circ$

NATIONAL ADVISORY
COMMITTEE FOR AERONAUTICS

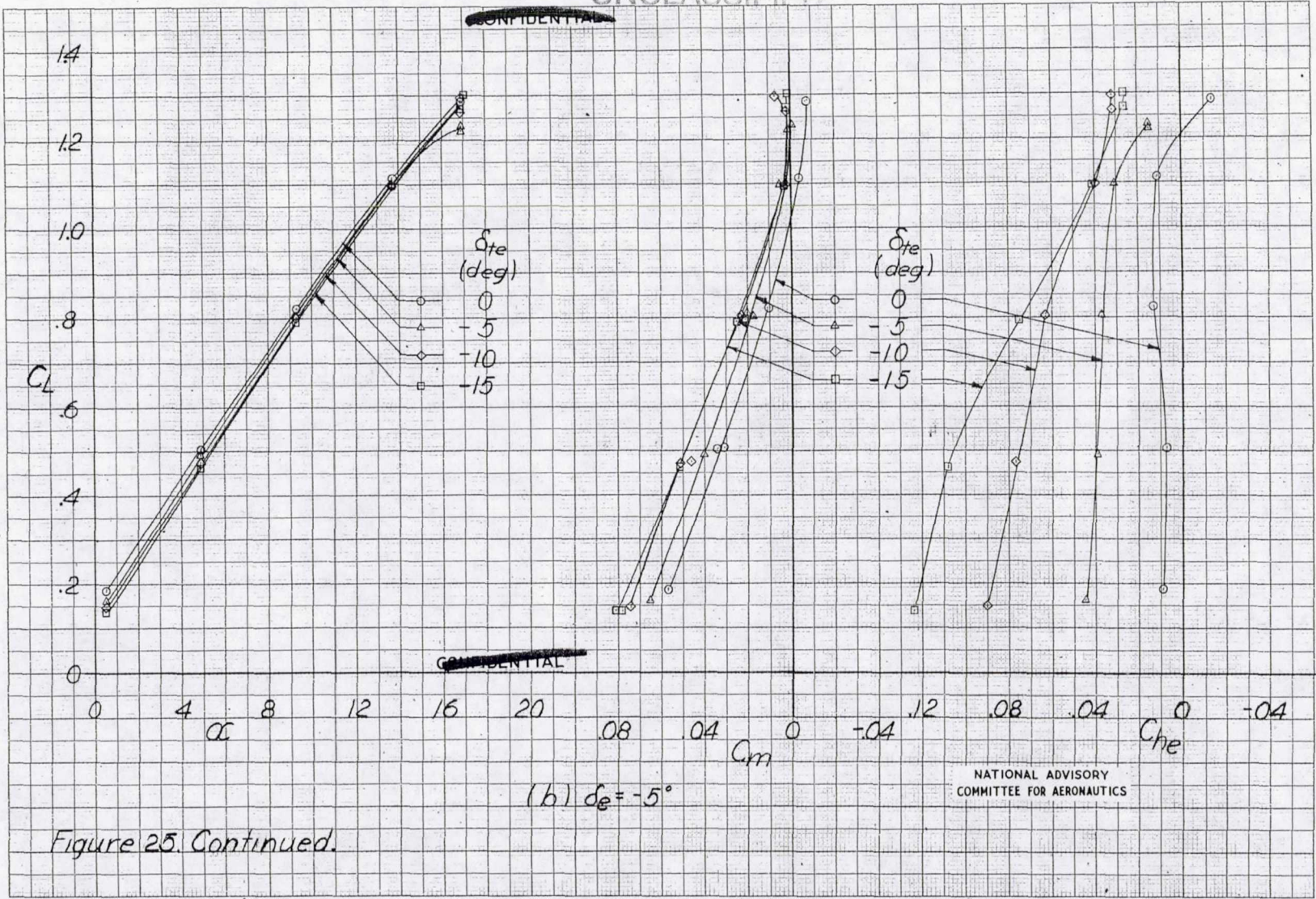
Figure 24.- Concluded.

UNCLASSIFIED



1949

UNCLASSIFIED



CONFIDENTIAL

(b) $\delta_e = -5^\circ$

NATIONAL ADVISORY
COMMITTEE FOR AERONAUTICS

Figure 25. Continued.

UNCLASSIFIED

MR No. 15127

~~CONFIDENTIAL~~ UNCLASSIFIED

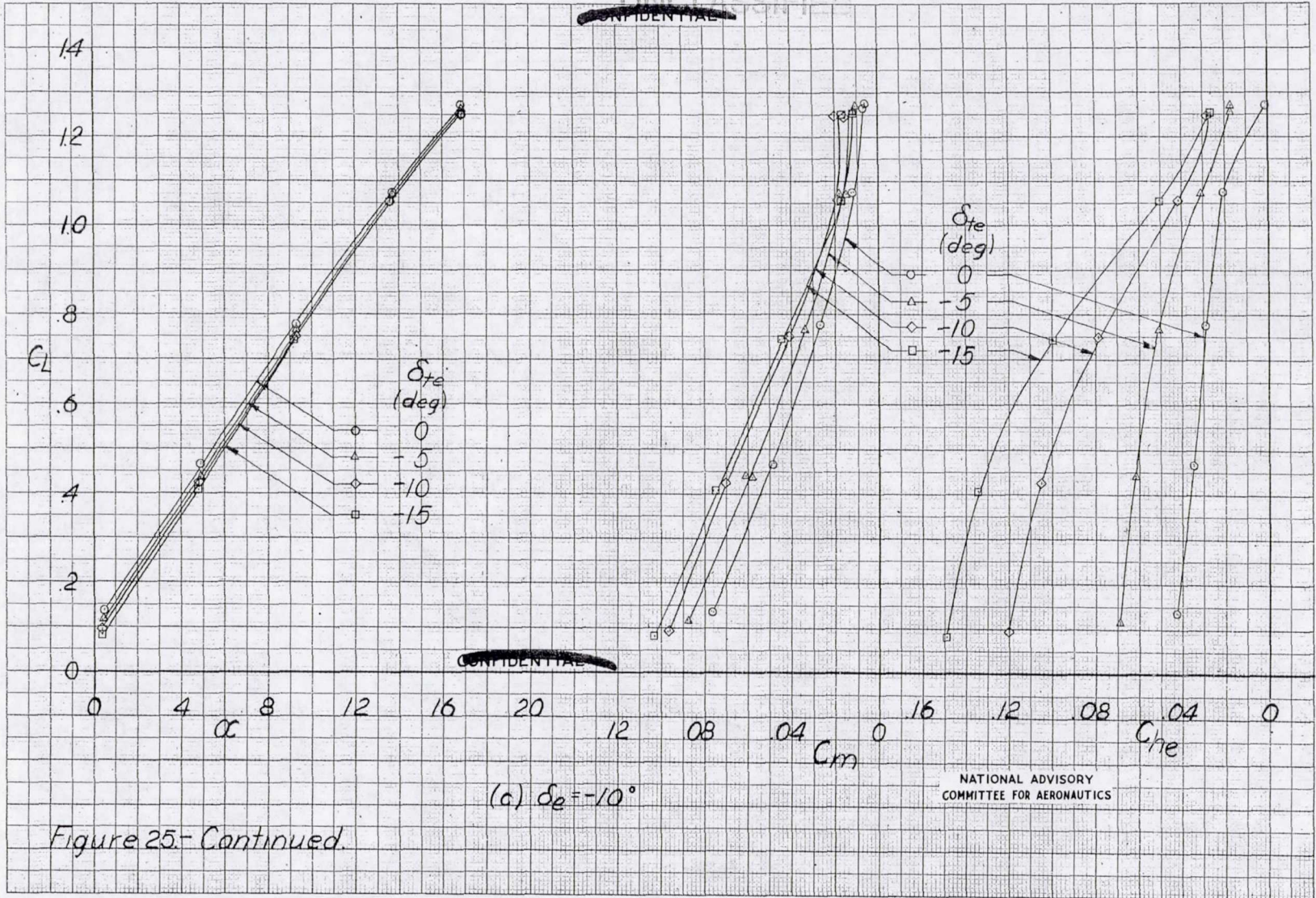
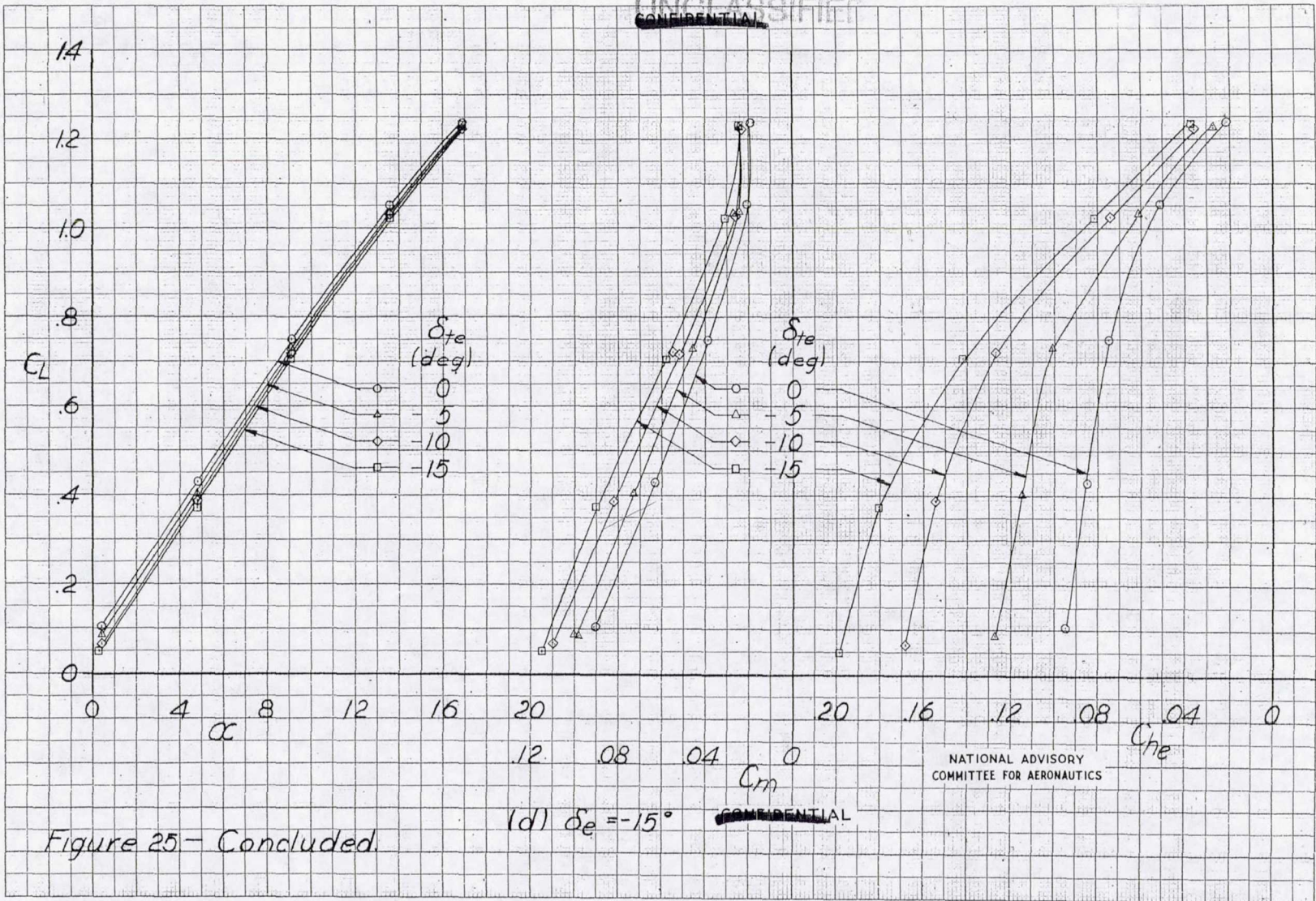


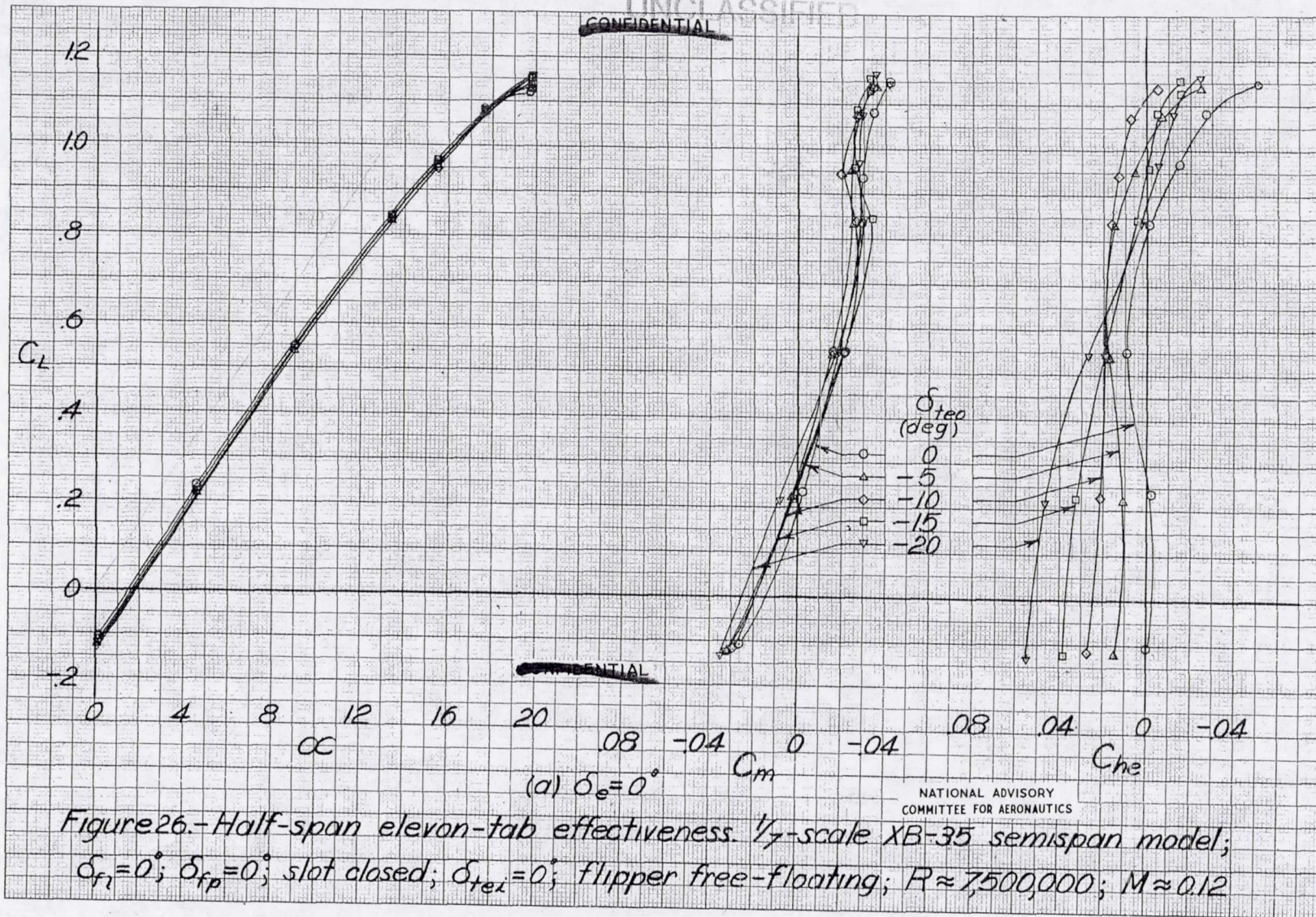
Figure 25.- Continued.

UNCLASSIFIED

~~CONFIDENTIAL~~



UNCLASSIFIED



164508

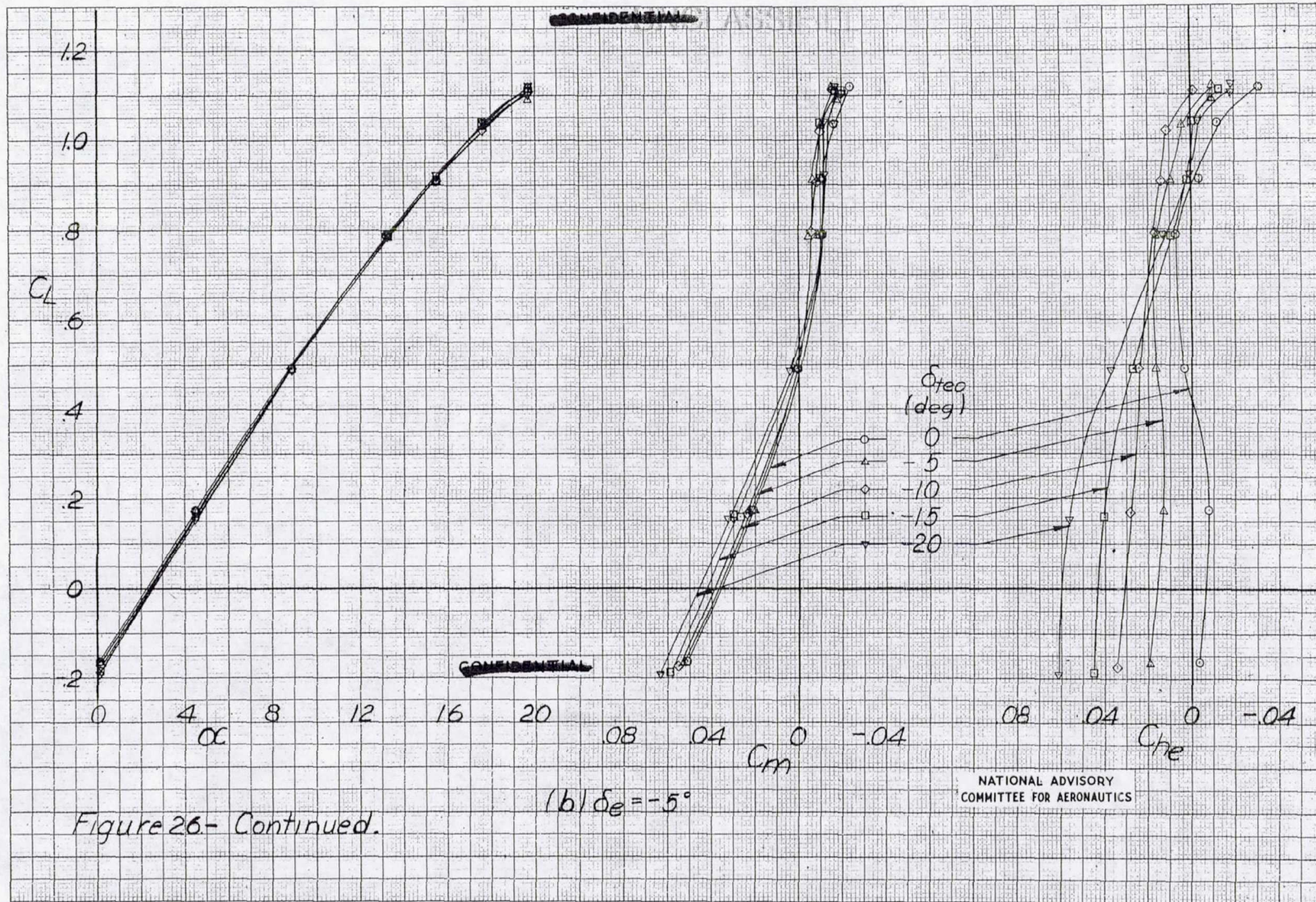


Figure 26- Continued.

MR No. 15L27

UNCLASSIFIED

184506

UNCLASSIFIED

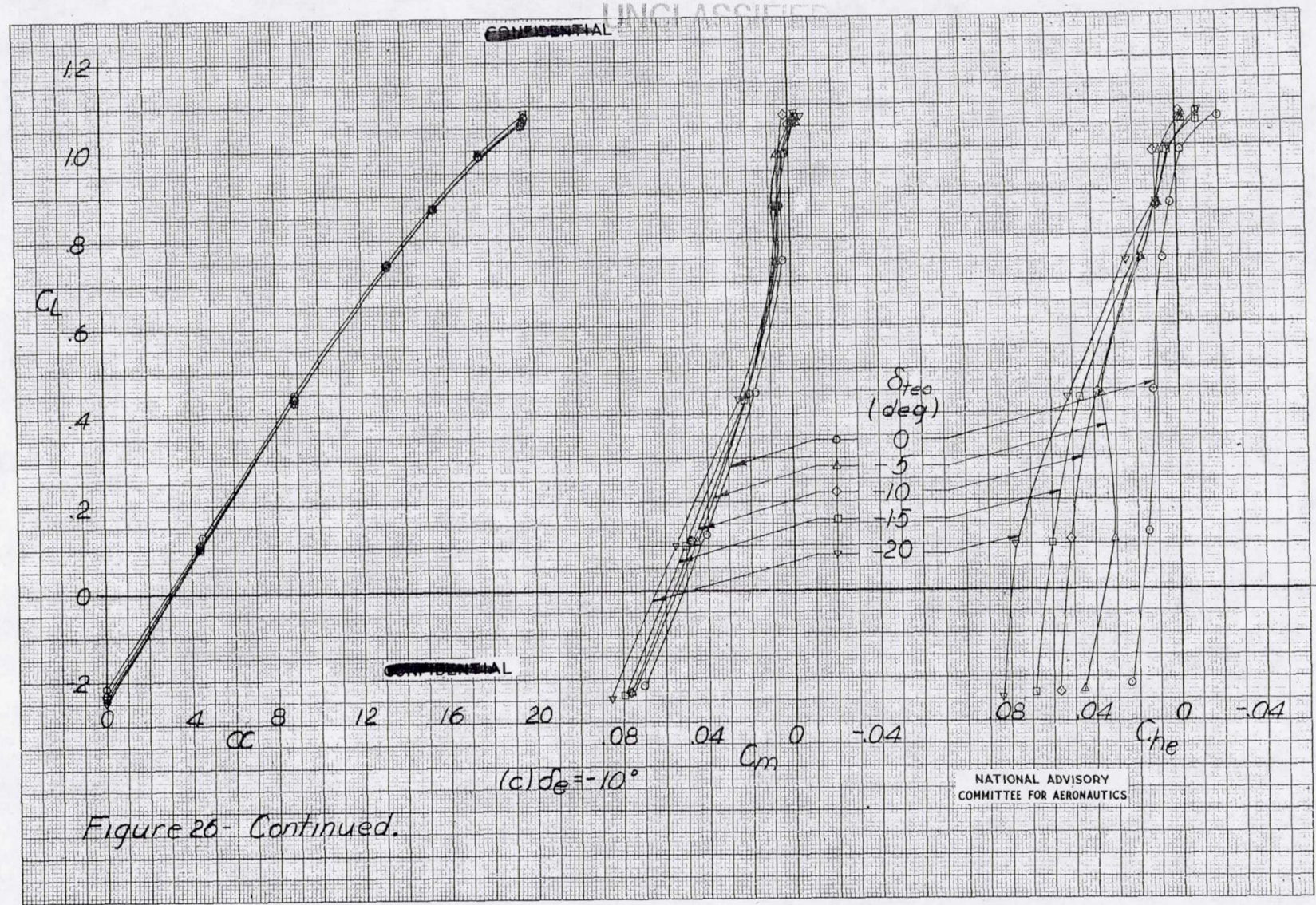


Figure 26-Continued.

MR No. L5L27

UNCLASSIFIED

104506

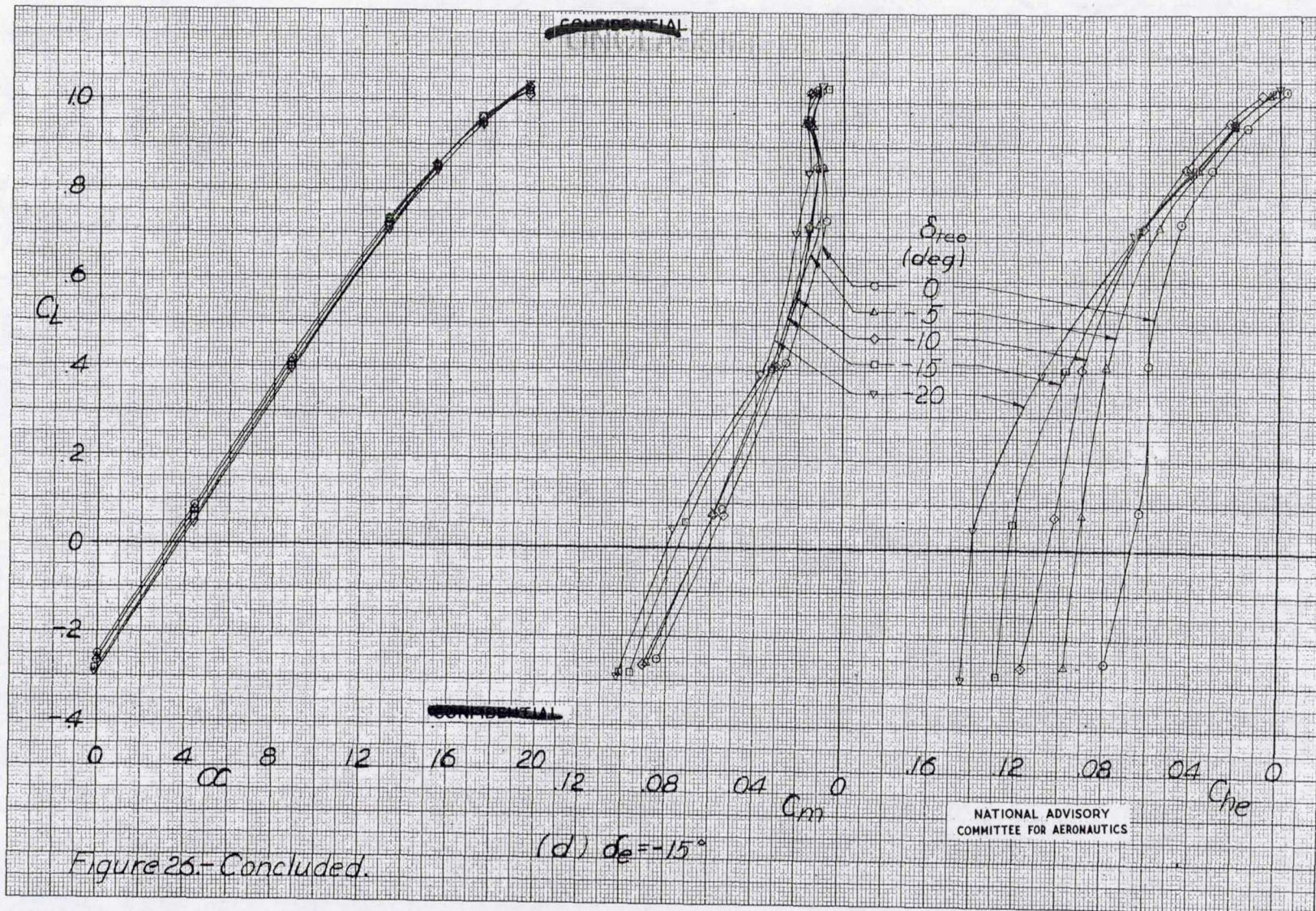
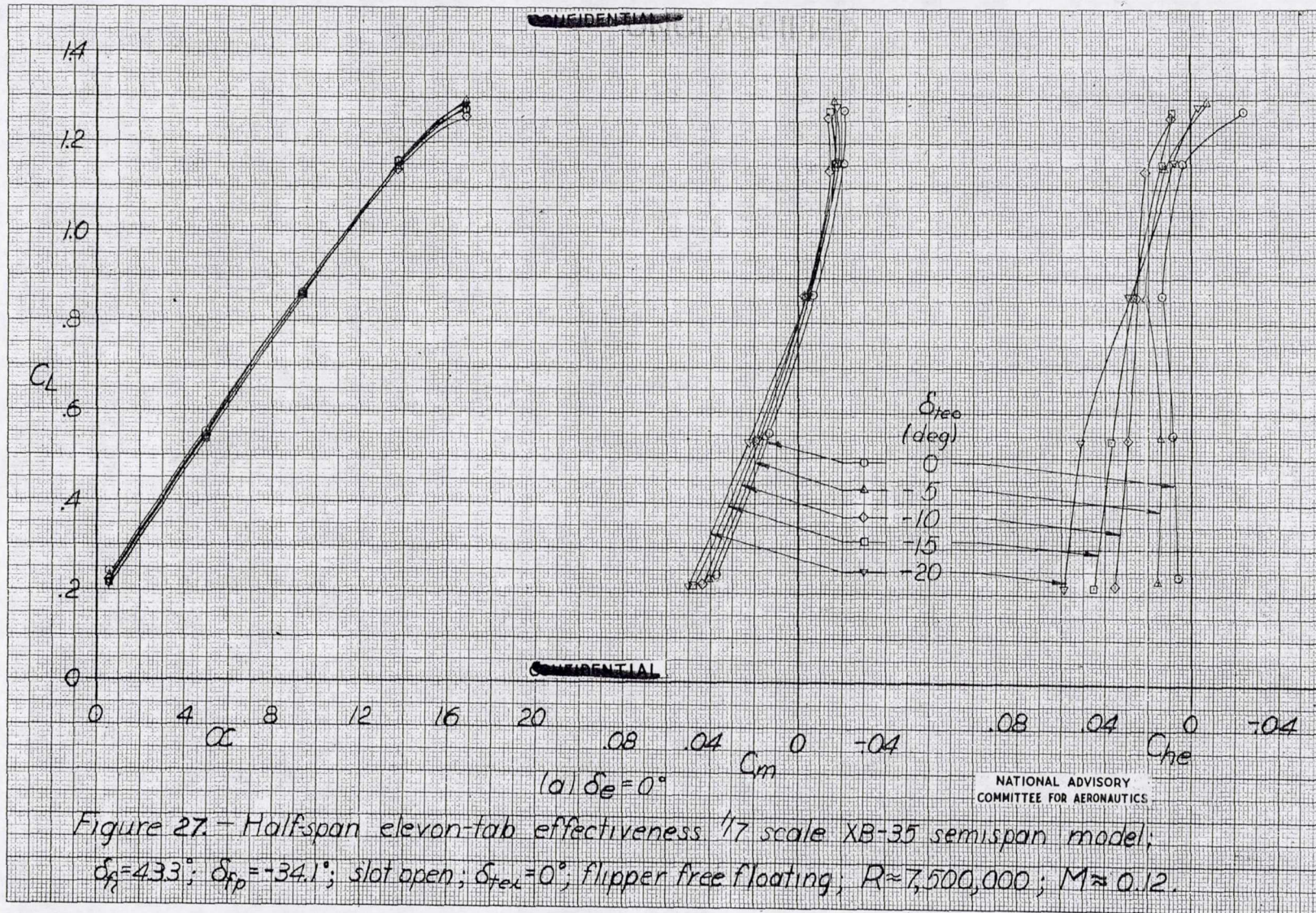


Figure 26.-Concluded.

MR No. L5L27

164507



MR No. 15127

UNCLASSIFIED

184527

UNCLASSIFIED

~~CONFIDENTIAL~~

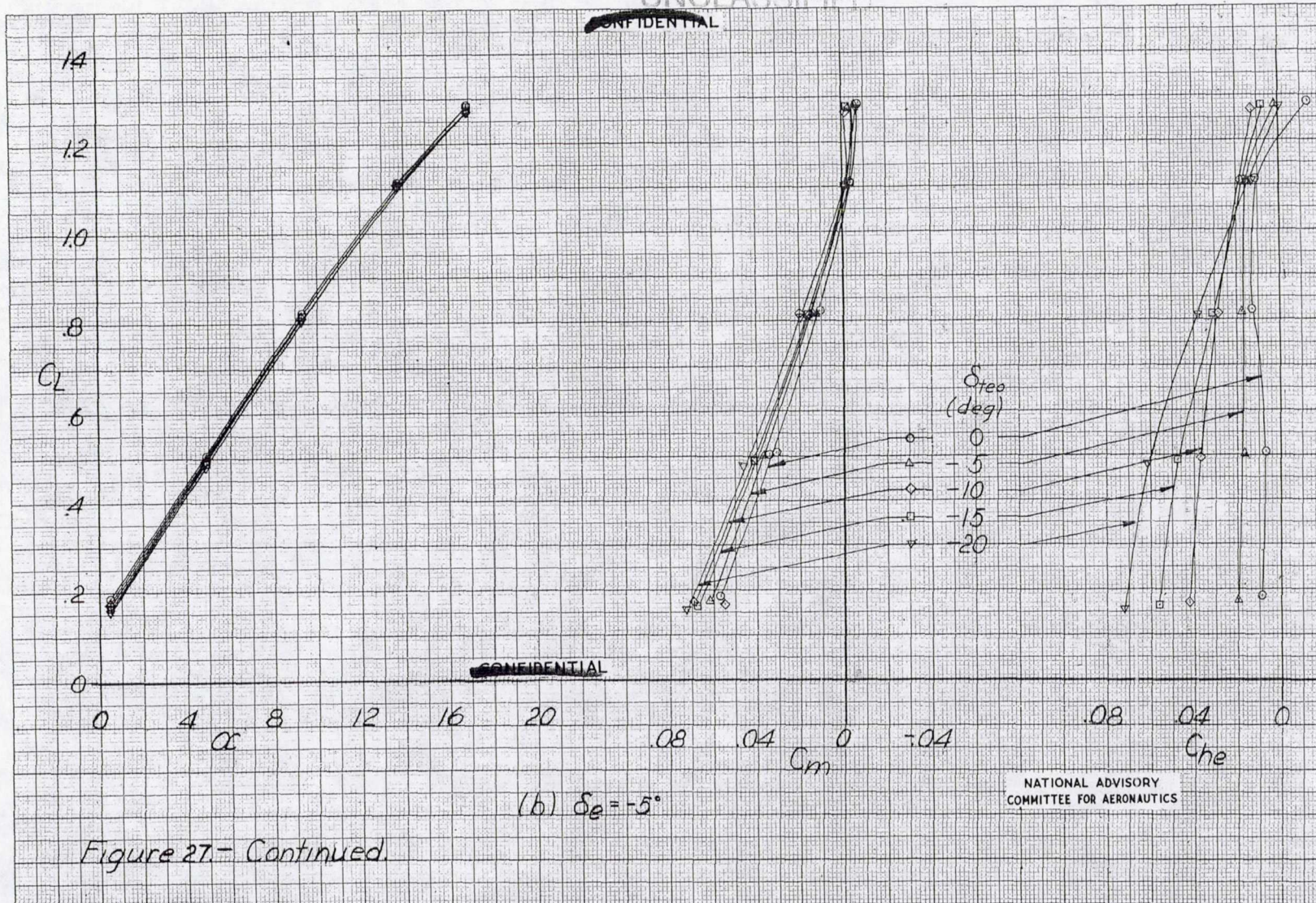


Figure 27- Continued.

MR No. 15127

UNCLASSIFIED

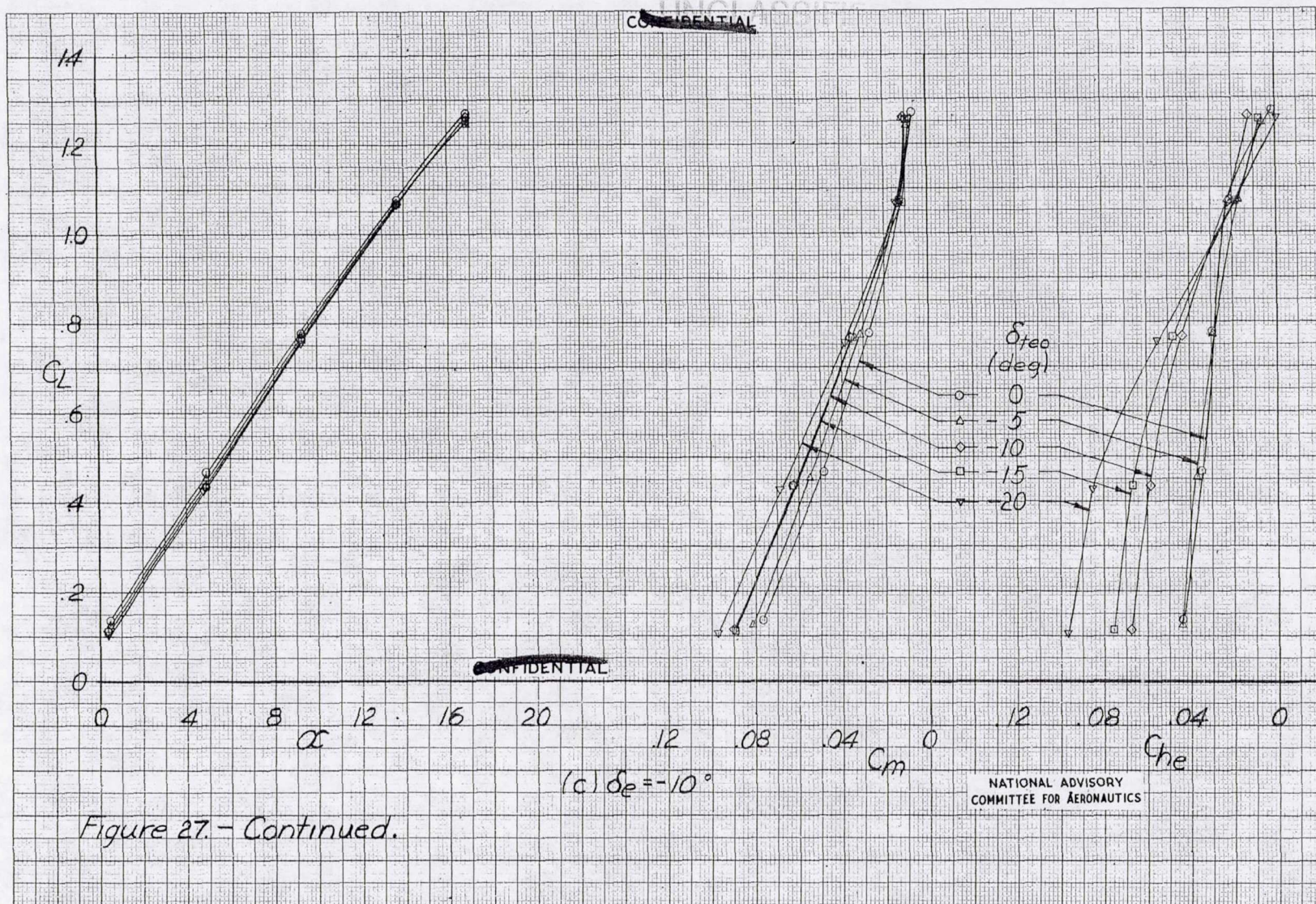


Figure 27. - Continued.

MR. NO. L5L27

164507

UNCLASSIFIED

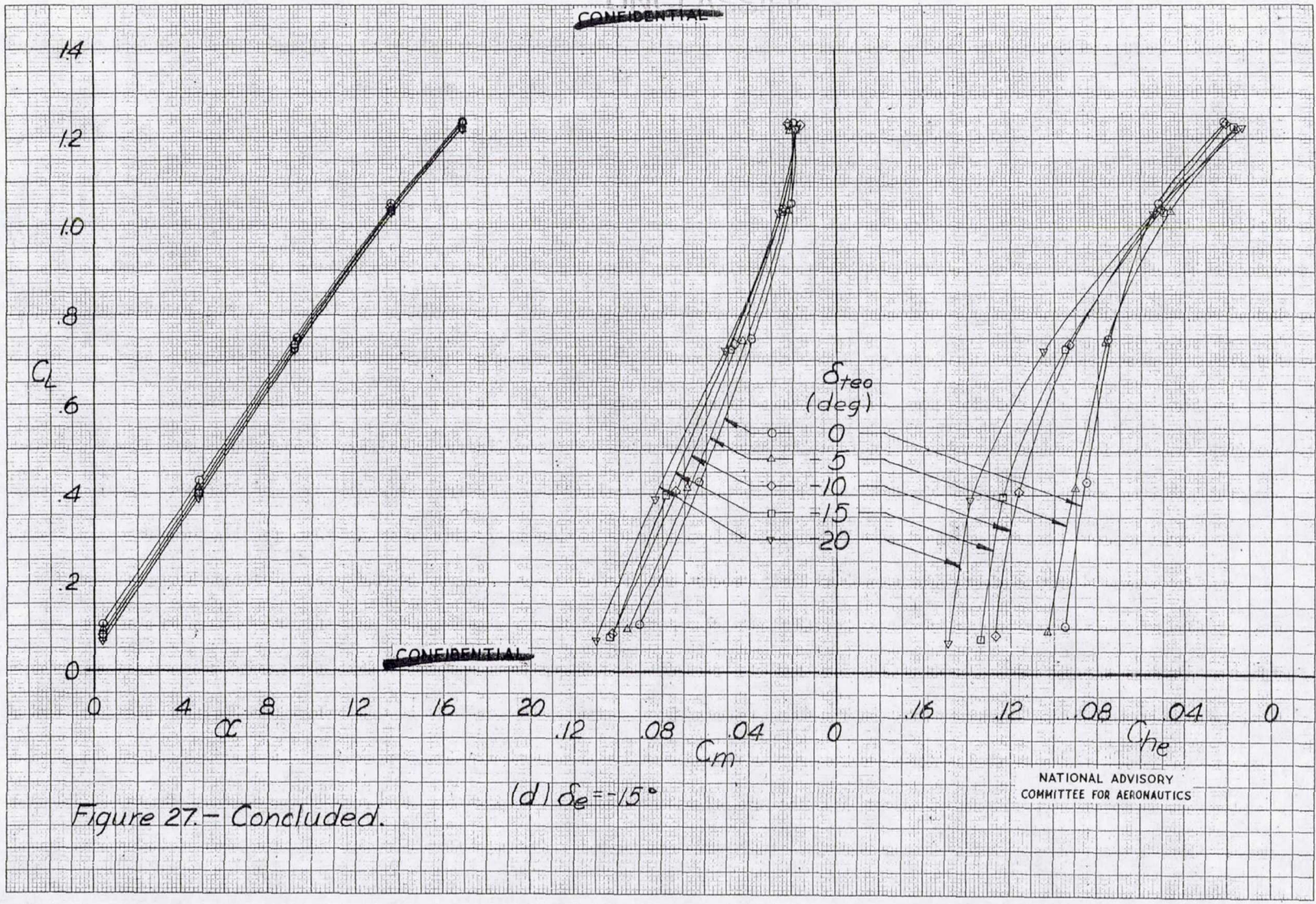


Figure 27.- Concluded.

(d) $\delta_e = -15^\circ$

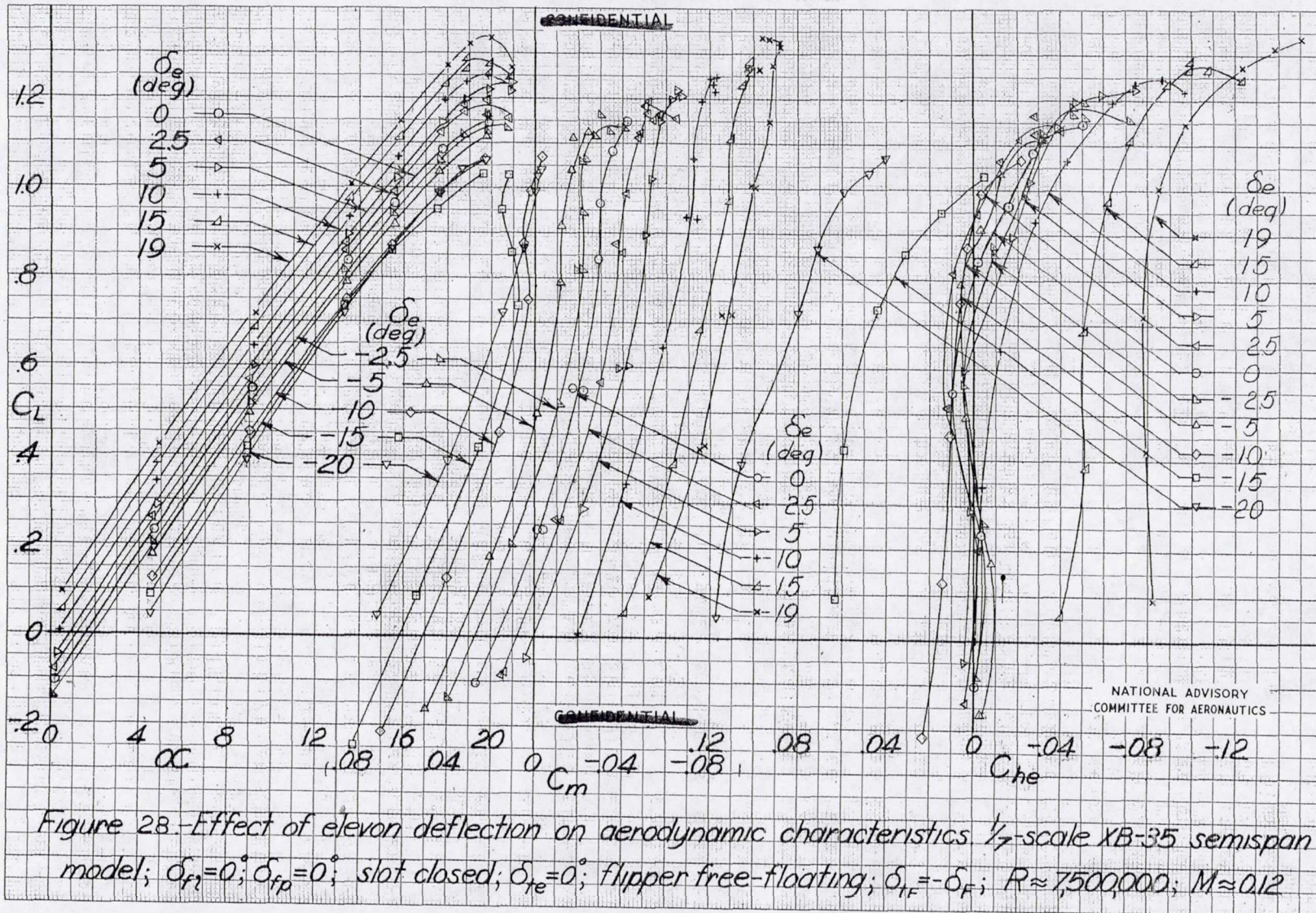
NATIONAL ADVISORY
COMMITTEE FOR AERONAUTICS

MR No. L5L27

UNCLASSIFIED

104508

UNCLASSIFIED



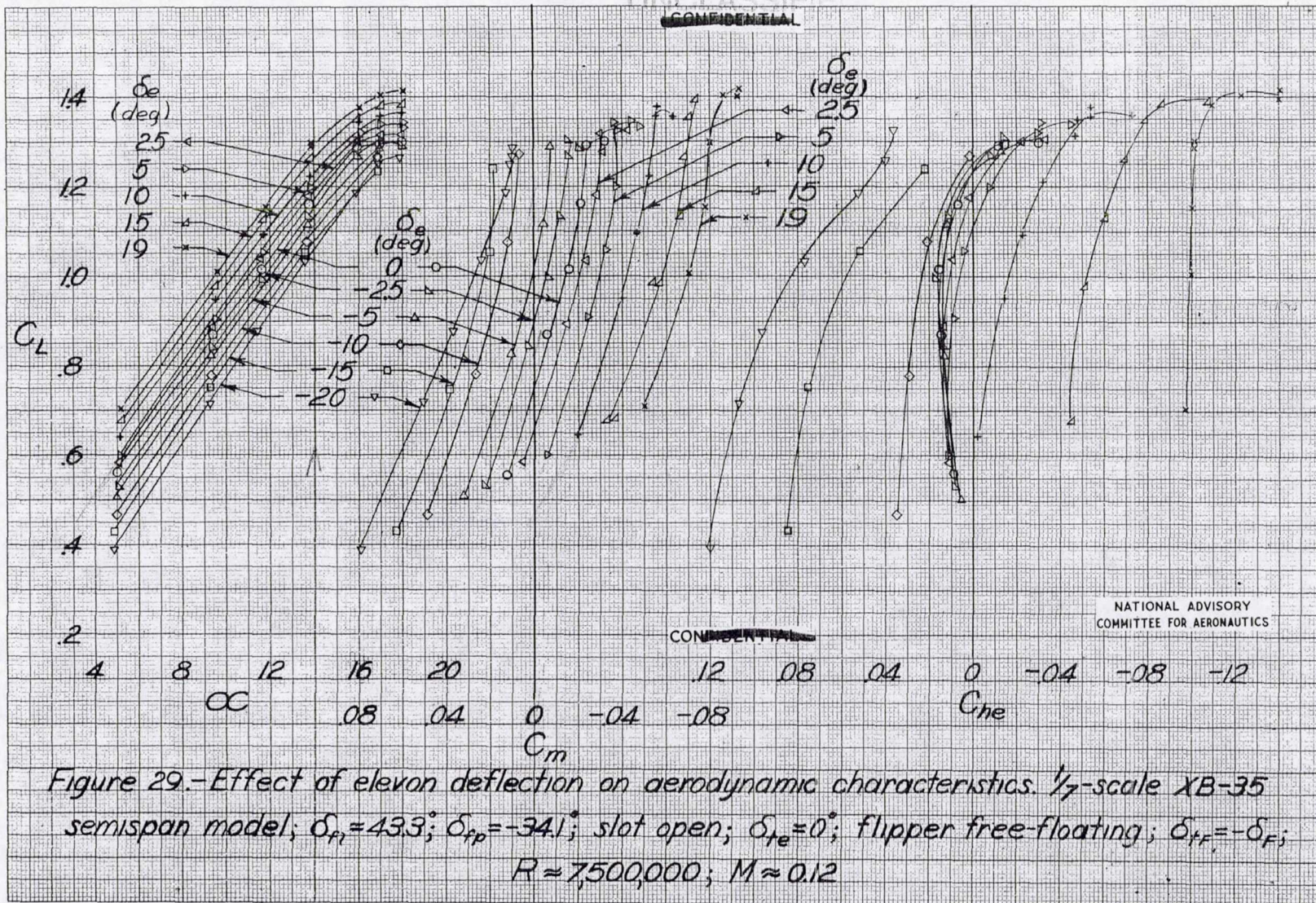
MR No. L5L27

UNCLASSIFIED

164509

UNCLASSIFIED

CONFIDENTIAL



NATIONAL ADVISORY COMMITTEE FOR AERONAUTICS

CONFIDENTIAL

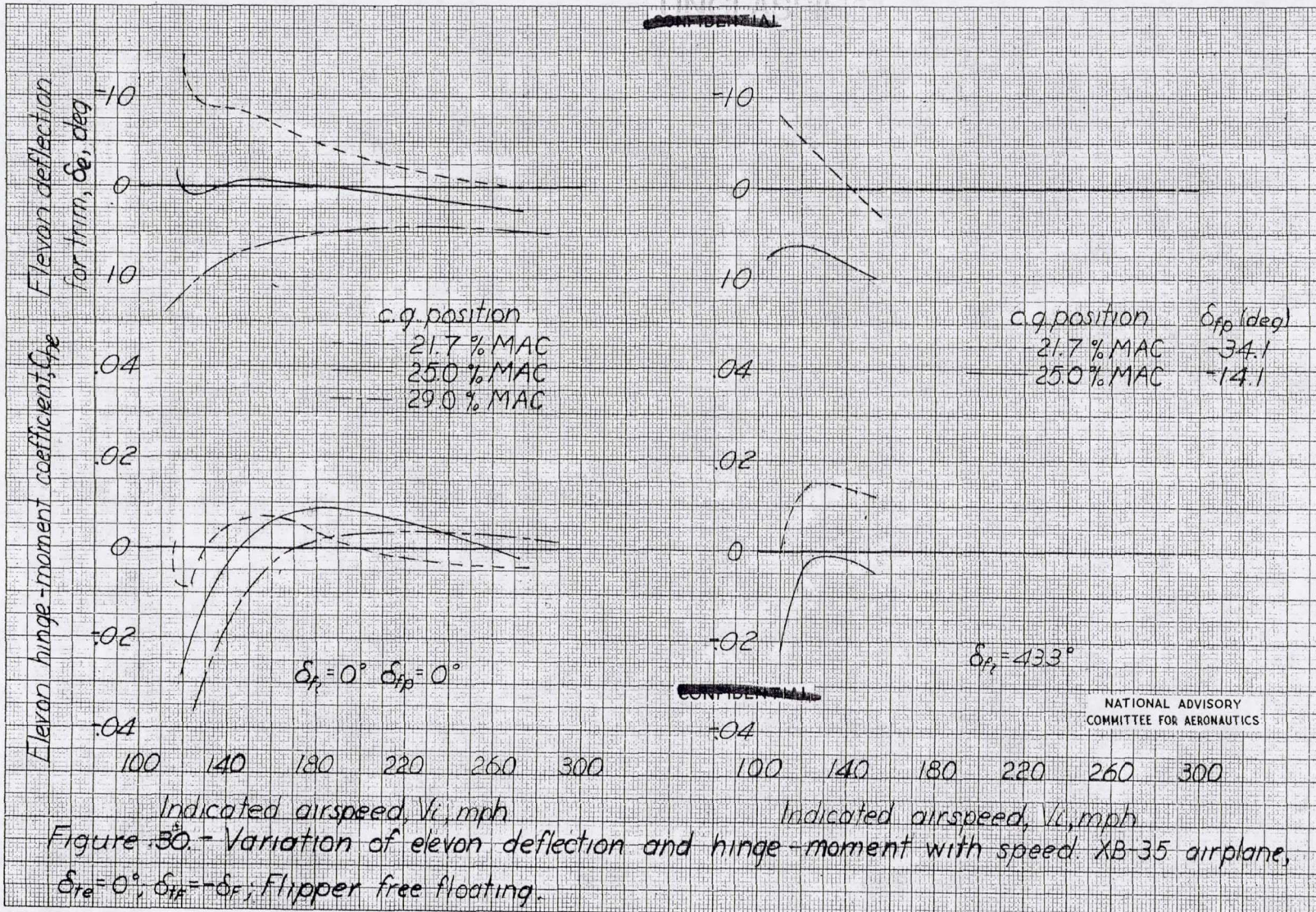
Figure 29.- Effect of elevon deflection on aerodynamic characteristics. $1/7$ -scale XB-35 semispan model; $\delta_{F1} = 43.3^\circ$; $\delta_{F2} = -34.1^\circ$; slot open; $\delta_{Te} = 0^\circ$; flipper free-floating; $\delta_{FF} = -\delta_F$; $R = 7,500,000$; $M \approx 0.12$

MR No. 15127

UNCLASSIFIED

164530

~~CONFIDENTIAL~~



~~CONFIDENTIAL~~

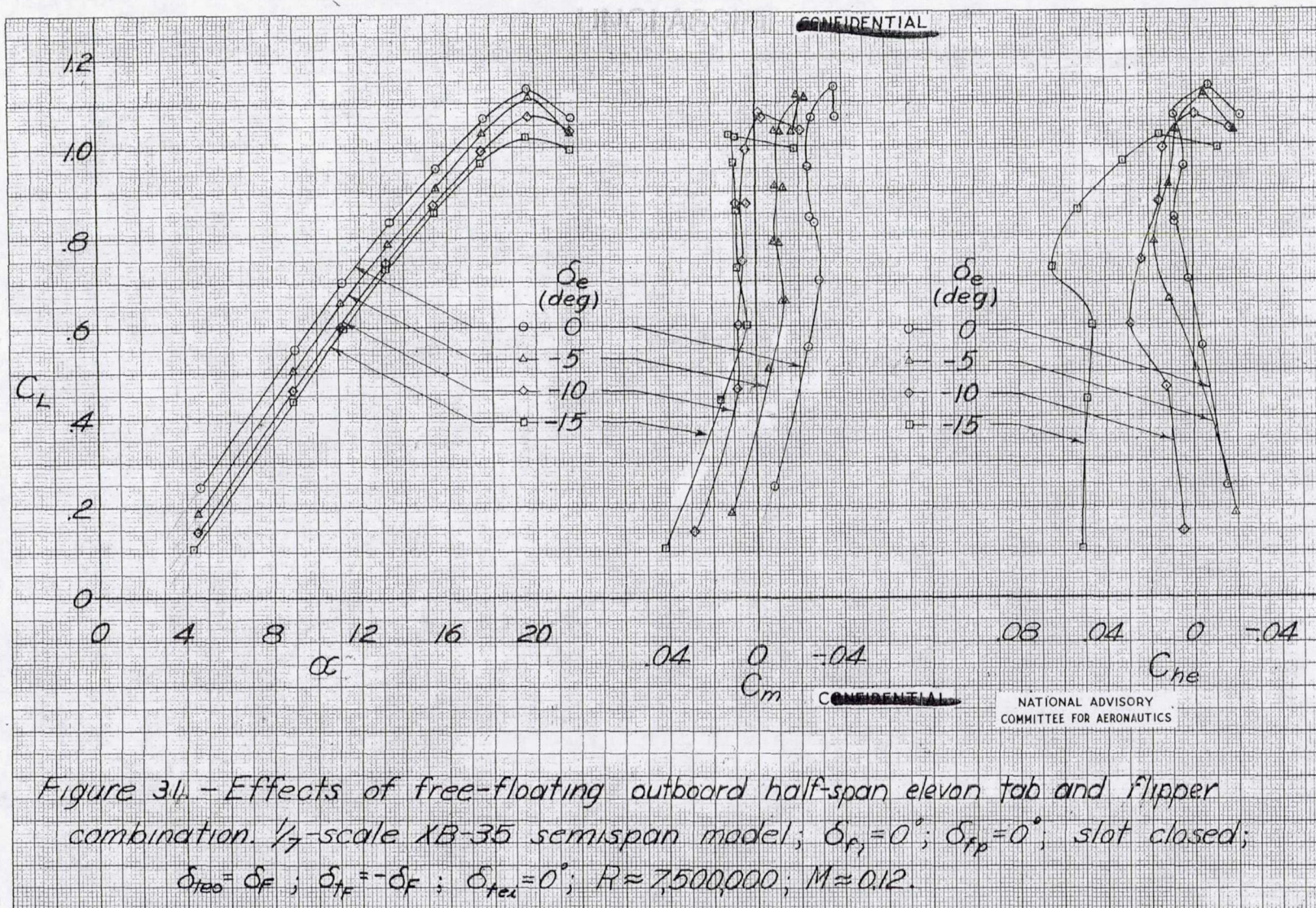
NATIONAL ADVISORY COMMITTEE FOR AERONAUTICS

Figure 30. - Variation of elevon deflection and hinge-moment with speed. XB-35 airplane, $\delta_{re} = 0^\circ$; $\delta_{ra} = -\delta_r$; Flipper free floating.

MR No. L5L27

UNCLASSIFIED

104531

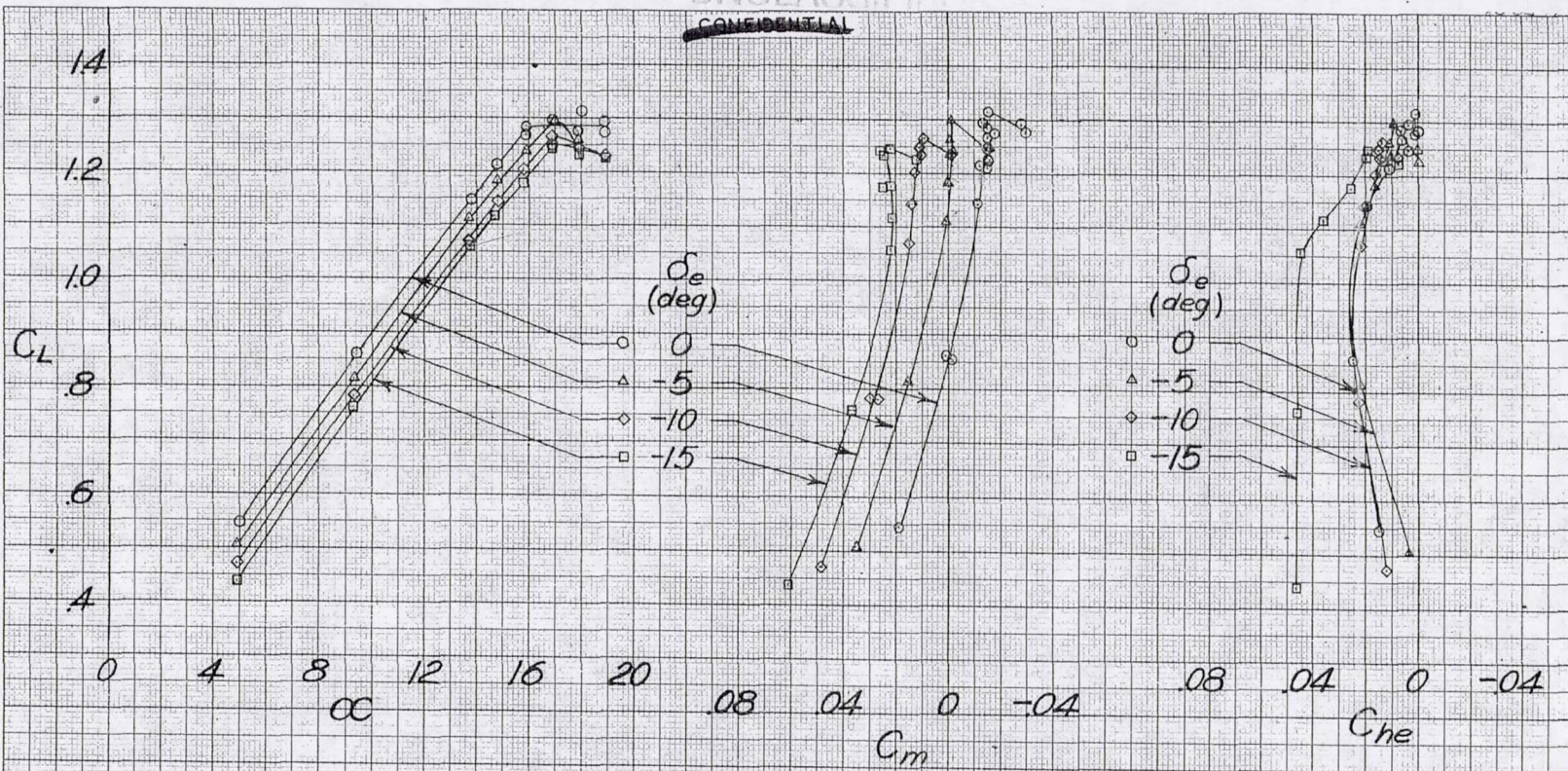


MR No. L5L27

UNCLASSIFIED

UNCLASSIFIED

~~CONFIDENTIAL~~



~~CONFIDENTIAL~~

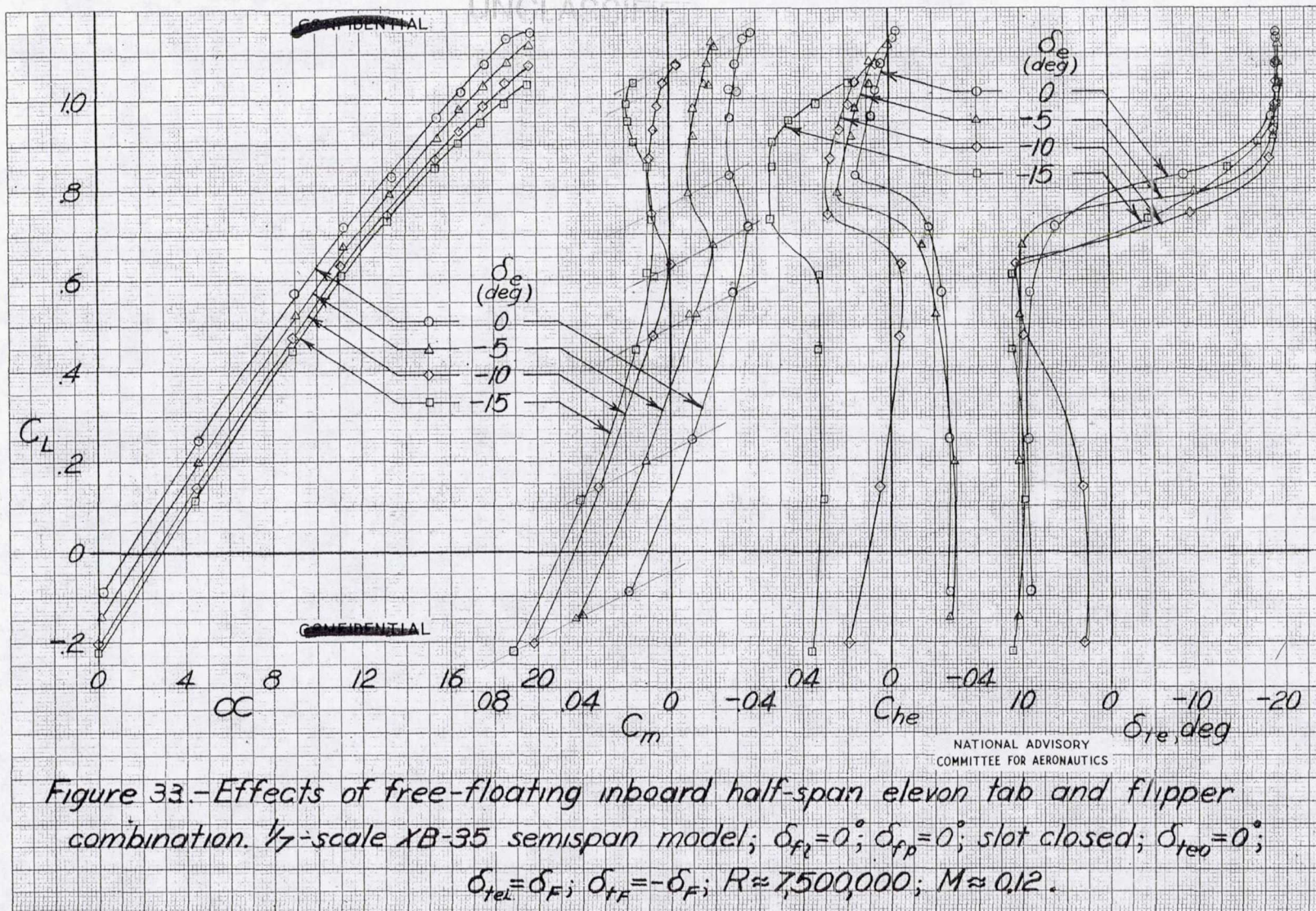
NATIONAL ADVISORY
COMMITTEE FOR AERONAUTICS

Figure 32.- Effects of free-floating outboard half-span elevon tab and flipper combination.

$1/7$ -scale XB-35 semispan model; $\delta_r = 43.3^\circ$; $\delta_{fp} = -34.1^\circ$; slot closed; $\delta_{tex} = 0^\circ$; $\delta_{teo} = \delta_F$;
 $\delta_{TF} = -\delta_F$; $R = 7,500,000$; $M \approx 0.12$.

MR No. L5L27

UNCLASSIFIED



UNCLASSIFIED

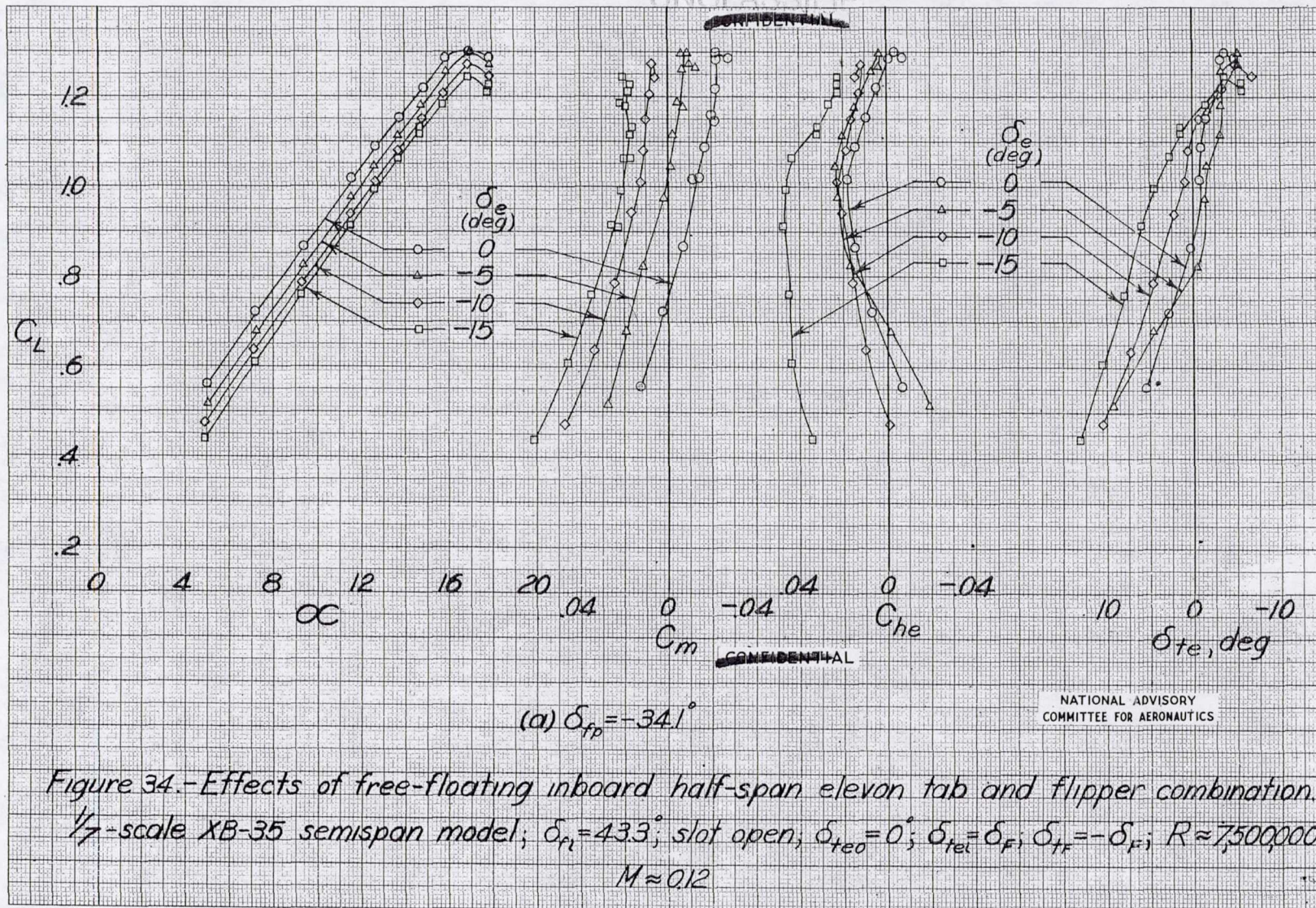


Figure 34.- Effects of free-floating inboard half-span elevator tab and flipper combination. $1/7$ -scale XB-35 semispan model; $\delta_{fi} = 43.3^\circ$; slot open; $\delta_{te0} = 0^\circ$; $\delta_{te} = \delta_{fi}$; $\delta_{te} = -\delta_{fi}$; $R \approx 7,500,000$; $M \approx 0.12$

MR No. L5L27

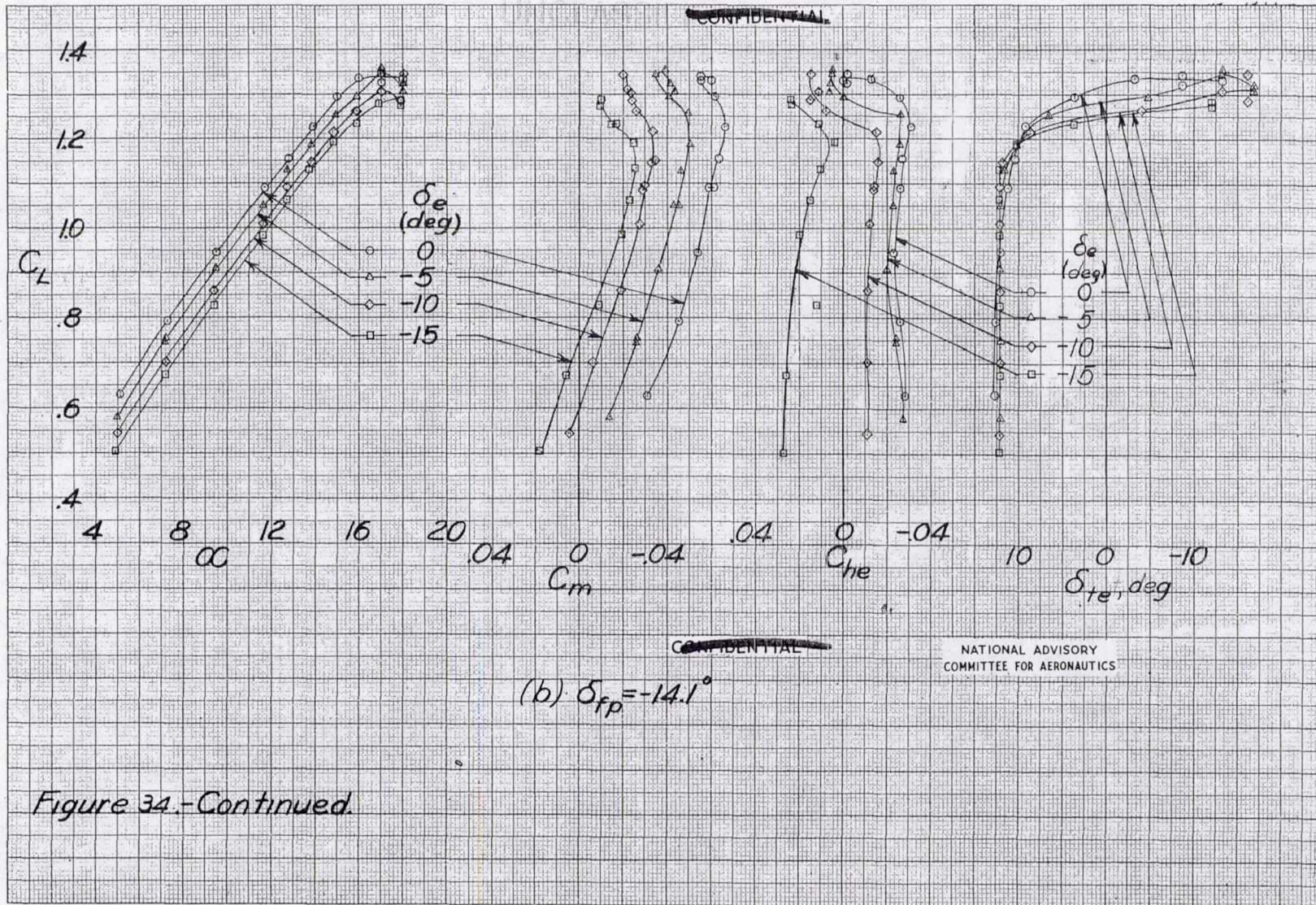


Figure 34.-Continued.

194504

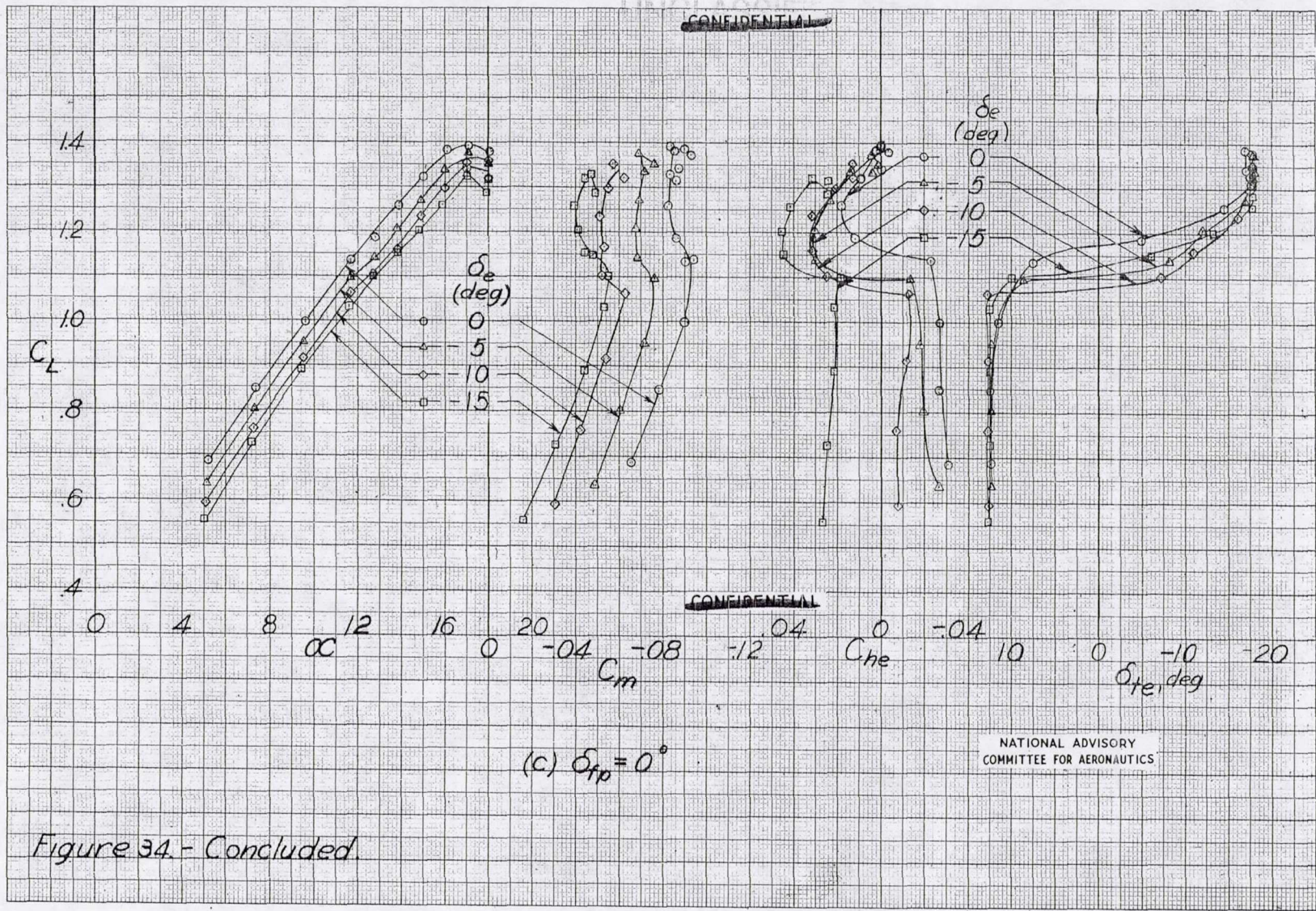
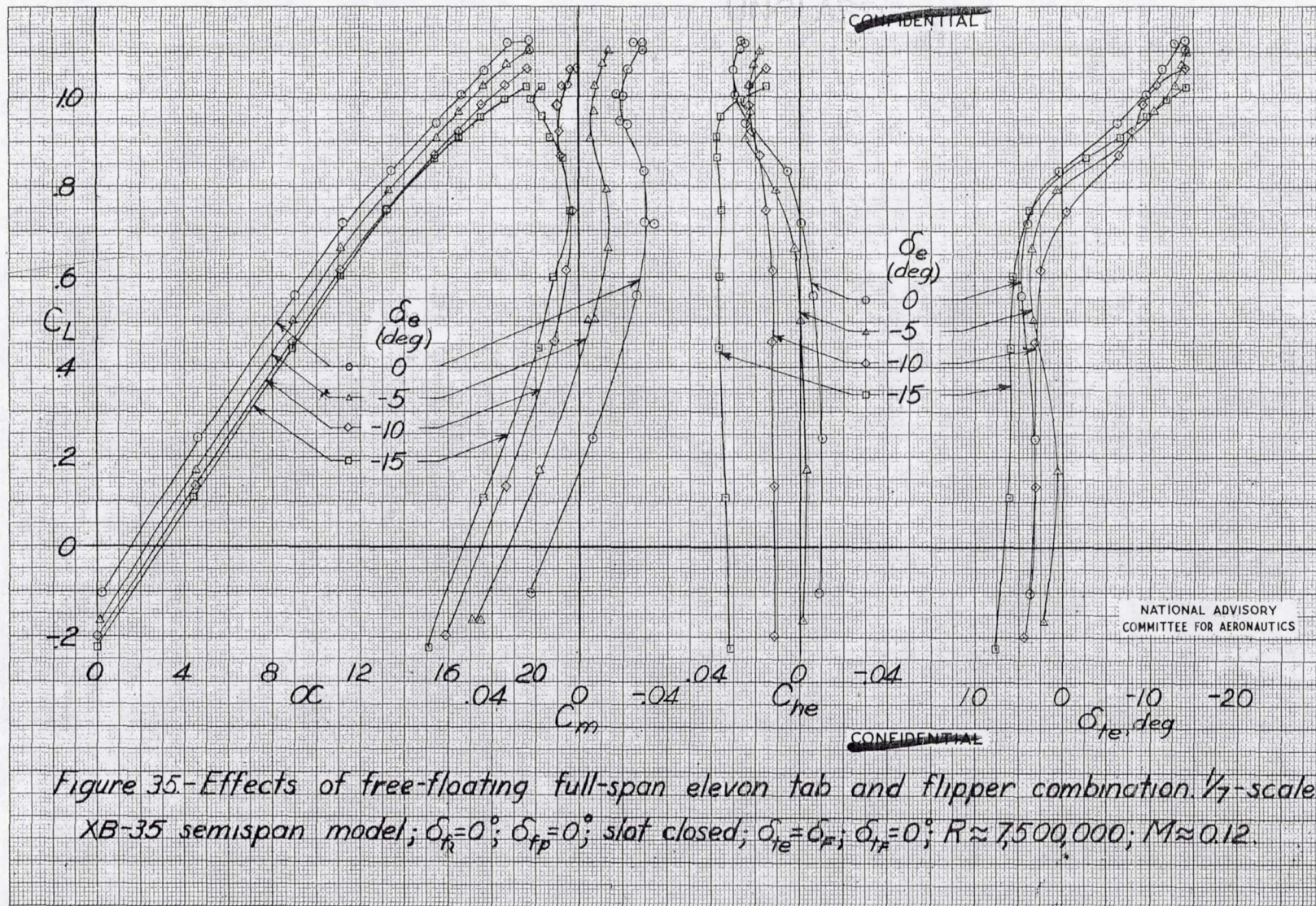


Figure 34 - Concluded

MR No. 15127

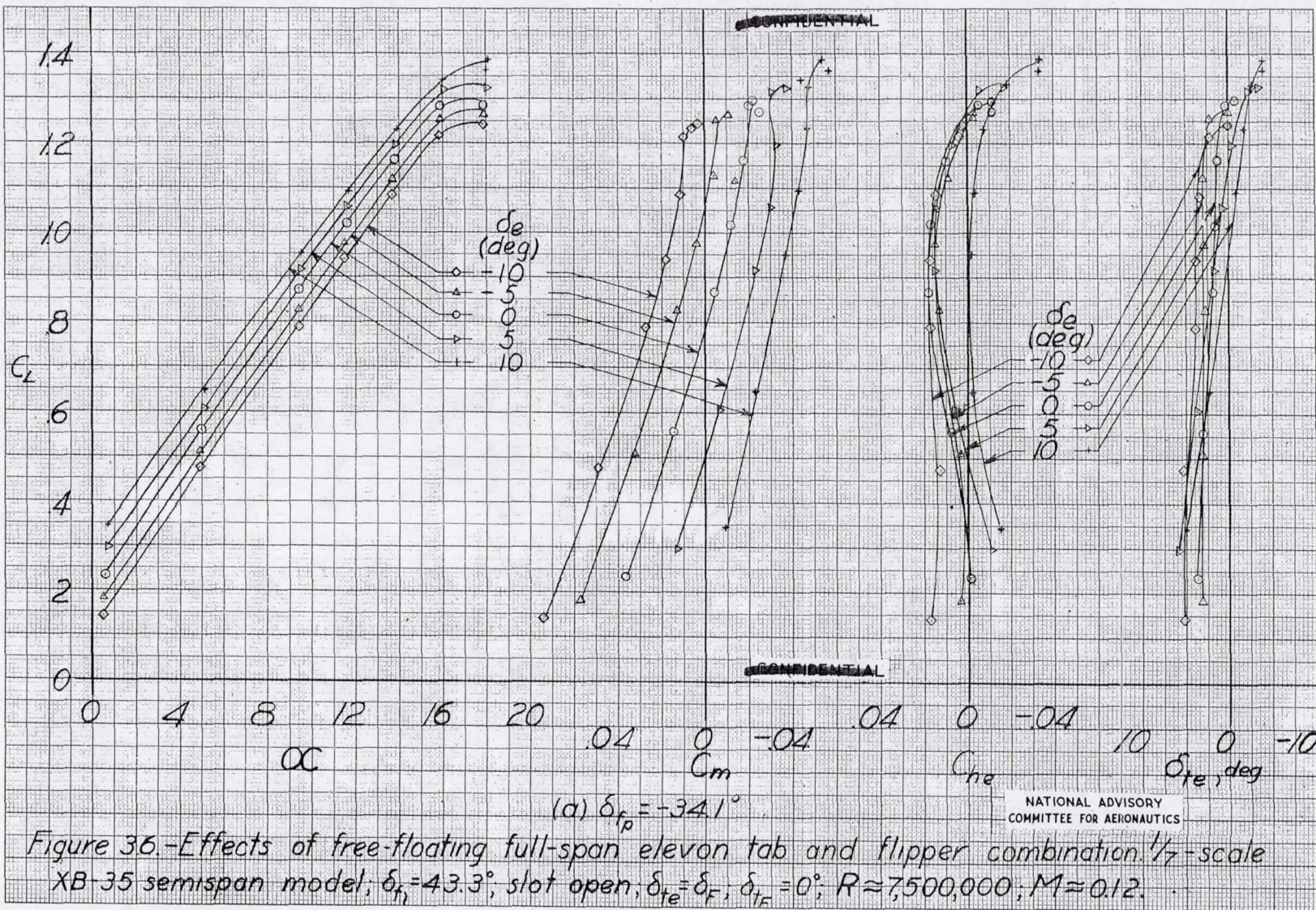
UNCLASSIFIED

104505



MR No. L5L27

UNCLASSIFIED



MR No. L5L27

104535

UNCLASSIFIED
CONFIDENTIAL

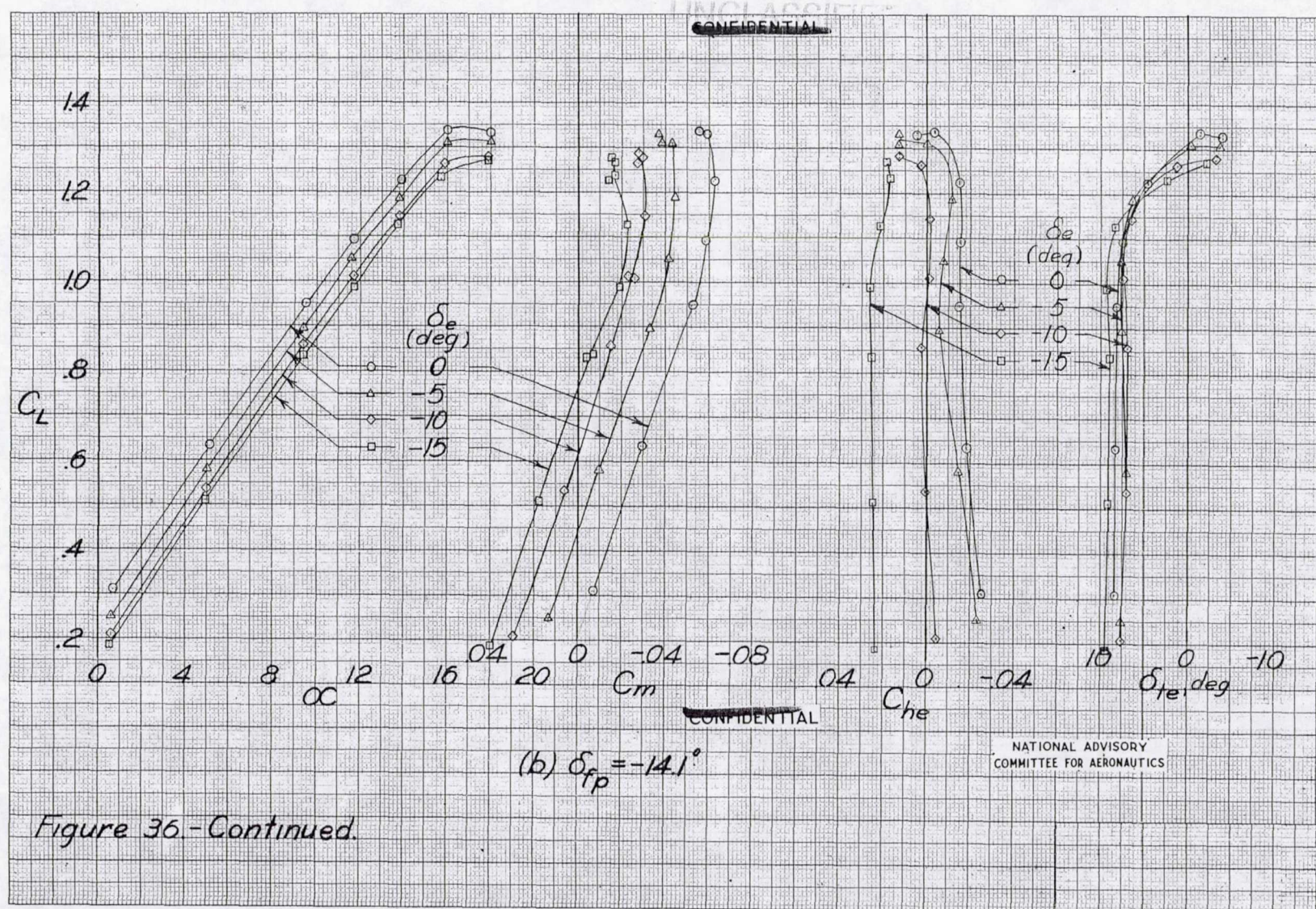


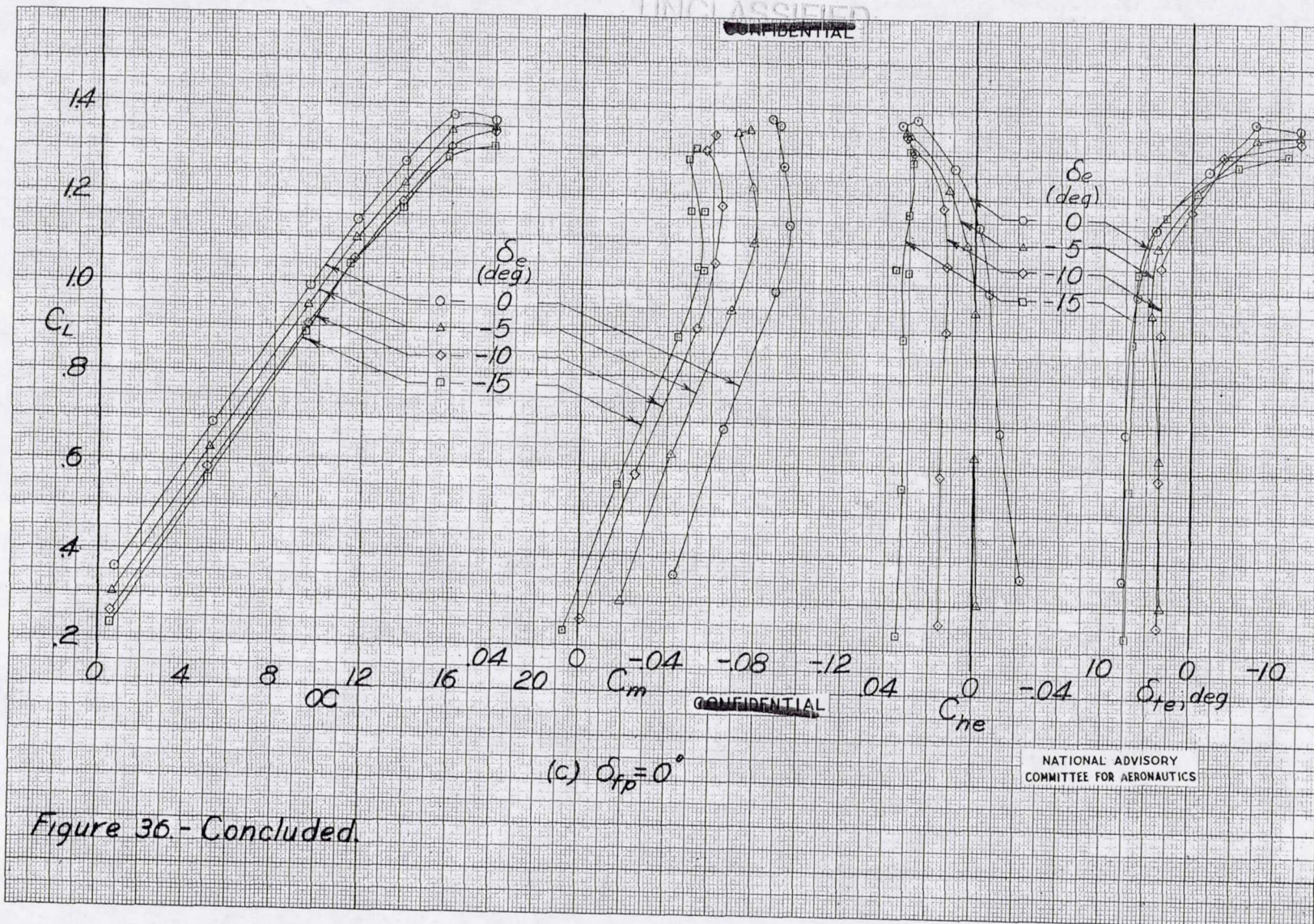
Figure 36 - Continued.

NATIONAL ADVISORY
COMMITTEE FOR AERONAUTICS

MR No. L5L27

UNCLASSIFIED

UNCLASSIFIED
CONFIDENTIAL



CONFIDENTIAL

NATIONAL ADVISORY
COMMITTEE FOR AERONAUTICS

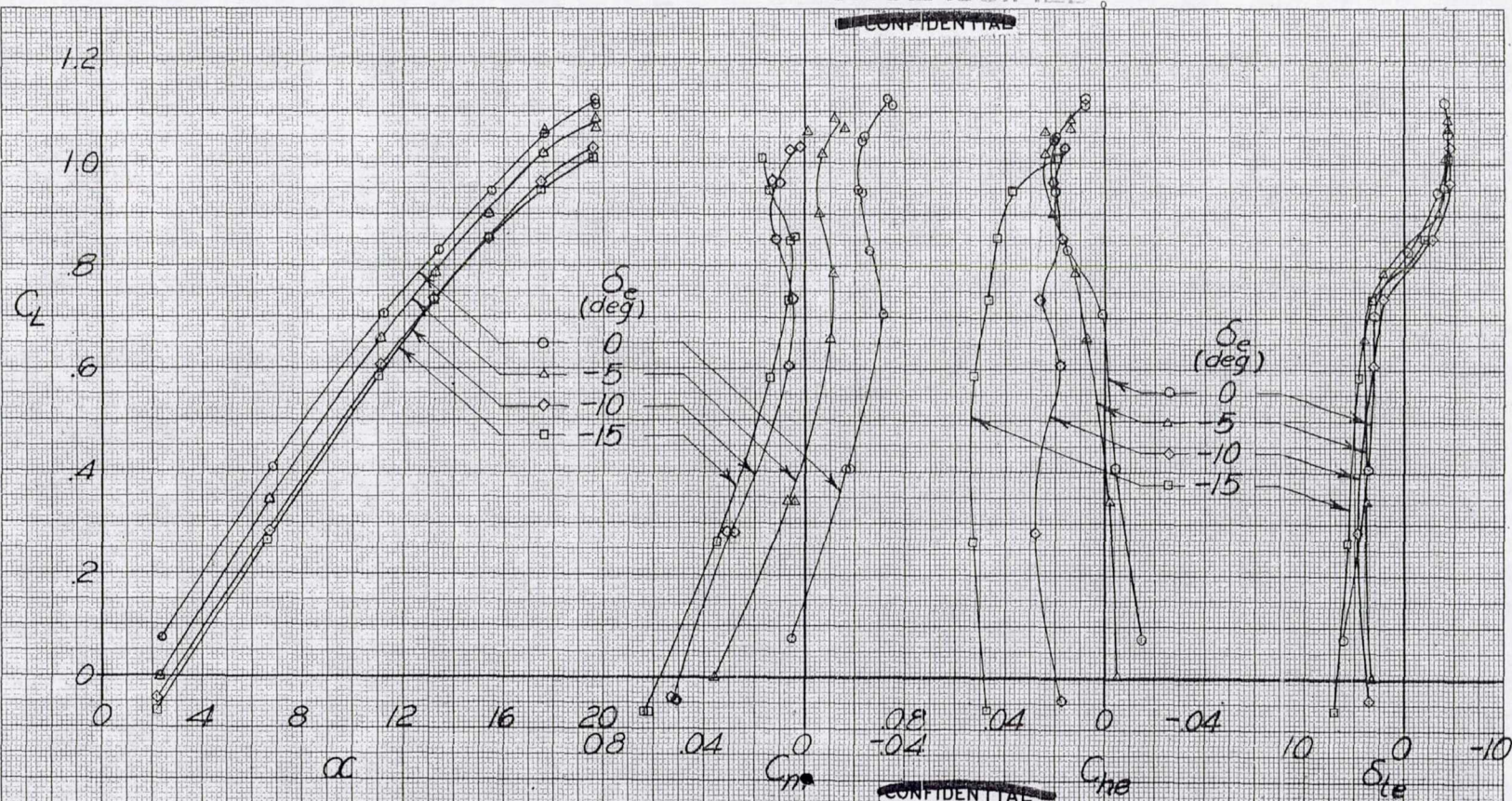
Figure 36 - Concluded.

MR No. L5L27

164537

UNCLASSIFIED

~~CONFIDENTIAL~~



~~CONFIDENTIAL~~

NATIONAL ADVISORY
COMMITTEE FOR AERONAUTICS

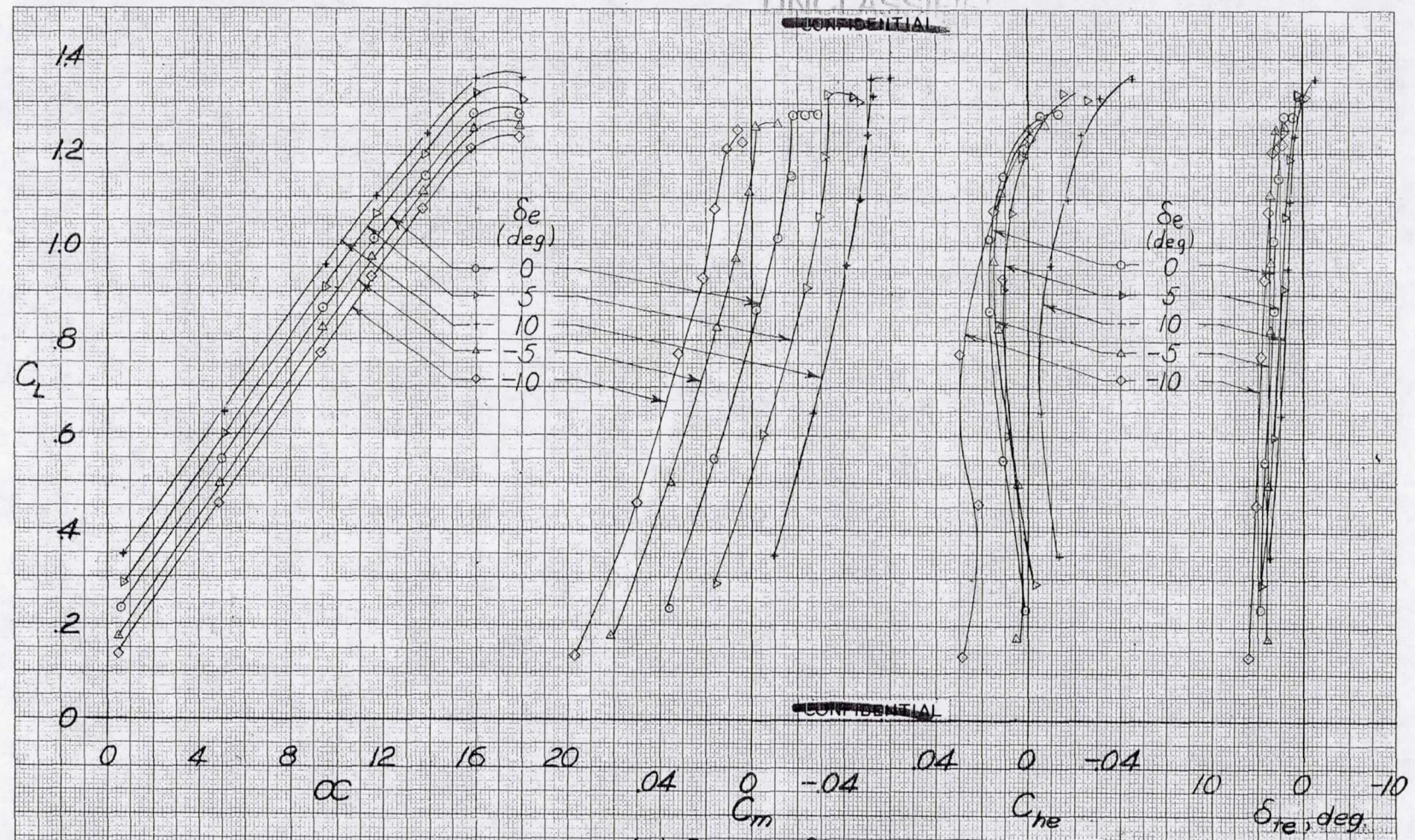
Figure 37 - Effects of free-floating full-span elevator tab and flipper combination
 1/7-scale XB-35 semispan model; $\delta_f = 0^\circ$; $\delta_{fp} = 0^\circ$; slot closed; $\delta_{te} = 1/2 \delta_f$; $\delta_{te} = 0^\circ$; $R \approx 7,500,000$; $M \approx 0.12$.

MR No. 15127

UNCLASSIFIED

104538

UNCLASSIFIED
CONFIDENTIAL



CONFIDENTIAL

(a) $\delta_{fp} = -34.1^\circ$

NATIONAL ADVISORY
COMMITTEE FOR AERONAUTICS

Figure 38.-Effects of free-floating full-span elevon tab and flipper combination.
1/7 scale XB-35 semispan model; $\delta_{fl} = 43.3^\circ$; slot open; $\delta_{te} = 1/2 \delta_{fl}$; $\delta_{re} = 0^\circ$; $R \approx 7,500,000$; $M \approx 0.12$.

MR No. L5L27

UNCLASSIFIED

164538

UNCLASSIFIED

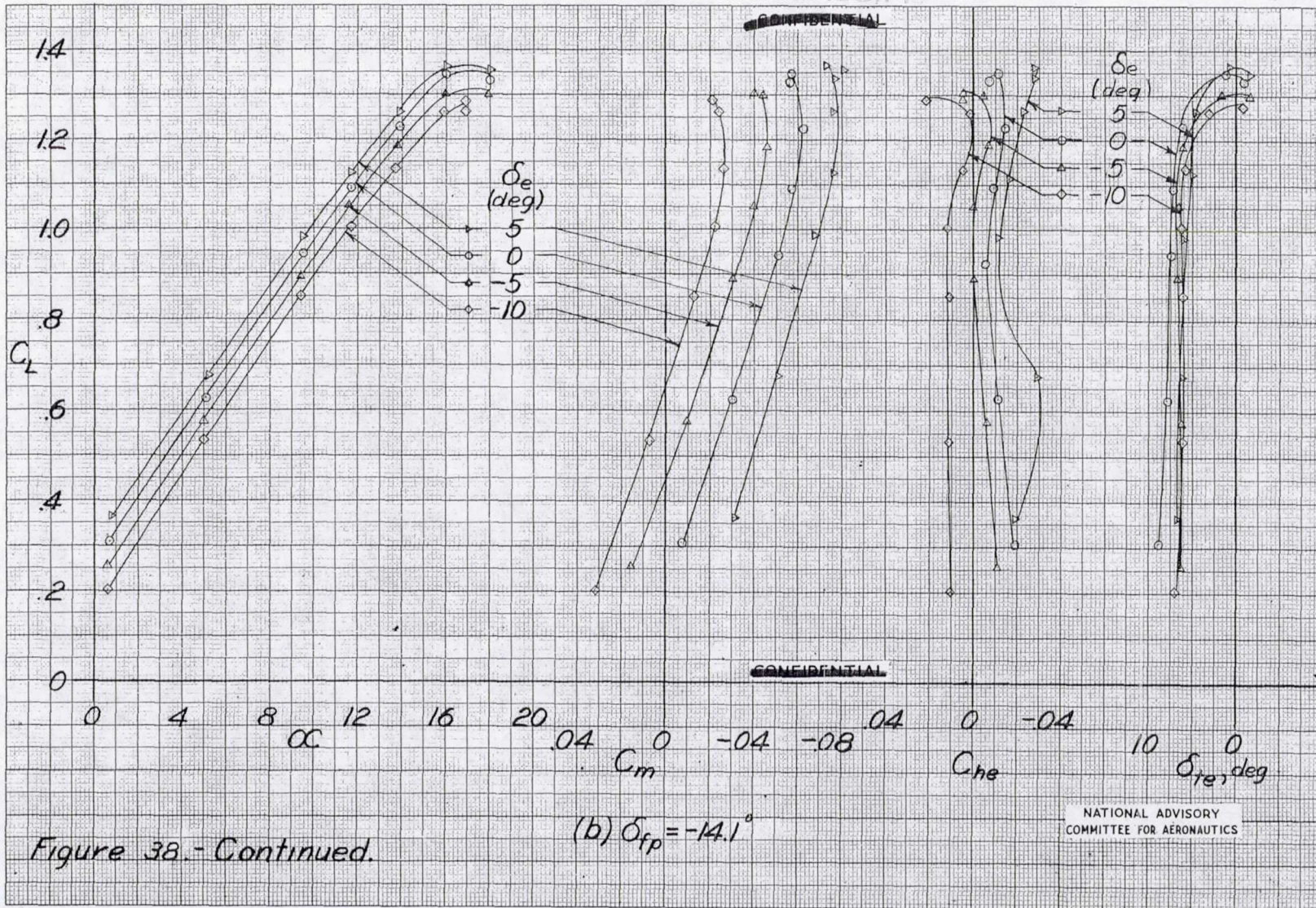


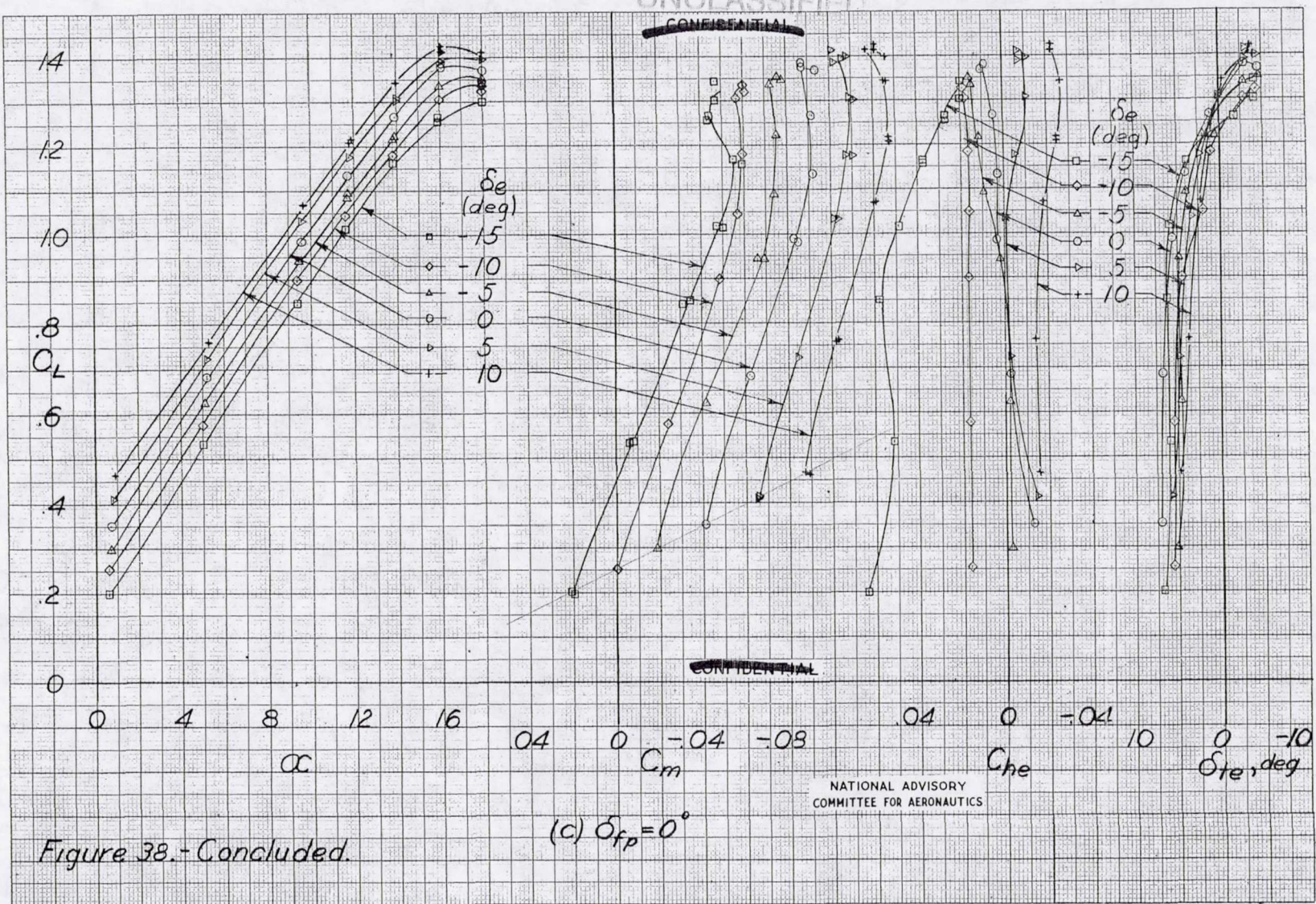
Figure 38.-Continued.

MR No. 15127

UNCLASSIFIED

164538

UNCLASSIFIED
CONFIDENTIAL



CONFIDENTIAL

CONFIDENTIAL

NATIONAL ADVISORY
COMMITTEE FOR AERONAUTICS

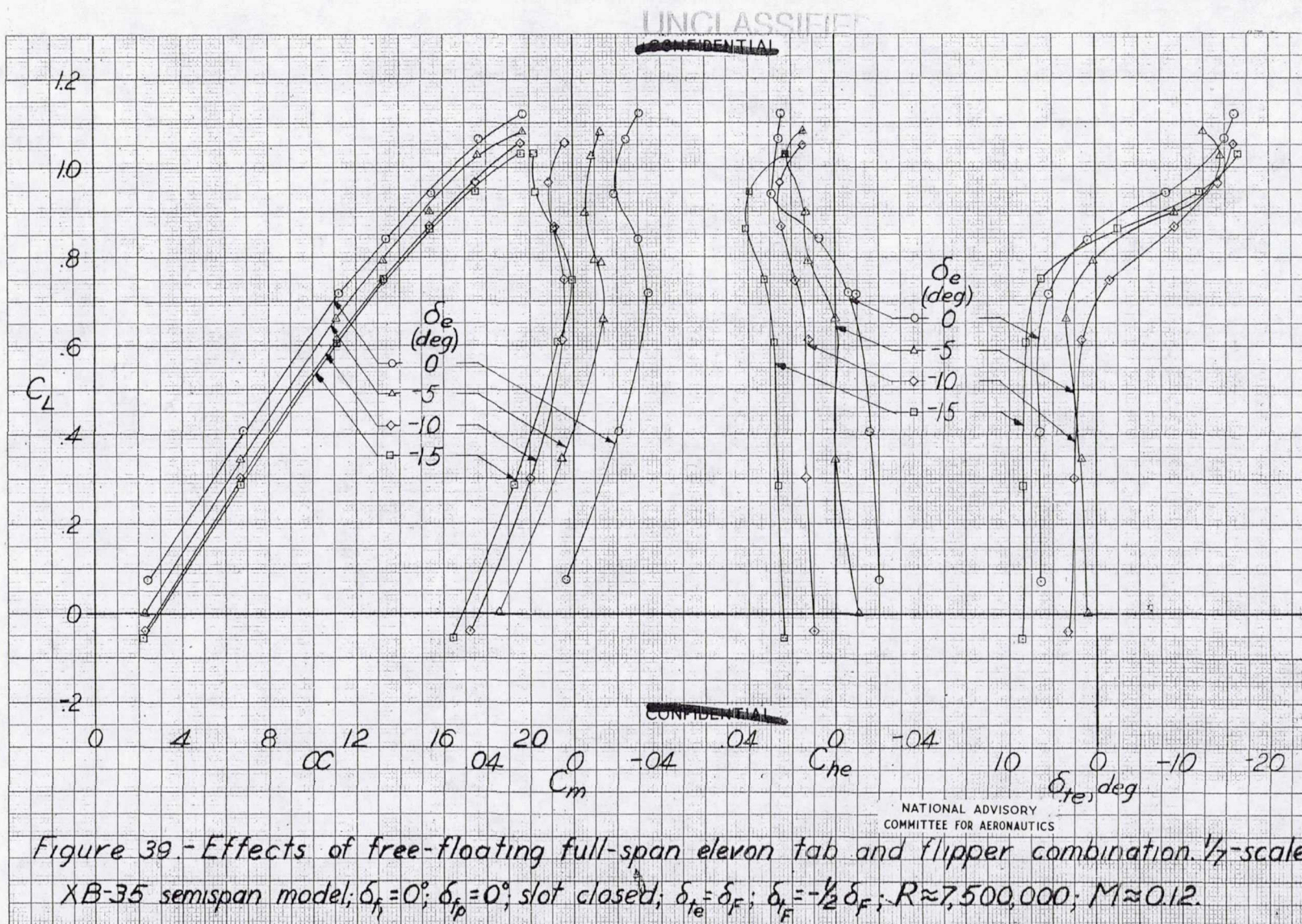
Figure 38.- Concluded.

(c) $\delta_{fp} = 0^\circ$

UNCLASSIFIED

MR No. L5L27

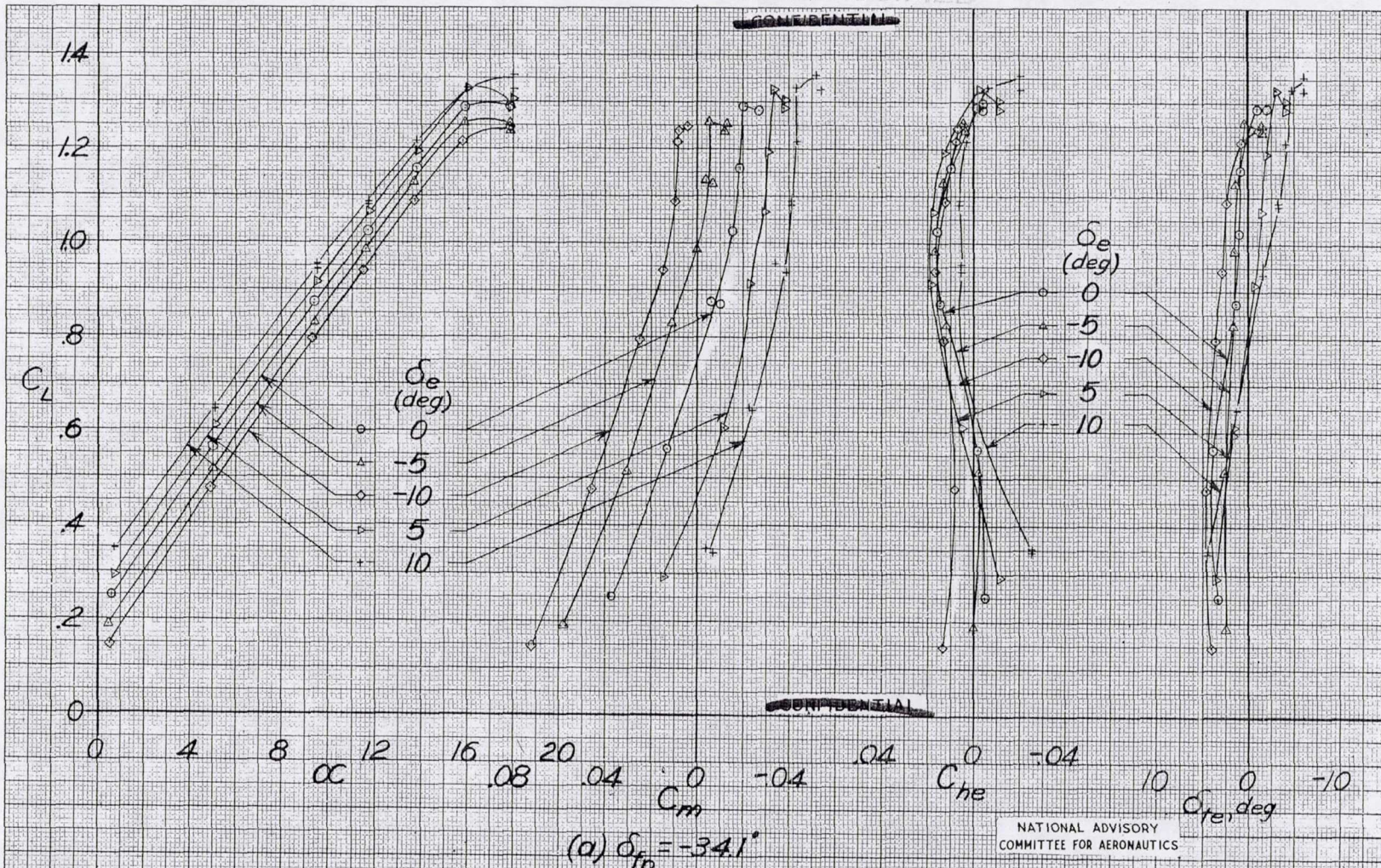
154539



MR No. L5127

~~CONFIDENTIAL~~

UNCLASSIFIED



(a) $\delta_{fp} = -34.1^\circ$

NATIONAL ADVISORY COMMITTEE FOR AERONAUTICS

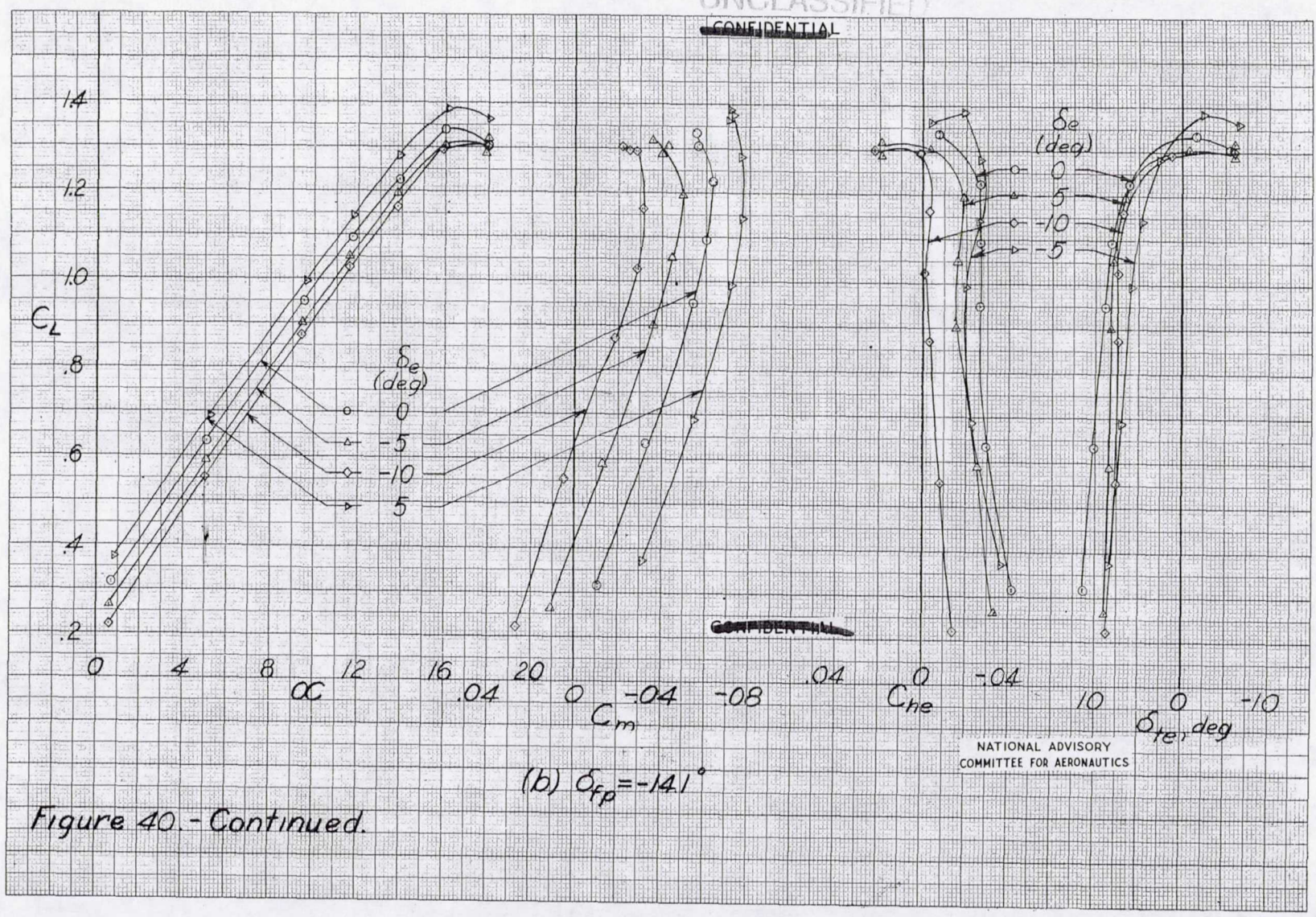
Figure 40.-Effects of free-floating full-span evelon tab and flipper combination. $1/7$ -scale XB-35 semispan model. $\delta_a = 43.3^\circ$; slot open; $\delta_{te} = \delta_{Fi}$; $\delta_{TF} = -1/2 \delta_{Fi}$; $R \approx 7,500,000$; $M = 0.12$

MR No. L5L27

UNCLASSIFIED

104540

UNCLASSIFIED
~~CONFIDENTIAL~~



(b) $\delta_{fp} = -14.1^\circ$

Figure 40 - Continued.

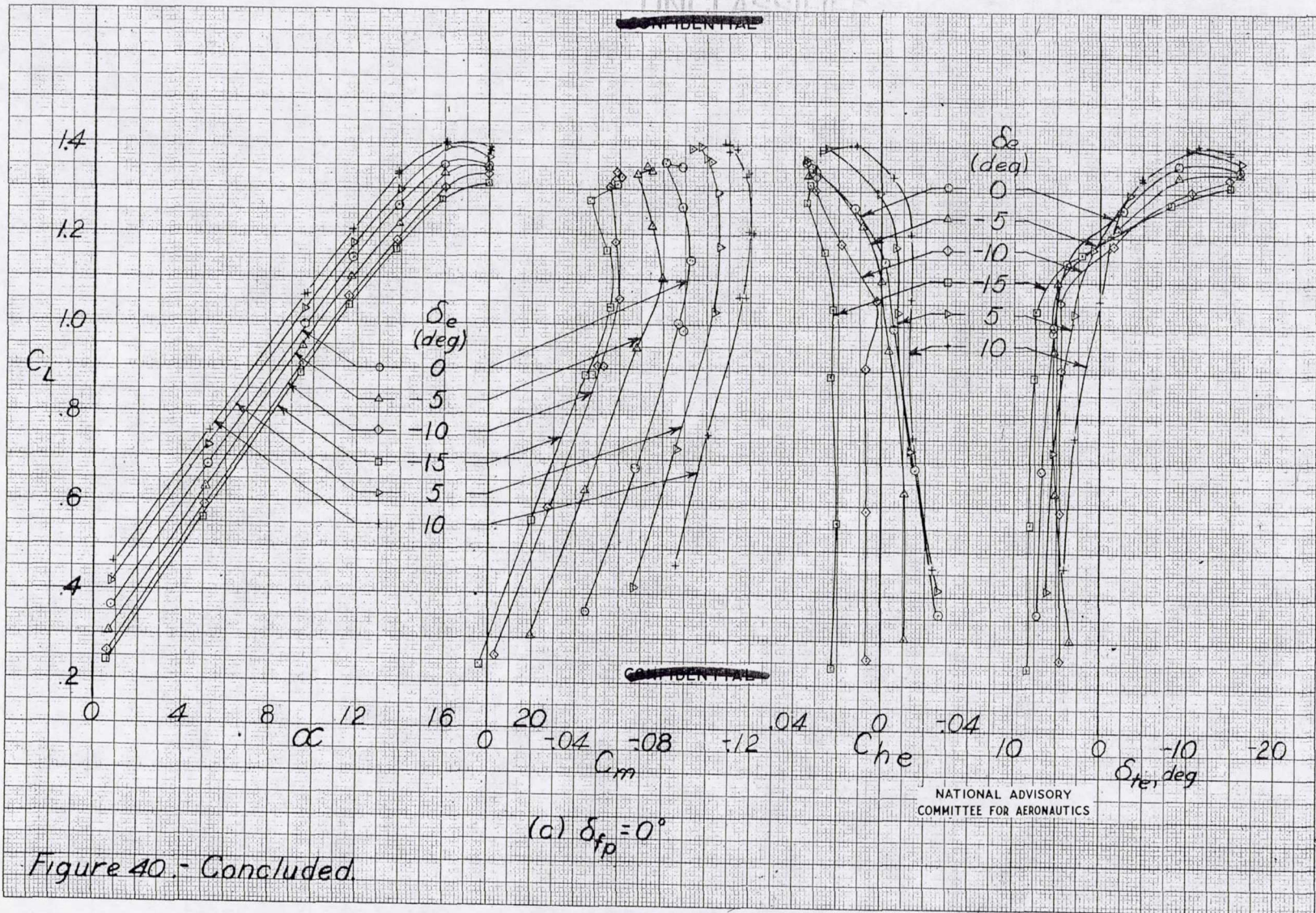
NATIONAL ADVISORY
COMMITTEE FOR AERONAUTICS

MR No. L5L27

UNCLASSIFIED

UNCLASSIFIED

~~CONFIDENTIAL~~



~~CONFIDENTIAL~~

(c) $\delta_{fp} = 0^\circ$

Figure 40.- Concluded.

MR No. L5L27

1944

UNCLASSIFIED

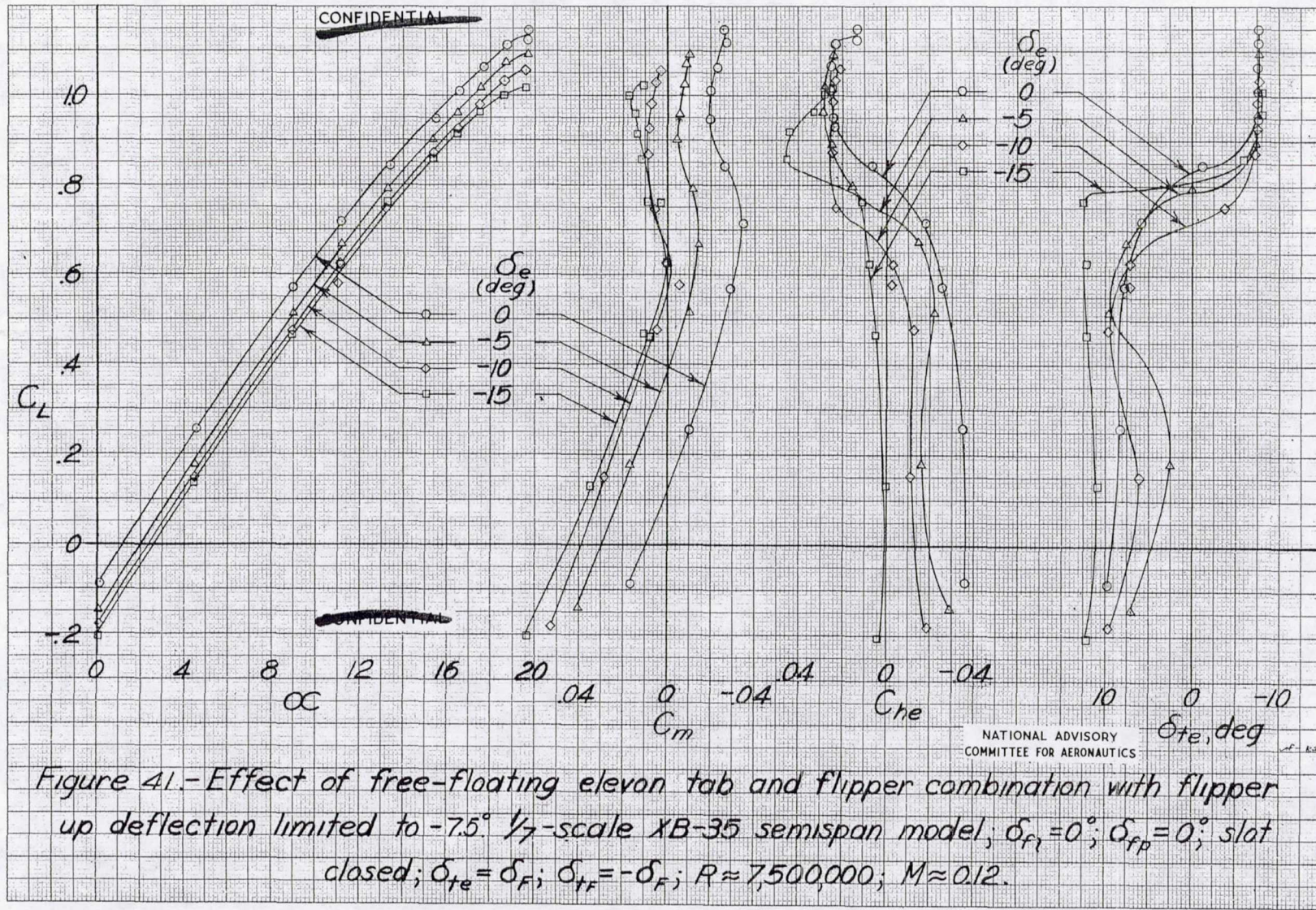


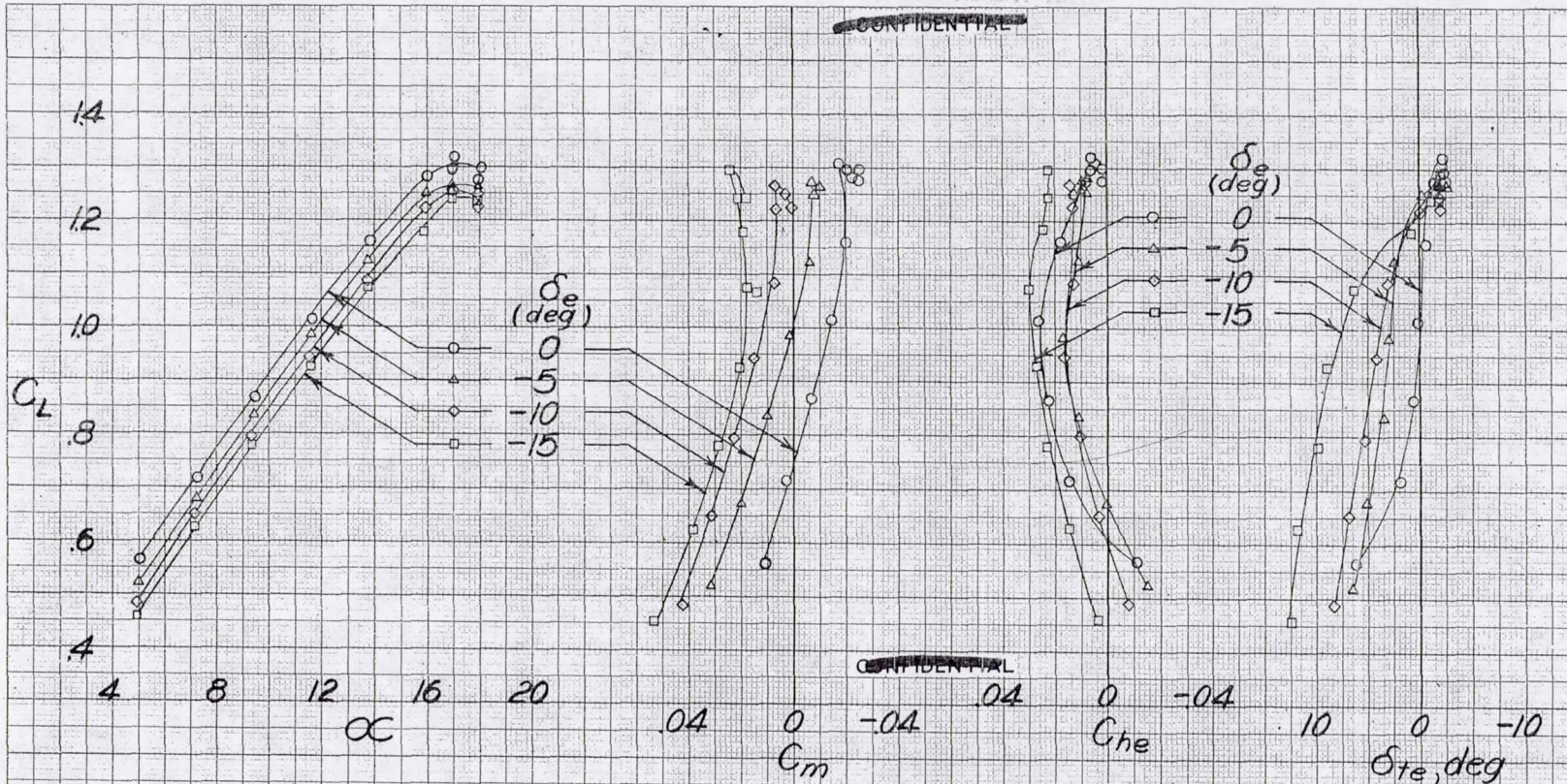
Figure 41.- Effect of free-floating elevator tab and flipper combination with flipper up deflection limited to -7.5° . $1/7$ -scale XB-35 semispan model; $\delta_{F1} = 0^\circ$; $\delta_{FP} = 0^\circ$; slot closed; $\delta_{te} = \delta_F$; $\delta_{tr} = -\delta_F$; $R \approx 7,500,000$; $M \approx 0.12$.

MR No. L5L27

UNCLASSIFIED

UNCLASSIFIED

~~CONFIDENTIAL~~



~~CONFIDENTIAL~~

NATIONAL ADVISORY
COMMITTEE FOR AERONAUTICS

(a) $\delta_{fp} = -34.1^\circ$

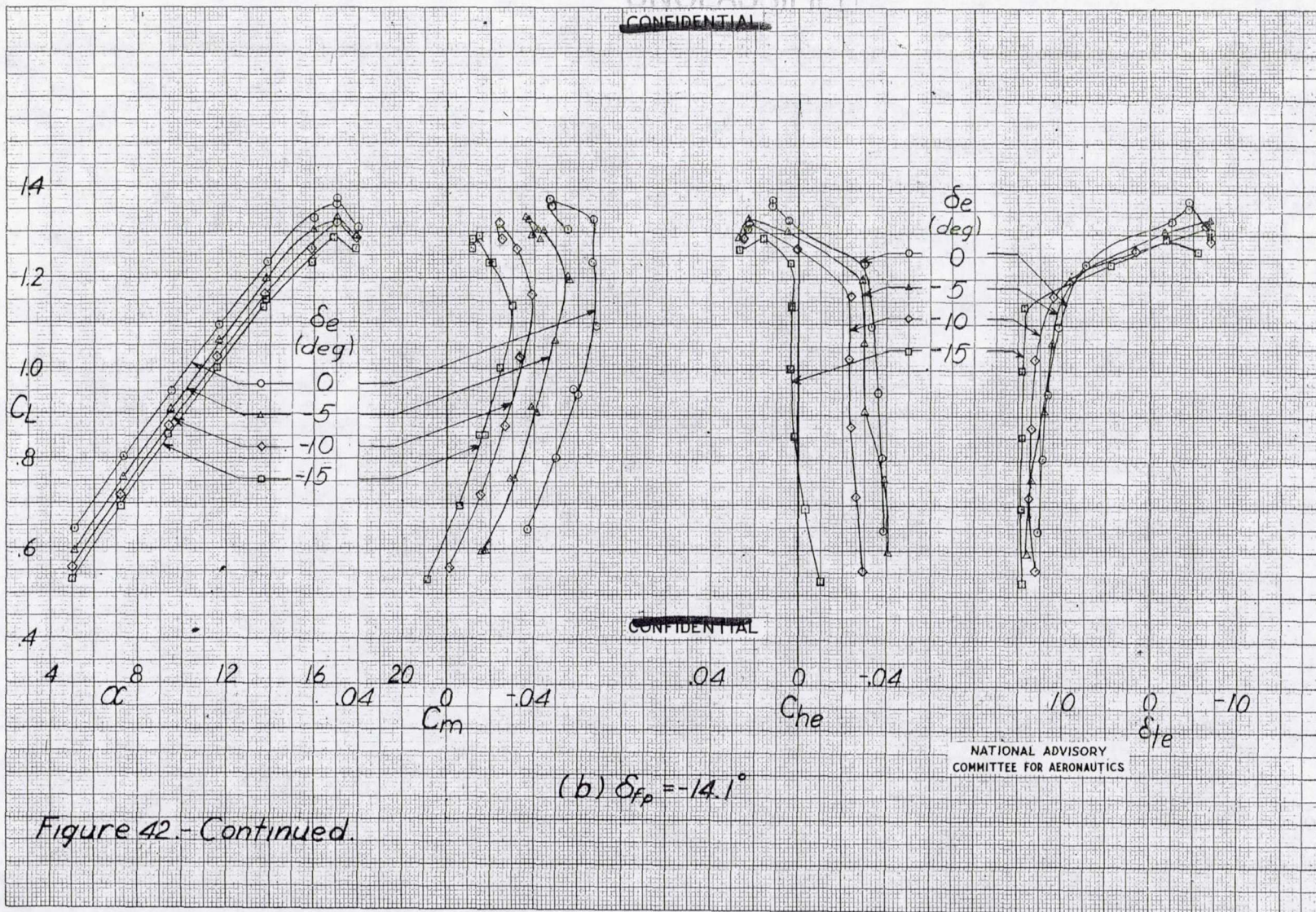
Figure 42.-Effect of free-floating elevon tab and flipper combination with flipper up deflection limited to -7.5° $1/7$ -scale XB-35 semispan model; $\delta_{fl} = 43.3^\circ$; slot open; $\delta_{te} = \delta_F$; $\delta_{tf} = -\delta_F$; $R \approx 7,500,000$; $M \approx 0.12$

MR No. 15127

UNCLASSIFIED

15492

UNCLASSIFIED
CONFIDENTIAL

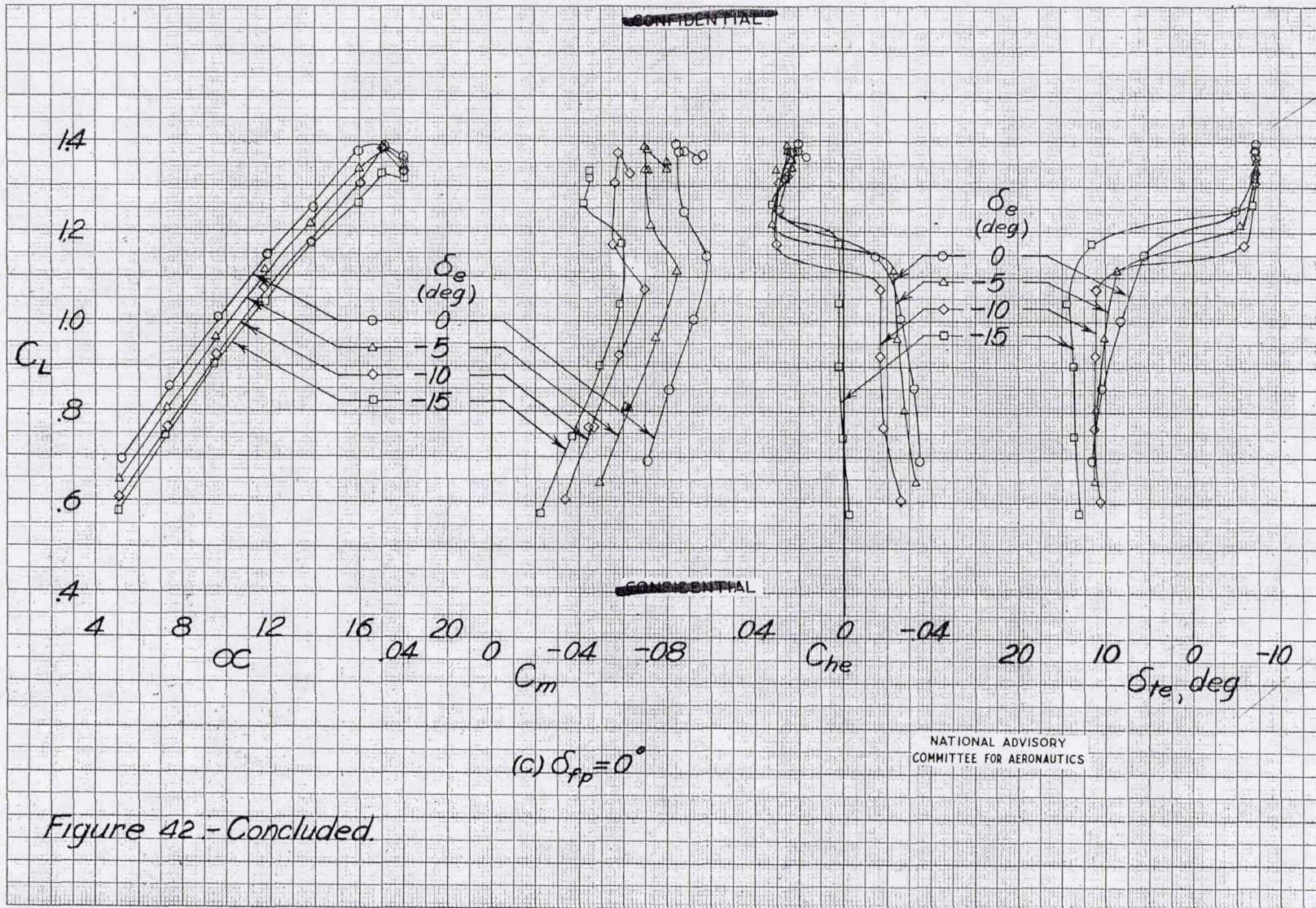


NATIONAL ADVISORY
COMMITTEE FOR AERONAUTICS

MR No. L5L27

UNCLASSIFIED

UNCLASSIFIED

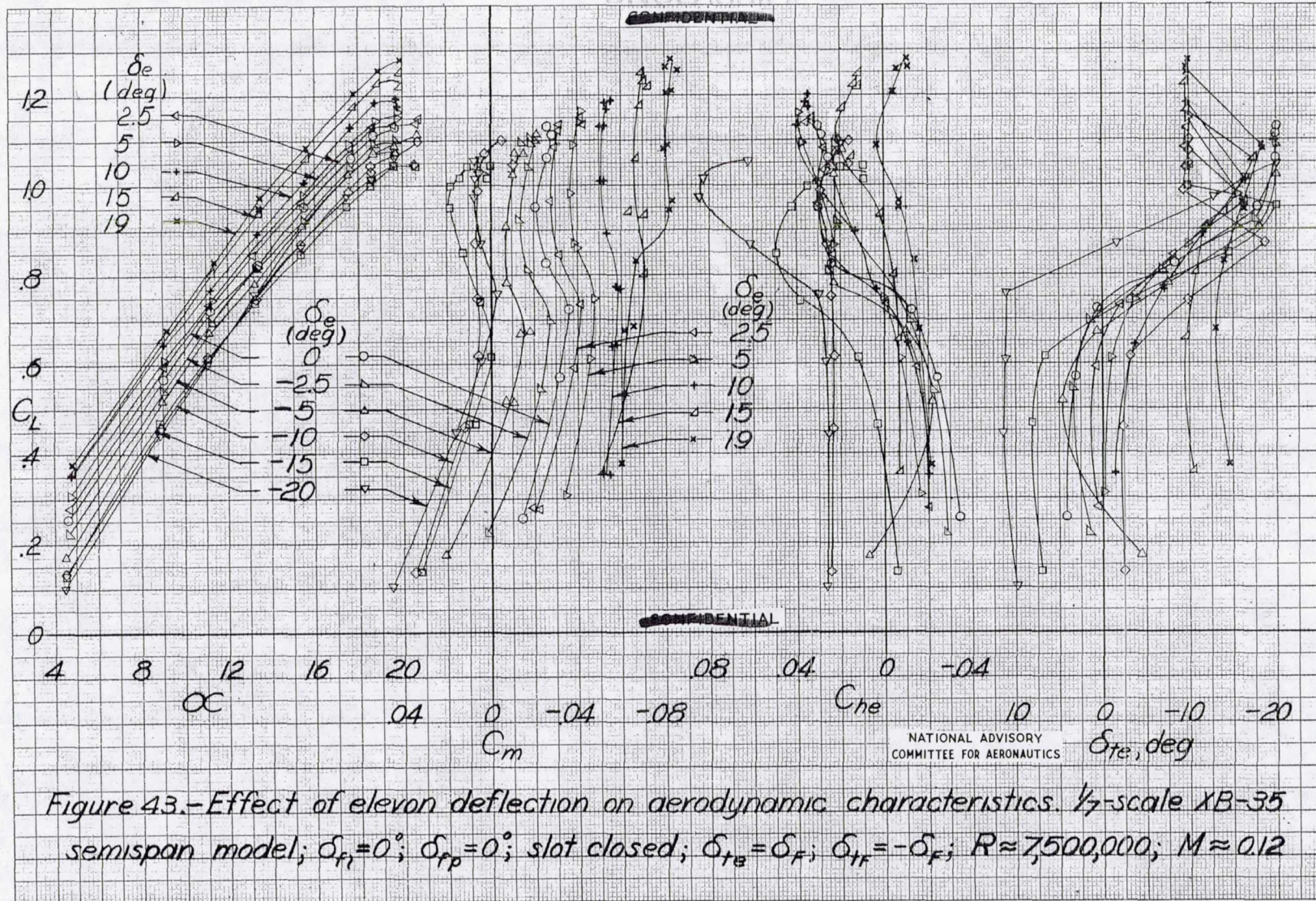


MR No. 15127

UNCLASSIFIED

154843

UNCLASSIFIED



Handwritten notes on the right side of the graph:

$\alpha = 5^\circ$
 15° 10°
 $-.09$ $-.09$
 $|||$ $|||$
 2018 2018

NATIONAL ADVISORY
 COMMITTEE FOR AERONAUTICS

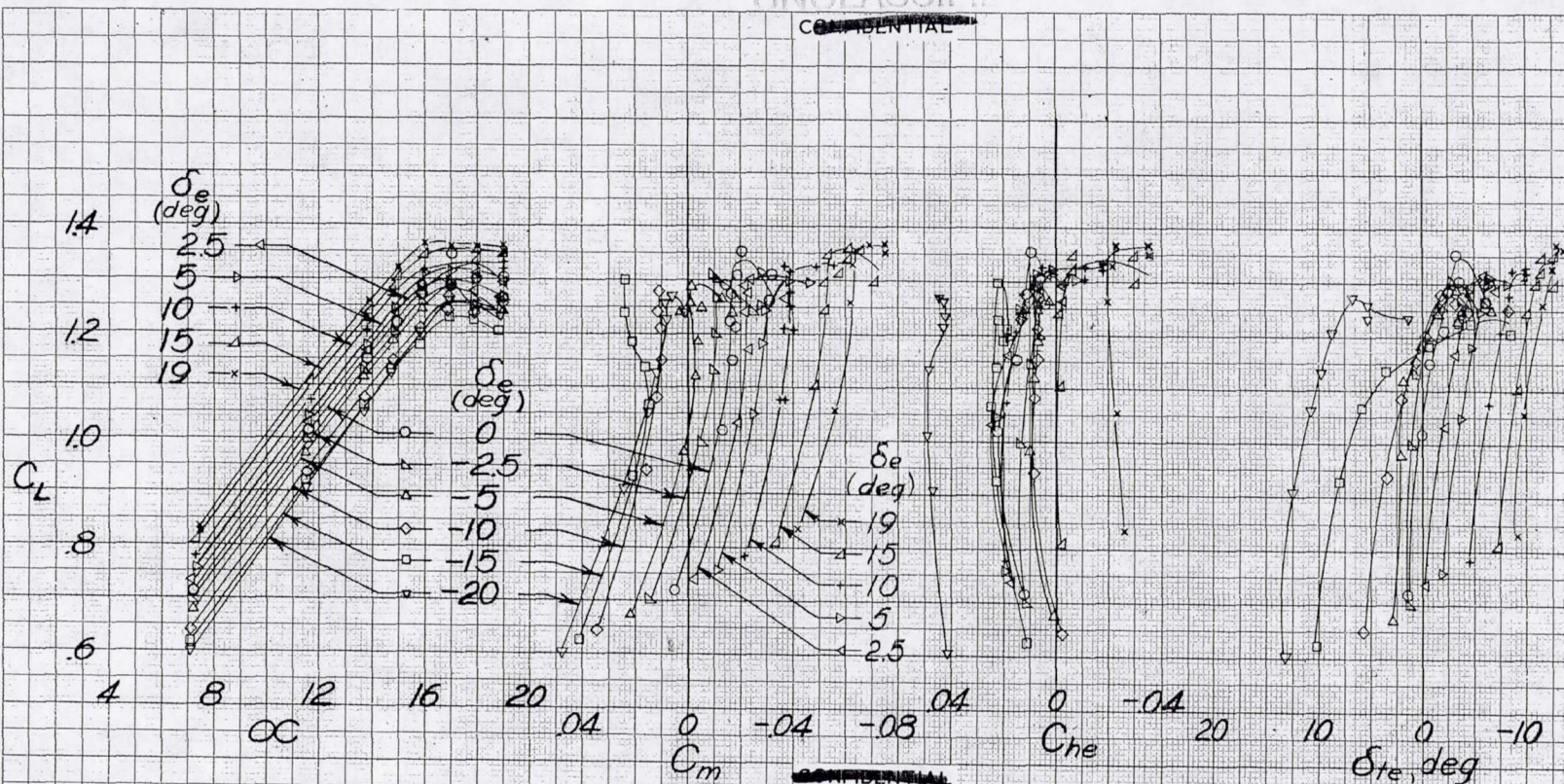
Figure 43.-Effect of elevon deflection on aerodynamic characteristics. 1/7-scale XB-35 semispan model; $\delta_{F1} = 0^\circ$; $\delta_{F2} = 0^\circ$; slot closed; $\delta_{TE} = \delta_F$; $\delta_{TF} = -\delta_F$; $R \approx 7,500,000$; $M \approx 0.12$

MR No. L5L27

UNCLASSIFIED

10454

UNCLASSIFIED
~~CONFIDENTIAL~~



(a) $\delta_{fp} = -34.1^\circ$

NATIONAL ADVISORY
 COMMITTEE FOR AERONAUTICS

Figure 44 - Effects of free floating full span elevon tab and flipper combination, 1/7 scale XB-35 semispan model; $\delta_{fp} = 433^\circ$; slot open; $\delta_{te} = \delta_f$; $\delta_{tf} = -\delta_f$; $R \approx 7,500,000$; $M \approx 0.12$.

MR No. L5L27

UNCLASSIFIED

154544

UNCLASSIFIED

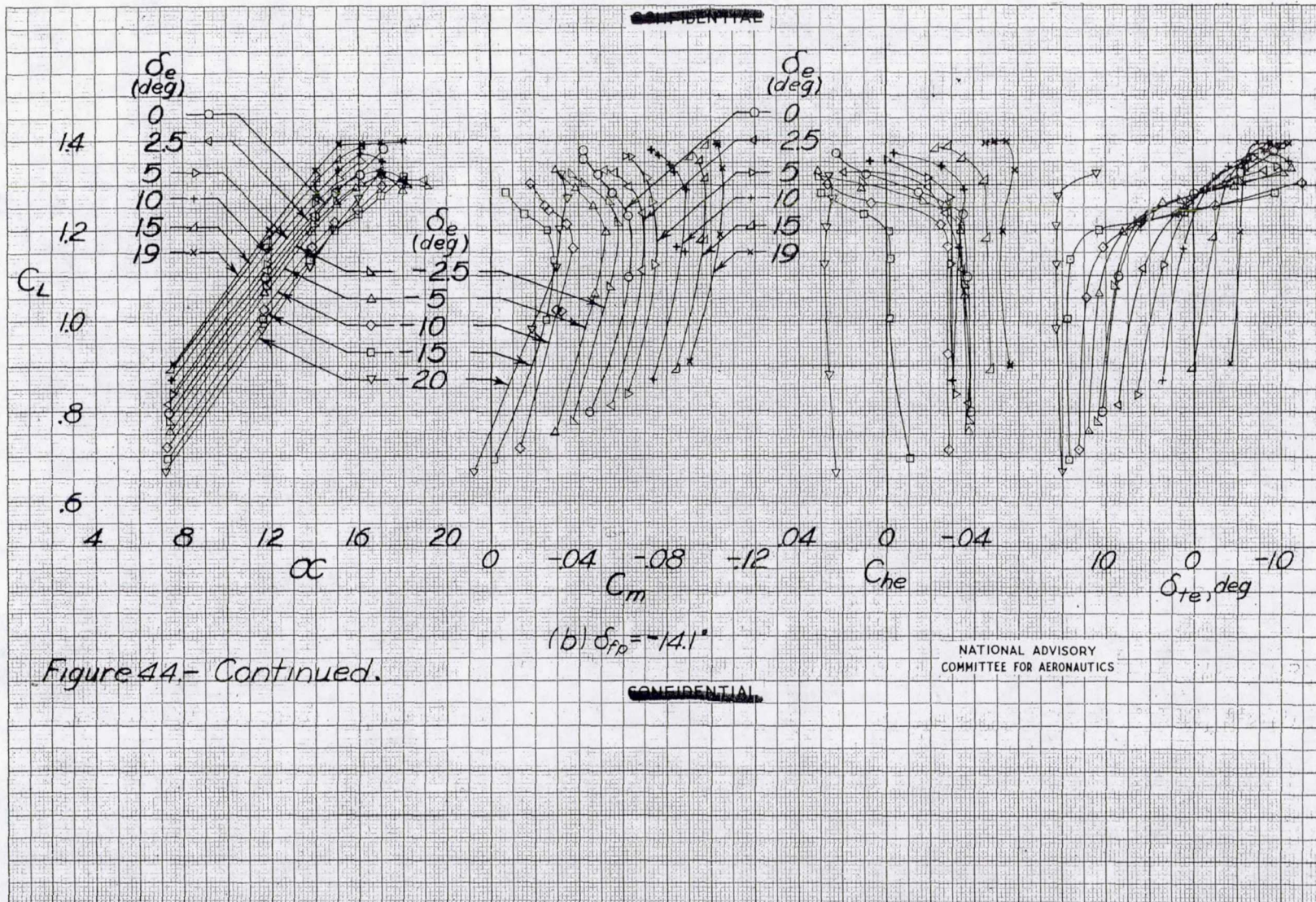


Figure 44.- Continued.

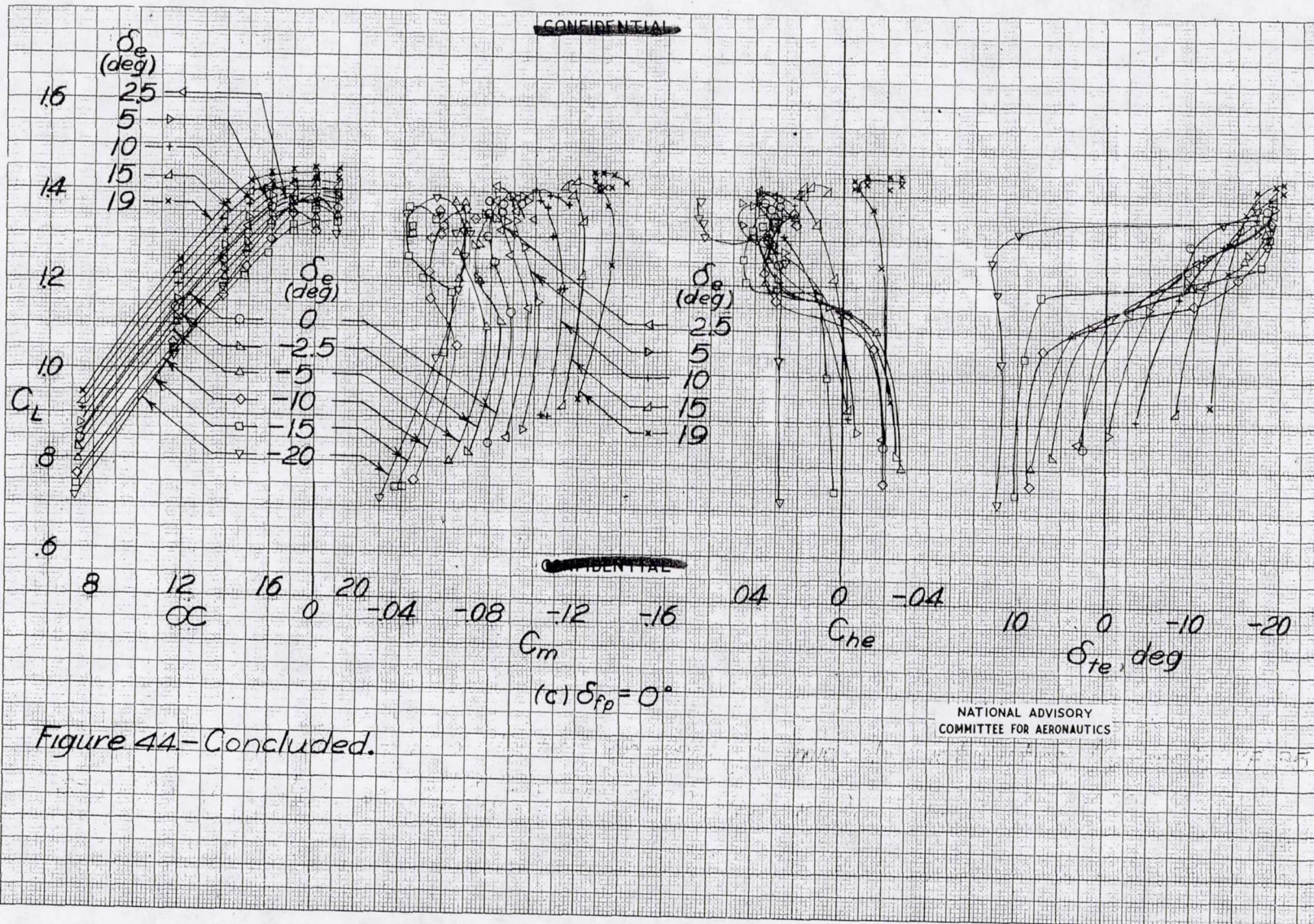
MR No. L5L27

UNCLASSIFIED

1945

UNCLASSIFIED

~~CONFIDENTIAL~~



~~CONFIDENTIAL~~

Figure 44-Concluded.

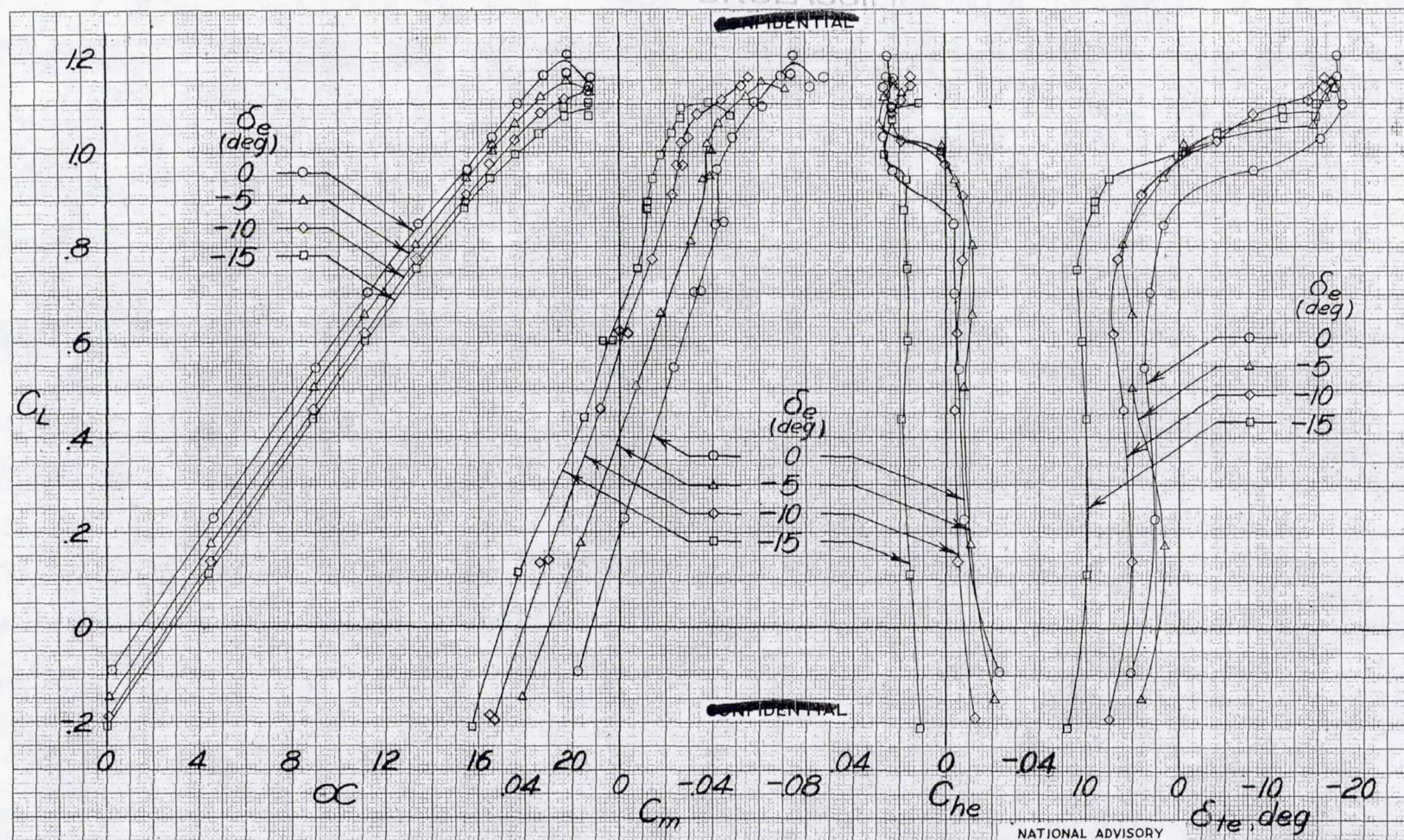
NATIONAL ADVISORY
COMMITTEE FOR AERONAUTICS

MR No. 15127

UNCLASSIFIED

1945

UNCLASSIFIED



CONFIDENTIAL

NATIONAL ADVISORY
COMMITTEE FOR AERONAUTICS

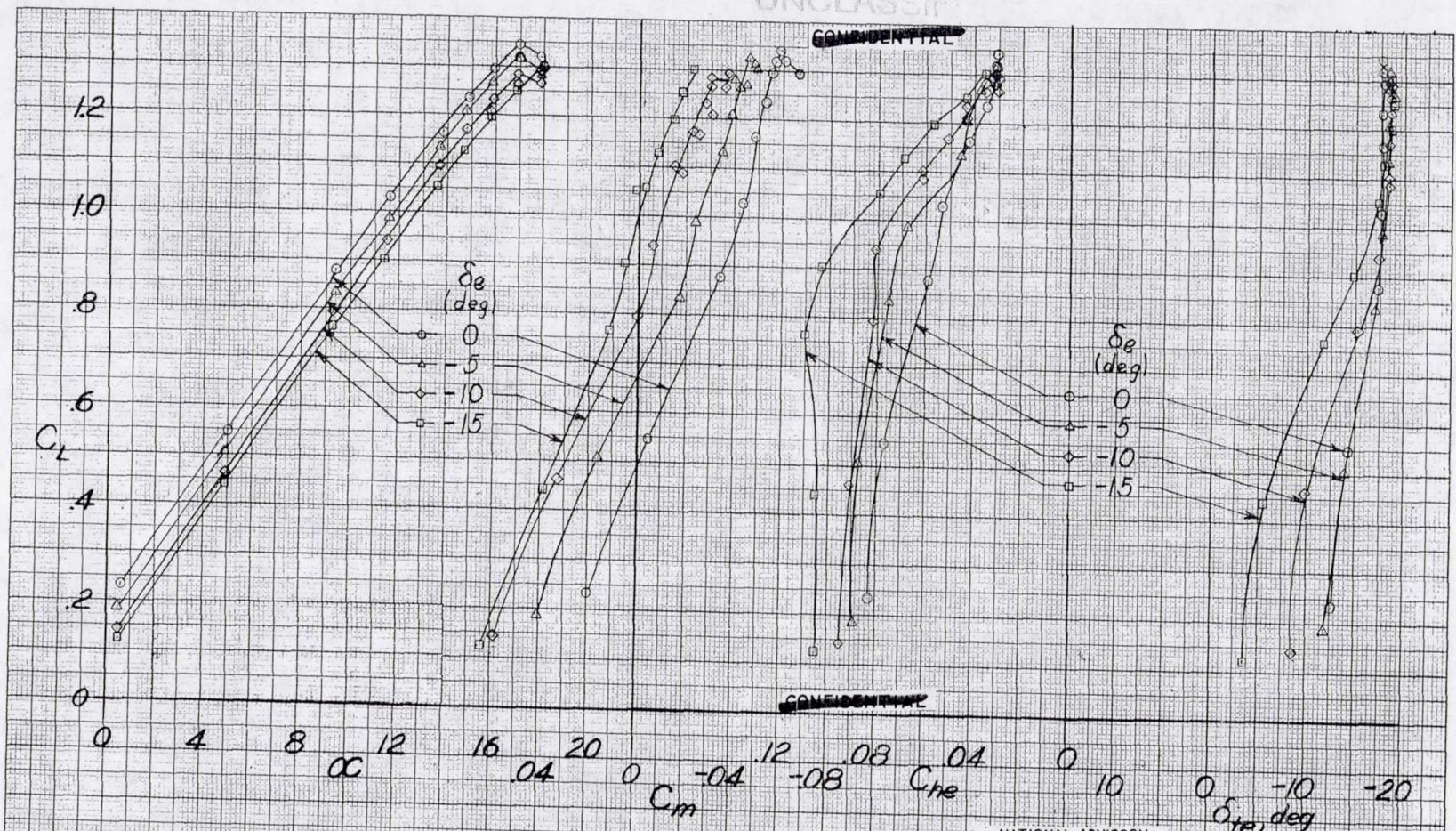
Figure 45-Effects of split rudder on floating characteristics of free-floating elevator tab and flipper combination $1/7$ -scale XB-35 semispan model; $\delta_{f1}=0^\circ$; $\delta_{f2}=0^\circ$; slot closed; $\delta_{te}=\delta_{f1}$; $\delta_{tf}=-\delta_{f1}$; $R \approx 7,500,000$; $M \approx 0.12$

MR No. 15127

UNCLASSIFIED

154545

UNCLASSIFIED



CONFIDENTIAL

NATIONAL ADVISORY COMMITTEE FOR AERONAUTICS

(a) $\delta_{fp} = -34.1^\circ$

Figure 46.-Effects of split rudder on floating characteristics of free-floating elevator tab and flipper combination. 1/7-scale XB-35 semispan model; $\delta_{f1} = 43.3^\circ$; slot open; $\delta_{te} = \delta_F$; $\delta_{tp} = -\delta_F$; $R \approx 7,500,000$; $M \approx 0.12$.

UNCLASSIFIED

MR No. L5L27

UNCLASSIFIED
CONFIDENTIAL

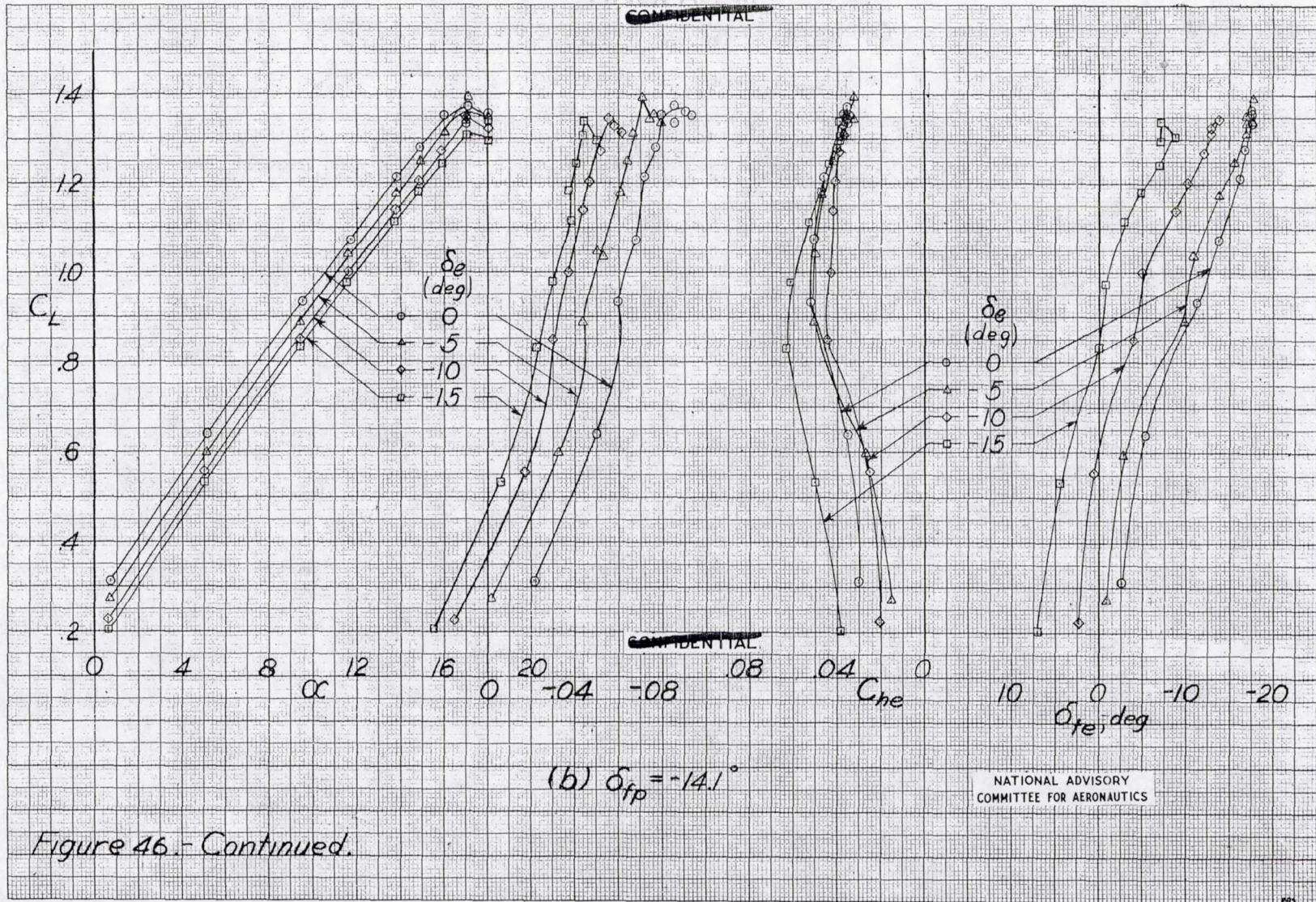


Figure 46 - Continued.

MR No. 15127

UNCLASSIFIED

104545

UNCLASSIFIED

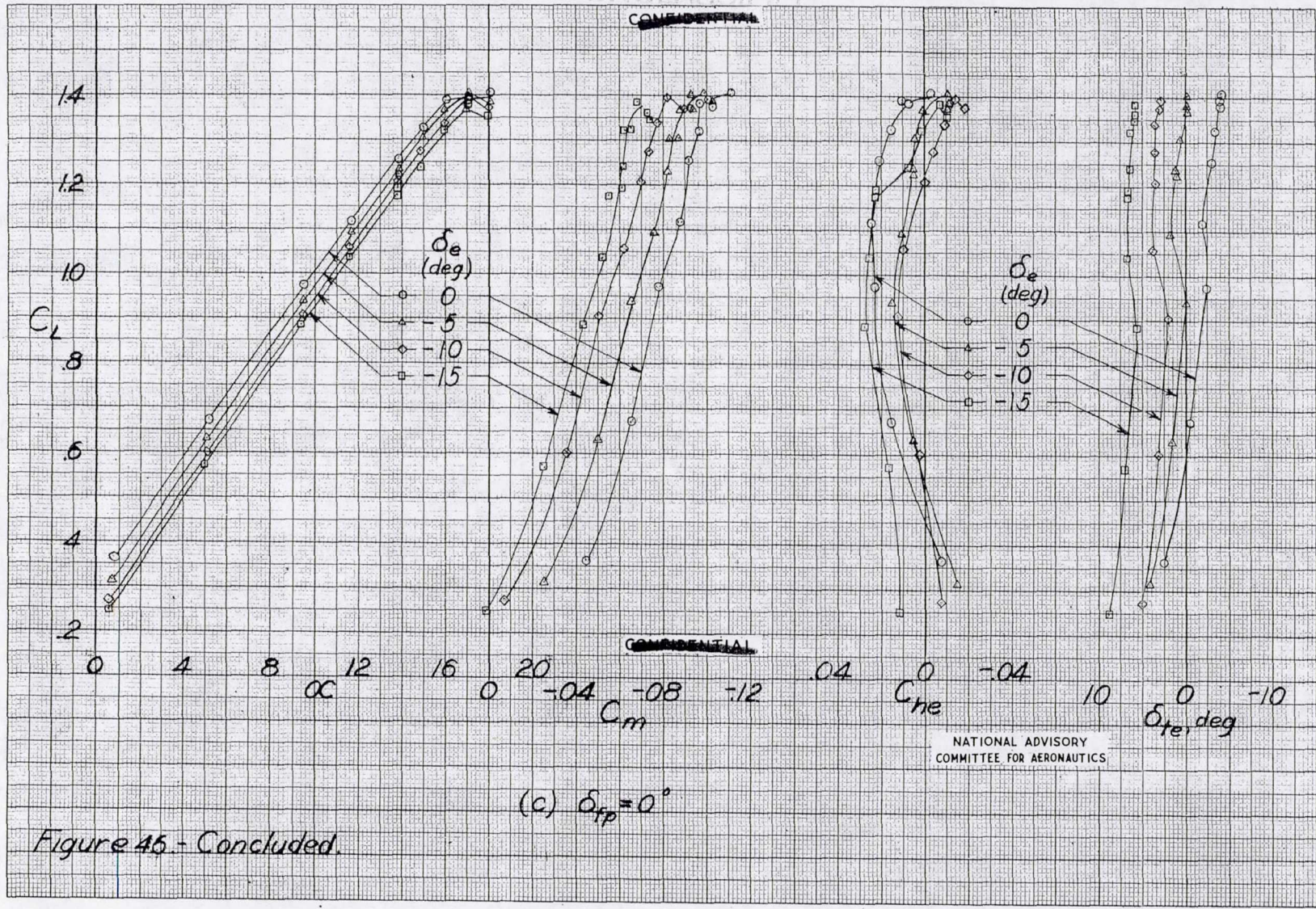


Figure 45 - Concluded.

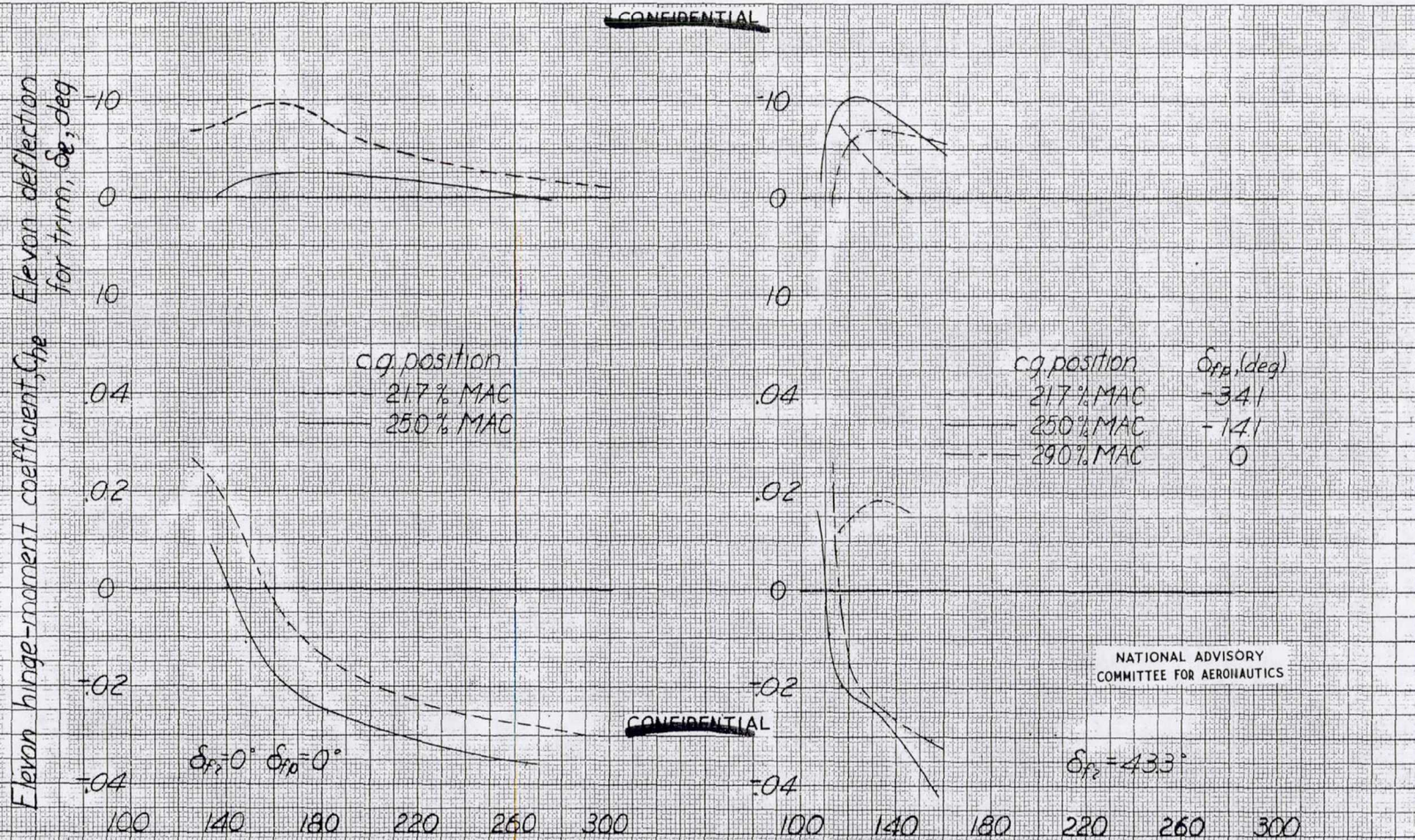
MR No. 15L27

UNCLASSIFIED

164547

UNCLASSIFIED

~~CONFIDENTIAL~~



~~CONFIDENTIAL~~

NATIONAL ADVISORY COMMITTEE FOR AERONAUTICS

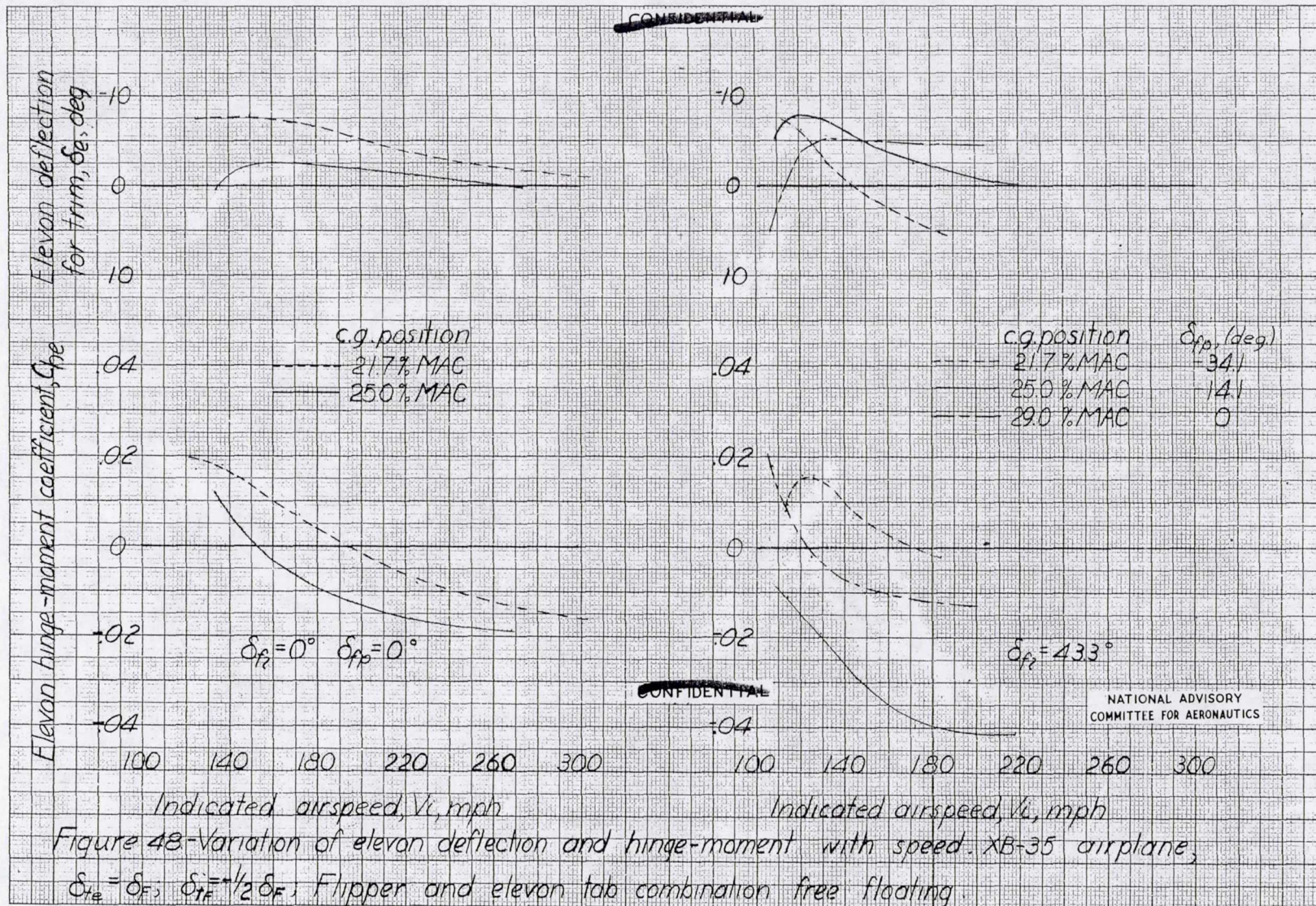
Indicated airspeed, V_i , mph
 Figure 47-Variation of elevon deflection and hinge-moment with speed. XB-35 airplane, $\delta_{Te} = \delta_F$, $\delta_{Te} = -\delta_F$, Flipper and elevon tab combination free floating; Maximum negative $\delta_F = -7.5^\circ$.

MR No. L5L27

UNCLASSIFIED

164840

UNCLASSIFIED



MR No. 15127

UNCLASSIFIED

154549

UNCLASSIFIED

~~CONFIDENTIAL~~

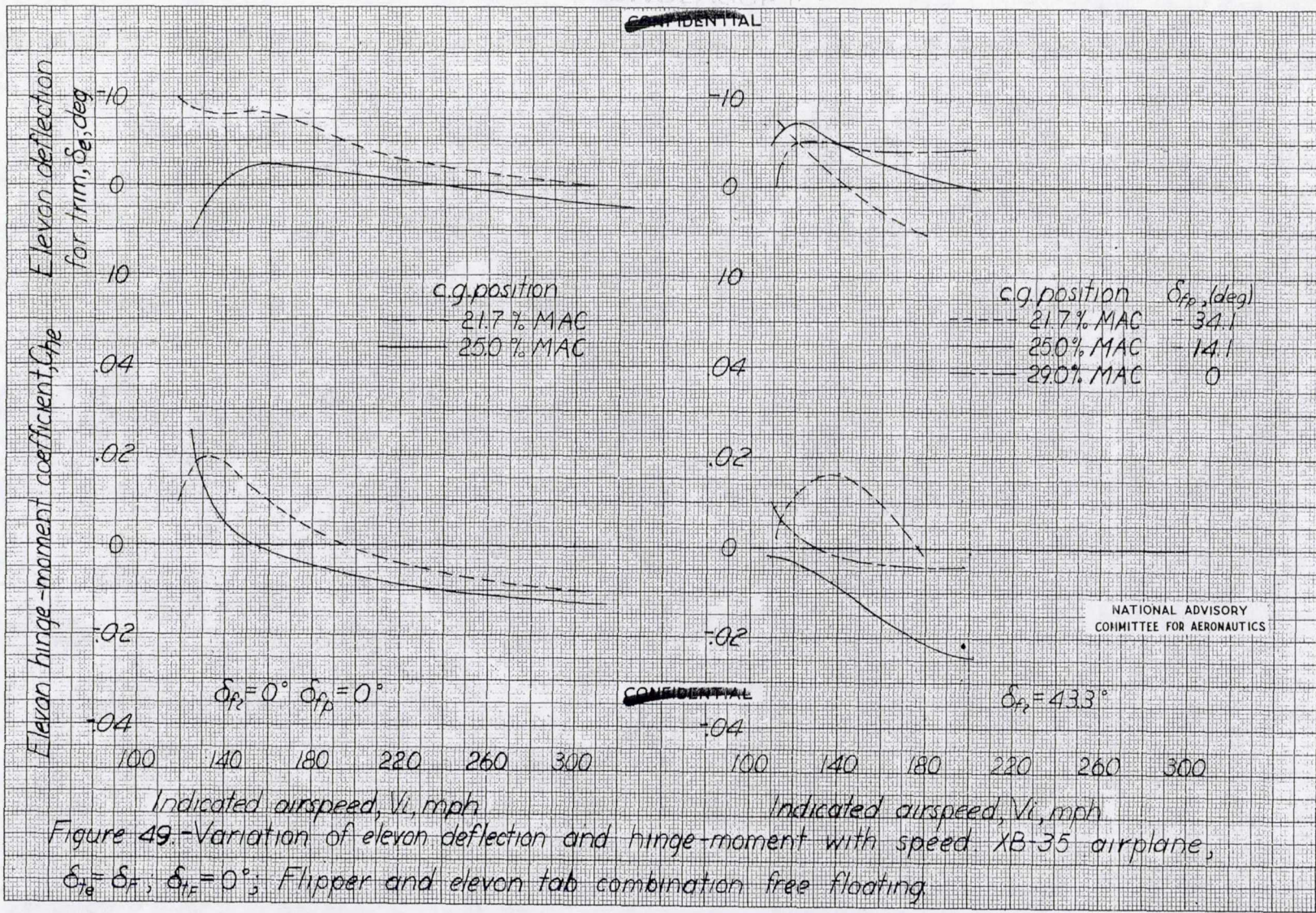


Figure 49.-Variation of elevon deflection and hinge-moment with speed XB-35 airplane, $\delta_{T_e} = \delta_T$; $\delta_{T_e} = 0^\circ$; Flipper and elevon tab combination free floating.

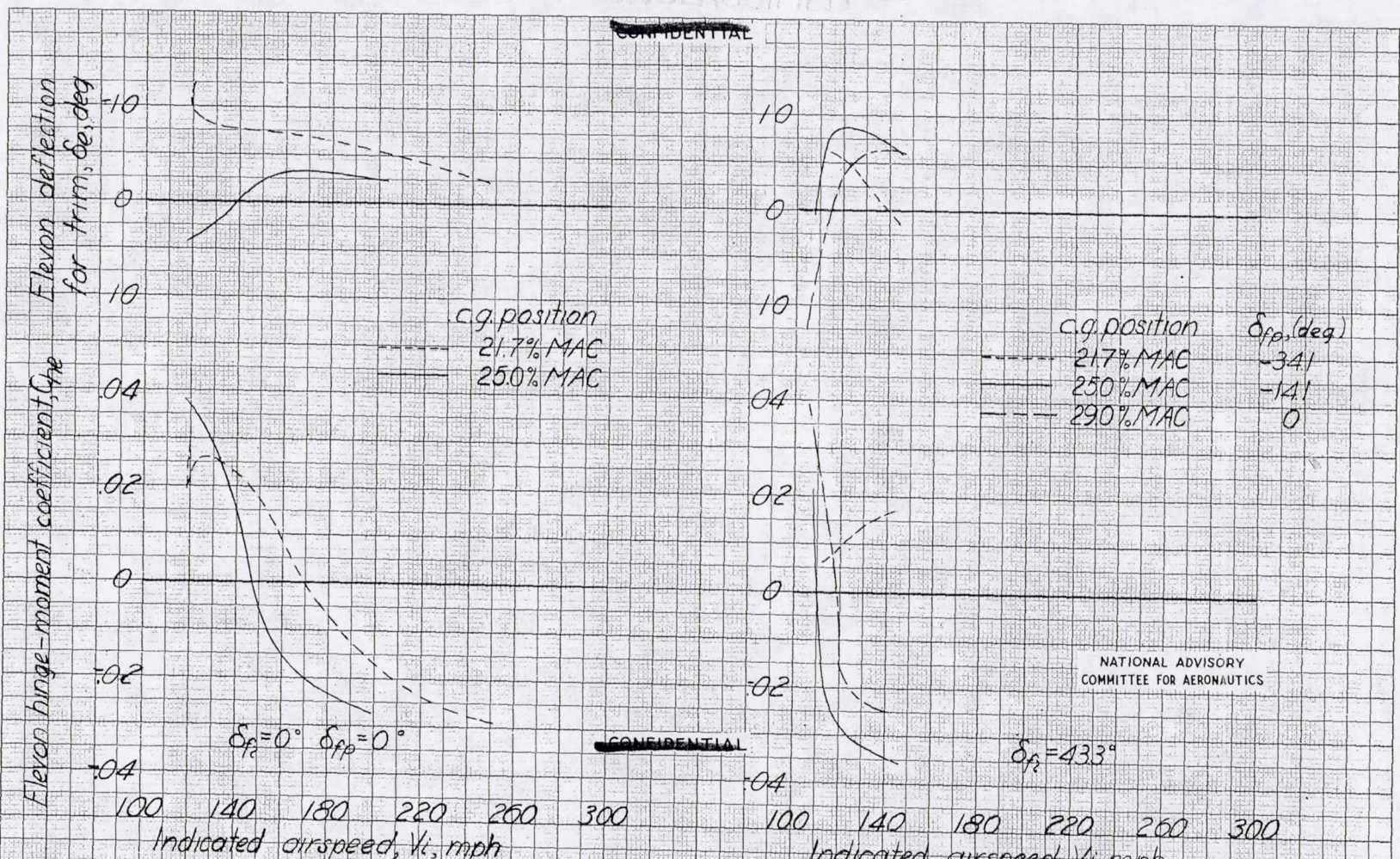
MR No. L5L27

UNCLASSIFIED

154850

UNCLASSIFIED

~~CONFIDENTIAL~~



NATIONAL ADVISORY COMMITTEE FOR AERONAUTICS

~~CONFIDENTIAL~~

Figure 50-Variation of elevon deflection and hinge-moment with speed, XB-35 airplane, $\delta_{te} = \delta_F$; $\delta_{tf} = -\delta_F$; Flipper and elevon tab combination free floating.

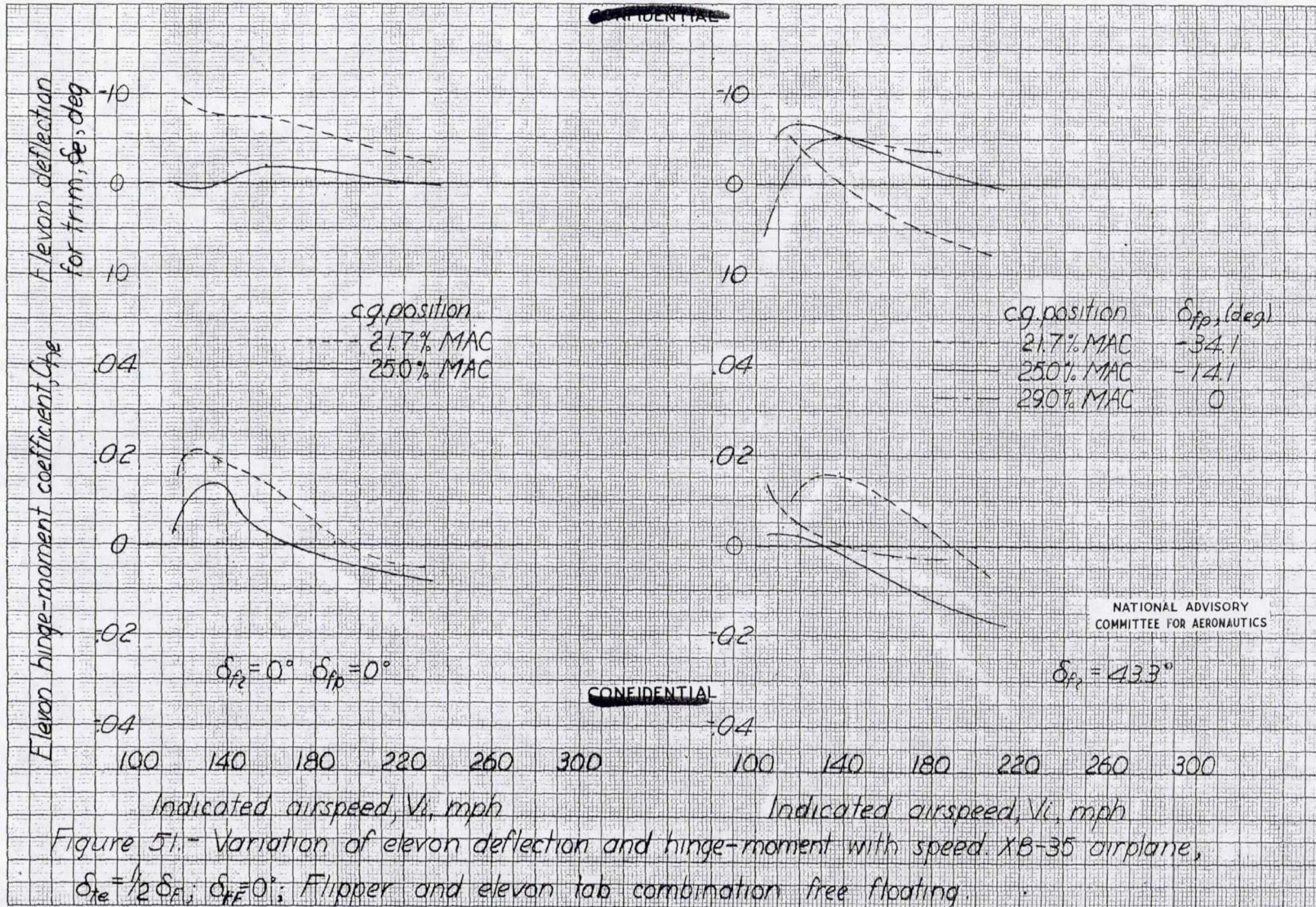
MR No. L5L27

UNCLASSIFIED

104551

UNCLASSIFIED

~~CONFIDENTIAL~~



~~CONFIDENTIAL~~

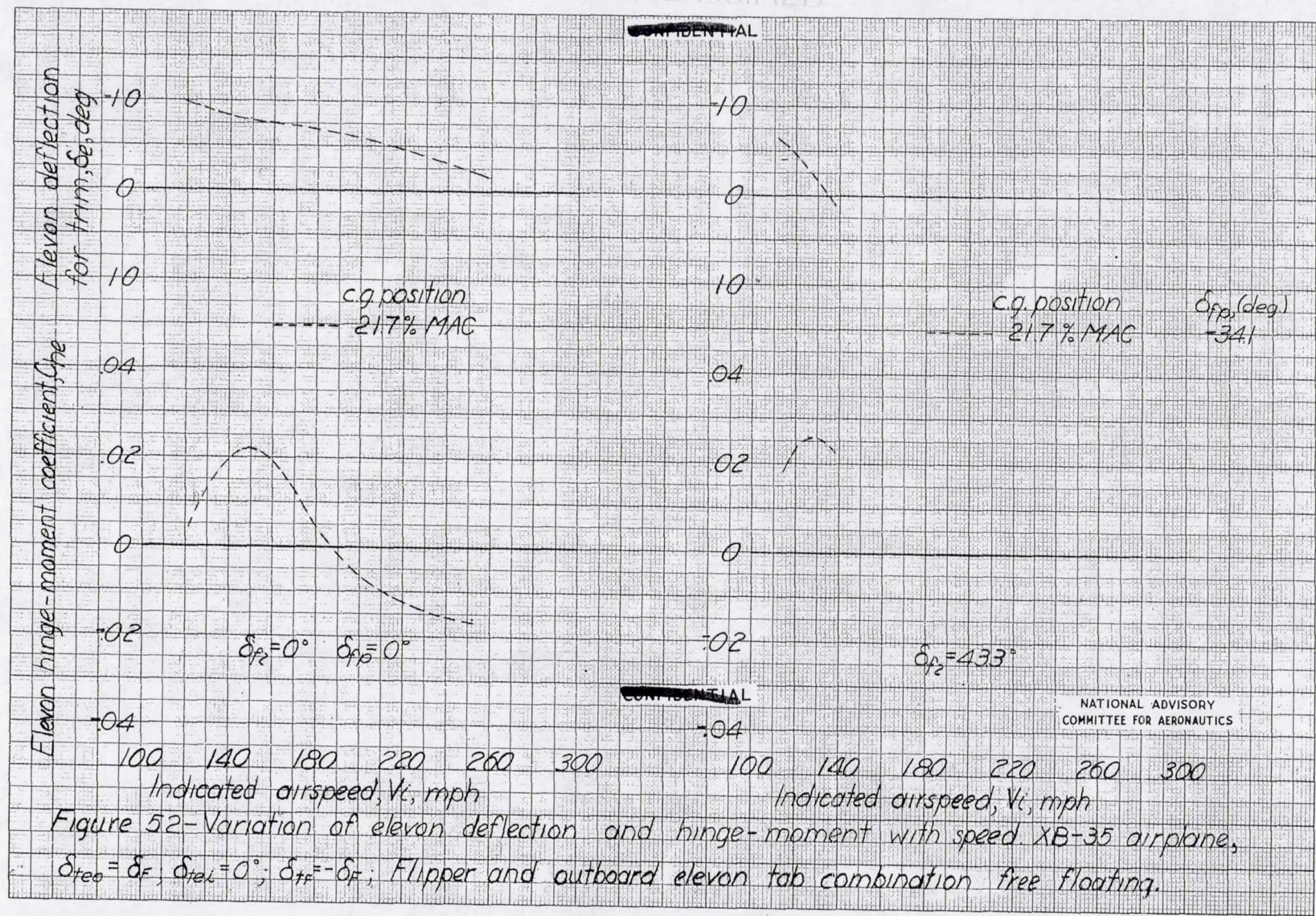
NATIONAL ADVISORY
COMMITTEE FOR AERONAUTICS

MR No. L5L27

UNCLASSIFIED

184502

UNCLASSIFIED



CONFIDENTIAL

NATIONAL ADVISORY COMMITTEE FOR AERONAUTICS

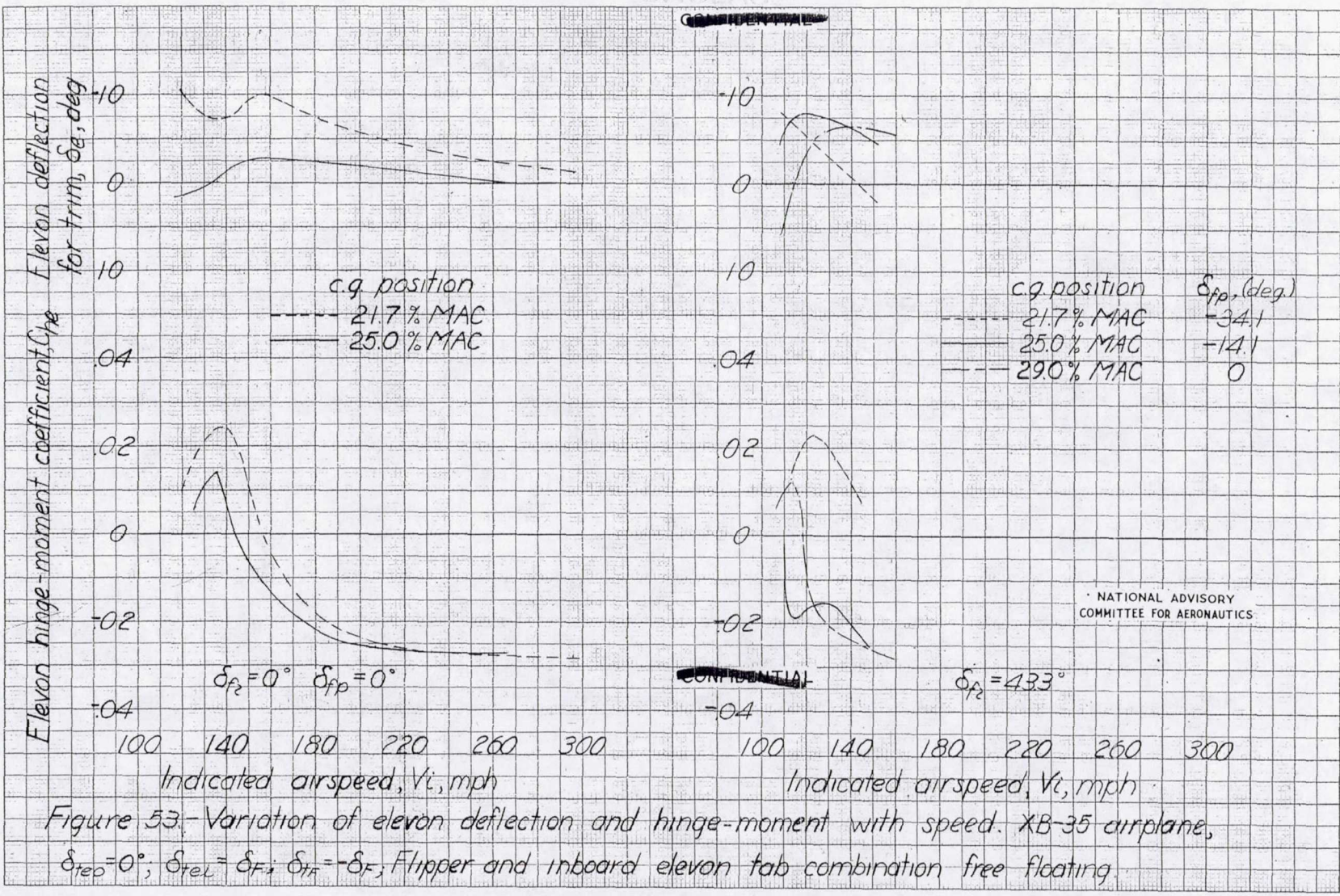
Figure 52-Variation of elevon deflection and hinge-moment with speed XB-35 airplane, $\delta_{te0} = \delta_F$; $\delta_{tel} = 0^\circ$; $\delta_{tr} = -\delta_F$; Flipper and outboard elevon tab combination free floating.

MR No. L5L27

UNCLASSIFIED

10455

UNCLASSIFIED



NATIONAL ADVISORY COMMITTEE FOR AERONAUTICS

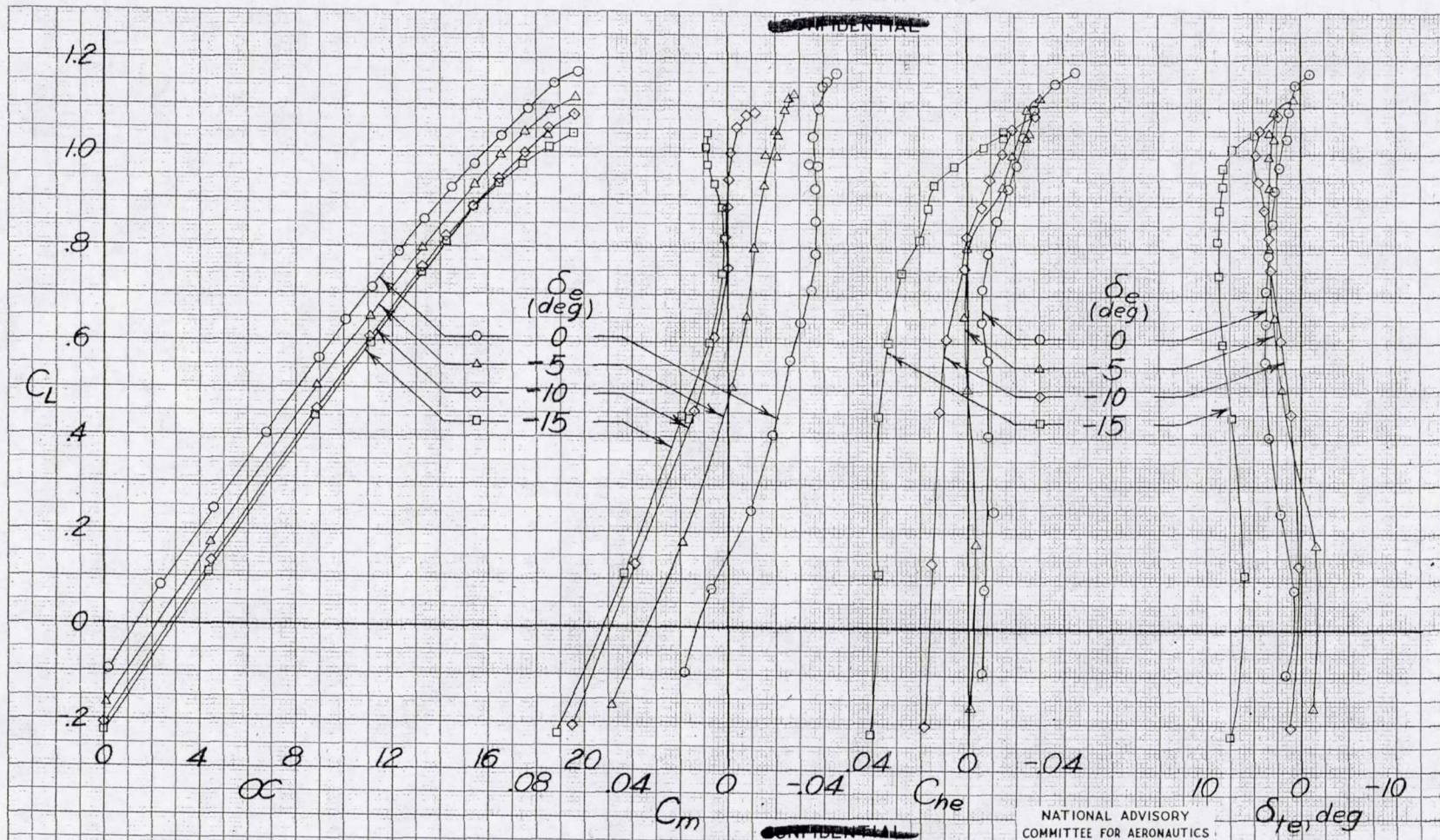
Figure 53.- Variation of elevon deflection and hinge-moment with speed. XB-35 airplane, $\delta_{te0} = 0^\circ$; $\delta_{tel} = \delta_{F}$; $\delta_{tr} = -\delta_{F}$, Flipper and inboard elevon tab combination free floating.

MR No. 15127

UNCLASSIFIED

10454

UNCLASSIFIED



MR No. L5127

Figure 54-Effects of free-floating inboard half-span elevon tab. $1/2$ -scale XB-35 semispan model; $\delta_{f1} = 0^\circ$; $\delta_{fp} = 0^\circ$; slot closed; $\delta_{te0} = 0^\circ$; flipper free floating; $\delta_{tf} = -\delta_F$; $R \approx 7,500,000$, $M \approx 0.12$

UNCLASSIFIED

164505

UNCLASSIFIED

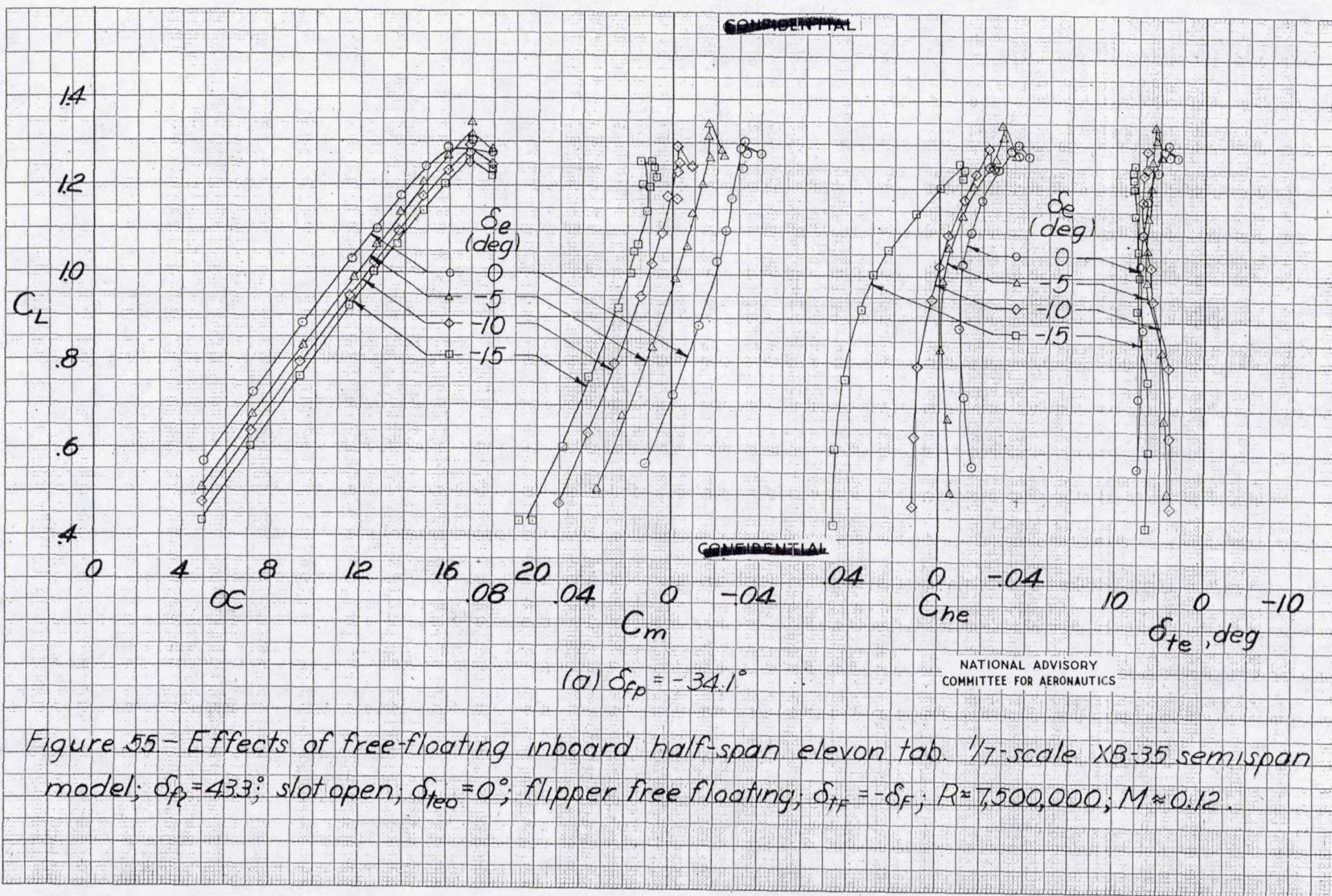


Figure 55 - Effects of free-floating inboard half-span elevon tab. 1/7-scale XB-35 semispan model; $\delta_{fp} = 43.3^\circ$; slot open, $\delta_{teo} = 0^\circ$; flipper free floating; $\delta_{ff} = -\delta_F$; $R \approx 7,500,000$; $M \approx 0.12$.

MR No. L5L27

UNCLASSIFIED

15455

UNCLASSIFIED

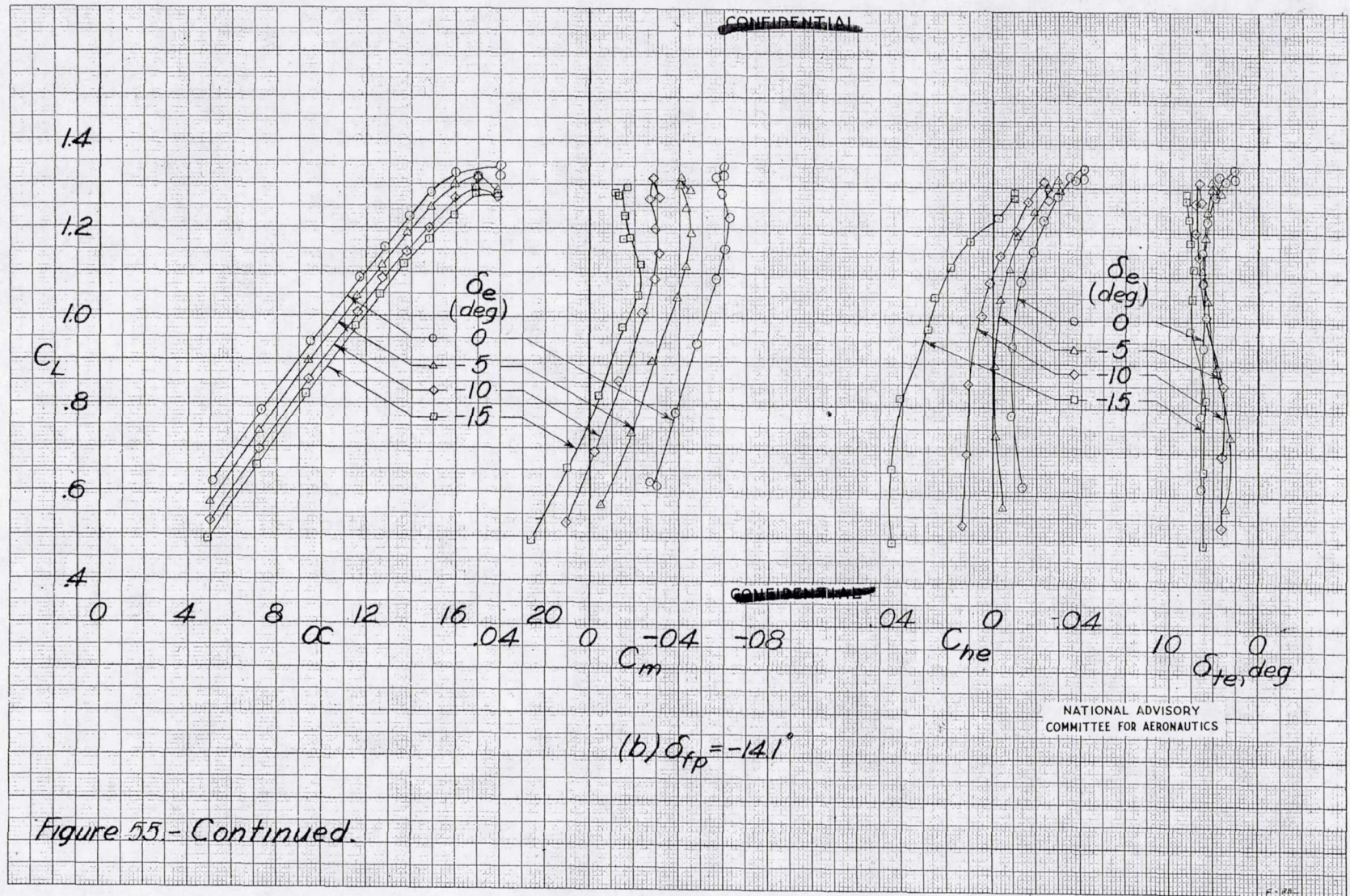


Figure 55 - Continued.

MR No. L5L27

UNCLASSIFIED

104505

UNCLASSIFIED

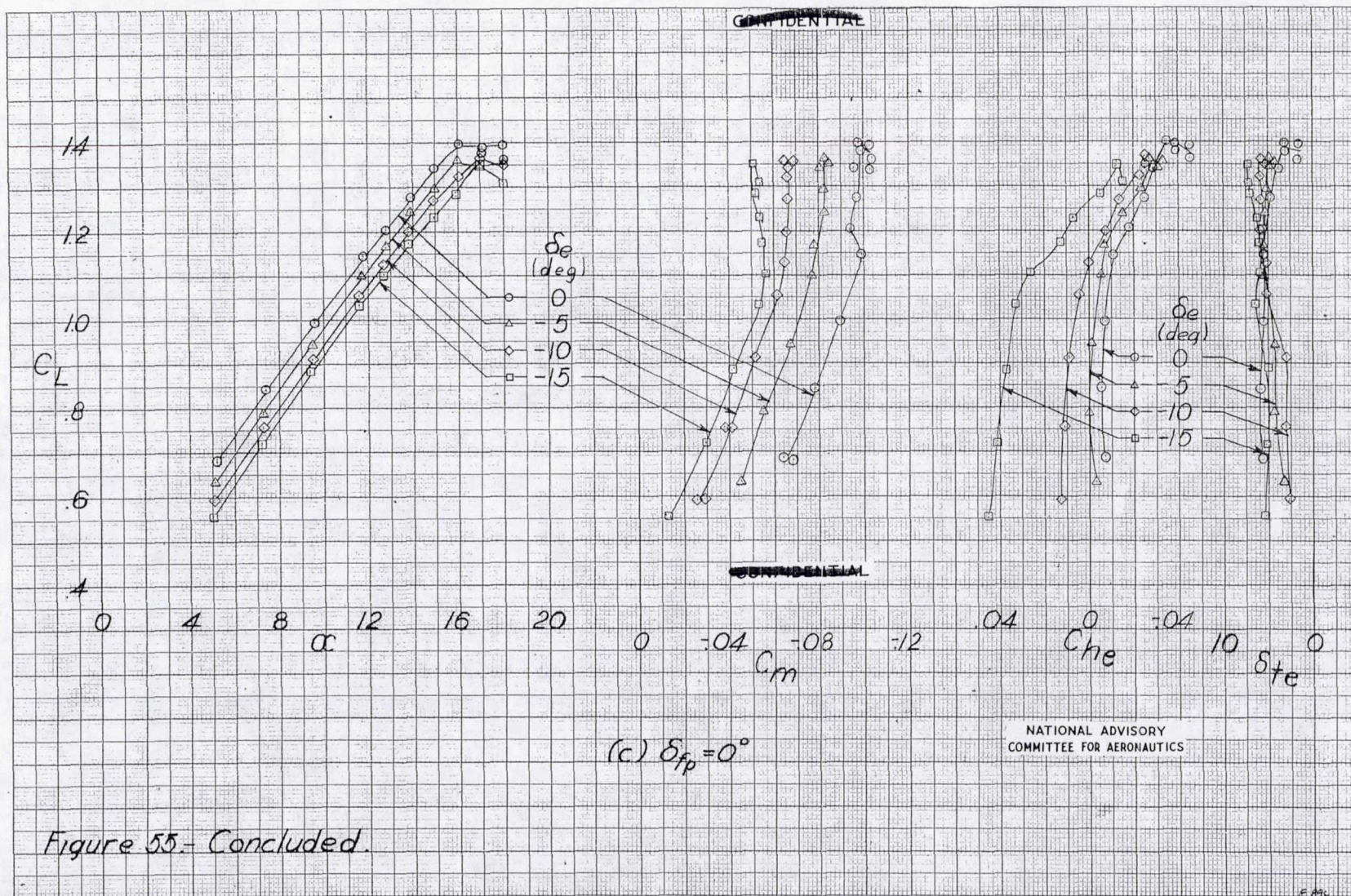
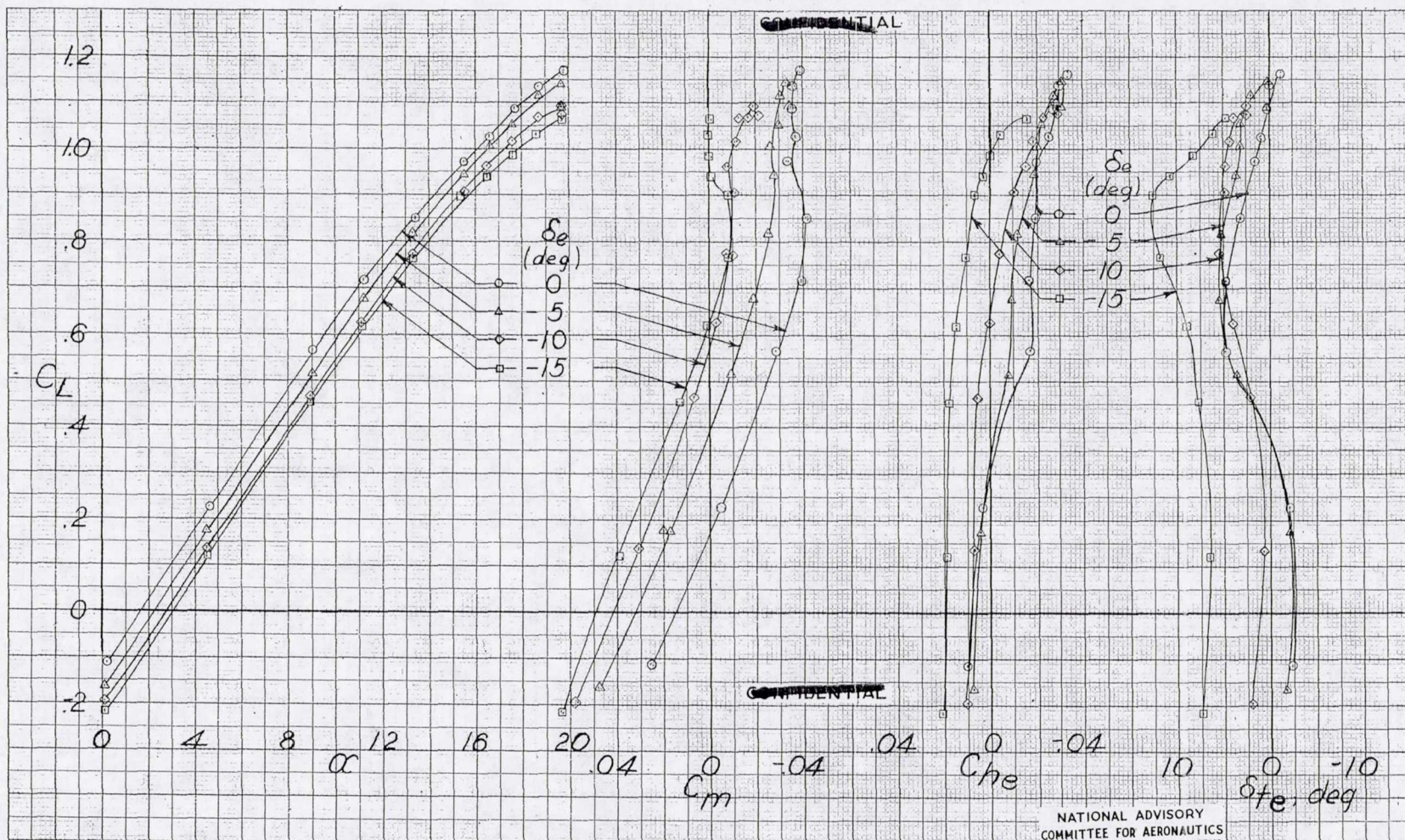


Figure 55- Concluded.

UNCLASSIFIED

UNCLASSIFIED



NATIONAL ADVISORY
COMMITTEE FOR AERONAUTICS

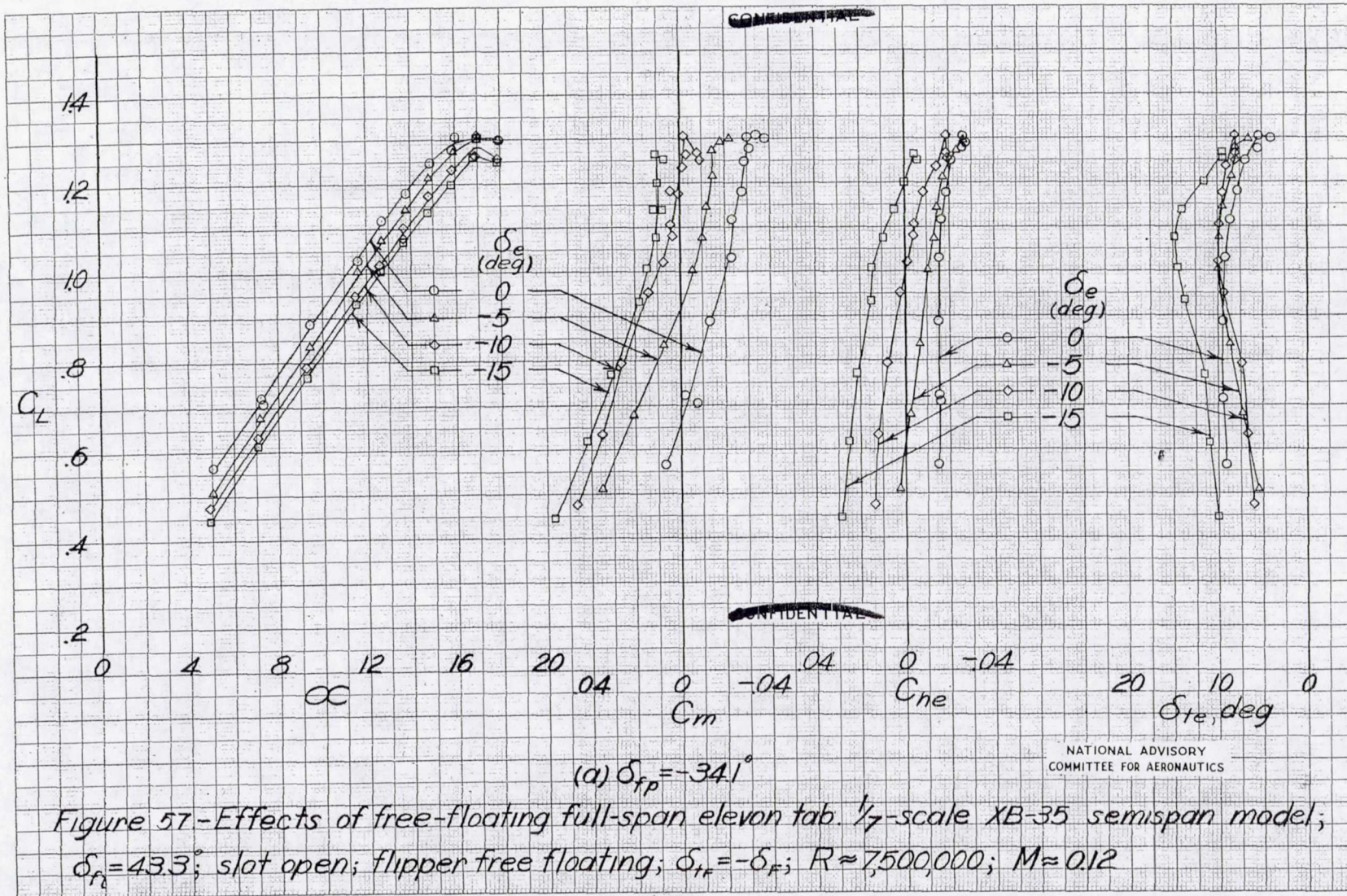
MR No. 15127

Figure 55.- Effects of free-floating full-span elevon tab. 1/7-scale XB-35 semispan model, $\delta_{F_c} = 0^\circ$; $\delta_{F_p} = 0^\circ$; slot closed, flipper free floating, $\delta_{F_r} = -\delta_F$, $R \approx 7,500,000$, $M \approx 0.12$.

UNCLASSIFIED

18457

UNCLASSIFIED



MR No. L5L27

UNCLASSIFIED

10455

UNCLASSIFIED

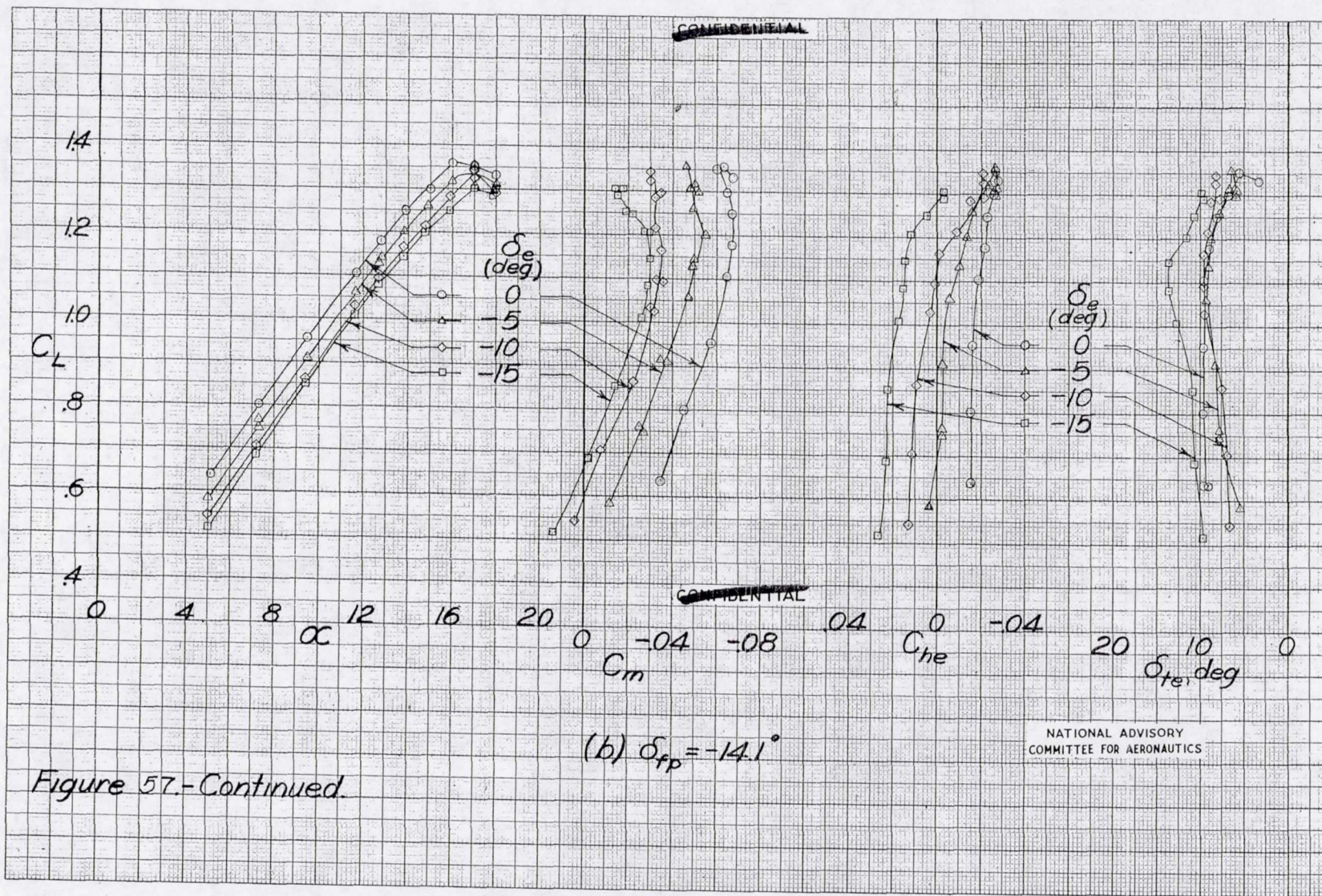


Figure 57.-Continued.

MR No. 15127

UNCLASSIFIED

10457

UNCLASSIFIED

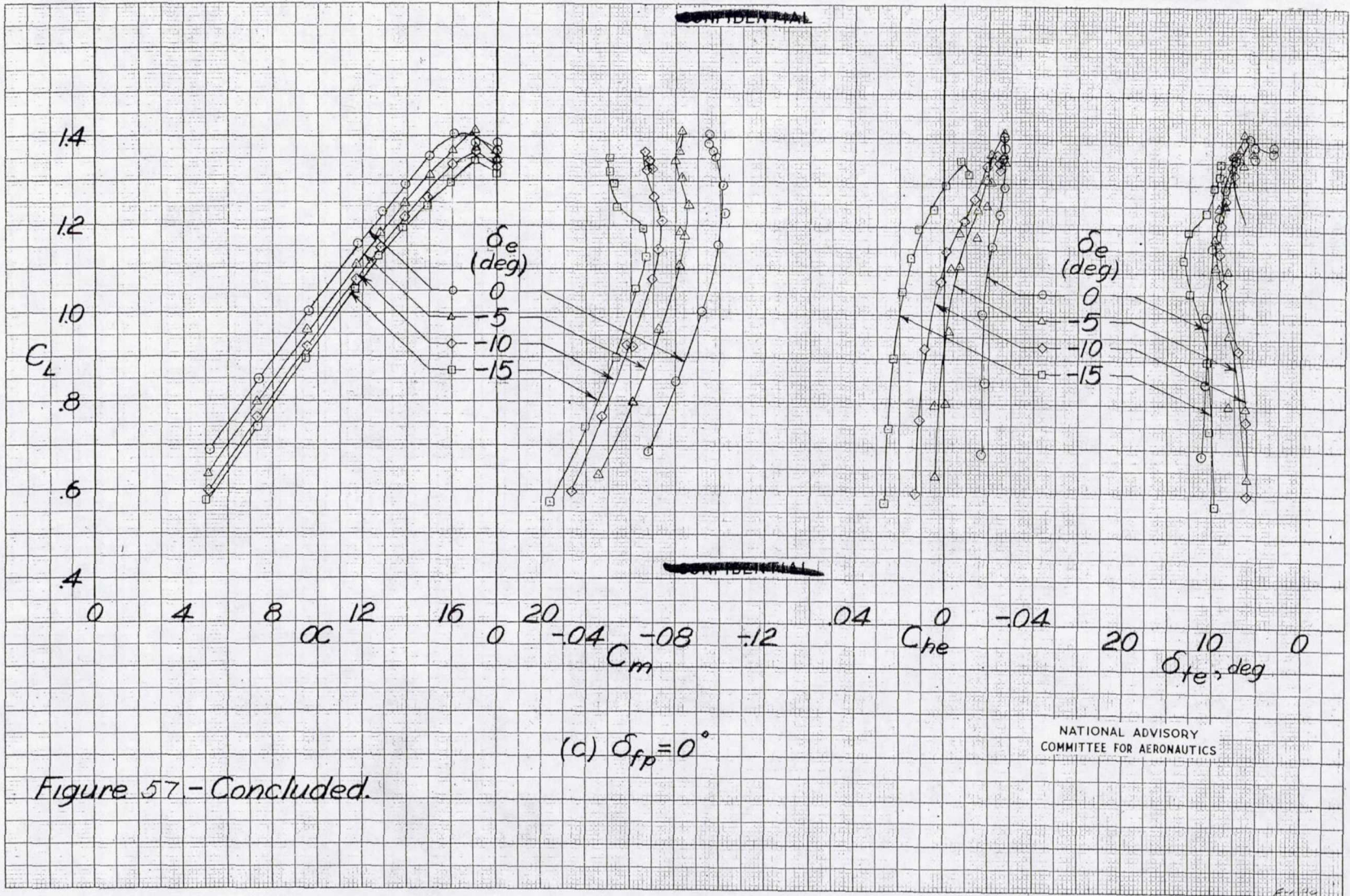


Figure 57 - Concluded.

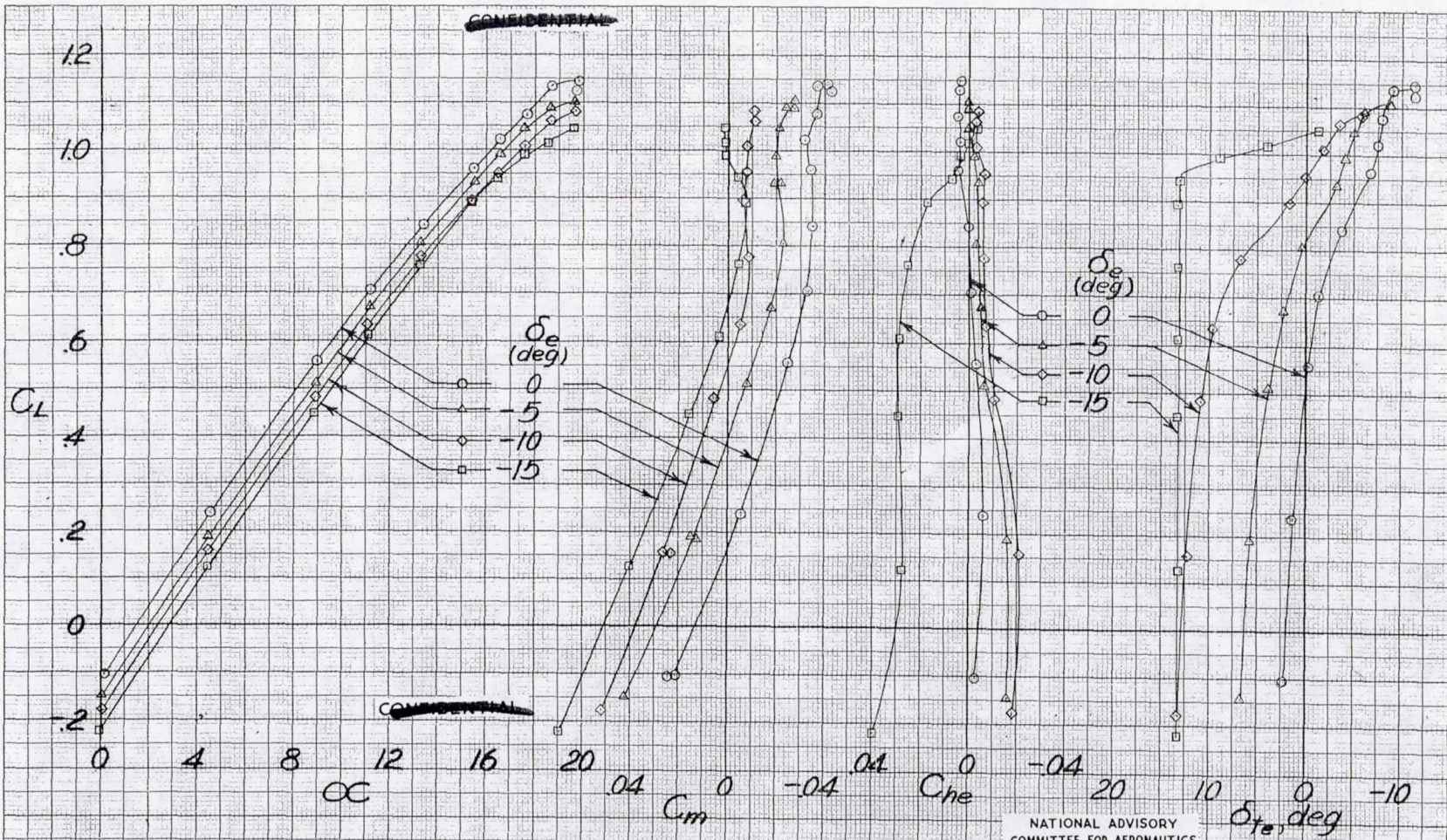
(c) $\delta_{fp} = 0^\circ$

NATIONAL ADVISORY COMMITTEE FOR AERONAUTICS

MR No. L5L27

UNCLASSIFIED

UNCLASSIFIED



NATIONAL ADVISORY COMMITTEE FOR AERONAUTICS

Figure 5B.-Effects of free-floating full-span elevon tab with splines. 1/7-scale XB-35 semispan model; $\delta_{fl} = 0^\circ$; $\delta_{fp} = 0^\circ$; slot closed; flipper free floating; $\delta_{TF} = -\delta_F$; $R \approx 7,500,000$; $M \approx 0.12$

MR No. L5127

UNCLASSIFIED

1945

UNCLASSIFIED

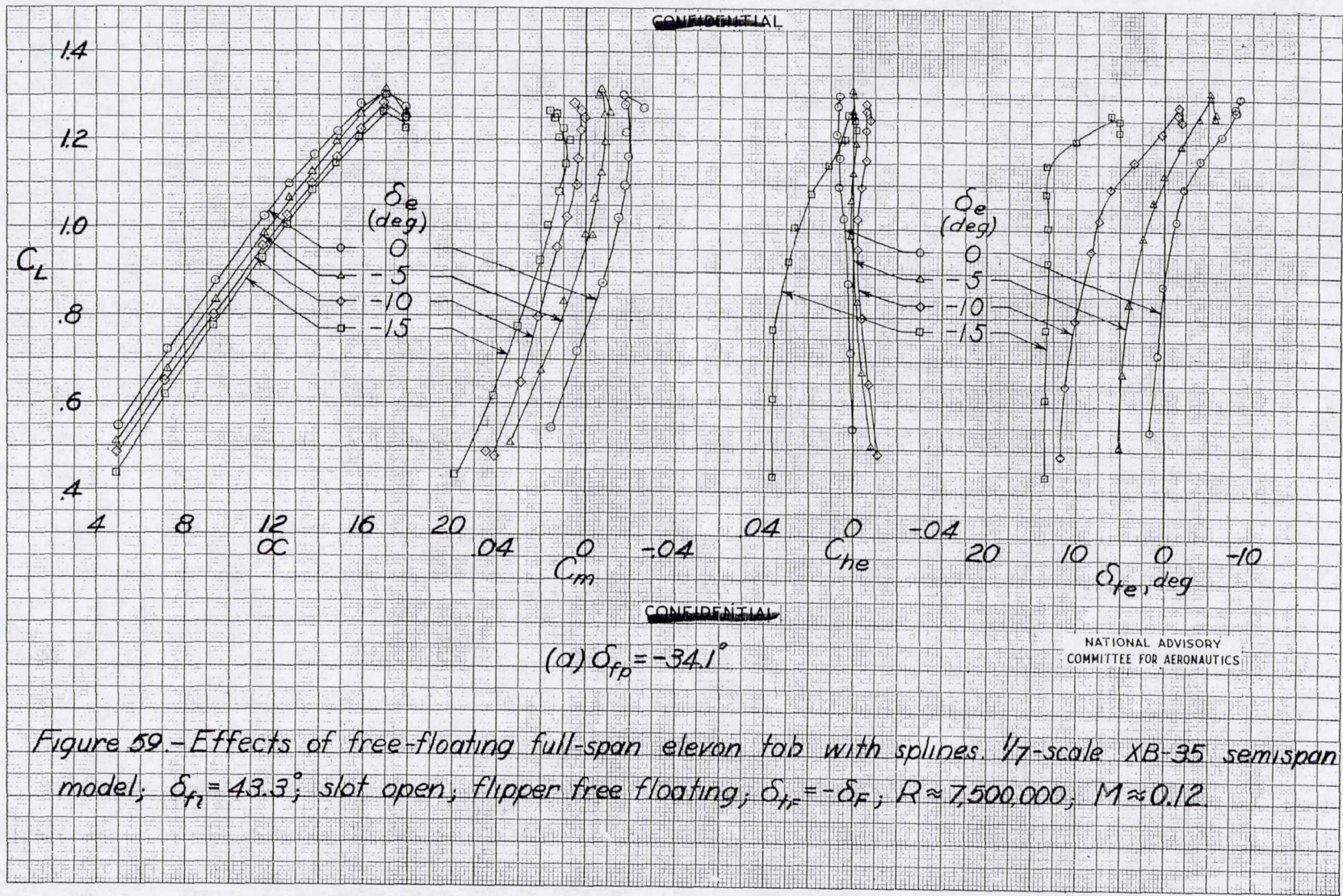


Figure 59.- Effects of free-floating full-span elevator tab with splines. 1/7-scale XB-35 semispan model; $\delta_{ft} = 43.3^\circ$; slot open, flipper free floating; $\delta_{fr} = -\delta_F$; $R \approx 7,500,000$; $M \approx 0.12$

MR No. L5L27

UNCLASSIFIED

154559

UNCLASSIFIED

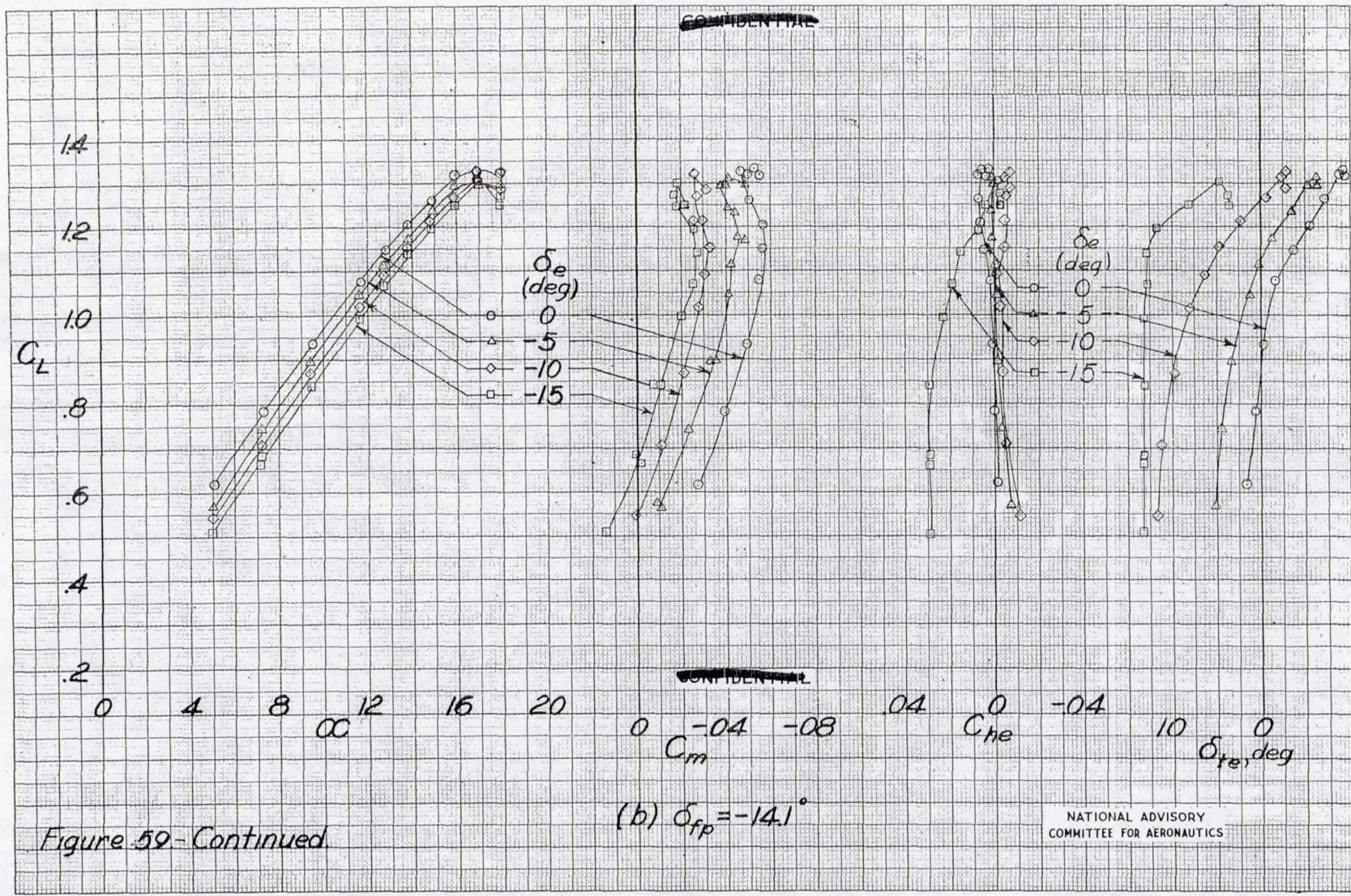


Figure 59-Continued

(b) $\delta_{fp} = -14.1^\circ$

NATIONAL ADVISORY
COMMITTEE FOR AERONAUTICS

MR No. 15127

UNCLASSIFIED

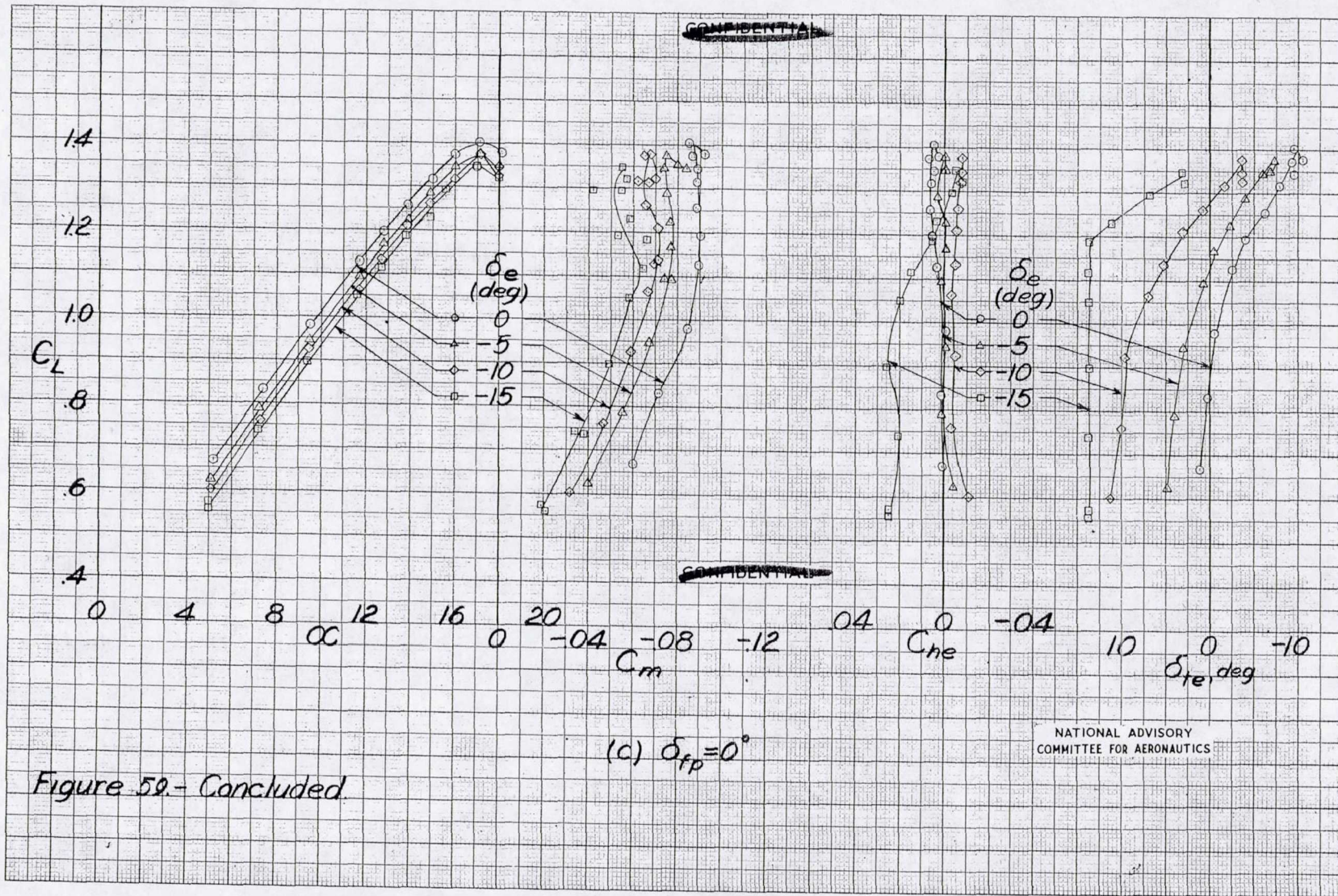
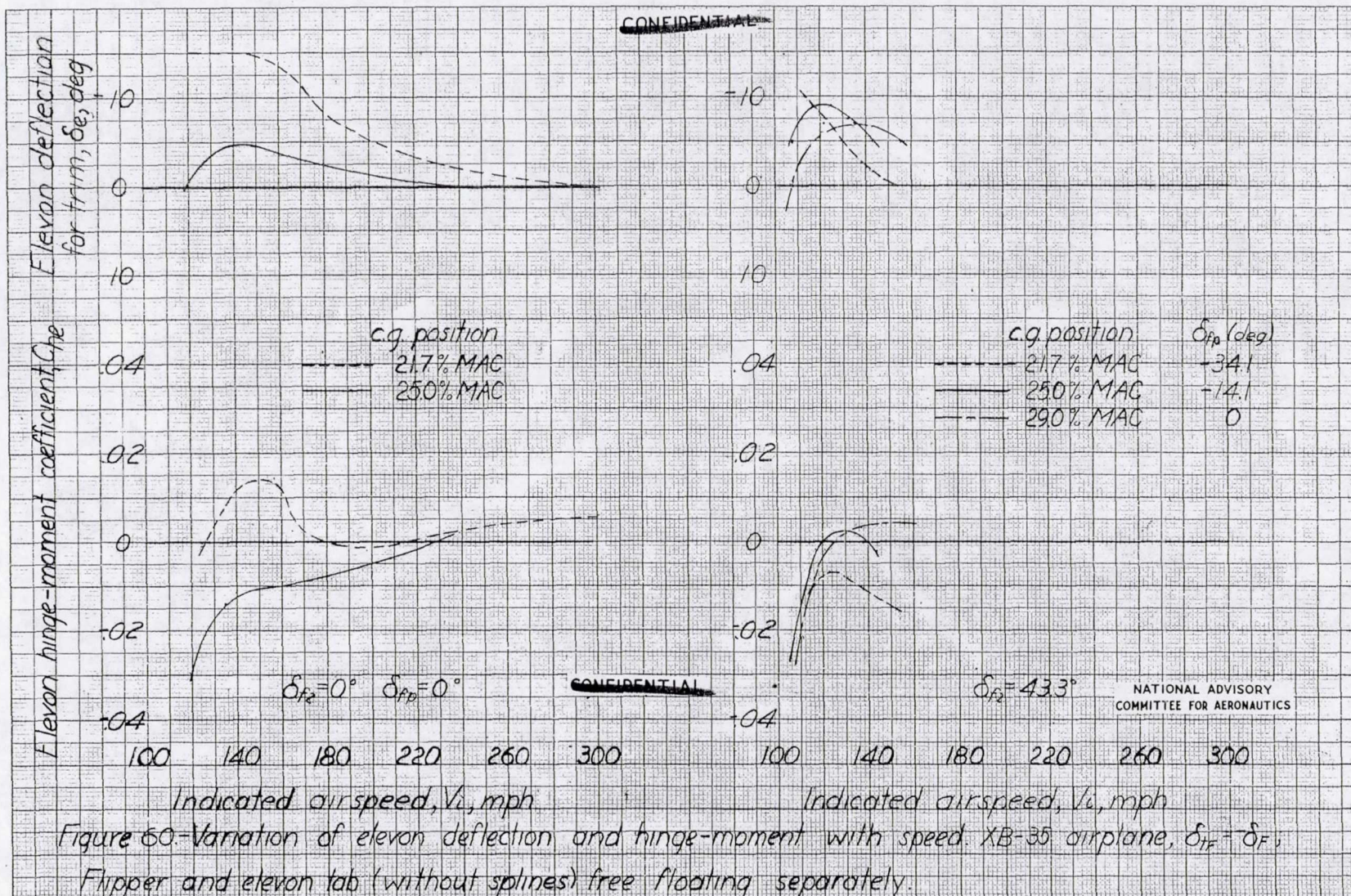


Figure 59.- Concluded.

MR No. L5L27

184550

UNCLASSIFIED



MR No. L5L27

UNCLASSIFIED

10454

UNCLASSIFIED

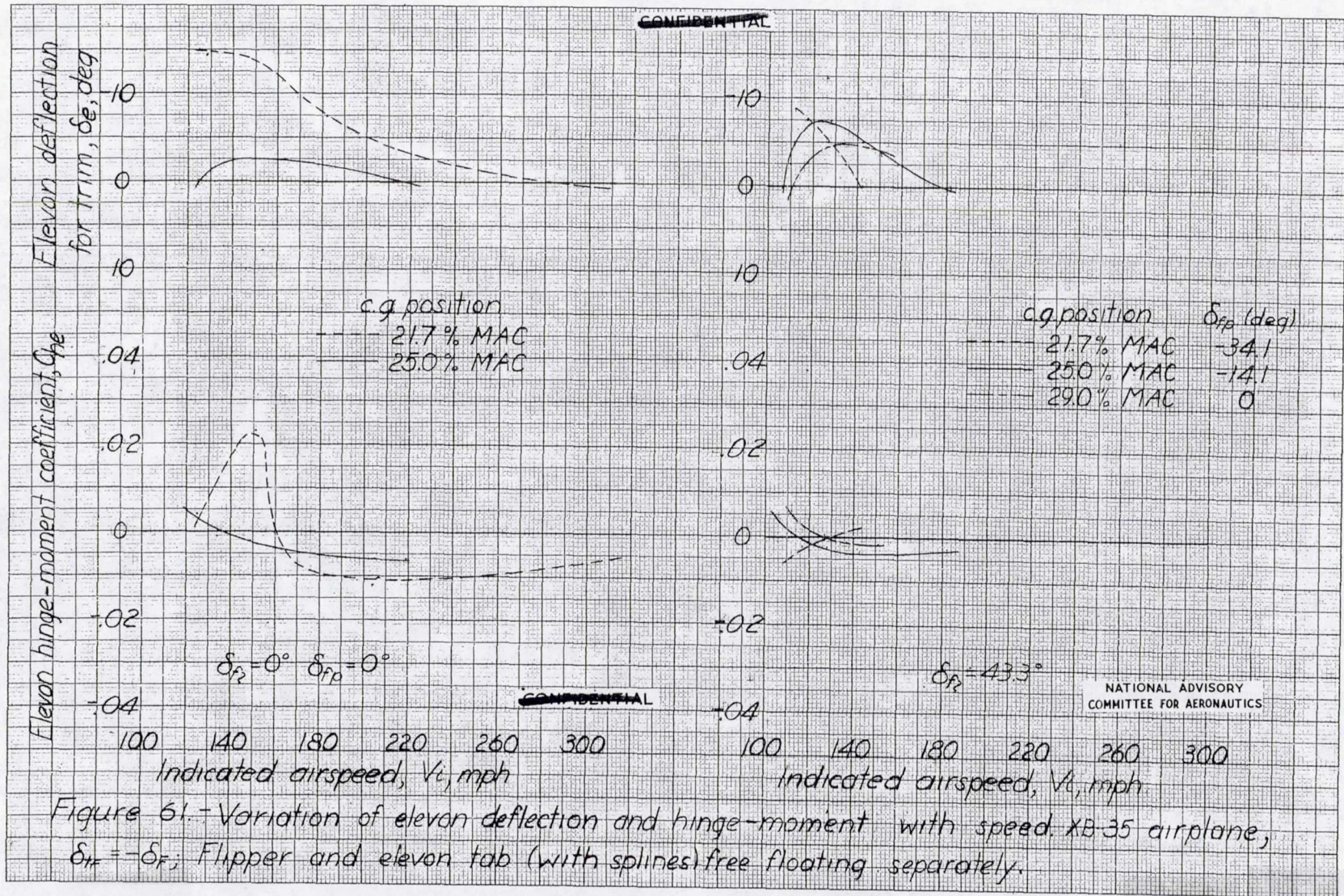


Figure 61. - Variation of elevon deflection and hinge-moment with speed. XB-35 airplane, $\delta_{F11} = -\delta_{F1}$; Flipper and elevon tab (with splines) free floating separately.

MR No. L5L27

UNCLASSIFIED

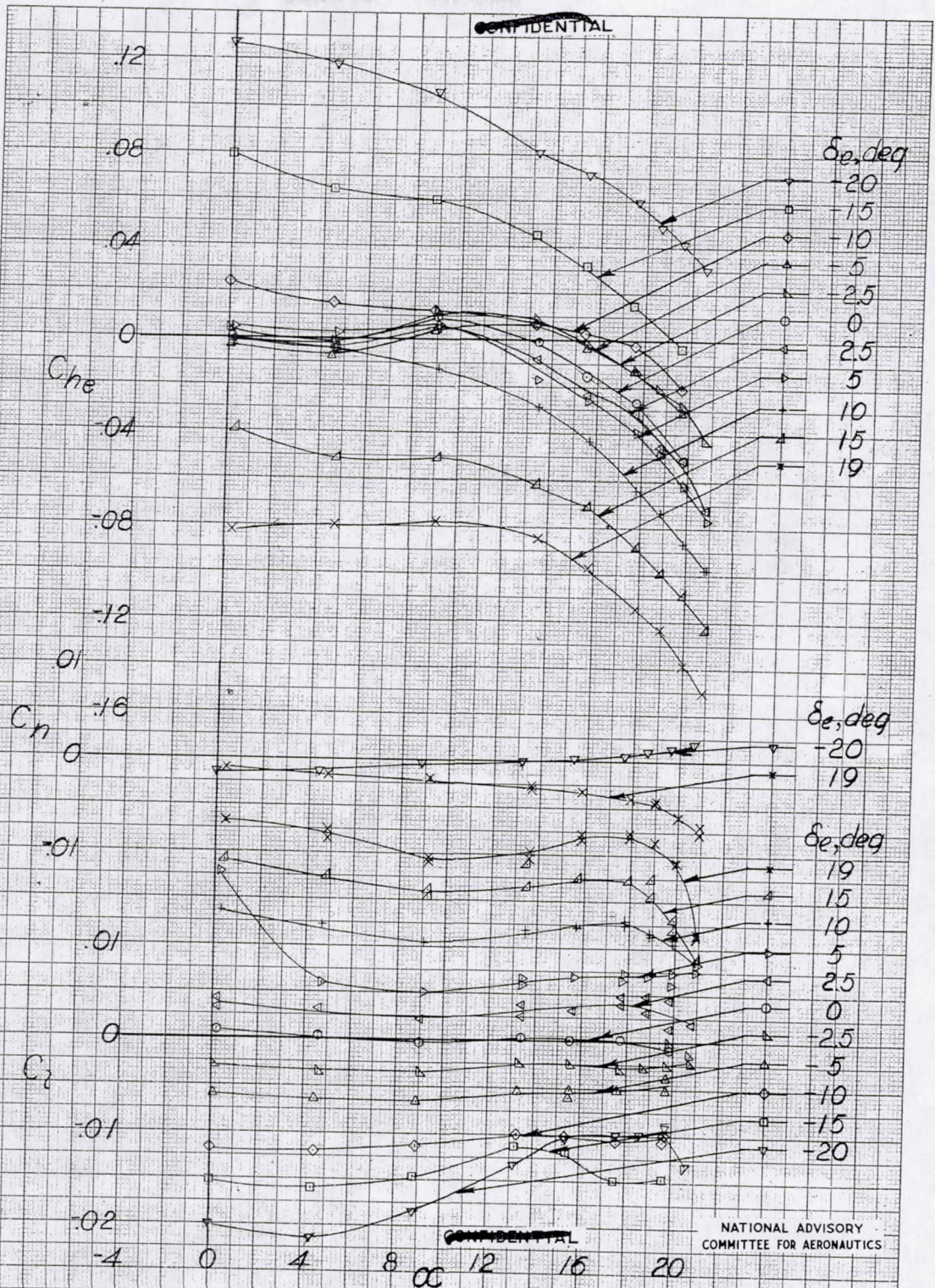


Figure 62 - Aileron characteristics with elevon tabs locked.
 $1/2$ -scale XB-35 semispan model; $\delta_{fl} = 0^\circ$; $\delta_{fp} = 0^\circ$; slot closed;
 flipper free-floating; $\delta_{TF} = -\delta_F$; $R \approx 7,500,000$; $M \approx 0.12$

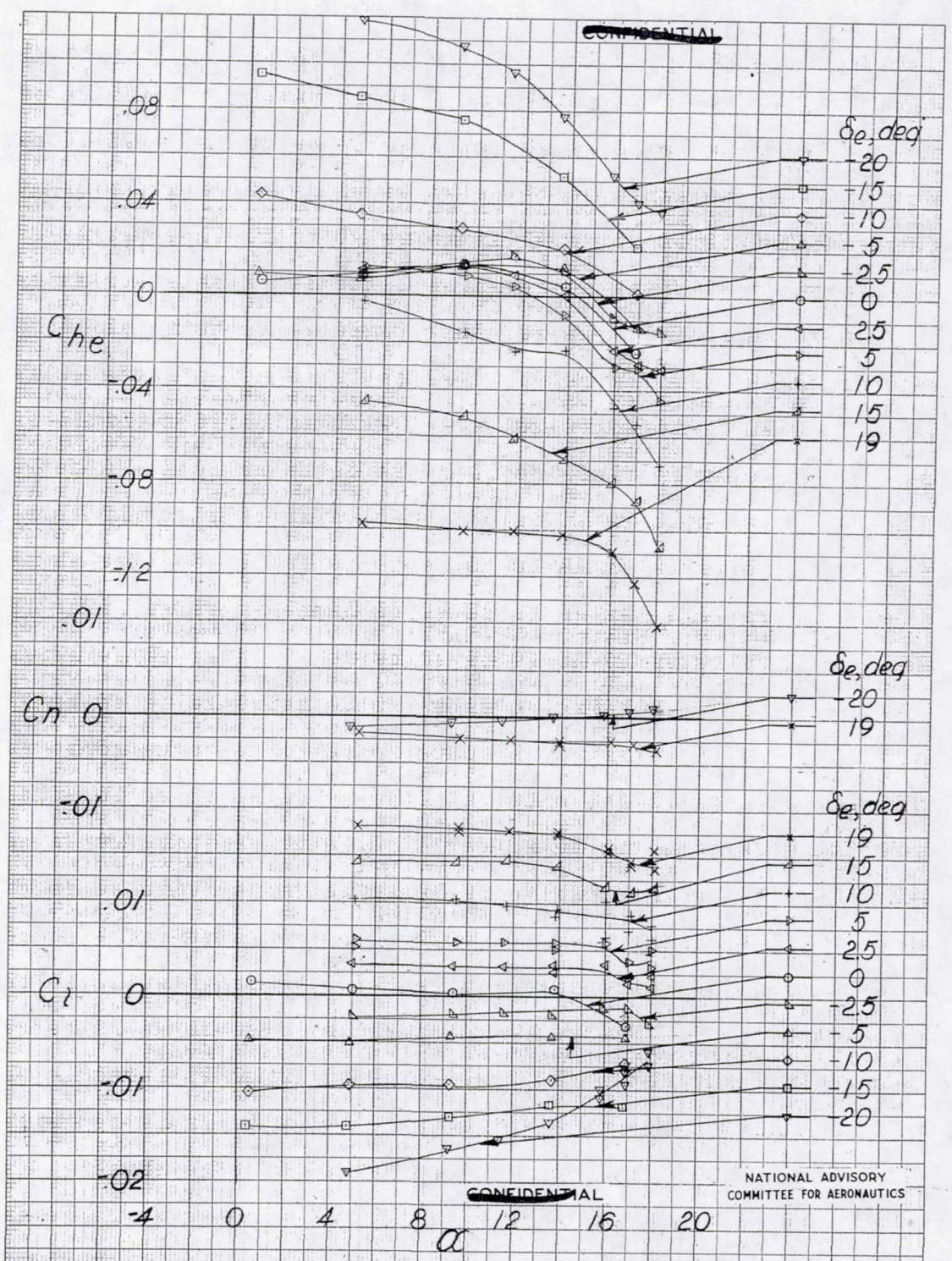
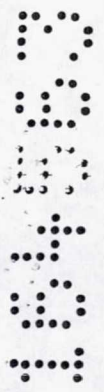
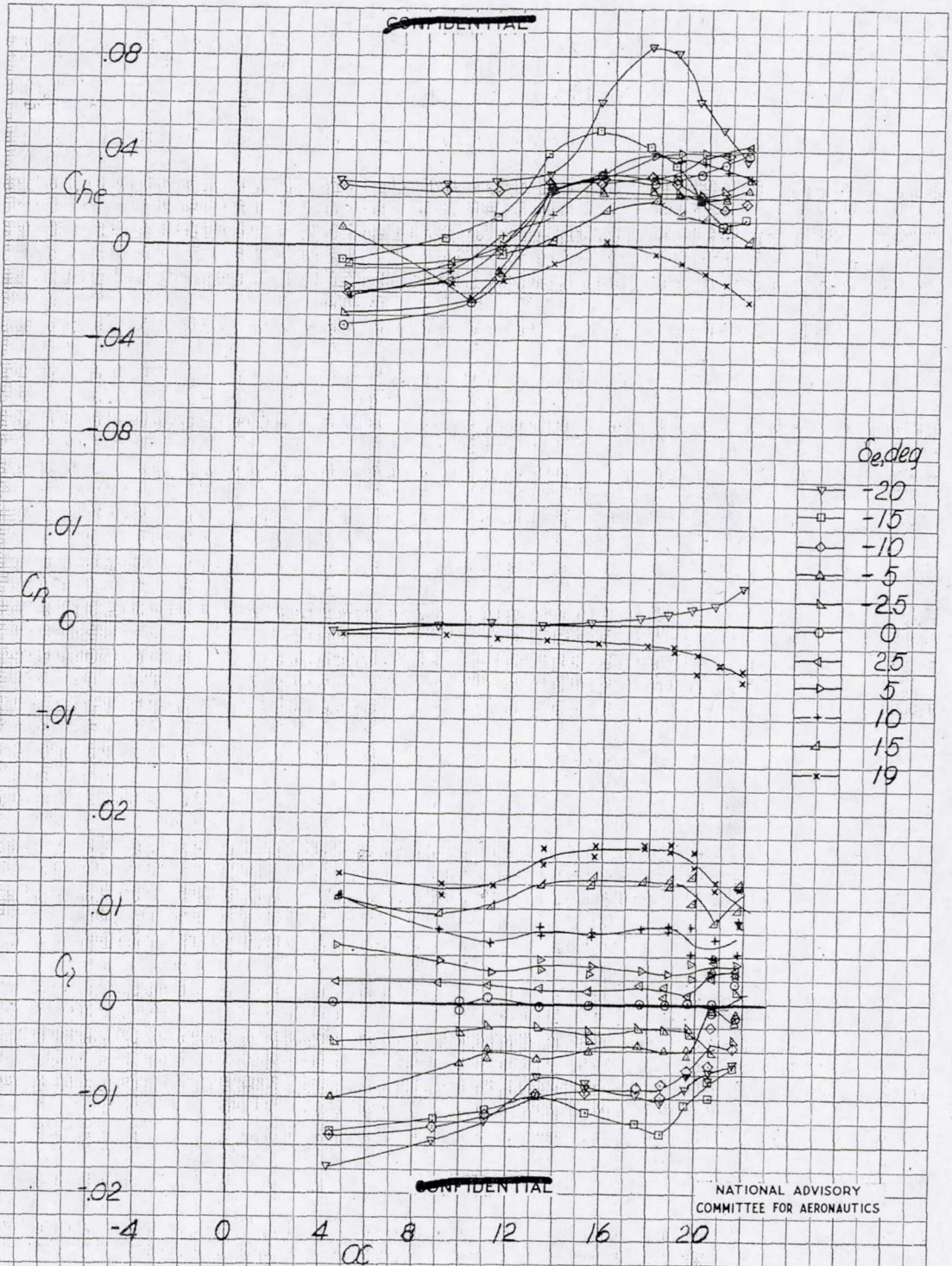


Figure 63.-Aileron characteristics with elevon tabs locked
 1/7-scale XB-35 semispan model; $\delta_{F1} = 43.3^\circ$; $\delta_{F2} = -34.1^\circ$; slot open; flipper free-floating; $\delta_{TF} = -\delta_F$; $R \approx 7,500,000$; $M \approx 0.12$

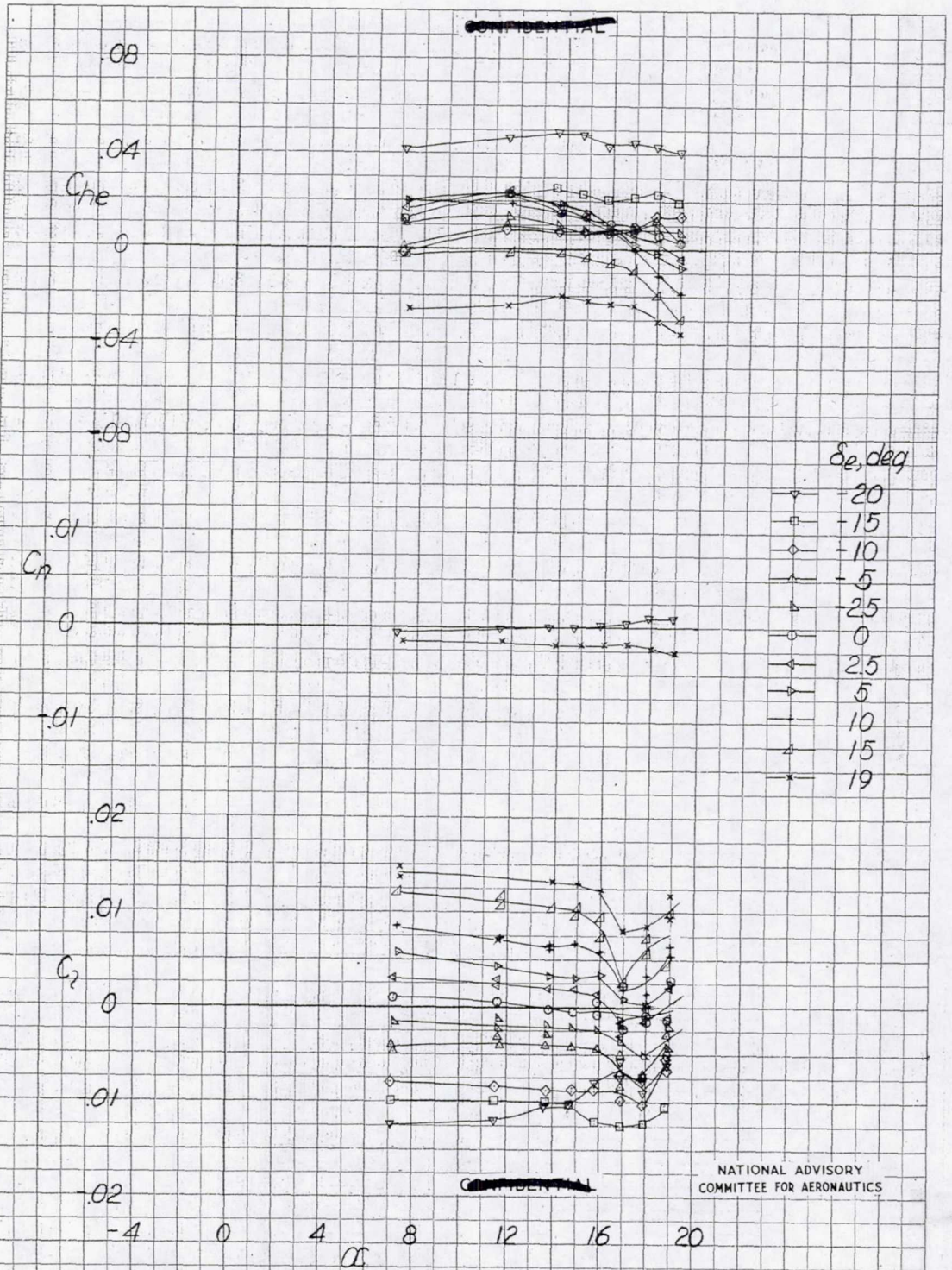
UNCLASSIFIED



NATIONAL ADVISORY COMMITTEE FOR AERONAUTICS

Figure 64-Aileron characteristics with a free-floating elevon tab and flipper combination $1/7$ -scale XB-35 semispan model; $\delta_{f_i} = 0^\circ$; $\delta_{f_p} = 0^\circ$; slot closed; $\delta_{f_e} = \delta_{f_i}$; $\delta_{f_f} = -\delta_{f_i}$; $R \approx 7,500,000$; $M \approx 0.12$

UNCLASSIFIED



NATIONAL ADVISORY COMMITTEE FOR AERONAUTICS

Figure 65 - Aileron characteristics with a free-floating elevator tab and flipper combination. $1/7$ -scale XB-35 semispan model; $\delta_{fl} = 43.3^\circ$; $\delta_{fp} = -34.1^\circ$; slot open; $\delta_{te} = \delta_F$; $\delta_{tf} = -\delta_F$; $R \approx 7,500,000$; $M \approx 0.12$



UNCLASSIFIED

MR No. L5L27

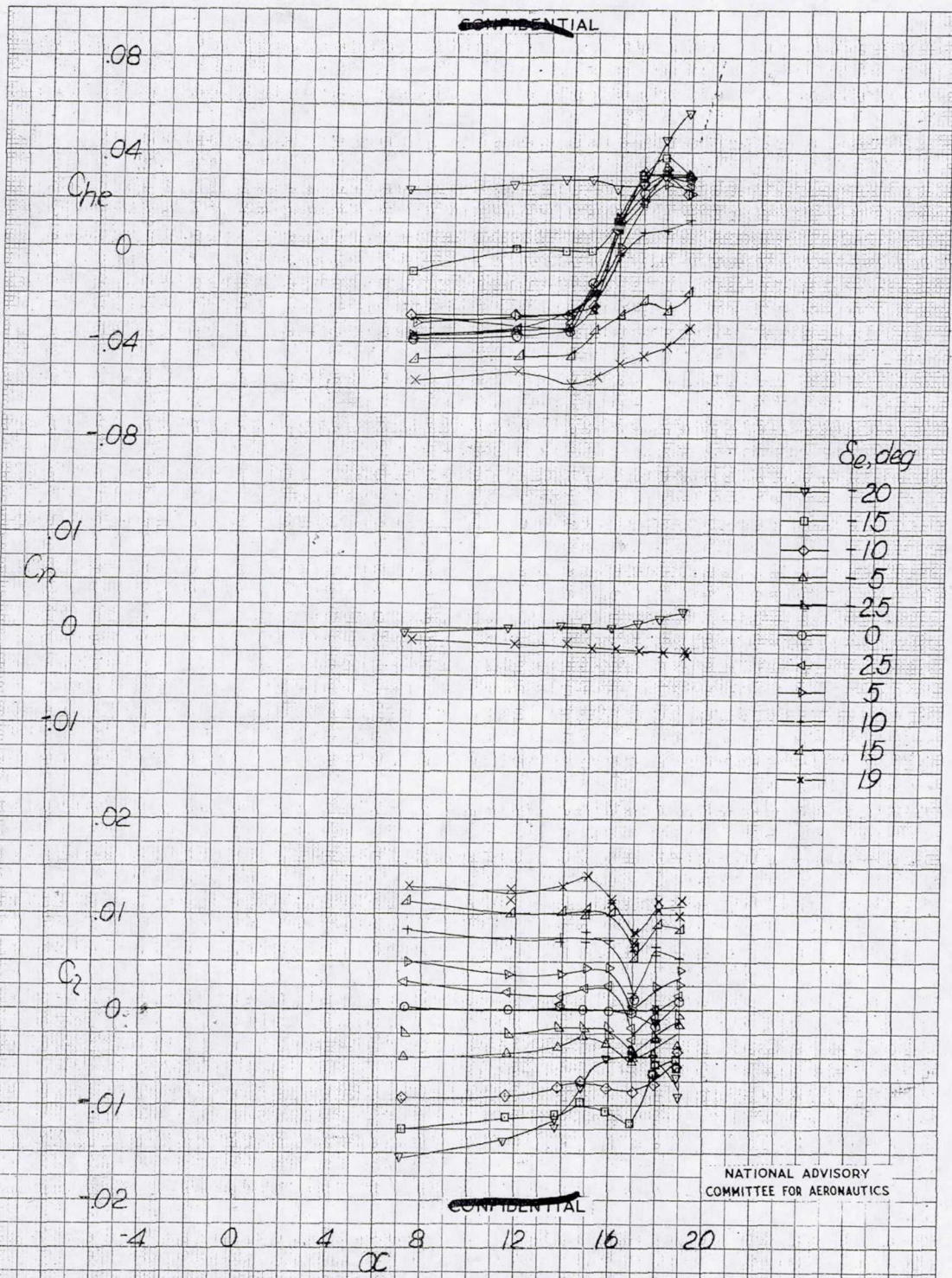


Figure 66.-Aileron characteristics with a free-floating elevator tab and flipper combination. $1/7$ -scale XB-35 semispan model; $\delta_{Ft} = 43.3^\circ$; $\delta_{Fp} = -14.1^\circ$; slot open; $\delta_{Te} = \delta_{Ft}$; $\delta_{Tp} = -\delta_{Ft}$; $R \approx 7,500,000$; $M = 0.12$

UNCLASSIFIED

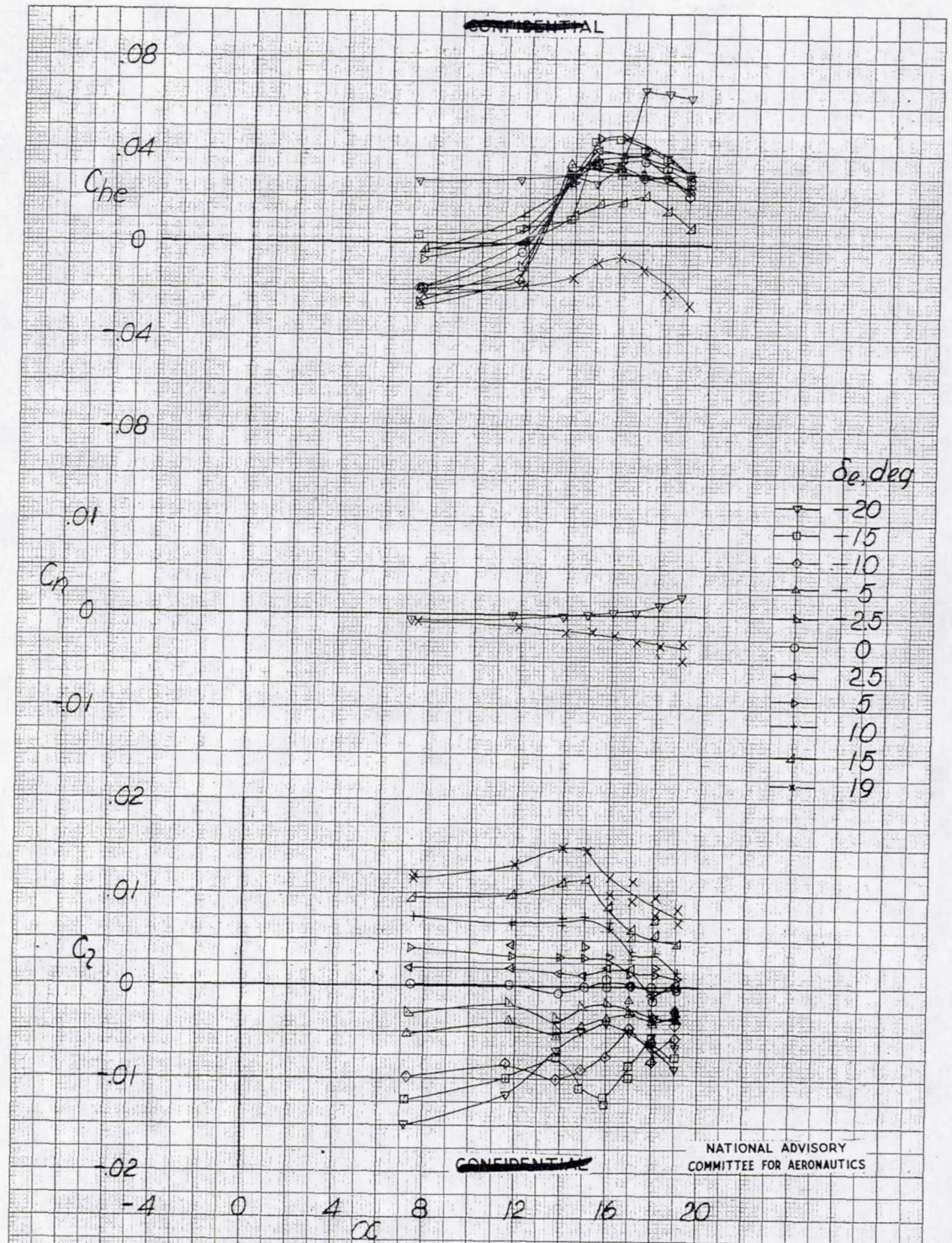
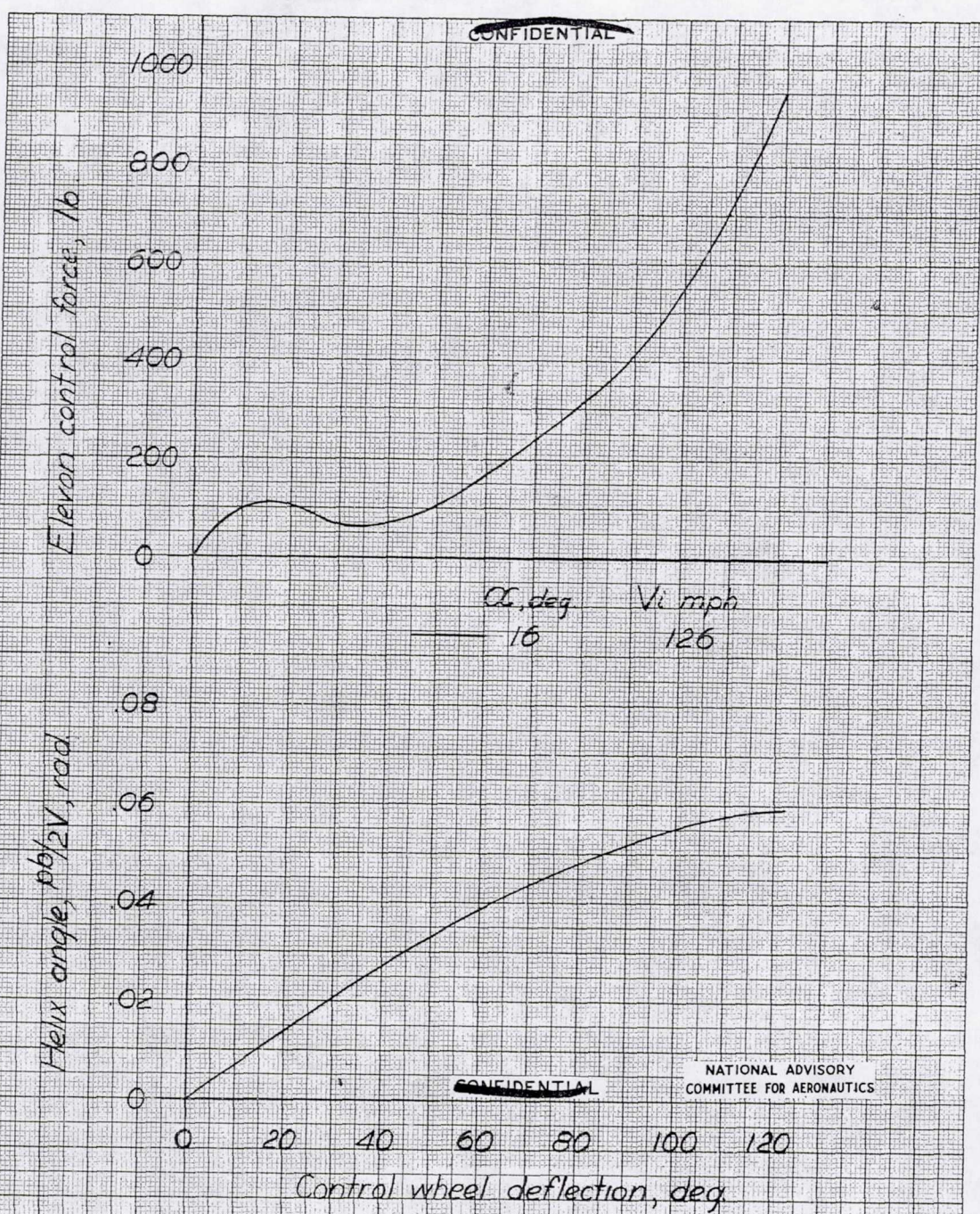


Figure 67 - Aileron characteristics with a free-floating elevon tab and flipper combination. $1/7$ -scale XB-35 semispan model; $\delta_{fl} = 43.3^\circ$; $\delta_{fp} = 0^\circ$; slot open; $\delta_{te} = \delta_F$; $\delta_{tf} = -\delta_F$; $R \approx 7,500,000$; $M \approx 0.12$



UNCLASSIFIED

MR No. L5L27



(a) $\delta_{F_2} = 0^\circ$; $\delta_{F_p} = 0^\circ$; slot closed

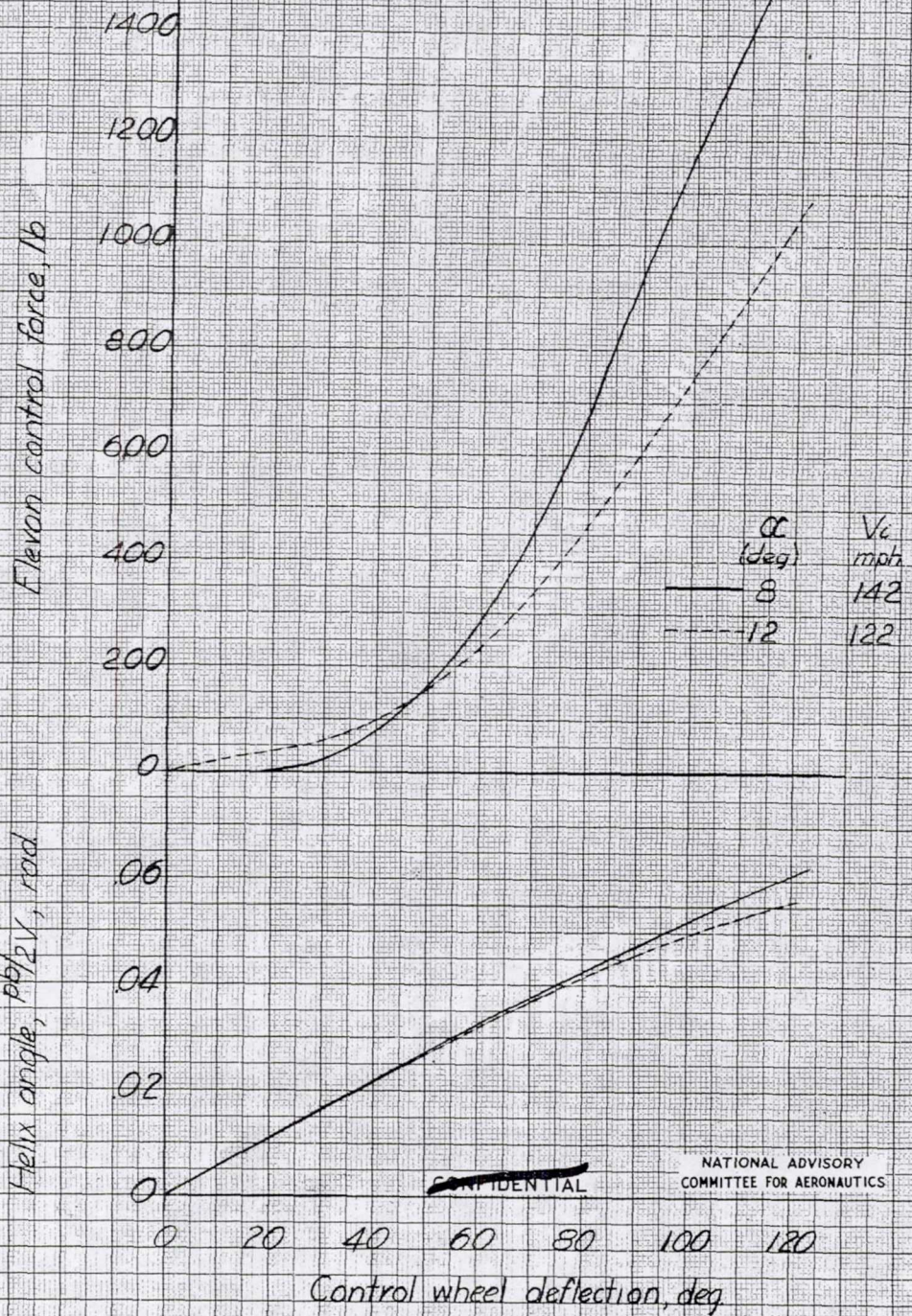
Figure 68 - Variation of estimated helix angle and lateral control force with control-wheel deflection. XB-35 airplane with free-floating flipper $\delta_{F_e} = 0^\circ$; $\delta_{F_r} = -\delta_r$;

UNCLASSIFIED

CONFIDENTIAL

UNCLASSIFIED

~~CONFIDENTIAL~~



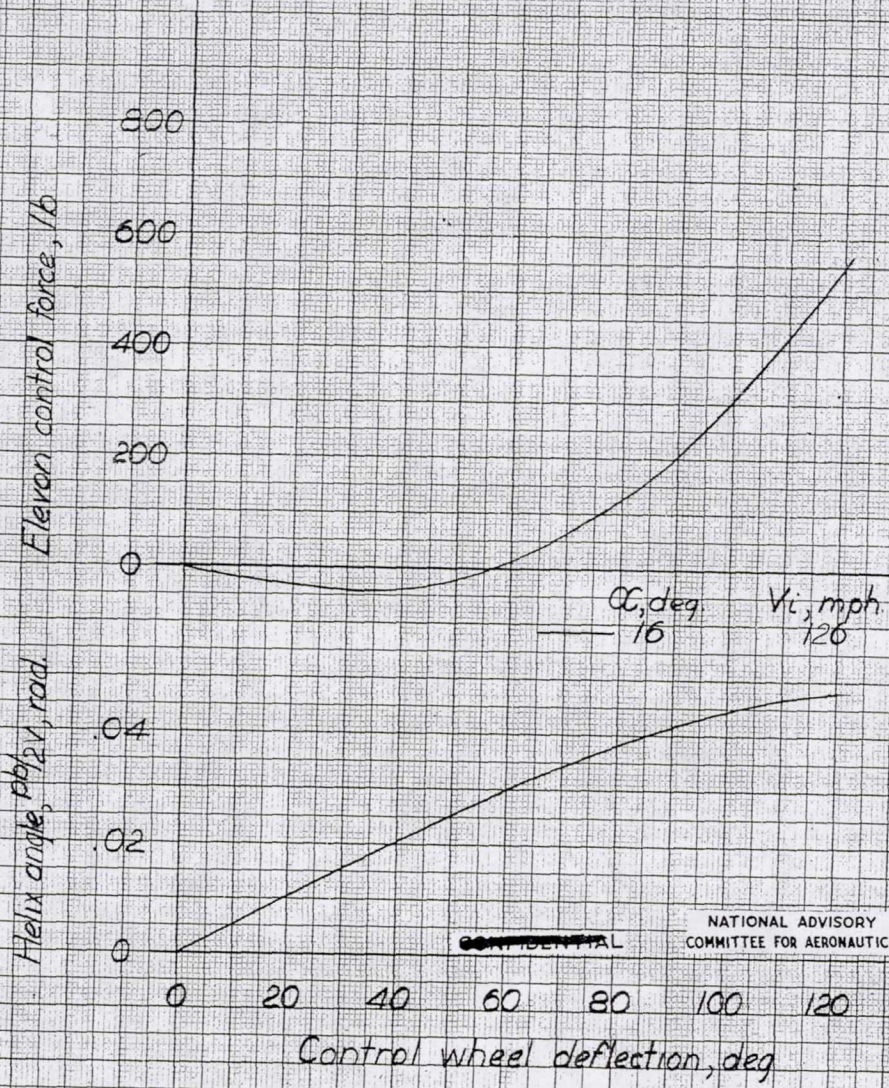
NATIONAL ADVISORY COMMITTEE FOR AERONAUTICS

~~CONFIDENTIAL~~

(b) $\delta_{F_1} = 43.3^\circ$; $\delta_{F_2} = -34.1^\circ$; slot open

Figure 68- Concluded.

~~CONFIDENTIAL~~



~~CONFIDENTIAL~~

NATIONAL ADVISORY COMMITTEE FOR AERONAUTICS

(a) $\delta_{F_e} = 0^\circ$; $\delta_{F_f} = 0^\circ$; slot closed

Figure 69 - Variation of estimated helix angle and lateral control force with control-wheel deflection XB-35 airplane with free-floating elevon tab and flipper combination.

$\delta_{T_e} = \delta_F$; $\delta_{T_f} = -\delta_F$



UNCLASSIFIED

MR No. L5L27

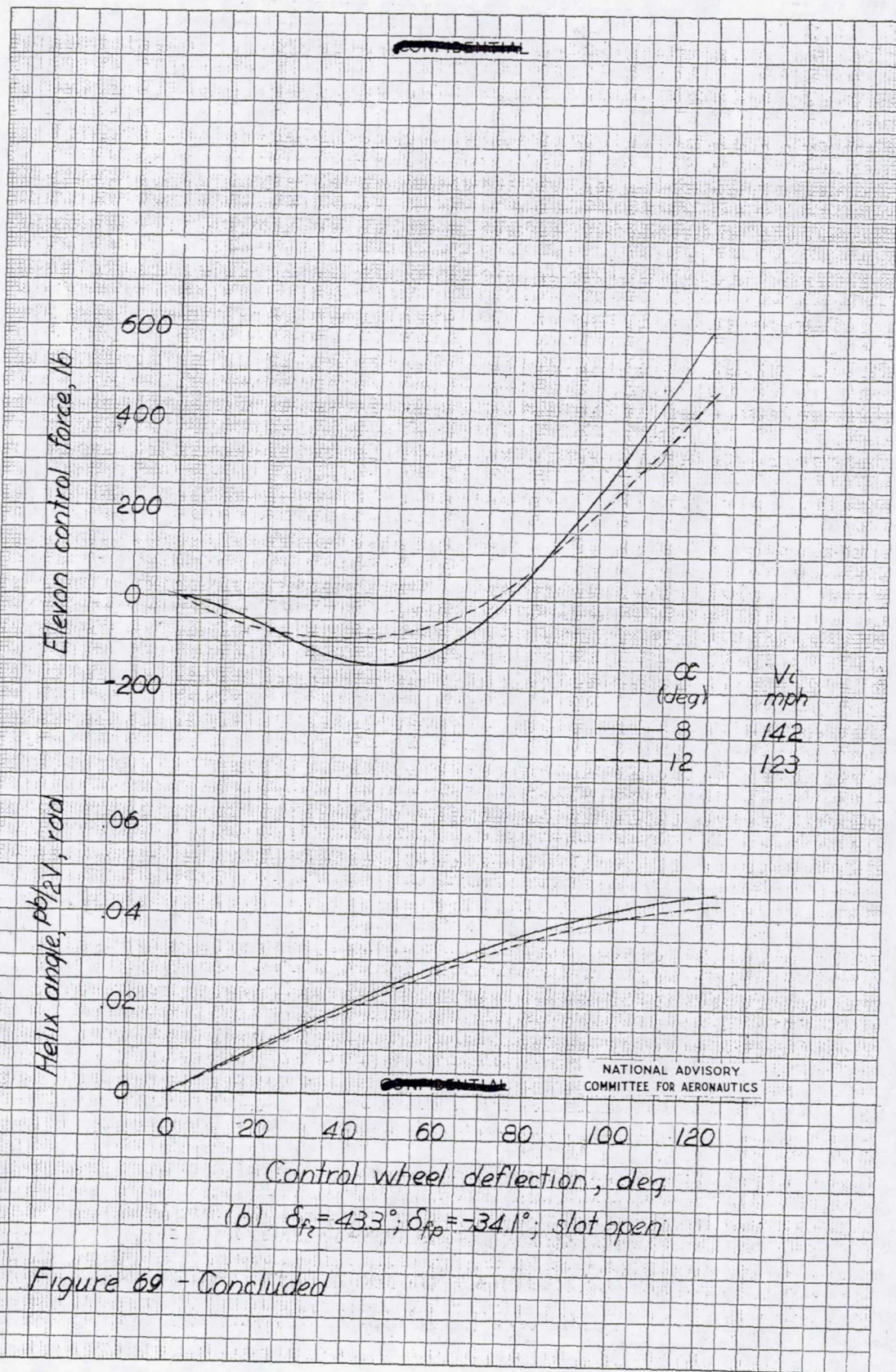


Figure 69 - Concluded

15437

UNCLASSIFIED

UNCLASSIFIED

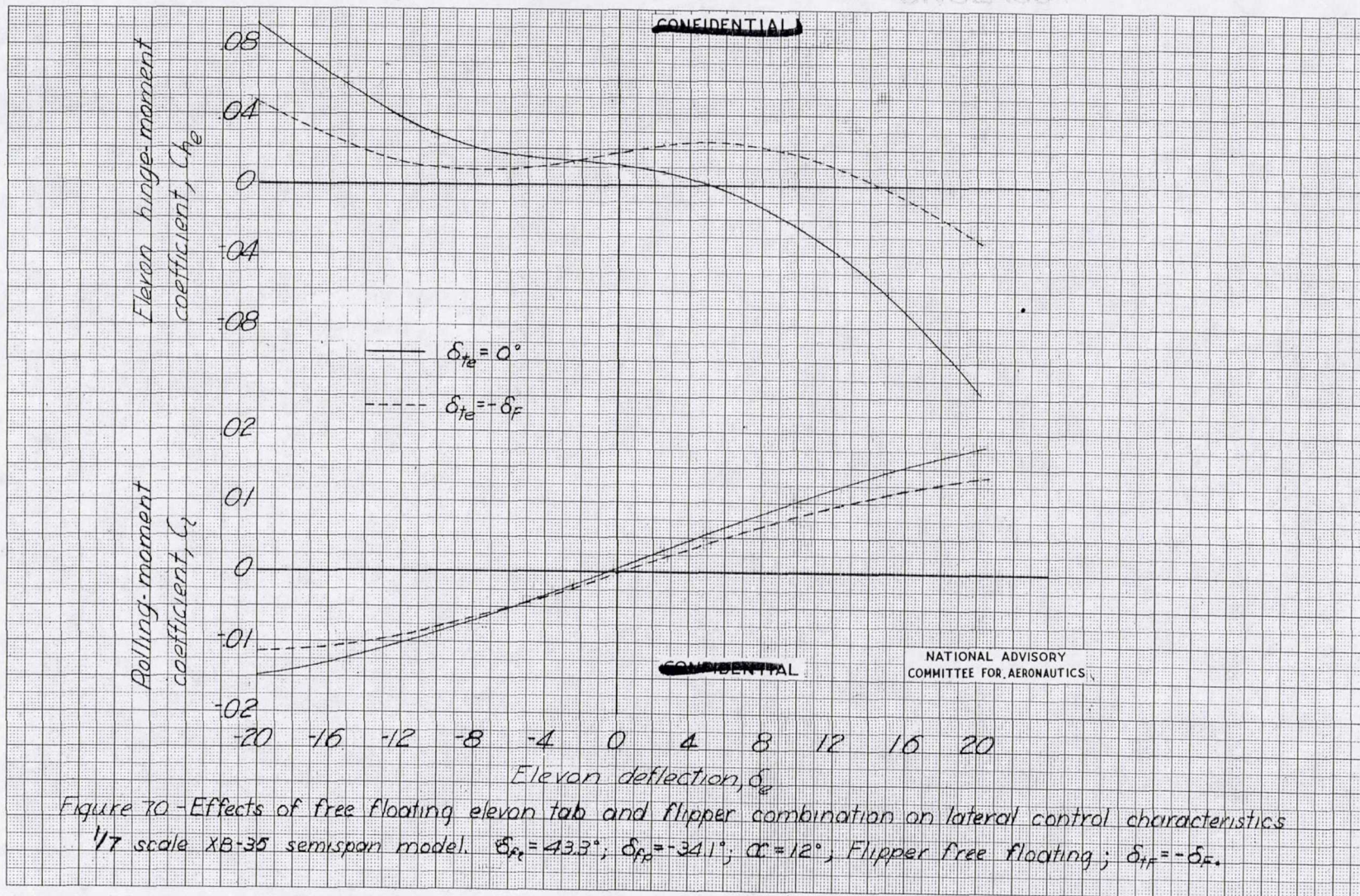


Figure 70 - Effects of free floating elevon tab and flipper combination on lateral control characteristics
 1/7 scale XB-35 semispan model. $\delta_{Ft} = 43.3^\circ$; $\delta_{Fb} = -34.1^\circ$; $\alpha = 12^\circ$; Flipper free floating; $\delta_{tr} = -\delta_F$.

MR No. 15127

UNCLASSIFIED